

AFRL-PR-WP-TR-1999-2122

**PROBABILISTIC ROTOR DESIGN
SYSTEM (PRDS)**

GAS TURBINE ENGINE DESIGN



P.G. ROTH

**GENERAL ELECTRIC AIRCRAFT ENGINES
ADVANCED ENGINEERING PROGRAMS DEPARTMENT
ONE NEUMANN WAY
CINCINNATI, OHIO 45215-6301**

DECEMBER 1998

FINAL REPORT FOR 01/23/1991 – 12/12/1998

APPROVED FOR PUBLIC RELEASE; DISTRIBUTION UNLIMITED

**PROPULSION DIRECTORATE
AIR FORCE RESEARCH LABORATORY
AIR FORCE MATERIEL COMMAND
WRIGHT-PATTERSON AIR FORCE BASE OH 45433-7251**

20000622 125

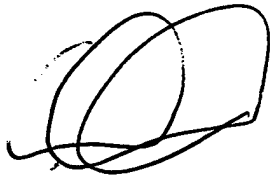
DTIC QUALITY INSPECTED 4

NOTICE

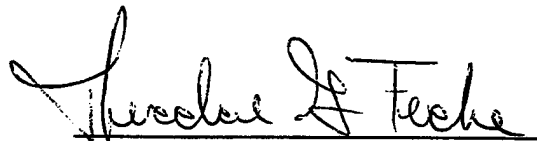
Using Government drawings, specifications, or other data included in this document for any purpose other than Government procurement does not in any way obligate the U.S. Government. The fact that the Government formulated or supplied the drawings, specifications, or other data does not license the holder or any other person or corporation; or convey any rights or permission to manufacture, use, or sell any patented invention that may relate to them.

This report is releasable to the National Technical Information Service (NTIS). At NTIS, it will be available to the general public, including foreign nations.

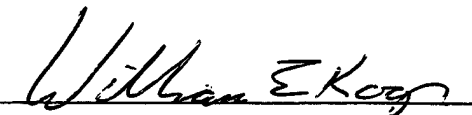
THIS TECHNICAL REPORT HAS BEEN REVIEWED AND IS APPROVED FOR PUBLICATION.



RICHARD FRIEND, SQN LDR, RAF
Project Engineer
Components Branch



THEODORE G. FECKE
Chief, Components Branch
Turbine Engine Division



WILLIAM E. KOOP
Chief of Technology
Turbine Engine Division
Propulsion Directorate

Do not return copies of this report unless contractual obligations or notice on a specific document requires its return.

REPORT DOCUMENTATION PAGE			Form Approved OMB No. 0704-0188	
Public reporting burden for this collection of information is estimated to average 1 hour per response, including the time for reviewing instructions, searching existing data sources, gathering and maintaining the data needed, and completing and reviewing the collection of information. Send comments regarding this burden estimate or any other aspect of this collection of information, including suggestions for reducing this burden, to Washington Headquarters Services, Directorate for Information Operations and Reports, 1215 Jefferson Davis Highway, Suite 1204, Arlington, VA 22202-4302, and to the Office of Management and Budget, Paperwork Reduction Project (0704-0188), Washington, DC 20503.				
1. AGENCY USE ONLY (Leave blank)		2. REPORT DATE DECEMBER 1998		3. REPORT TYPE AND DATES COVERED FINAL REPORT FOR 01/23/1991 - 12/12/1998
4. TITLE AND SUBTITLE PROBABILISTIC ROTOR DESIGN SYSTEM (PRDS) -- GAS TURBINE ENGINE DESIGN			5. FUNDING NUMBERS C F33615-90-C-2070 PE 62203 PR 3066 TA 12 WU 80	
6. AUTHOR(S) P.G. ROTH				
7. PERFORMING ORGANIZATION NAME(S) AND ADDRESS(ES) GENERAL ELECTRIC AIRCRAFT ENGINES ADVANCED ENGINEERING PROGRAMS DEPARTMENT ONE NEUMANN WAY CINCINNATI, OHIO 45215-6301			8. PERFORMING ORGANIZATION REPORT NUMBER	
9. SPONSORING/MONITORING AGENCY NAME(S) AND ADDRESS(ES) PROPULSION DIRECTORATE AIR FORCE RESEARCH LABORATORY AIR FORCE MATERIEL COMMAND WRIGHT-PATTERSON AFB, OH 45433-7251 POC: SON LDR RICHARD FRIEND, AFRL/PRTC, 937-255-2734			10. SPONSORING/MONITORING AGENCY REPORT NUMBER AFRL-PR-WP-TR-1999-2122	
11. SUPPLEMENTARY NOTES				
12a. DISTRIBUTION AVAILABILITY STATEMENT APPROVED FOR PUBLIC RELEASE, DISTRIBUTION UNLIMITED.			12b. DISTRIBUTION CODE	
13. ABSTRACT (Maximum 200 words) The USAF Probabilistic Rotor Design System (PRDS) contract (F33615-90-C-2070) was designed to develop, validate and demonstrate a probabilistic alternative to existing deterministic design philosophy. This report is a final summary of the work done for disk applications (a second team at GE Aircraft Engines is continuing work on a contract extension focusing on blades). Included in this report are: 1) A summary of physical mechanisms relevant to disk design. 2) A review of records on disk failures. 3) Extensive discussion of the concept of risk based design and recommendations for applications. 4) Description of a Probabilistic Design Analysis System developed by GE. 5) In depth review of validation testing of Probabilistic Fracture Mechanics base on fatigue testing of seeded push-pull and model disk specimens. 6) An introduction to risk based design optimization with an example application. 7) Specific suggestions for incorporating elements of risk based design into the Engine Structural Integrity Program (ENSIP, MIL SPEC 1783).				
14. SUBJECT TERMS Gas turbine engine design, Probabilistic methods, Risk analysis, Risk			15. NUMBER OF PAGES	
			16. PRICE CODE	
17. SECURITY CLASSIFICATION OF REPORT UNCLASSIFIED	18. SECURITY CLASSIFICATION OF THIS PAGE UNCLASSIFIED	19. SECURITY CLASSIFICATION OF ABSTRACT UNCLASSIFIED	20. LIMITATION OF ABSTRACT SAR	

Table of Contents

	<u>Page</u>
1.0 Introduction	1
1.1 Summary of Completed Contract Phases	3
2.0 Data Acquisition	7
2.1 Federal Aviation Administration Data	7
2.2 GEAE Disk Cracking Experience	9
3.0 Correlation of Failure Experience	11
3.1 Thermal Prediction	11
3.2 Stress/Displacement Prediction	12
3.3 Burst Prediction	18
3.4 LCF Prediction	19
3.4.1 Stratification of Fatigue Distributions and Size Effect Translations	20
3.4.2 The Interpretation of Strain- Controlled Fatigue Data	27
3.4.3 The Effect of Specimen Preparation on Fatigue Life	31
3.5 Sharp Crack Fracture Mechanics Prediction	31
3.6 Probabilistic Fracture Mechanics Prediction	39
3.7 Statistical Competition	42
3.8 Quality Control and NDE Prediction	43
3.8.1 Background	43
3.8.2 The Log-Logistic Prior Model	46
3.8.3 The \hat{a} versus a Model	52
4.0 Probabilistic Rotor Design System Parameters	55
5.0 Algorithm Flowcharting and Development	57
5.1 Response Surface Formulation of Risk Calculation	57
5.2 Program Organization	57
5.3 Database Architectures	59
5.4 ANSYS Parametric Modeling and Analysis	59
5.5 SIESTA (System for Integrated Engineering STructural Analysis)	62
5.6 MISSYDD Fracture Mechanics and Fatigue	62

Table of Contents (Continued)

	<u>Page</u>
5.7 Statistical Combination	62
5.7.1 F_{lcf}	62
5.7.2 F_{flaws}	63
5.7.3 F_{burst} and F_{yield}	63
5.7.4 Competition between Mechanisms	66
5.8 Nondestructive Evaluation	66
5.9 Optimization	67
5.10 Distributed Processing	67
6.0 Development of Acceptable (or Appropriate) Risk Criteria	69
6.1 Analysis of FAA/NAPC Data	69
6.2 Application of Probabilistic Methods	74
6.3 Appropriate Risk	76
6.4 System Risk versus Component Risk and Some Final Considerations ...	78
Phase I – References	81
7.0 Introduction to Probabilistic Design Analysis	85
7.1 An Example	86
7.2 Discussion of the Estimation Algorithms	87
7.3 Probabilistic Design Analysis System (PDAS)	89
8.0 Probabilistic Fracture Mechanics	91
8.1 Outline of the PFM Risk Calculation	91
8.2 Note on the Statistical Size Effect	92
9.0 Dealing with Variability: The Probabilistics Target	93
9.1 Example – Factoring In Dimensional Variability	95
9.2 Example – Factoring in Variability in Inclusion Distribution	97
9.3 Example – Factoring in Variability in Inclusion Behavior	98
10.0 Statistical or Not?	101
10.1 Application Strategies	102
11.0 PDAS Template Programming	105

Table of Contents (Continued)

	<u>Page</u>
11.1 Keywords	106
11.2 Table Manipulation	107
11.3 Text Entries	107
11.4 Equalities	108
11.5 Expressions	110
11.5.1 Algebraic Functions	110
11.5.2 Digitized Functions	110
11.6 Response Surfaces	112
11.7 Algebraic Operations	113
11.8 Distribution Handling	115
11.9 Loops	115
11.10 Subroutines	116
11.11 Regression Functions	117
11.12 Optimization	117
11.12.1 Optimization Notes	120
11.13 Plotting	121
11.14 Model, Mission and Calculation Libraries	121
11.15 General Commands	122
11.16 Response Surfaces	124
Phase II References	125
12.0 Probabilistic Fracture Mechanics (PFM)	127
12.1 Probabilistic Fracture Mechanics (PFM)	127
13.0 An Early PFM Validation Study	129
13.1 Background	129
13.2 Specimen Preparation	129
13.3 Evaluation of Seeding Practice	130
13.4 Fatigue Testing	134
13.5 Fracture Mechanics Analysis	137
13.6 MISSYDD Analysis	140

Table of Contents (Continued)

	<u>Page</u>
14.0 PRDS Validation Program	145
14.1 Specimen Preparation	145
14.2 Evaluation of Seeding Practice	147
14.3 Fatigue Testing	152
15.0 Analysis	155
15.1 Life Models	155
15.2 Inclusion Distributions	155
15.2.1 Image Analysis	155
15.2.2 Dirtiness Distributions	157
15.2.3 Inclusion Orientation	159
15.3 MISSYDD Analysis	161
15.3.1 Hourglass Tests	161
15.3.2 Other Push-Pull Tests	168
15.3.3 Model Disk Tests	173
16.0 Summary and Discussion	179
Phase III References	181
17.0 An Introduction to Design Optimization	183
18.0 Probabilistic Fracture Mechanics	187
18.1 Outline of the PFM Risk Calculation	187
19.0 Probabilistic Design Analysis System	189
20.0 Optimization of the IHPTET HPT Disk	191
20.1 First Step of Optimization	191
20.2 Second Step of Optimization	191
20.3 Recognizing Other Variabilities	196
20.4 Optimization Results	198
21.0 Closing Thoughts	207
Phase IV – References	209

Table of Contents (Continued)

	<u>Page</u>
22.0 Conservatism	211
23.0 Damage Tolerance	215
23.1 Flaws are Rare	215
23.2 Flaws Are Not Attracted to Stress Concentrations	217
23.3 Flaws Are Not Sharp Cracks	220
24.0 Recommendations	229
24.1 Specific Recommendations	231
Phase VI – References	233
Appendix A – Statement of Work	235
1.0 Introduction	235
2.0 Scope	235
3.0 Background	235
4.0 Technical Requirements	235
4.1 Phase I – Data Acquisition	232
4.1.1 Data Acquisition	236
4.1.2 Correlation of Failure Experience	236
4.1.3 Evaluation of Loads and Temperatures	236
4.1.4 Probabilistic Rotor Design System Parameters	236
4.1.5 Development of Acceptable Risk Criteria	236
4.2 Phase II – Method Development	236
4.2.1 Failure Models Development	237
4.2.2 Statistical Analysis Models	237
4.2.3 Methodology Description	237
4.3 Phase III – Validation	237
4.3.1 Test Definition	237
4.3.2 Test Evaluation	237
4.3.3 PRDS Design Tool Refinement	238
4.4 Phase IV – Application	238

Table of Contents (Concluded)

	<u>Page</u>
4.4.1 Probabilistic Redesign	238
4.5 Phase V – Application Test	238
4.5.1 Rotor Components Detail Design	238
4.5.2 Rig Test and Validation for Gas Generator Testing	238
4.5.3 Hot Cyclic Spin of Component	238
4.6 Phase VI – Method Extension	238
4.6.1 PRDS for Metal Matrix Composite (MMC) Rotors	238
4.6.2 Modifications to Military Standard 1783	238
4.6.3 PRDS Modifications	238
5.0 Data and Other Deliverables	238
Appendix B – Sampling Scatter	239
Appendix C – PDAS Analysis Templates	243
Appendix D - Introduction to Response Surface Methodology and Factorial Designs	249

List of Illustrations

Figure	Title	Page
1.	Thermal Analysis – Comparison of ANSYS Finite Element Calculations with Measured Temperatures (ATEGG Engine, Transient Condition).	11
2.	Elastic-Plastic Stress/Displacement Analysis – Comparison of Finite Element Calculated Stresses with Theoretical Solution (Pressurized Thick-Walled Cylinder).	12
3.	Instrumented Fatigue Specimens.	13
4.	Burst Analysis – CF6-50 Stages 3-9 Compressor Spool Deflected Shape (CYANIDE Elastic-Plastic Calculation).	20
5.	Fatigue Analysis – Model Comparison to Experiment.	21
6.	Cutup Plan (First Size-Effect Study).	21
7.	Comparison of Large and Small Bar Failure Distributions (First Size-Effect Study).	22
8.	Small Bar Distribution Scaled by 50 – Compares Conservatively with Large Bar Distribution (First Size-Effect Study).	22
9.	Small Bar Distribution Scaled by 20 – Compares Conservatively with Large Bar Distribution (First Size-Effect Study).	23
10.	Small Bar Distribution Scaled by 2.5 – Good Agreement with Large Bar Distribution (First Size-Effect Study).	23
11.	Failed Large Bars – Rim Ends Down (First Size Effect Study).	24
12.	Large & Small Bar Failure Distributions Separated by Layer (First Size Effect Study.)	24
13.	Cutup Plan and Comparison of Fore and Aft Layer Failure Distributions (ENSIP Study).	25
14.	Cutup Plan and Comparison of Fore and Aft Layer Failure Distributions (Second Size Effect Study).	25
15.	Failed Large Bars – Aft Ends Down (Second Size Effect Study).	26
16.	Large Bar Failure Distribution Compared to Fore and Aft Layer Small Bar Failure Distributions (Second Size Effect Study).	27
17.	Extensometer Array.	29
18.	Second Size Effect Failure Distributions with Tabulation of Stabilized A- and B-Strains – Questionable Points Circled.	30
19.	Life is Correlated to Maximum Compressive Residual Stresses – Data Compares Three GEAE Machining Vendors.	31
20.	Fracture Mechanics Analysis – Model Comparison to Experiment (Two Materials, Multiple Specimen Geometries).	32

List of Illustrations (Continued)

Figure	Title	Page
21.	Fracture Mechanics Analysis – Model Comparison to Experiment (As–HIP PM René 95 Kb Bars).	33
22.	Crack Growth Rate Data for Specimen K1062 (As–HIP PM René 95, Four Load Sheds).	34
23.	Crack Growth Rate Data for Specimen K1063 (As–HIP PM René 95, Four Load Sheds).	34
24.	Crack Growth Rate Data for Specimen K1064 (As–HIP PM René 95, Four Load Sheds)	35
25.	Crack Growth Rate Data for Specimen K1065 (As–HIP PM René 95, Four Load Sheds)	35
26.	Crack Growth Rate Data for Specimen K1066 (As–HIP PM René 95, Four Load Sheds).	36
27.	Crack Growth Rate Data for Specimen K1067 (As–HIP PM René 95, Four Load Sheds).	36
28.	Second Load Sheds Compared (As–HIP PM René 95 Specimens).	37
29.	Third Load Sheds Compared (As–HIP PM René 95 Specimens).	37
30.	Fourth Load Sheds Compared (As–HIP PM René 95 Specimens).	38
31.	Threshold Benchmarks – Comparison of Typical As–HIP René 95 Specimen (K102) to Typical DA Inconel 718 Specimen (K1096).	38
32.	First Load Sheds Compared (DA Inconel 718 Specimens).	39
33.	Second Load Sheds Compared (DA Inconel 718 Specimens).	39
34.	Third Load Sheds Compared (DA Inconel 718 Specimens).	40
35.	Fourth Load Sheds Compared (DA Inconel 718 Specimens).	40
36.	MISSYDD Validation Study – Predicted Defect Failure Distribution Compared to Data.	41
37.	MISSYDD Validation Study – Natural Fatigue Competes with Seeds.	42
38.	MISSYDD Validation Study– Natural Fatigue Failure Distribution Compared to Data.	42
39.	MISSYDD Validation Study– Predicted Defect Failure Distribution Combined with Natural Fatigue Distribution Compared to Data.	43
40.	(a) Binomial Simulation of 30 Inspections of a Single Crack, (b) Simulation Repeated 1000 Times.	44

List of Illustrations (Continued)

Figure	Title	Page
41.	(a) Histogram of Simulation Results. (b) Theoretical Binomial Distribution Function (Binomial Parameter is 0.90).	45
42.	Two Data Sets from the Have-Cracks-Will-Travel Study and Log-Logistic Fits.	47
43.	Average POD Curve with Distribution of Detectability.	48
44.	(a) Beta Simulation of 1000 Cracks. (b) Histogram of Detectabilities.	49
45.	Beta Simulation of Crack Detectability Combined with Binomial Simulation of Inspections.	50
46.	Berens-Hovey \hat{a} -versus-a NDE Response Model – POD at a is the Probability that \hat{a} Exceeds a Threshold.	52
47.	Berens-Hovey \hat{a} -versus-a NDE Response Model – POD Curve Construction. . .	53
48.	Eddy Current Amplitude Plotted against Crack Area – Area Inferred from Optical Measurement.	54
49.	Eddy Current Amplitude Plotted against Crack Area – Area Inferred from Replica Measurement – The Scatter Decreases.	54
50.	PDAS (Probabilistic Design Analysis System).	58
51.	MISSYDD Data Base Index.	60
52.	Baseline ANSYS Disk Model (Center) Plus Eight Parametric Perturbations. . .	61
53.	MISSYDD Calculation of Fflaws.	64
54.	Computation of Fburst.	65
55.	ADS Design Optimization.	68
56.	Dual Pressure Waves Hitting a Target.	86
57.	Failure Regions.	86
58.	First Order Approximation to Failure Region.	87
59.	Polyhedral Approximation to Failure Region.	87
60.	Correlated (x,y) Sequences Generated by MLC Algorithm.	89
61.	Peened Specimens Tested at One Temperature/Strain Condition.	93
62.	Predicted Failure Distributions for Nine Disk Perturbations.	94
63.	Strategy for Implementation of Probablistics.	95
64.	Dimensional Distribution Probability Density Functions.	96
65.	Risk Response Surface Integrated against Dimensional Distributions.	96

List of Illustrations (Continued)

Figure	Title	Page
66.	Lot-to-Lot Variability in Inclusion Distribution.	97
67.	Weibull Fit to Predicted/Observed Distribution.	99
68.	Material Variability Integrated into Specimen Predictions of 61.	99
69.	Material Variability Integrated into Other Cylindrical Specimen Data Sheets. ..	100
70.	Digitized Goodman Curves: Polar in Theta ... Linear in Temperature.	112
71.	Response Surface Example.	113
72.	Response Surface Example – Grid Required for Interpolation.	113
73.	Response Surface of Monte Carlo Estimate (Z) as Function of Alpha (X) and Beta (Y).	113
74.	Weibull Fit to Predicted/Observed Distribution.	128
75.	MV2 Specimen Design.	130
76.	SMC Blending Study – Evaluation Based on Poisson Model.	135
77.	MV2 Elastic/Plastic Stress Distribution.	137
78.	Fracture Mechanics Comparisons Using 7505 F Vacuum Data.	140
79.	Revised Fracture Mechanics Comparisons.	141
80.	MV2 MISSYDD Analysis.	142
81.	Revised MV2 MISSYDD Analysis.	142
82.	Revised MV2 MISSYDD Analysis – – Focus on Natural Initiations.	143
83.	HG1 Hourglass Geometry.	146
84.	HG2 Hourglass Geometry.	147
85.	Forging Mult Coding.	147
86.	Forging Cutup.	148
87.	MD–9 Model Disk Geometry.	149
88.	MD–10 Model Disk Geometry.	149
89.	Cameron Blending Study – Evaluation Based on Poisson Model.	151
90.	Schematic of Can Filling Experiment.	151
91.	Comparison of Hourglass Test Stresses to René 88 DT Stress-Strain Curve.	152
92.	Heavy Liquid Separation.	156
93.	SEM Image of an HLS Recovered Inclusion.	156
94.	Size Distributions.	158

List of Illustrations (Continued)

Figure	Title	Page
95.	Aspect Ratio Distributions.	158
96.	Predicted and Observed Distributions Compared.	160
97.	Simulation Example.	161
98.	Lot-to-Lot Variability in Inclusion Distribution.	162
99.	Oriented and Unoriented Distributions Compared.	162
100.	Predicted and Observed Distributions Compared Assuming Orientation.	163
101.	Algorithm 1 — Comparison of Predicted and Observed Distributions.	163
102.	Comparison of Data Sets.	164
103.	Stratification.	165
104.	Stratification.	165
105.	Strategy for Implementation of Probabilistics.	166
106.	Censored Data Set Comparison.	167
107.	Censored Data Set Comparison.	167
108.	HG1/S1	168
109.	HG2/S2	169
110.	HG1/S0	169
111.	Algorithm 2 – Peened Specimens Tested at One Temperature/Strain Condition. .	170
112.	Comparison of Data Sets.	171
113.	Distributions of Maximum Stresses.	171
114.	Distributions of Minimum Stresses.	172
115.	Distributions Broadened by Stress Variability.	172
116.	Stress Variability Factored into Cylindrical Data.	173
117.	Other Cylindrical Specimen Data Sets.	174
118.	MD-9 Comparison of Predicted and Observed Failure Distributions.	175
119.	Individual Fracture Mechanics Calculations.	176
120.	MD-10 Comparison of Predicted and Observed Failure Distributions.	176
121.	Rectangular Window.	183
122.	Trials - Feasible Solutions.	183
123.	Optimal Solution.	184

List of Illustrations (Continued)

Figure	Title	Page
124.	Objective Function $23/2 x + y$.	185
125.	Constraint Function $(2x + 21/2 y)/(2x(x + 21/2 y))$	186
126.	Constraint Function $1/2(x + 21/2y)$	186
127.	Volume Optimization.	191
128.	ADS-based Stacked Shell Optimization Program. Rough Outline	193
129.	ADS-based Stacked Shell Optimization Program Flanges and a Rim added.	193
130.	BOFF, WOFF AND ROFF Judgement.	193
131.	Optimized Outline.	194
132.	Dual Alloy Disk Concept Variability; PDAS Probabilities.	198
133.	Evolution of Design and Response Parameters.	199
134.	Evolution of Design and Response Parameters.	199
135.	Evolution of Design and Response Parameters.	200
136.	Evolution of Design and Response Parameters.	200
137.	Evolution of Design and Response Parameters.	201
138.	Evolution of Design and Response Parameters.	201
139.	Evolution of Design and Response Parameters.	202
140.	Evolution of Design and Response Parameters.	202
141.	Evolution of Design and Response Parameters.	203
142.	Evolution of Design and Response Parameters.	203
143.	Evolution of Design and Response Parameters.	204
144.	Minor Outline Changes Between Iteration 2 and 4.	204
145.	Location 1: Web Narrows Slightly.	205
146.	Location 2: Web Narrows Slightly.	205
147.	Location 3: Bore Shifts Slightly.	206
148.	Location 4: Bore Shifts Slightly.	206
149.	Strategy for Implementation of Probabilistics.	212
150.	POD Function.	216
151.	Size Distributions.	216
152.	Integrated POD.	217

List of Illustrations (Concluded)

Figure	Title	Page
153.	F110 Bolthole Model.	218
154.	Monte Carlo Simulation.	219
155.	Geometric Failure Probability at 5,000 Cycles Compared to POD Function. ...	219
156.	Integrated Failure Probability at 5,000 Cycles.	220
157.	Revised MD9 Predictions.	221
158.	Revised MD10 Predictions.	221
159.	MD10 Internal Initiations.	222
160.	René 88 DT, Subsurface.	223
161.	René 88 DT, Subsurface.	223
162.	René 88 DT, Surface.	224
163.	René 88 DT, Surface	224
164.	As-HIP René 95, Subsurface.	225
165.	As-HIP René 95, Subsurface.	225
166.	As-HIP René 95, Surface.	226
167.	As-HIP René, Surface.	226
168.	Flaw Distribution Compared to POD Function.	230
B.1.	Reproducibility – 10 Random Samples of Size 20.	241
B.2.	Reproducibility – 20 Random Samples of Size 20.	241
B.3.	Reproducibility – 30 Random Samples of Size 20.	241
B.4.	Reproducibility – 40 Random Samples of Size 20.	241
D.1.	Average Hoop Stress on Bore Offset.	252

List of Tables

Table	Title	Page
1.	Rotor Failures (1972 to 1987)	7
2.	Disk/Rim Failures by Cause.	8
3.	Disk/Rim Failures by Flight Conditions.	9
4.	Strain Comparison for Specimens.	14
4.	Strain Comparison for Specimens (Continued).	15
4.	Strain Comparison for Specimens (Continued).	16
4.	Strain Comparison for Specimens (Continued)	17
4.	Strain Comparison for Specimens (Concluded).	18
5.	Comparison of Experimental Results for Disk Burst Speed with Empirical Method and CYANIDE Predictions.	19
6.	AB Strain Comparisons for SEL2-22 (13,451 Cycle Life).	30
7.	Threshold Stress Intensity Range, ksi in ²	33
8.	Dimensions of Simulated Cracks Measured by Eddy Current.	54
9.	Average Number of Engines in Operation.	70
10.	Number of Disk/Rim Failures.	71
11.	Failure Rates – Disk/Rim Failures per 1000 Engines.	71
12.	Engine Hours Accrued (Millions).	72
13.	Hours Accrued per Engine.	72
14.	Engine Hours Accrued (Millions).	73
15.	Failure Rates – Disk/Rim Failures (Number per Million Engine Flight Hours). .	73
16.	Failure Results Comparison.	87
17.	Seeding Definition.	130
18.	Inspection Comparisons.	132
18.	Inspection Comparisons. (Concluded)	133
19.	Blending Study.	134
20.	Test Orientations.	136
21.	Test Results Summary.	138
21.	Test Results Summary (Concluded).	139
22.	Seeding Definition.	145
23.	Forging Dispositions.	146

List of Tables (Concluded)

Table	Title	Page
24.	Blending Study.	150
25.	Can Fill Study.	150
26.	Model Disk Test Matrix.	153
27.	Seed Weights and Seeding Rates.	157
28.	Inclusion Orientation Study.	160
29.	Model Disk Test Results Summary.	175
30.	Fractional Factorial Design.	195
31.	Normalized Deviations Results.	196
32.	Design Point Defined by Seventeen Perturbations.	197

Phase I – Data Acquisition

1.0 Introduction

The USAF Probabilistic Rotor Design System (PRDS) contract (F33615-90-C-2070) was funded to develop, validate and demonstrate a probabilistic alternative to existing deterministic design philosophy.

Traditional design practices recognize that determinism has limits, that predictions are averages, that there is some risk of failure. But risk is addressed only indirectly: Maximum loadings (e.g. plus 3σ) are kept below minimum properties (e.g. minus 3σ), and additional safety factors may be applied if confidence needs further boosting. The presumption is that critical components can (and should) be designed with enough conservatism that they never fail.

While the traditional approaches have worked well in integrating the lessons of experience, recognizing and then compensating for problems as technology pushes ahead, there is a common perception that their conservatism is extreme, and there are pressures pushing for a change. Aerospace designers are moving towards lighter weight structures operating nearer theoretical limits to increase efficiency, speed and maneuverability, but as designs are slimmed and demands on them increased, the possibility of failure inevitably will increase. Moreover, new materials are being developed (intermetallics, ceramics, composites) which potentially provide quantum improvements over conventional metallic alloys in some properties (strength, density, temperature capability). They also present, however, new modes of failure which are not addressed by current design practices.

It is becoming more and more common to evaluate designs by assessing (and controlling) risk of failure. While some analyses are overly simplistic (and a few may be fraudulent), the state of the art of risk analysis is improving, and it is an art. There is a proliferation of different phi-

losophies, formulations and computational techniques. GEAE and Pratt & Whitney have each developed their own probabilistic approaches to support the Air Force. NASA has contracted for at least two new probabilistic software packages (from JPL and Southwest Research Institute) to analyze Shuttle fleet experience, and to apply in the designing of new vehicles, satellites and space stations. Other agencies and industries estimate risks using other tools for other applications (regulatory assurance of nuclear safety, evaluations of toxicity and carcinogenicity). There are several reasons for this diversity, some good, some bad.

First, there is diversity in the range of disciplines relevant to a specific problem. For example, many factors are significant to the integrity of a structure: Loading and environment, thermal and stress distribution, failure mechanisms and material capability. While SRI's Nessus (*Reference 1*) attempts to be self-contained (to the point that it includes its own finite element stress code) it misses important pieces (life algorithms). This is a limitation but not a shortcoming; there is no need to have a single ultimate program which serves all purposes. A modular programming approach is preferred with individual computational modules being soundly based, assumptions clearly stated, limitations recognized, and educated, open minds in charge. Also, given that modules may need to interact (even if their equations are independent), it helps to develop common formats for data exchange.

Second, risk analyses deal in uncertain terms, usually extrapolating far from obtainable experience. In some cases their input is not well quantified, and in many cases the predictions can not be meaningfully tested. When information is lacking, assumptions are substituted which sometimes gain indomitable credibility

by the persistence of their application. Consequently, competing alternative formulations often can not be reasonably compared.

Third, there often seems to be a misplaced confidence in the universality of probabilistic methods. Thus, given discovery of an alloy heat inadvertently contaminated by incompatible scrap chips, a request may be made to calculate the risk to the fleet. This reflects a very common belief that all random factors are probabilistically random. The contamination in this example is likely not. While it is recommended that statistical approaches be applied when appropriate, it is emphasized that they can mislead if not properly based and accompanied by physical understanding.

The PRDS (Probabilistic Rotor Design System) contract will develop and demonstrate a probabilistic approach to design.

A tool, PDAS (Probabilistic Design Analysis System) will be developed to calculate risk associated with statistically distributed parameters, facilitate evaluation of the effect of non-statistical parameters on risk, and enable risk-based optimization. PDAS will but exemplify a philosophy. While it will be a flexible tool, it will be structured with disk design in mind. The system will be comprised of modules identified with specific functions (e.g. geometric modeling, thermal/stress/displacement analysis, fatigue and fracture mechanics calculation). The logic which connects the modules, the basic probabilistic algorithms, should be broadly applicable, but other problems may require different component modules. For example, the risk analysis of a structural design such as a space platform would require a different set of finite element types (beams, plates), a different set of failure modes (bending, buckling), and so on.

Individual modules will be selected based on demonstrated performance and will be a mix of GEAE-developed and commercial packages.

GEAE's SIESTA (System for Integrated Engineering STructural Analysis, *Reference 2*) will provide a common language to tie them together.

The PRDS contract was divided into six phases:

- Phase I - Data Acquisition and Planning – Review experience to assess the performance of traditional design practices. Compare analytical models against experiment. Identify sources of scatter which contribute to the probabilistic nature of risk. Outline the probabilistic approach. Address questions of interpretation: What is the meaning of a calculated risk and what is an appropriate level of risk for design?
- Phase II - Method Development – Turn the flowchart developed in Phase I into a usable tool. Identify data needed for application.
- Phase III - Validation – Design and execute a testing program incorporating both small scale feature specimens and more realistic model disks which evaluates the probabilistic models developed in Phases I and II.
- Phase IV - Application – Utilize the tools developed in Phase II to optimize the design of an advanced technology engine disk.
- Phase V - Application Test – Test the full scale disk redesigned in Phase IV. Following limited engine exposure to demonstrate operability, It was intended that the disk be tested to failure in a spin pit facility. While the single test would do little to validate the statistical predictions, post-test failure analysis could boost confidence in the new design tool. Scheduling problems eventually led to the Air Force agreeing to cancel this item.
- Phase VI - Method Extension – Evaluate the lessons learned in Phases I through IV and make recommendations for the next step. Develop a modified Military Standard 1783 which incorporates PRDS. A

program extension has been awarded to incorporate blades into the probabilistic framework.

The full statement of work is reproduced in Appendix A.

1.1 Summary of Completed Contract Phases

Individual Interim Reports were completed for Phases I, II, III, IV and VI.

The Phase I (Data Acquisition) Interim Report documented the following:

- Compilation of data from FAA failure statistics, GEAE cracking investigations and laboratory method validations. This data was used both to support analysis of the effectiveness of current design practices and analytical tools, and as background for a definition of acceptable risk.
- Review of GEAE cracking investigations to identify occasions of excessive stress or temperature, poor material properties, inherent material inclusions, manufacturing damage and so forth, to assess the effectiveness of current design practices which are largely based on safety factors.
- Analysis of laboratory data to assess the accuracy of specific analytic tools used during the design process.
- Identification of the principal failure modes to be incorporated into the probabilistic design analysis system and listing of the potential drivers or failure causes (which include stresses, temperatures and gradients).
- Algorithmic development and program flowcharting addressing four principal failure modes. As part of this development, relevant parameters such as part dimensions, inclusion sizes, speeds, temperatures and so forth were identified, and the approaches to be taken to integrate variations

in these parameters into estimated risk outlined.

- Utilization of the FAA statistics gathered in Task 1 to draw conclusions concerning risk of disk failure in today's commercial engine fleet. It was assumed that design practices and analytical tools are largely the same regardless of the application (i.e. military or commercial), and hence that conclusions drawn from the FAA data are broadly applicable. Data was sorted by failure cause at the component level, and some trends were observed. E.g. Failure of turbine disks is more likely than failure of compressor disks is more likely than failure of fan disks. E.g. Disk failures are most often not design related.
- Developed a rationale for the application of probabilistic design and used the FAA data to suggest an acceptable level of risk for design.

The Phase II (Method Development) Interim Report documented the following:

- An introduction to the concept of designing probabilistically against failure and a comparison of three standard approaches to estimating failure probability.
- Following this, the philosophy was laid out for PDAS (PDAS — Probabilistic Design Analysis System), a software package which facilitates application to the design process of probabilistic algorithms and optimization tools.
- A general strategy was outlined for application of probabilistics with three specific examples provided to demonstrate the integration of statistically describable variability into design analyses.
- Specific proposals were made for setting part lives using probabilistics.
- The report concluded with a detailed summary of the PDAS Template Language and

its application to managing response surface analyses.

The Phase III (Validation) Interim Report documented the following:

- The theory and formulas basing GEAE's Probabilistic Fracture Mechanics (PFM) methodology were summarized.
- An early PFM validation study was described. The study employed hourglass push-pull fatigue specimens machined from As-HIP PM René 95 seeded with a broad distribution of alumina inclusions. The failure distribution of a sample of fifty of these specimens tested at room temperature was accurately predicted.
- PRDS PFM validation testing included both hourglass push-pull specimens and small model disks. The hourglass concept was again chosen to simulate stress gradients present in real hardware while allowing adequate numbers of tests to enable proper statistical comparisons. The model disks more closely simulate real hardware: Machining conformed to production practices. The stress field is generally multiaxial. But given their much higher costs (both of manufacturing and of testing), far fewer could be run. Considerable detail was presented detailing fabrication and testing of the hourglass and model disk specimens, and comparison of the test results with predictions.
- The results of GEAE's validation studies were considered in the context of the probabilistics application strategy introduced in the Phase II Interim report as a three ring target:
 - *A Bull's Eye* – Apply what we know as well as we know how.
 - *A Middle Ring* – Evaluate sensitivities to known deviations and bound the results.

- *An Outer Ring* – Back off from the calculations until accumulated experience justifies doing otherwise.

Validation exercises evaluate our ability to hit the Bull's Eye given what we do know. In design applications, middle ring assumptions and outer ring conservatisms are often necessary and usually prudent given less than complete understanding of all factors potentially affecting performance and/or safety.

The Phase IV (Method Application) Interim Report documented the following:

- A brief introduction to the concept of design optimization.
- The main PFM algorithm and the PDAS design tool.
- The application of PDAS to the optimized design of the HPT disk of the XTC-76/3 IHPTET. The application was successful in that it moved the disk geometry to a configuration conforming to GEAE design practices, but weight was added in the process.

The Phase VI (Method Extension) Interim Report documented the following:

- The lessons learned were pulled together to support proposed revisions to the ENSIP MIL SPEC 1783.
- Modifications were recommended which both recognize the established rarity of the flaws which the ENSIP damage tolerance approach is intended to protect against, and more accurately reflect their behavior.

At the request of the USAF, these separate reports have been gathered into this single volume. Editing has been done to eliminate some of the duplications between the reports, but some themes have been left to repeat as was felt appropriate for clarity or emphasis, often accompanied by variations which reflect the evolution of our understanding over the nearly ten years of this contract.

Acknowledgements

The author wishes to acknowledge the enormous contributions of John Coomer and Norman Austin who shared technical responsibility for this contract for its first several years and initiated the PRDS seeded testing program. Also, Don Beeson, Greg Blanc, Bob Maffeo, Bob McClain, Steve Schrantz, JR Engebretsen and Tim Stone for contributions to the development of PDAS, Greg Bechtel and (again) Tim Stone who provided their finite element expertise for the various analyses, Jean Murray-Stewart, Eric Huron, Tom Daniels, Ron Grant and Agnes Berszeyi who helped with material preparation, testing and post-test fractography, Keith Megow who executed a successful spin pit testing program, Dave Crall, Dan Lang,

Mark Tipton and (again) Bob McClain who assisted greatly with setting up parametric disk models for the XTC-70 HPT disk, Jeanette Sturgill, Mike O'Hair and Dorothy Reese who patiently assisted in preparation of this document, Paul Domas for always asking the right questions, and my multiple generations of USAF program sponsors and monitors, Ted Fecke, Mike McIntyre, Chris Pomfret and Sqn. Ldr. Andrew Green.

Disclaimer

The examples developed in this report have been constructed for purpose of demonstration. While some data may be real, the applications do not represent hardware produced by GE Aircraft Engines.

2.0 Data Acquisition

Engine field data was reviewed to identify types of problems that have been encountered. Two sources were used: FAA/NAPC commercial engine failure statistics, and GEAE field cracking investigations.

2.1 Federal Aviation Administration Data

FAA/NAPC reports were gathered for the years 1972 through 1987 (*References 3-18*). The tabularized data from each report was converted into ASCII data files with the aid of an optical character scanner and analyzed. The reports attempt to be inclusive in that they summarize the experience of tens of thousands of engines and many millions of hours of operation. However, there are questionable irregularities in fleet sizes, and at least one known failure that was investigated by the FAA but does not appear in the data. The FAA/NAPC reports are limited in that the age distributions of individual parts, engines, and engine fleets are not included.

Failure modes are broadly grouped into seven classes, as shown in *Table 1*. Observations from the data are as follows:

- The engine is a system, and blades are the weak link. Out of 2,493 failures of large engines during this 16-year period, 1,536 involved fragments. Of these 1,536, 1,453 were blades, 29 were from seals, and 54 were from disks. There were 206 failures with no reported cause (oil problems, etc.). There were 751 failures linked to specific components, but no fragments were released, and no details were presented. (Refer to *Table 1*.)
- Compressor and turbine failure numbers are comparable (24 and 26 respectively) and much higher than the number of fan failures (4). (*Table 2*.)
- For those disk failures which could be assigned a cause (30 out of 54), a significant number (13) were considered to be directly design related. Another 13 were attributed to unspecified secondary causes. Only 2 of

Table 1. Rotor Failures (1972 to 1987)

Engine	Blade	Seal	Disk	Rim	None	Other	All
JT3	156	1	6	2	77	18	260
JT4	34	0	1	1	16	1	53
JT8	631	13	13	8	378	118	1,161
JT9	282	14	3	4	76	20	399
PWA2037	6	0	0	0	1	0	7
CF6	205	1	2	10	67	19	304
CFM56	8	0	0	0	18	1	27
RB-211	131	0	2	2	11	29	282
ALL	1,453	29	27	27	751	206	2,493

Table 2. Disk/Rim Failures by Cause.

Engine	CAUSE CODE							All
	1	2	3	4	5	6	7	
JT3	1C	2T	1F				1F 3C	2F 4C 2T
JT4		1T					1C	1C 1T
JT8	1F 4C 2T	3C 2T		1C			3C 5T	1F 11C 9T
JT9	2C 1T	1C 1T					1C 1T	4C 3T
PWA2037								
CF6	1C	3T	1T	1T			2C 4T	3C 9T
CFM56								
RB-211	1C						1F 2T	1F 1C 2T
ALL	1F 9C 3T	4C 9T	1F 1T	1C 1T			2F 10C 12T	4F 24C 16T
Codes: F – Fan C – Compressor T – Turbine 1 – Design and Life Prediction Problems 2 – Secondary Causes 3 – Foreign Object Damage 4 – Quality Control 5 – Operational 6 – Assembly and Inspection Error 7 – Unknown								

- the 30 were attributed to foreign object damage, and 2 to quality control. (*Table 2*)
- Twenty-four disk failures could not be attributed to a specific cause.
- Disk failures occurred almost exclusively at takeoff and climb (43 out of 54) supporting a fatigue interpretation. (*Table 3*)

Table 3. Disk/Rim Failures by Flight Conditions.

ENGINE	FLIGHT CONDITION CODE									
	1	2	3	4	5	6	7	8	9	10
JT3	0	1	2	2	0	3	0	0	0	0
JT4	0	0	1	1	0	0	0	0	0	0
JT8	0	0	10	7	3	1	0	0	0	0
JT9	0	0	2	4	0	1	0	0	0	0
PWA2037	0	0	0	0	0	0	0	0	0	0
CF6	0	0	6	6	0	0	0	0	0	0
CFM56	0	0	0	0	0	0	0	0	0	0
RB-211	0	0	1	1	1	0	0	0	0	1
All	0	1	22	21	8	1	0	0	0	1
CODES: 1 - Inspection/Maintenance 2 - Taxi/Ground Handling 3 - Takeoff 4 - Climb 5 - Cruise 6 - Descent 7 - Approach 8 - Landing 9 - Hovering (Not Applicable to these Engines) 10 - Unknown										

These data will be considered further in Section 6.1, Development of Acceptable Risk Criteria.

2.2 GEAE Disk Cracking Experience

The history of our large engine disk cracking was reviewed. The review included the CF6, CFM56, F101 and F110 engine lines. All cracking was considered, whether failure resulted or not. The information from their analysis is considerably more detailed than that available from the FAA summaries.

GEAE cracking history can be divided into nine categories:

1. Parts within blueprint tolerances, but tolerances too large given stress sensitivity: Design analysis problem.
2. Parts out of blueprint: Quality control problem.
3. Manufacturing induced damage (surface damage): Process problem; quality control problem.
4. Fretting: Design problem; materials problem.
5. Material inclusions: Process problem; materials problem; and quality control problem.
6. Assembly (as simple as leaving a tool in the engine): Quality control problem.
7. Temperatures not understood: Design analysis problem.
8. Stresses not understood (misanalysis, complex stress fields not recognized): Design analysis problem.

9. Secondary failure (e.g. loss of cooling):
Systems analysis problem.

Comparing with the FAA data: Disk cracking problems are rare (in agreement with *Table 1*). Turbines are more prone to cracking than compressors, which are more prone to cracking than fans. While six GE failures appear in the FAA data as uninterpretable at the time of reporting (*Table 2*), all were eventually explained. Design and analysis oversights were judged to be

responsible for a large fraction of our cracking problems, consistent with the 13/30 industry average. There have been fewer than the industry average of 13/30 secondary cause events. Most cracking events were caught before failure. Correlation with flight conditions (as in *Table 3*) is not relevant.

Experimental data relevant to specific failure modes has been reviewed and will be discussed in the next section.

3.0 Correlation of Failure Experience

While we are sometimes surprised by a problem, response is swift. Analysis and testing are initiated to quickly understand it, identify a fix, and implement a management plan. We do not believe that problems are due to inherent limitations in methodology, but rather to improper application of good methodology, lack of appropriate data, or oversights. Safety factors do not guarantee safety.

In each of Sections 3.1 through 3.8, a specific analysis method will be considered. The average success of our deterministic methods will be supported by experimental data (if available), and potential sources of variability will be discussed (if recognized). GEAE's probabilistic fracture mechanics methodology can also be supported experimentally; the results of a validation study will be summarized.

3.1 Thermal Prediction

ANSYS (*Reference 19*) will be incorporated as the PDAS thermal analysis module. Used properly, it should produce accurate results. *Figure 1* shows comparison of predicted and measured temperatures for the final compressor stage of an ATEGG engine (the probable choice for the component demonstration phase of PRDS) (*Reference 20*).

(Note: An advanced turbine disk was eventually selected).

Proper use requires attention to the numerical details of the calculation (e.g. good meshing), but this is in some sense a minor concern if the basic physical models are correct. Based on the generally good agreement shown in *Figure 1*, we suspect that the quality of the necessary

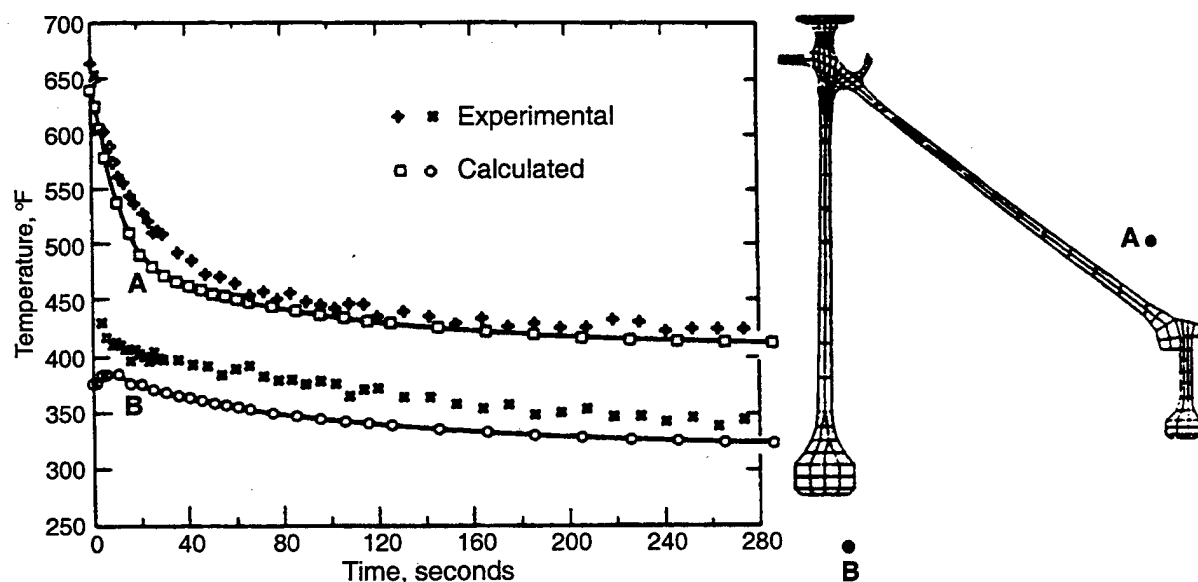


Figure 1. Thermal Analysis - Comparison of ANSYS Finite Element Calculations with Measured Temperatures (ATEGG Engine, Transient Condition).

boundary condition data is a more important consideration (air flows and temperatures).

3.2 Stress/Displacement Prediction

GEAE uses a variety of advanced finite element codes for analysis of stresses and displacements (ANSYS (*Reference 19*), CLASS/MASS (*Reference 21*), CYANIDE (*Reference 22*)), oftentimes supported by correlation with experimental photoelastic testing. As with the thermal analysis codes, these programs will produce accurate results provided the inputs are correct. *Figure 2* shows the CYANIDE (Cyclic ANalysis of Inelastic Deformation) calculations for the elastic/plastic expansion of a thick-walled cylinder subject to internal pressure compared both to the theoretical solution by Hodge and White (*Reference 23*) and a nu-

merical calculation of another well known code, ADINA (*Reference 24*).

The greatest challenge to providing good stress/displacement numbers will be in understanding details of the constitutive data used in the inelastic calculations. The following discussion describes a 1985 study of strain variations in smooth specimens taken from conventional forgings. Variation was insignificant in the elastic regime, but was sometimes significant following yielding, even at modest strain levels (0.7%).

Nine specimens were machined from random pieces of forged DA (Direct Aged) Inconel 718 and instrumented with precision strain gages, four to each specimen (as shown in *Figure 3*). The specimens were mounted one by one in a standard MTS load frame and instrumented for feedback control with a one inch bridge exten-

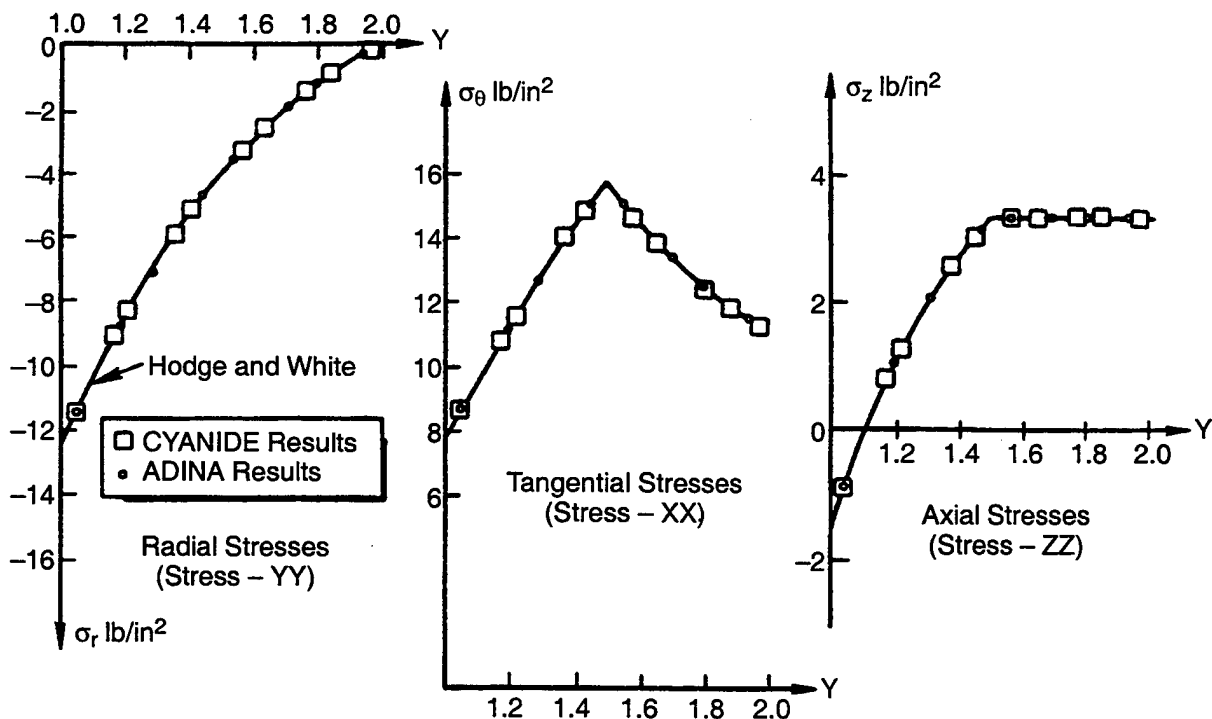


Figure 2. Elastic-Plastic Stress/Displacement Analysis – Comparison of Finite Element Calculated Stresses with Theoretical Solution (Pressurized Thick-Walled Cylinder).

someter mounted towards the upper end of the specimen gage between two of the gages. All but two of the samples were also monitored by a second identical extensometer mounted simi-

larly towards the bottom end. Each was strained from 0.00% to 0.20%, held for 25 minutes, reversed to 0.00%, held for 25 minutes, strained to 0.40%, and so on.

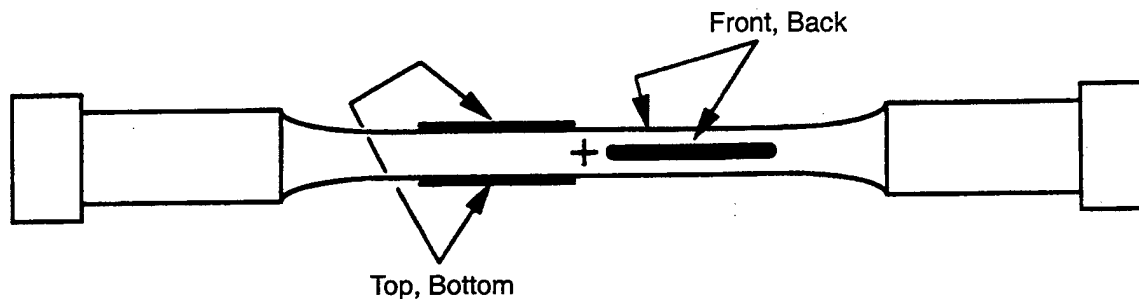


Figure 3. Instrumented Fatigue Specimens.

At each plateau, six readings were taken at five minute intervals from the four strain gages and from the reference extensometer (the controlling extensometer was, of course, fixed). Averages of the groups of six are summarized in **Table 4**. Readings within a group showed some fluctuation but typically held within a 50 microstrain range (0.005% in strain). Only the first two decimal places of the strain percentages will be considered significant.

Referring to **Table 4**, it is seen that the gages and extensometer at the top end of any given specimen always agreed to within about 2% of their average. Variations among the gages and extensometer at the bottom of a specimen were typically somewhat greater, but were still less than about 5% at low strain levels (levels < 0.8%).

Variations within single specimens were circumferential, or longitudinal, or both. Referring again to **Table 4**, it is seen that very large

differences in strain were recorded longitudinally for some specimens. Most interesting were specimens 12 and 13. These were cut radially from a single forging piece, and therefore most closely simulate the specimens of a size effect study which will be discussed in Section 3.4.1.

The extensometer controlling test 12 was located at the rim end of the specimen; it is seen that the strains at the opposite end of the specimen (the bore end) tend to be lower upon yielding. The situation was reversed for test 13. The controlling extensometer was located at the bore end of the specimen, and the strains at the opposite (rim) end were higher upon yielding. Both observations would seem to suggest a decrease in yield strength from bore to rim.

The effect of yield strength variations on calculated stresses and displacements will be analytically investigated. If there is significant

Table 4. Strain Comparison for Specimens.

Specimen 02 (Percent)

EXT 1	GAGE 1	GAGE 2	GAGE 3	GAGE 4	EXT 2
0.000	-0.001	-0.001	-0.002	-0.001	0.000
0.200	0.205	0.200	0.205	0.198	0.200
0.000	-0.006	0.007	0.004	-0.004	0.000
0.400	0.399	0.396	0.399	0.393	0.400
0.000	-0.030	0.015	-0.003	-0.012	0.002
0.600	0.606	0.592	0.588	0.582	0.603
0.000	-0.022	0.011	-0.011	-0.023	0.004
0.700	0.714	0.696	0.671	0.665	0.695
0.000	0.001	0.004	-0.026	-0.035	0.005
0.800	0.817	0.792	0.747	0.743	0.776
0.000	0.016	0.005	-0.039	-0.044	-0.005
0.900	0.917	0.889	0.832	0.827	0.862
0.000	0.025	0.012	-0.043	-0.050	-0.006
1.020	1.031	1.006	0.933	0.930	0.961
0.000	0.033	0.022	-0.043	-0.054	-0.015

Specimen 03 (Percent)

EXT 1	GAGE 1	GAGE 2	GAGE 3	GAGE 4	EXT 2
0.000	0.002	0.002	0.001	0.002	0.000
0.200	0.196	0.202	0.196	0.199	0.198
0.000	0.000	-0.000	0.001	-0.002	-0.003
0.400	0.397	0.405	0.395	0.402	0.395
0.000	0.004	0.004	0.007	0.001	0.000
0.602	0.603	0.602	0.594	0.605	0.594
0.000	0.008	-0.003	0.005	-0.000	-0.005
0.700	0.700	0.694	0.684	0.697	0.685
0.000	0.008	-0.012	-0.003	-0.007	-0.011
0.800	0.804	0.796	0.777	0.794	0.775
0.000	0.016	-0.009	-0.009	-0.006	-0.020
0.908	0.909	0.906	0.868	0.895	0.870
0.000	0.014	-0.013	-0.025	-0.010	-0.033
1.000	0.000	1.000	0.951	0.978	0.945
0.000	0.014	-0.013	-0.033	-0.014	-0.040

Table 4. Strain Comparison for Specimens (Continued).

Specimen 04 (Percent)

EXT 1	GAGE 1	GAGE 2	GAGE 3	GAGE 4	EXT 2
0.000	0.001	0.001	0.001	0.000	0.000
0.200	0.205	0.210	0.207	0.209	0.200
0.000	0.005	0.010	0.008	0.005	0.000
0.400	0.410	0.418	0.413	0.416	0.400
0.000	0.011	0.018	0.017	0.011	0.000
0.600	0.613	0.615	0.609	0.614	0.596
0.000	0.017	0.016	0.015	0.013	-0.008
0.700	0.723	0.725	0.708	0.717	0.690
0.000	0.022	0.013	0.003	0.011	-0.020
0.800	0.825	0.829	0.794	0.807	0.775
0.000	0.021	0.011	-0.015	0.004	-0.035
0.900	0.902	0.922	0.928	0.871	0.852
0.000	0.019	0.007	-0.038	-0.003	-0.057
1.000	1.019	1.025	0.949	0.979	0.932
0.000	0.015	-0.000	-0.062	-0.013	-0.073

Specimen 06 (Percent)

EXT 1	GAGE 1	GAGE 2	GAGE 3	GAGE 4	EXT 2
0.000	0.001	0.002	0.001	0.002	0.000
0.200	0.202	0.208	0.205	0.206	0.200
0.000	0.004	0.004	0.004	0.004	0.004
0.400	0.403	0.413	0.405	0.414	0.400
0.000	0.009	0.012	0.008	0.013	0.003
0.600	0.608	0.620	0.606	0.621	0.610
0.000	0.009	0.016	0.004	0.016	0.000
0.700	0.704	0.718	0.701	0.718	0.705
0.000	0.004	0.013	-0.001	0.013	0.000
0.800	0.799	0.816	0.797	0.815	0.800
0.000	0.006	0.016	0.000	0.017	0.000
0.900	0.897	0.917	0.896	0.916	0.905
0.000	0.003	0.015	-0.002	0.016	0.000
1.000	0.990	1.012	0.991	1.011	1.005
0.002	0.002	0.012	-0.005	0.016	0.000

Table 4. Strain Comparison for Specimens (Continued).

Specimen 07 (Percent)

EXT 1	GAGE 1	GAGE 2	GAGE 3	GAGE 4	EXT 2
0.000	0.001	0.002	0.001	0.002	0.000
0.205	0.205	0.205	0.202	0.203	0.200
0.000	0.004	0.003	0.003	0.001	0.000
0.405	0.405	0.407	0.401	0.403	0.403
0.000	0.001	0.003	0.002	-0.002	0.000
0.600	0.599	0.601	0.613	0.604	0.610
0.000	-0.003	0.002	0.020	-0.002	0.010
0.710	0.705	0.704	0.843	0.800	0.833
0.000	0.007	0.009	0.140	0.079	0.110
0.810	0.805	0.797	1.347	1.280	1.342
0.000	0.009	0.006	0.487	0.401	0.460
0.900	0.894	0.881	1.749	1.666	1.765
0.000	0.008	0.002	0.758	0.653	0.740
0.200	0.181	0.180	0.194	0.198	0.189
0.400	0.333	0.328	0.390	0.396	0.348

Specimen 08 (Percent)

EXT 1	GAGE 1	GAGE 2	GAGE 3	GAGE 4	EXT 2
0.000	0.003	0.003	0.003	0.003	0.000
0.200	0.199	0.201	0.198	0.200	0.200
0.000	-0.002	-0.004	-0.001	-0.006	0.000
0.400	0.400	0.409	0.402	0.402	0.400
0.000	-0.003	-0.002	0.003	-0.007	0.000
0.600	0.596	0.601	0.577	0.579	0.586
0.000	-0.006	-0.008	-0.014	-0.024	-0.020
0.700	0.698	0.700	0.630	0.632	0.640
0.000	-0.001	-0.007	-0.047	-0.059	-0.050
0.800	0.803	0.803	0.662	0.664	0.671
0.000	0.006	-0.001	-0.089	-0.110	-0.095
0.900	0.902	0.903	0.689	0.685	0.700
0.000	0.004	-0.004	-0.135	-0.166	-0.130
1.000	0.999	0.999	0.712	0.702	0.726
0.000	0.003	-0.008	-0.179	-0.216	-0.172

Table 4. Strain Comparison for Specimens (Continued)

Specimen 11 (Percent)

EXT 1	GAGE 1	GAGE 2	GAGE 3	GAGE 4	EXT 2
0.000	0.001	0.001	0.001	0.001	0.000
0.215	0.216	0.220	0.214	0.221	0.214
0.000	0.003	0.002	0.002	0.002	0.000
0.400	0.407	0.412	0.403	0.416	0.400
0.000	0.008	0.006	0.004	0.006	0.000
0.600	0.608	0.611	0.604	0.625	0.610
0.000	0.005	0.005	0.004	0.010	0.000
0.700	0.711	0.714	0.713	0.742	0.720
0.000	0.005	0.004	0.008	0.020	0.008
0.800	0.812	0.814	0.815	0.852	0.830
0.000	0.011	0.010	0.017	0.034	0.015
0.900	0.913	0.915	0.916	0.956	0.930
0.000	0.016	0.014	0.023	0.038	0.015
1.028	1.028	1.032	1.032	1.070	1.040
0.000	0.017	0.015	0.029	0.036	0.015

Specimen 12 (Percent)

EXT 1	GAGE 1	GAGE 2	GAGE 3	GAGE 4	EXT 2
0.000	-0.000	-0.000	0.000	-0.000	0.000
0.200	0.196	0.196	0.199	0.199	0.200
0.000	-0.000	-0.004	-0.001	-0.005	0.000
0.400	0.397	0.394	0.398	0.404	0.400
0.000	0.005	-0.002	0.003	-0.003	0.000
0.600	0.601	0.599	0.595	0.603	0.600
0.000	0.004	-0.001	-0.006	-0.013	-0.009
0.700	0.693	0.696	0.659	0.670	0.663
0.000	-0.005	-0.005	-0.039	-0.042	-0.040
0.800	0.778	0.790	0.707	0.723	0.715
0.000	-0.016	-0.006	-0.083	-0.076	-0.070
0.900	0.872	0.890	0.756	0.780	0.769
0.000	-0.026	-0.009	-0.132	-0.116	-0.113
1.000	0.955	0.974	0.803	0.833	0.822
0.000	-0.030	-0.011	-0.166	-0.145	-0.140

Table 4. Strain Comparison for Specimens (Concluded).

Specimen 13 (Percent)

EXT 1	GAGE 1	GAGE 2	GAGE 3	GAGE 4
0.000	0.001	0.001	0.001	0.001
0.200	0.203	0.202	0.201	0.200
0.000	0.002	0.002	0.006	-0.000
0.400	0.400	0.401	0.397	0.397
0.000	-0.001	0.003	0.006	-0.002
0.600	0.601	0.607	0.607	0.612
0.000	-0.007	0.006	0.010	0.007
0.700	0.690	0.703	0.727	0.746
0.000	-0.009	0.013	0.034	0.047
0.810	0.793	0.815	0.901	0.940
0.000	-0.020	0.009	0.081	0.115
0.900	0.879	0.900	1.011	1.059
0.000	-0.019	0.009	0.108	0.155
1.000	0.979	0.993	1.121	1.178
0.000	-0.014	0.006	0.119	0.172

impact, recommendations for statistical characterization will be made.

The study leads to other implications. The level of variance is generally consistent with that observed in fatigue studies monitored by multiple extensometers. For DA Inconel 718, a 2% error in strain easily yields 20% error in life; a 5% error in strain, 50% error in life. Clearly, when fatigue tests are controlled by single extensometers, their interpretation will be impacted if the bars are not uniformly strained. This observation is supported by an earlier study of variations in diametral strain about hourglass specimens of cast René 80 (*Reference 25*). In this paper, LF Coffin recommends for fatigue testing that extensometers be oriented so as to register the average strain as sampled about a specimen's circumference, and speculates that this will reduce the scatter. We will return to this in Section 3.4.2.

3.3 Burst Prediction

GEAE's burst design practice allows predictions based either on an empirical model sup-

ported by subscale tests or on elastic/plastic stress analysis. (*References 26 and 27*) The elastic-plastic approach is preferred for several reasons:

- The empirical model is questionable unless supported by testing of representative components (like geometry and material).
- The empirical approach is not expected to work well for some nonsymmetric structures, such as spacers and shafts.
- Even when the empirical model is well supported by tests, the temperature distribution of the tests will not usually match that of the disk in operation.
- Growth calculations are also needed. Unless the disk is truly elastic, these will require a non-linear analysis (possibly even including creep). Taking the analysis to burst incurs only small additional expense.

Table 5 shows the comparison of 14 disk tests with both empirical and elastic/plastic based predictions (*Reference 28*). The empirical model actually appears better, but it must be

recognized that the model was generated from the same data being compared to prediction. Also, since these calculations were performed in 1983, improvements in the CYANIDE finite element code could conceivably improve the elastic/plastic predictions.

A final example **Figure 4** shows the cross section of a CF6-50 compressor 3-9 spool along with the deflected shape predicted by CYANIDE. This disk was burst at 16,909 rpm; the CYANIDE prediction was 16,850 rpm (**Reference 29**).

The data on variability in yielding presented in Section 3.2 is potentially relevant. It seems clear that significant variability in the high end of the stress-strain curve (post-yield) should be reflected in burst speeds. This will be inves-

tigated analytically. If the impact is significant, recommendations will be made for statistical characterization.

3.4 LCF Prediction

Deterministic understanding of fatigue is still developing. Shown in **Figure 5** are the results of an empirical model which shows good average agreement with a range of data. (**Reference 30**). Similar models will be incorporated as PDAS modules.

A considerable study has been made of the sources of scatter in fatigue. The importance of this is manifested when competition is explicitly recognized as called for in PRDS. In this section, some pertinent studies will be summarized.

Table 5. Comparison of Experimental Results for Disk Burst Speed with Empirical Method and CYANIDE Predictions.

Disk	Material	Experimental Burst Speed (RPM)	Empirical Model Burst Speed (RPM)	CYANIDE Burst Speed (RPM)
T1	Ti17A/B	89,400	90,960	89,800
T2	Ti17B	92,600	92,670	97,000
T3	Ti17B	84,140	Radial	83,750
T4	Ti17B	86,810	89,930	95,397
T6	Ti6-4	77,880	Radial	78,750
I1	IN718	62,600	65,400	65,050
I2	IN718	62,550	65,400	65,050
I3	IN718	87,500	85,930	88,800
R1	René 95	80,210	78,770	86,000
R3	René 95	77,550	84,030	90,000
R4	René 95	78,650	83,860	90,000
R5	René 95	68,500	Radial	70,100
R6	René 95	71,510	72,460	76,000
R7	René 95	72,680	74,230	79,500
R8	René 95	79,810	78,700	85,750
R9	René 95	86,570	89,610	96,750
R10	René 95	80,800	82,640	90,050

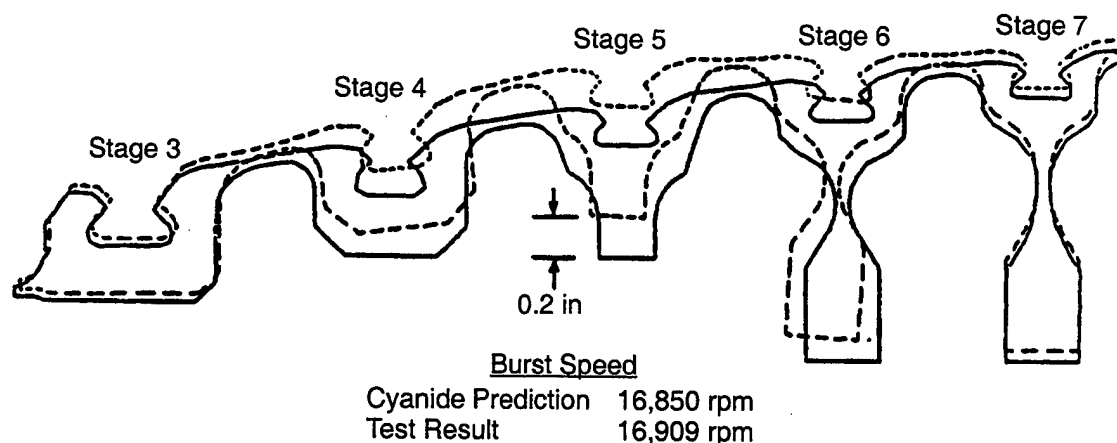


Figure 4. Burst Analysis – CF6-50 Stages 3-9 Compressor Spool Deflected Shape (CYANIDE Elastic-Plastic Calculation).

3.4.1 Stratification of Fatigue Distributions and Size Effect Translations

Three studies were completed by GEAE between 1982 and 1985 which demonstrated unmistakable stratification of fatigue distributions as a function of forging location. Two were IR&D investigations of the statistical size effect in fatigue, and the third supported the USAF F110-100 Engine Structural Integrity Program (ENSIP) as a first attempt at verification of GEAE's probabilistic fracture mechanics methodology. The significance of the stratification will be shown.

The first size effect study compared large and small bars taken radially from a single DA Inconel 718 CFM56 HPT forging according to the drawing of *Figure 6*. Nineteen large and twenty-one small specimens were tested at room temperature under identical loading conditions on the same machine.

The size effect hypothesis views a large specimen as an equivalent number of small specimens, and holds that it fails upon failure of any piece.

Statistically, at any given life, the failure probability of the large specimens should be greater than that of the small specimens. *Figure 7* shows the hypothesis to be qualitatively supported by the data; at any life the large bar failure probability is greater than the small bar failure probability.

The large and small bar failure distributions should be quantitatively related; most simply:

$$\begin{aligned}
 &\text{Prob (large bar failure)} \\
 &= \text{Prob (failure of any of the} \\
 &\quad \text{equivalent number of small bars)} \\
 &= 1 - \text{Prob (all the equivalent small} \\
 &\quad \text{bars survive)} \\
 &= 1 - \text{Prob (small bar survival)}^n \\
 &= 1 - (1 - \text{Prob (small bar failure)})^n \\
 &\text{or abbreviating,} \\
 &F_L = 1 - (1 - F_S)^n
 \end{aligned}$$

where n is the number of small bars equivalent to a single large bar.

This simple translation works only if the two sizes are comparable by a single factor, n . For example, the ratio of the volumes of the large and small specimens is about 50. Scaling the small bar distribution by this factor, however,

- 9 Points at A-Ratio 0.25
- 6 Points at A-Ratio 1.00
- 6 Points at A-Ratio 5.00
- 8 Points at A-Ratio 1.00
- 13 Points at A-Ratio 0.50
- 11 Points at A-Ratio 2.00
- 11 Points at A-Ratio 99.99
- Regression Line
- 3 Sigma Line

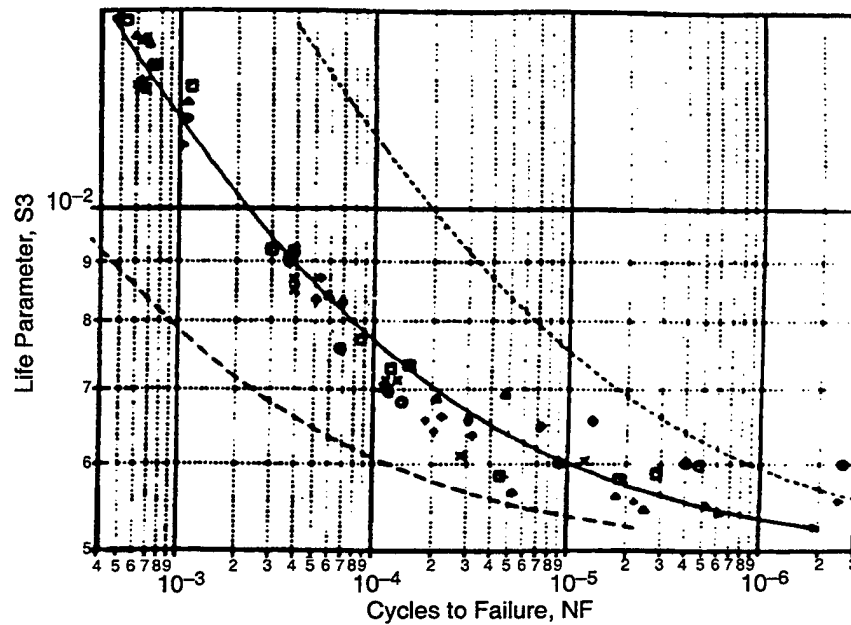


Figure 5. Fatigue Analysis - Model Comparison to Experiment.

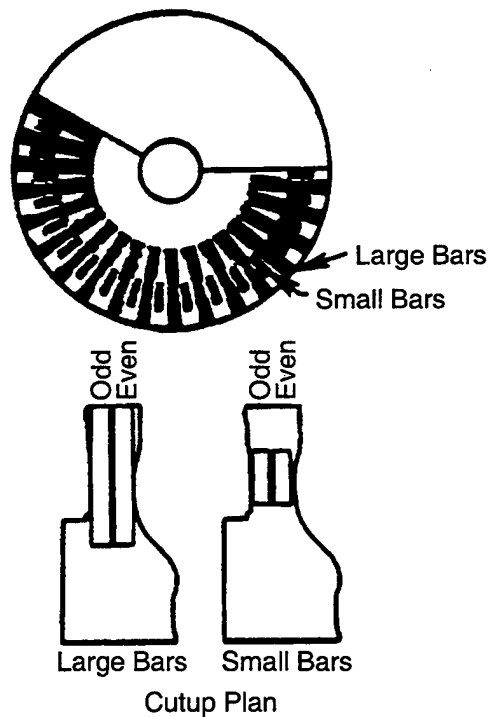


Figure 6. Cutup Plan (First Size-Effect Study).

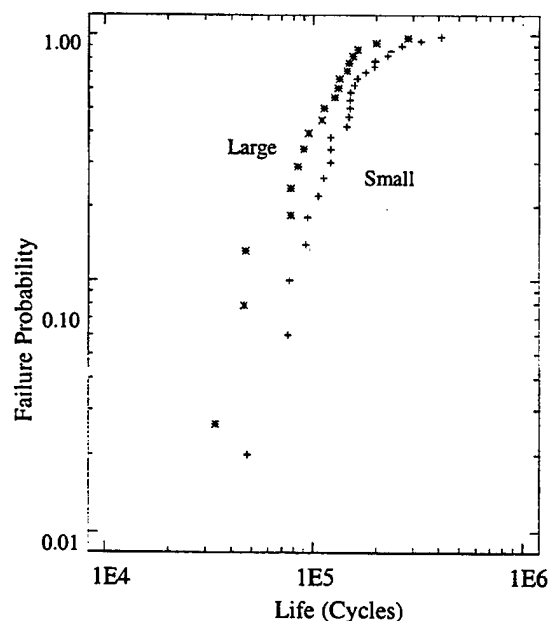


Figure 7. Comparison of Large and Small Bar Failure Distributions (First Size-Effect Study).

does not yield the observed large bar distribution; the scaling is very, very conservative (*Figure 8*).

In truth, the factor of 50 should not work. Almost all the failures were surface initiated; the experiment essentially compared the surface areas of the large and small specimens. Scaling by the appropriate ratio of 20 still yields very conservative results (*Figure 9*).

Again looking more closely at the data, it is not surprising that the factor of 20 does not work. Most of the failures occurred near the radius-gage transition. There is a very slight stress concentration at this point (a few percent); perhaps enough to attract initiation. The large specimen has about 2.5 times more surface material at the transition than the small specimen (the ratio of the diameters). *Figure 10* shows that scaling by this factor brings the small bar distribution in line with the large bar distribution; the agreement is excellent.

Not only does this analysis demonstrate the sensitivity of specimen size and the considerations which must be applied to avoid gross

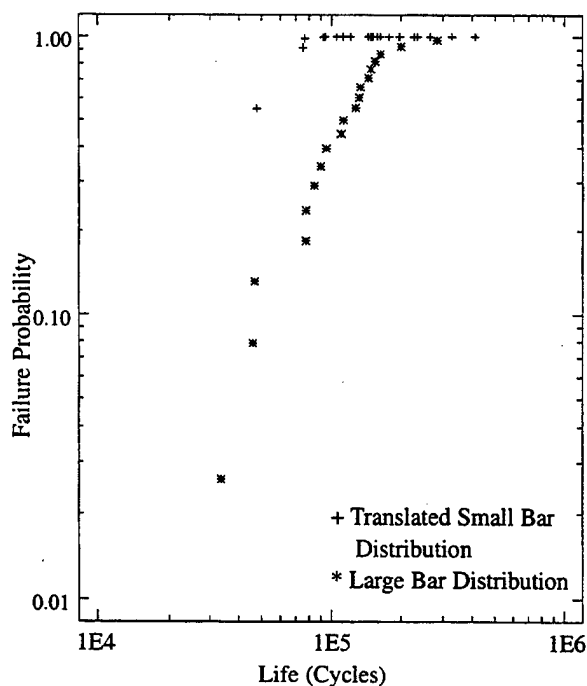


Figure 8. Small Bar Distribution Scaled by 50 – Compares Conservatively with Large Bar Distribution (First Size-Effect Study).

over conservatism in statistical translation between sizes, the analysis is also totally wrong.

In this study, the forging orientations of the specimens were recorded by scribe marks on their rim ends. The single fatigue machine was loaded with the scribe marks alternating between up and down. *Figure 11* shows the failed specimens lined up with their rim ends down. There clearly was a tendency for the bars to fail towards the bore of the forging.

Given that the orientations of the specimens in the test frame were alternated, this bias in failure location cannot be blamed on misalignment. It has been suggested that if the specimen blanks were all fixed identically in the lathe, some consistent machining problem might be responsible. While this cannot be checked, it seems doubtful. A microstructural assessment of one of the failed specimens did suggest a very slight gradient in structure along the gage section from rim to bore. It would have been

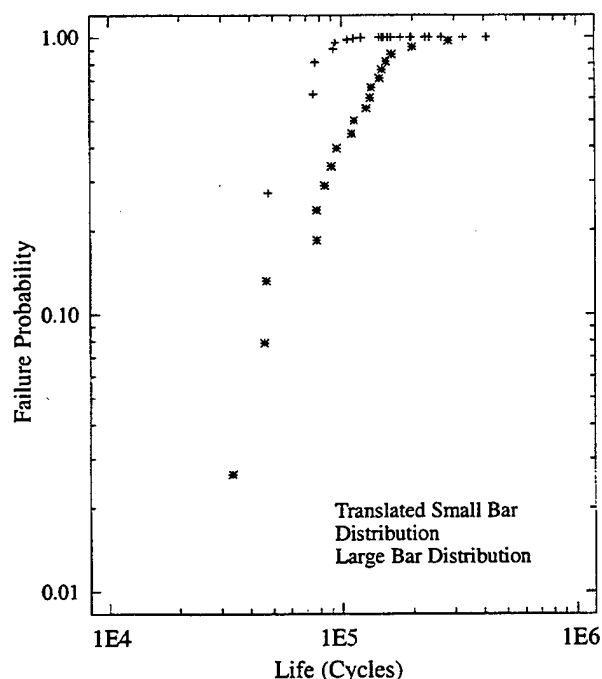


Figure 9. Small Bar Distribution Scaled by 20 - Compares Conservatively with Large Bar Distribution (First Size-Effect Study).

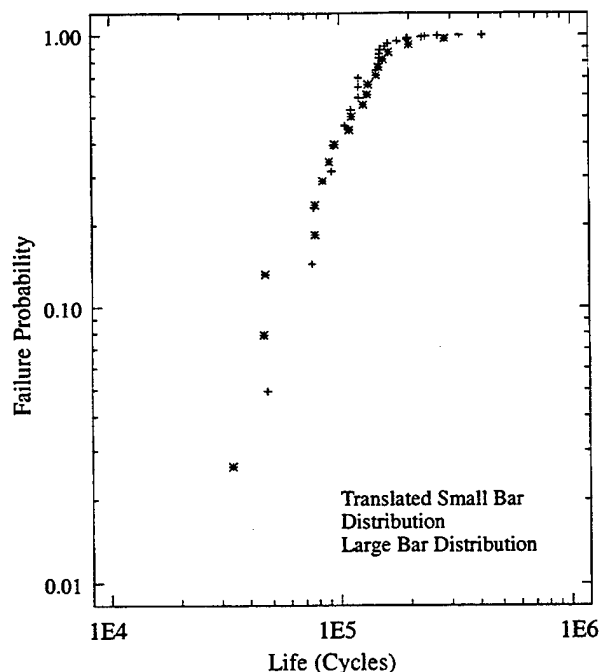


Figure 10. Small Bar Distribution Scaled by 2.5 - Good Agreement with Large Bar Distribution (First Size-Effect Study).

judged insignificant were it not for the observed bias.

The fatigue distribution of the large specimens is essentially that of the material near the bore ends. The small bars sampled material near the centers of the large bar gage sections, away from the bore, away from where the large bars failed. It can be concluded, therefore, that fatigue-capability of the small bar material must be statistically better than that of the large bar material. This, we feel, is the correct explanation for the bias in failure location and for the separation of the two distributions in *Figure 7*.

Figure 12 shows the failure distributions of the large and small bars separated by layer. The consistency of the shifts supports the existence of subtle gradients in fatigue capability. While such gradients have not been reported in the literature, their observation in this study is not a fluke.

The ENSIP study found similar gradients under more realistic test conditions. Twenty-four specimens were taken from an F110-100 HPT forging (-150 mesh E+I René 95) according to the cutup drawing of *Figure 13*. Again there are two layers of specimens, forward and aft. All specimens were cycled to failure through a simple mission composed of two major cycles followed by twelve minor cycles; the tests were run at 750° F.

Shown in the same figure are the separated experimental failure distributions of the forward and aft specimens (twelve of each). Note again the distinct separation between layers.

The second size effect study also supports the existence of fatigue gradients. Specimens were cut from a single CFM56 stage 9 compressor disk hot die DA Inconel 718 forging as shown in *Figure 14*. All bars were tested at room temperature under identical loading conditions. *Figure 15* shows the large bars lined up with their aft ends down. There is evident again a tendency to fail at one end (the forward end),

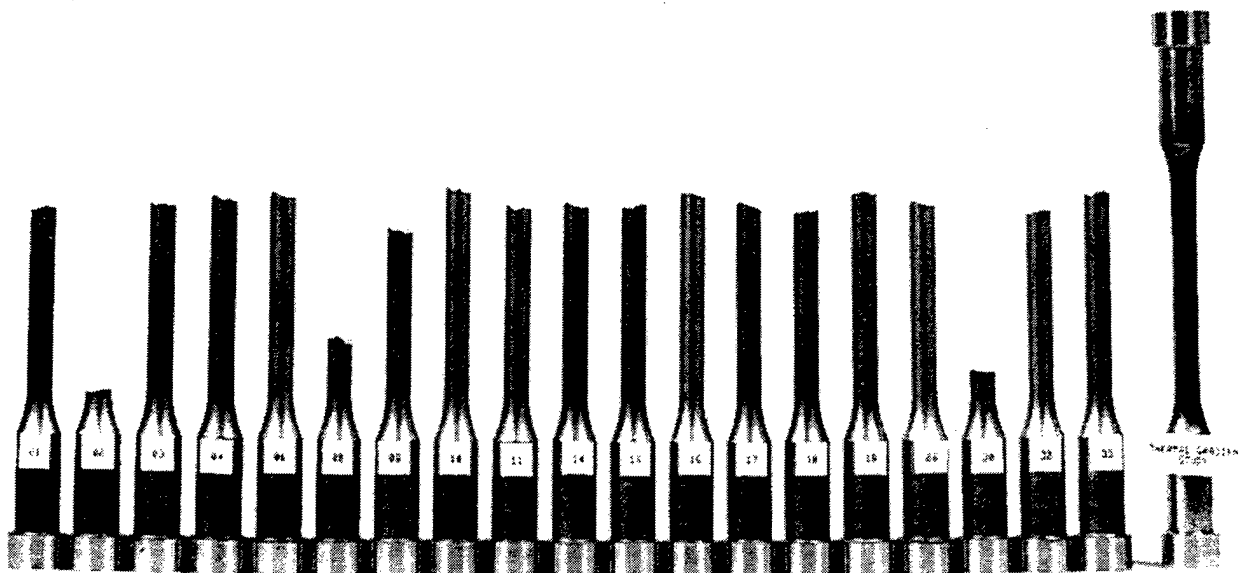


Figure 11. Failed Large Bars – Rim Ends Down (First Size Effect Study).

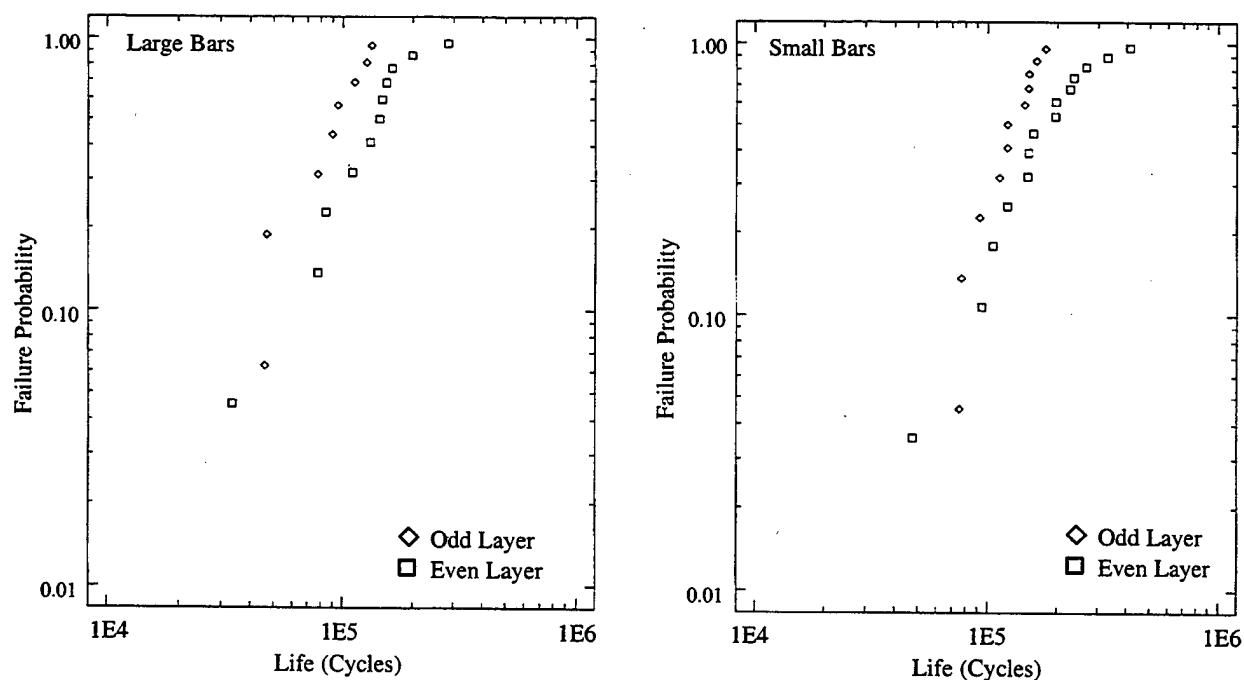


Figure 12. Large & Small Bar Failure Distributions Separated by Layer (First Size Effect Study.)

and this is consistent with the forward and aft failure distributions included in *Figure 14* which show the forward small bars statistically shifted to lower life.

The large specimens include material which would otherwise have been split into two small specimens. The failure distribution of the large specimens should reflect the minimum perfor-

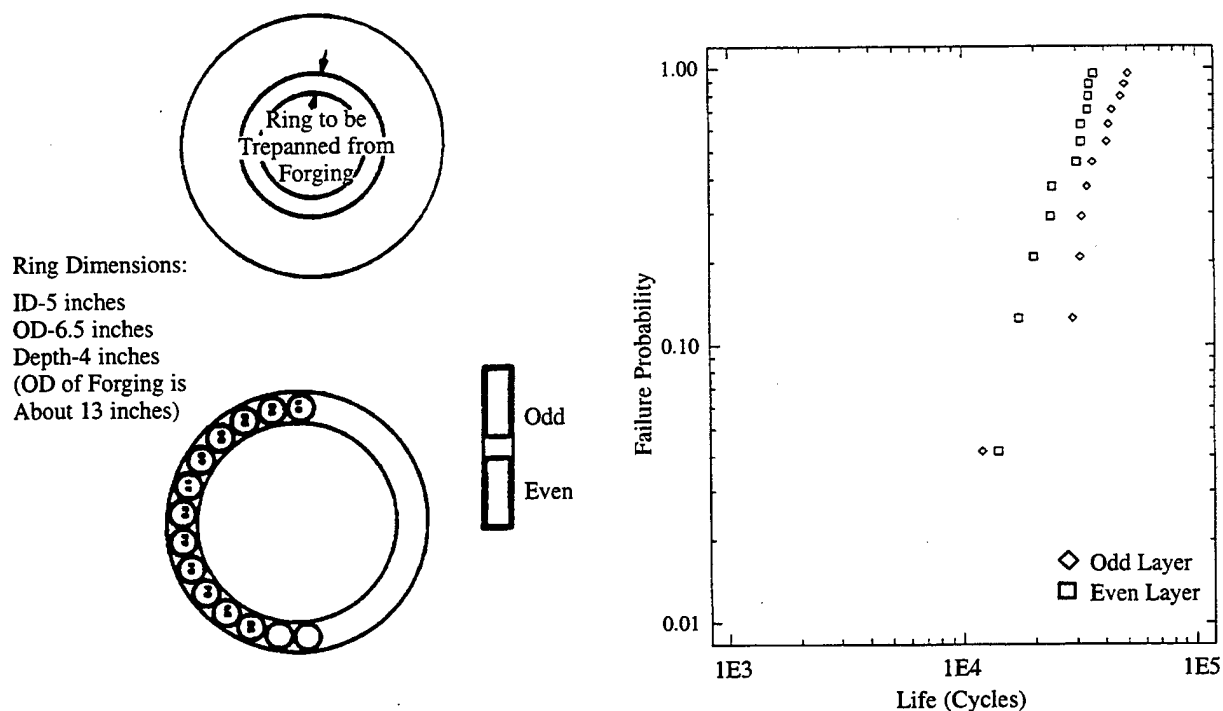


Figure 13. Cutup Plan and Comparison of Fore and Aft Layer Failure Distributions (ENSIP Study).

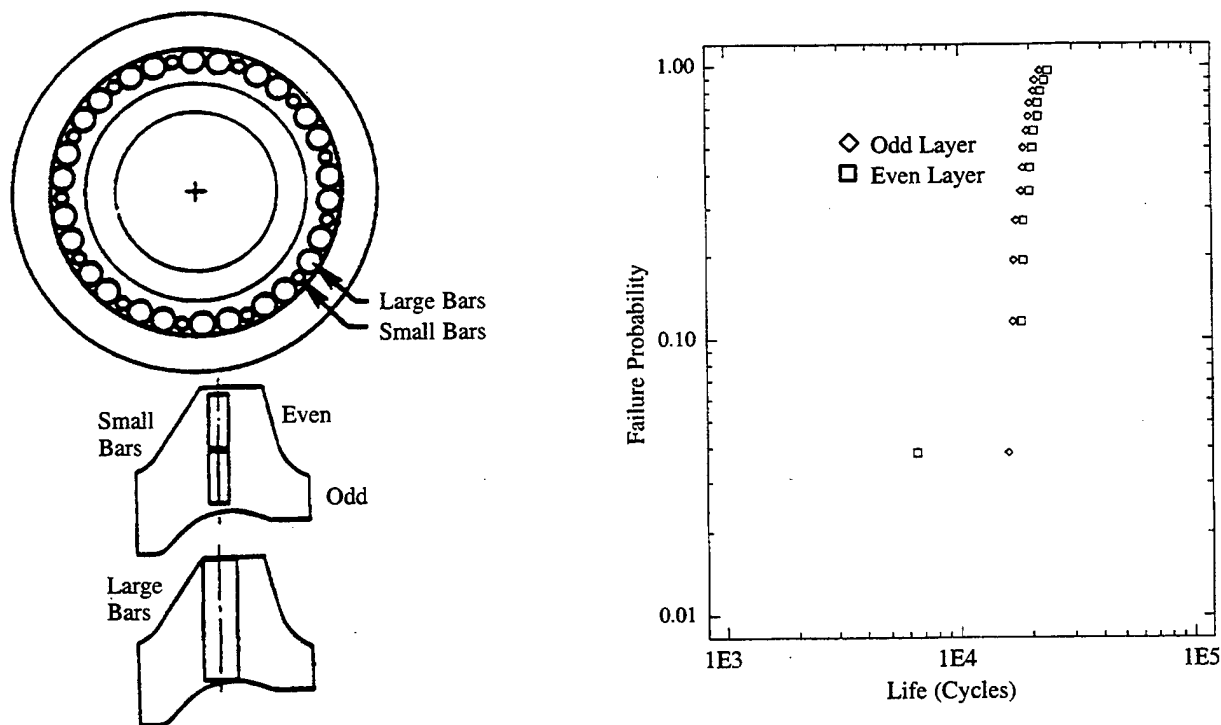


Figure 14. Cutup Plan and Comparison of Fore and Aft Layer Failure Distributions (Second Size Effect Study).

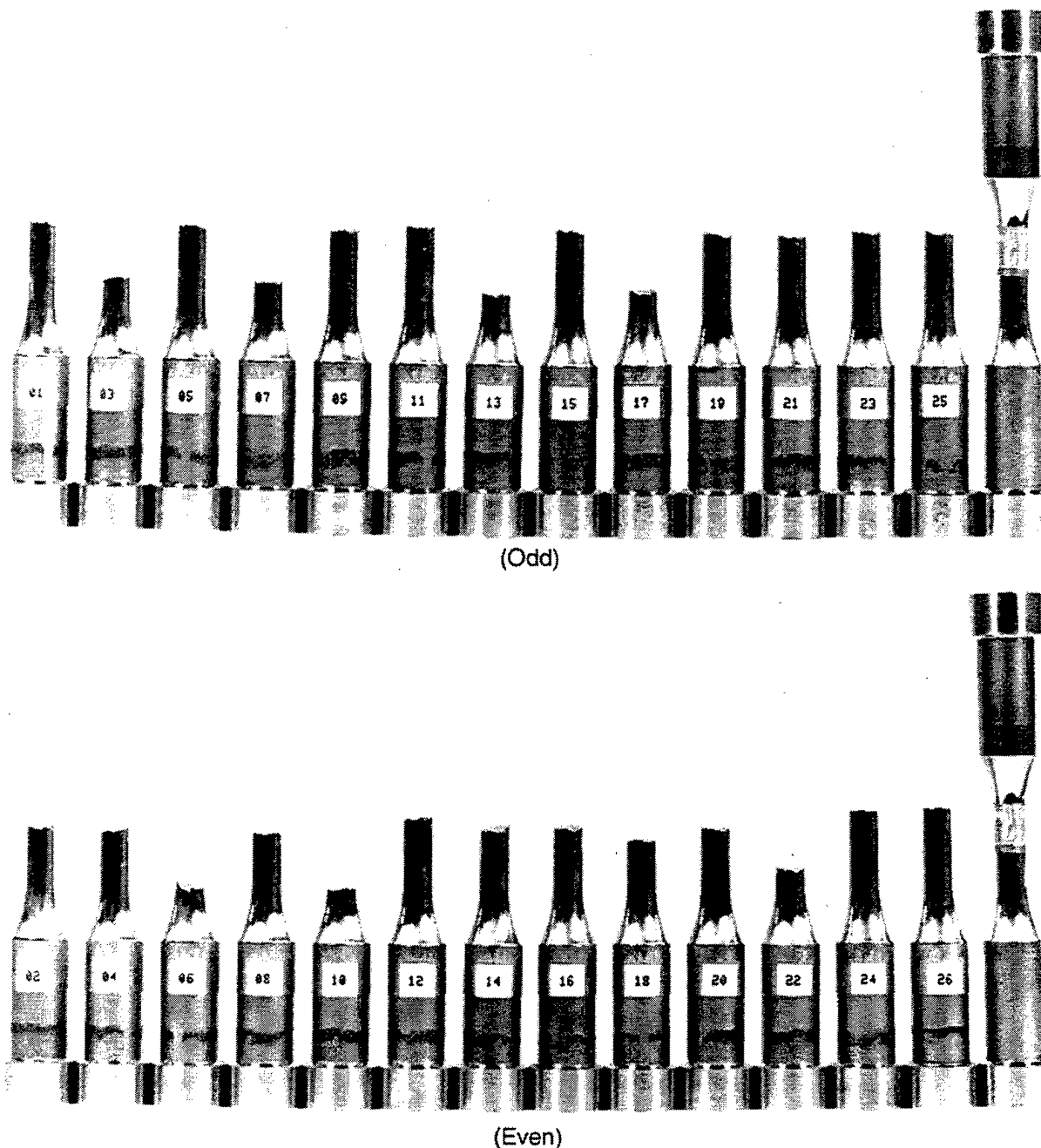


Figure 15. Failed Large Bars – Aft Ends Down (Second Size Effect Study).

ties of the volumes being tested. This is confirmed by *Figure 16* which superimposes the failure distributions of the large bars and the separated forward and aft small bars — the large bar distribution and the forward small bar distribution are nearly identical.

The point of these studies is that materials which are assumed to be homogeneous (in particular, powder alloy products) probably are not. This is perhaps not a major revelation; but it does suggest that the apparent scatter reported for a material may overestimate the true

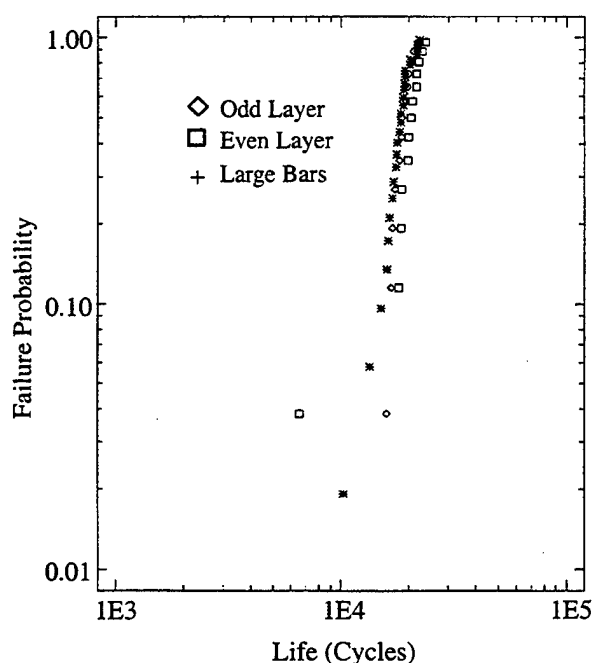


Figure 16. Large Bar Failure Distribution Compared to Fore and Aft Layer Small Bar Failure Distributions (Second Size Effect Study).

scatter at any given component location; minimum life estimates may be conservative. We have shown that the conservatism can become extreme when failure distributions are translated to larger volumes.

3.4.2 The Interpretation of Strain-Controlled Fatigue Data

The discussion at the end of Section 3.2 suggests that a large component of observed fatigue scatter is artifactual. Clearly, there would be a payoff if this component could be eliminated. One step in this direction begins by re-considering the definition of a strain controlled test. This section considers the potential application of multiple extensometers.

The three programs summarized in Section 3.4.1 all utilized dual longitudinal LVDT extensometers (labeled A and B) placed near the center of the cylindrically gaged specimens and oriented, respectively, at 0 and 90° relative

to the front of the test stand. The tests were started in strain control until stabilized loads were achieved, control being based on the A-extensometer, then switched to load control. All three programs showed significant discrepancies between the strains reported by the two extensometers.

The two size effect investigations each employed two specimen geometries, one large and one small. The gage lengths used in the first program were 3.8 inches for the large specimens and 0.6 inches for the small. Smaller gage lengths were chosen for the second program in an attempt (unsuccessful) to eliminate the effect of the graduated fatigue properties. The chosen lengths were 1.1 inches for the large specimens and 0.5 inches for the small.

Two-inch extensometers were applied to the 3.8-inch specimens, 1 inch extensometers to the 1.1-inch specimens, 0.5-inch extensometers to the 0.6-inch specimens, and 0.4-inch extensometers to the 0.5-inch specimens. The A-extensometers were, in every case, centered on the specimens; the B-extensometers were slightly offset to accommodate support cables.

It is suspected that the 0.5 inch extensometers might have been too large for the 0.6 inch gage sections, given that the B-extensometers were offset. It may be that the specimen radii interfered with the strain measurements.

There is some evidence to support this conjecture: Eighteen of the 0.6 inch specimens tested had higher maximum A-strains than B-strains; only 10 went the other way. The same pattern was observed for the 0.5 inch specimens instrumented with 0.4 inch extensometers; 15 had higher maximum A-strains than maximum B-strains and 4 higher B than A. The corresponding numbers for the 1.1 inch specimens instrumented with 1 inch extensometers were 11 and 9.

The 2-inch extensometers applied to the 3.8 inch gaged specimens were not so closely located to the specimen radii. Of the specimens

tested, 17 had higher A-strains than B-strains and 17 went the other way. These specimens showed interesting correlations between the measured strains and the observed fatigue lives.

Nineteen large bars were tested at room temperature with a 0.69% strain range. Spearman correlation coefficients (*Reference 31*) were calculated comparing fatigue life with the maximum A-strain, with the maximum B-strain and with the larger of these two maxima. A value of 0 for the correlation coefficient would imply total non-correlation of the variables; a correlation coefficient of -1 would imply perfect negative correlation (i.e. the higher the strain, the lower the life). The Spearman coefficient for life vs. maximum A-strain was about -0.263; for life vs. maximum B-strain, it was about -0.526; and for life vs. maximum AB-strain, the correlation coefficient was about -0.712.

Given that these tests were all run at the same strains, as determined by the A-extensometer, one could reasonably expect complete non-correlation between life and the maximum strain reported by this extensometer. As it turned out, however, the maximum A-strain was not always 0.69% upon switching to load control. This reflects, to some extent at least, the difficulty in defining a truly stabilized load given the limitations in current testing technology. It may be, therefore, that the -0.263 negative correlation (which is not large) is still meaningful.

The maximum B-strains showed large deviations from 0.69%, both positive and negative, and the high correlation of -0.526 suggests that the fibers of the specimens actually experienced these strains. If the hypothesis is adopted that the two extensometers measure the strains of two fibers of any given specimen, and that the maximum AB-strains are therefore better estimates of the true maximum strains, then the

very high correlation of -0.712 is not surprising.

A smaller number (10) of the 3.8 inch gage length specimens were tested at 750°F; the strain range was again 0.69%. The results were similar: there was a -0.134 correlation between life and maximum A-strain, a -0.297 correlation between life and maximum B-strain and a -0.505 correlation with maximum AB-strain.

Based on these observations (and supported by the Coffin paper (*Reference 25*)), it was suggested that fatigue scatter could be reduced by controlling tests with averaged multiple extensometers. An array of four was developed along with the associated electronics to implement this control (*Figure 17*), but funding was cut before the approach could be demonstrated. Still, even if tests are controlled by a single extensometer, bad tests can sometimes be identified by multiple instrumentation as we now show.

The composite *Figure 18* presents a plot of the failure distributions of the second size effect study and a tabulation of the A- and B-strains of each sample averaged over the duration of stabilized load control. At least one point of the small bar subset appears to be an outlier (6,535 cycles). The B-strain of this test is seen to be 0.91% compared to the 0.81% A-strain. This does not seem coincidental.

Also, the three lowest results in the large bar subset (10,262, 13,451 and 15,086 cycles) are seen to have the highest stabilized stresses (206, 192, and 193 ksi, respectively). Again, this seems to imply more than coincidence. Consider the 13,451 test. The strain variations apparent in *Table 6* confirm that there was a problem.

The 15,086 test was discrepant in that the change from strain to load control was not made, and the lowest of the large bar tests (10,262 cycles) experienced instability in the

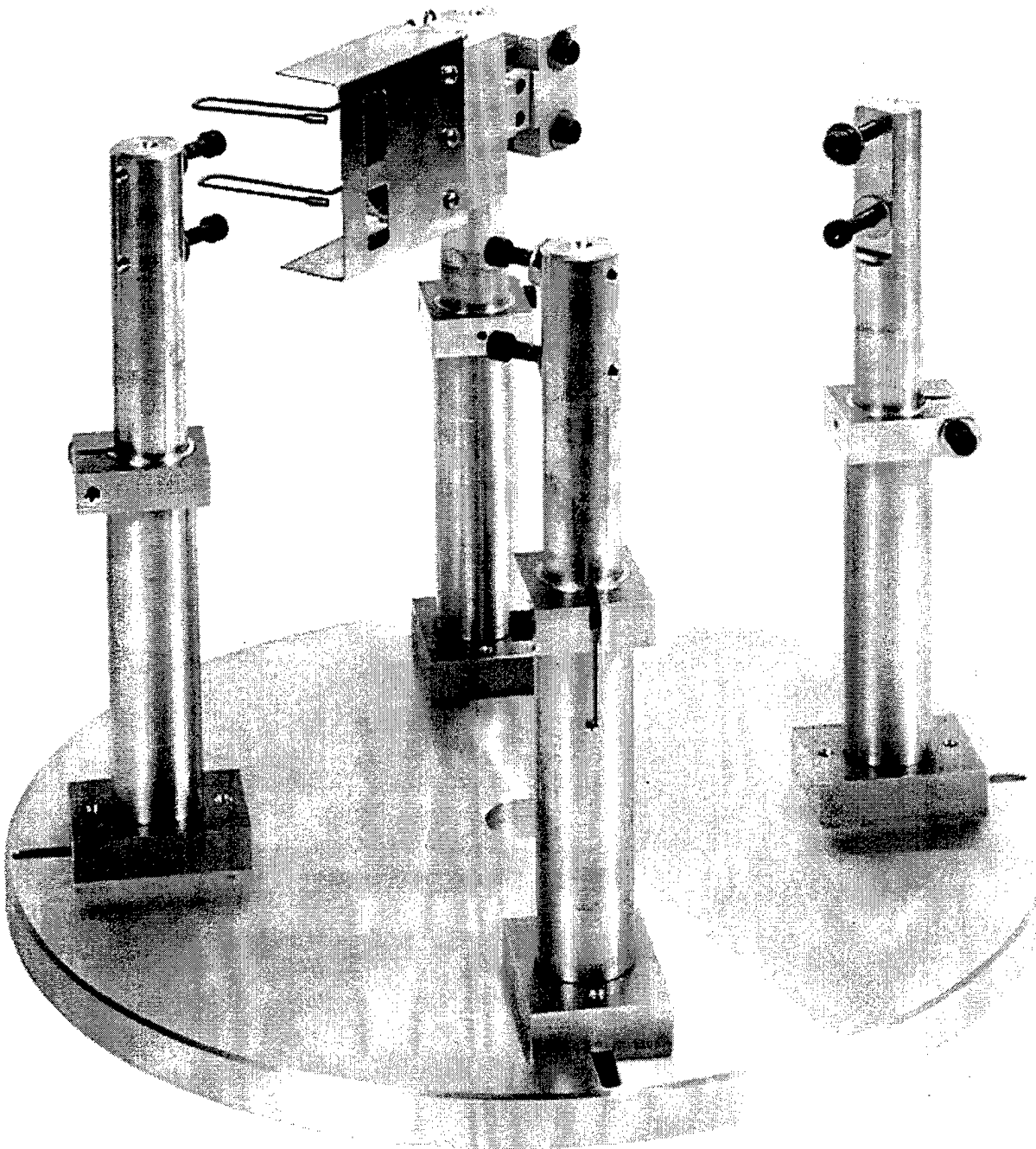


Figure 17. Extensometer Array.

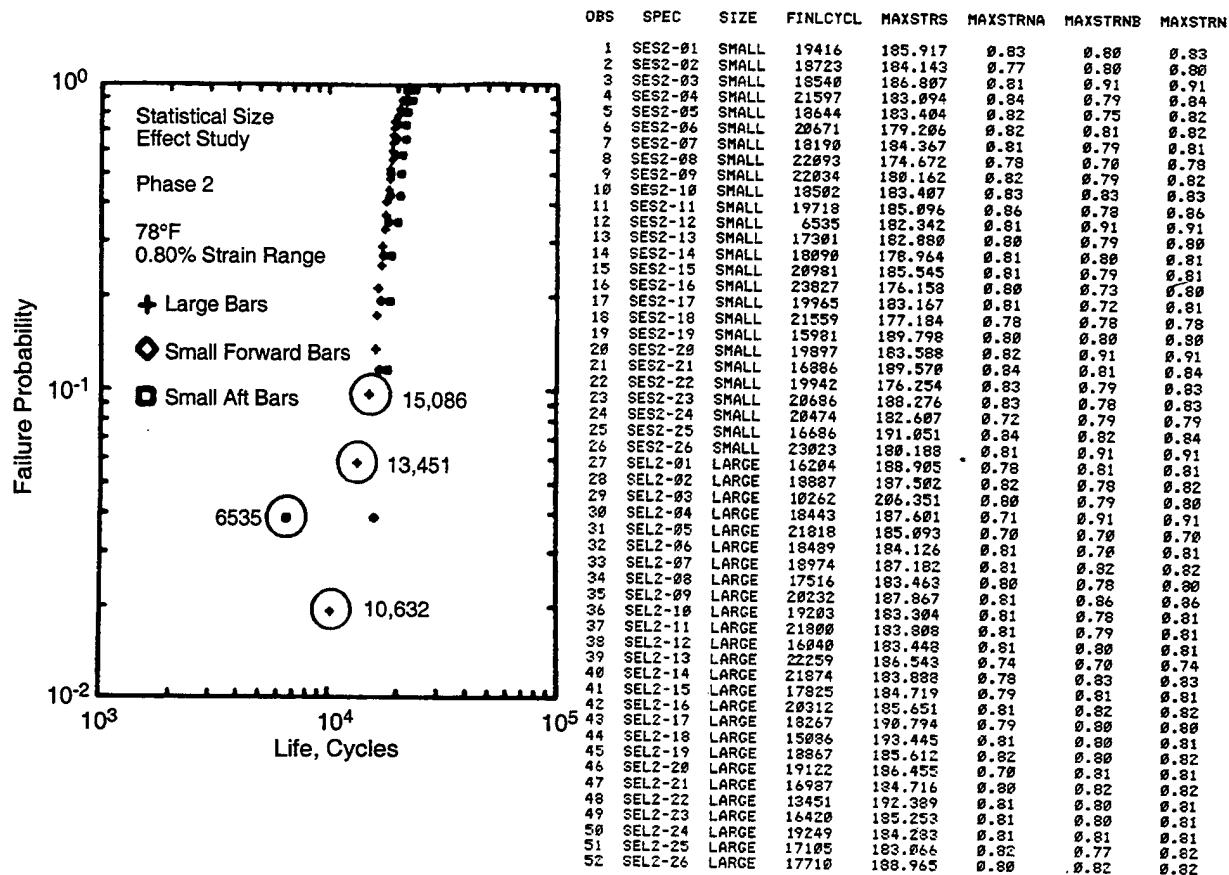


Figure 18. Second Size Effect Failure Distributions with Tabulation of Stabilized A- and B-Strains – Questionable Points Circled.

start-up which disabled the data acquisition system; averaged strains were not available.

Table 6. AB Strain Comparisons for SEL2-22 (13,451 Cycle Life).

Cycle	A-strain	B-strain
1,001	0.280%	0.340%
1,002	0.330	0.443
1,003	0.388	0.562
1,004	0.389	0.561
1,005	0.463	0.714
1,006	0.478	0.745
1,007	0.563	0.913
1,008	0.620	1.024
1,009	0.655	1.098
1,010	0.691	1.167

If these four points are deleted, the remaining lives range from about 16,000 cycles to about 24,000 cycles. It seems quite possible that much of this spread is due to deviations in strain from the nominal 0.8% value at which the tests were to be run. The work on yielding discussed in Section 3.2 demonstrates that sufficient strain variation is possible.

Should stress analyses be run incorporating variability and applied to average fatigue data, or should the observed variability in fatigue data be applied to average value stress analyses? We don't really know at this time, but it is clear that the tests which generate the supporting data are more complex than we are wont to recognize. Improvements may be called for.

3.4.3 The Effect of Specimen Preparation on Fatigue Life

Given that understanding of significant sources of fatigue scatter can potentially improve the accuracy of risk analyses, we conclude by mentioning that GEAE has studied the effect of machining practices on life.

Early round-robin studies showed large differences between fatigue specimens manufactured by different vendors, all to our internal specification for low stress ground and polished specimens (*Figure 19*).

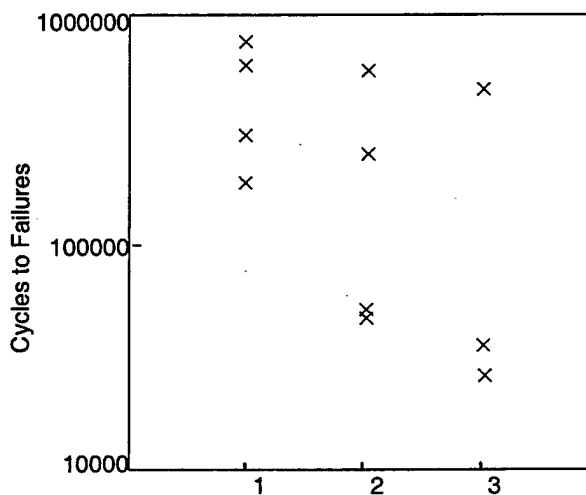


Figure 19. Life is Correlated to Maximum Compressive Residual Stresses - Data Compares Three GEAE Machining Vendors.

While this problem has since been corrected, of greater significance is on-going investigation of the effect of production machining practices on life. Lessons learned will be incorporated into his Phase III validation effort.

3.5 Sharp Crack Fracture Mechanics Prediction

The average prediction capability of GEAE's fracture mechanics methodology is supported by the correlation in *Figure 20* (*Reference 32*). The data, which encompasses two materials

and numerous specimen geometries, shows good agreement over a range of initial crack sizes. The central diagonal line represents perfect agreement between calculated and observed. The parallel dotted and solid lines represent, respectively, factors of 1.5 and 2 from perfect agreement. Most calculations are within a factor of 2 of the observations.

It should be recognized that fracture mechanics is one of the most complex phenomena analyzed in engineering. The following are the major assumptions:

- Crack growth rate is a simple function of stress intensity, a complex parameter incorporating stress distribution, crack size, shape, and local geometry.
- Crack growth rate curves can be represented by a standard multiparameter functional form.
- A small number of generic stress intensity solutions (e.g. surface semi-elliptical, corner quarter-elliptical) suffices to describe most crack problems.
- Approximations required for stress intensity calculations are adequate.
- Non-linear effects such as crack tip plasticity and loss of constraint can be accounted for by simple corrections.
- Crack growth rate data is referenced to zero-max loading. A simple stress intensity correction can be made to apply this data to more general min-max loading.
- Perturbations to the global stress field caused by a crack can be ignored.

For any initial crack these assumptions combine into a difference equation which is integrated to a critical crack size defining failure. While the deviations in *Figure 20* probably involve some systematic model error, there is scatter even for simple geometries of the most homogeneous materials. *Figure 21*, for example, summarizes the results of crack

growth testing of Kb-bars machined from As-HIP PM René 95 (See *Appendix A.4 of Reference 33*).

In a 1982 study, MF Henry concluded that significant differences in crack growth rates are possible within a single Inconel 718 forging depending on specimen location and orientation (*Reference 34*). This is consonant with the results of the low cycle fatigue studies described in the preceding Section 3.4.1.

Henry's investigation was extended under F110 development funding. Crack growth rate scatter was assessed for As-HIP PM René 95 (assumed homogeneous) as well as for forged DA Inconel 718 (assumed less homogeneous). Scatter in the wrought material was to be studied within a single forging and between different forgings. Only the same part testing was completed (actually 9 of the 10 same part speci-

mens) when the program was discontinued. Multiple tests were run on all specimens.

Five Single Edge Notch (SEN) specimens were machined from a single HIPped can of -150 mesh PM René 95 and were tested to assess baseline variability (the HIPped material is assumed more uniform than a forged product). An Electrical Potential Drop (EPD) system with microcomputer data logging was used to monitor crack growth and control the servo-hydraulic test machine. All tests were run at 750°F, at a stress ratio of 0.5 (to prevent closure effects) and at a frequency of 10 Hz. The cracks were initiated at electro-chemically machined notches and allowed to grow out of the notch field. Four thresholds were generated for each specimen by load shedding from a point corresponding to $20 \text{ ksi}\sqrt{\text{in}}$.

The twenty thresholds obtained for these five specimens are summarized in *Table 7*; plots of

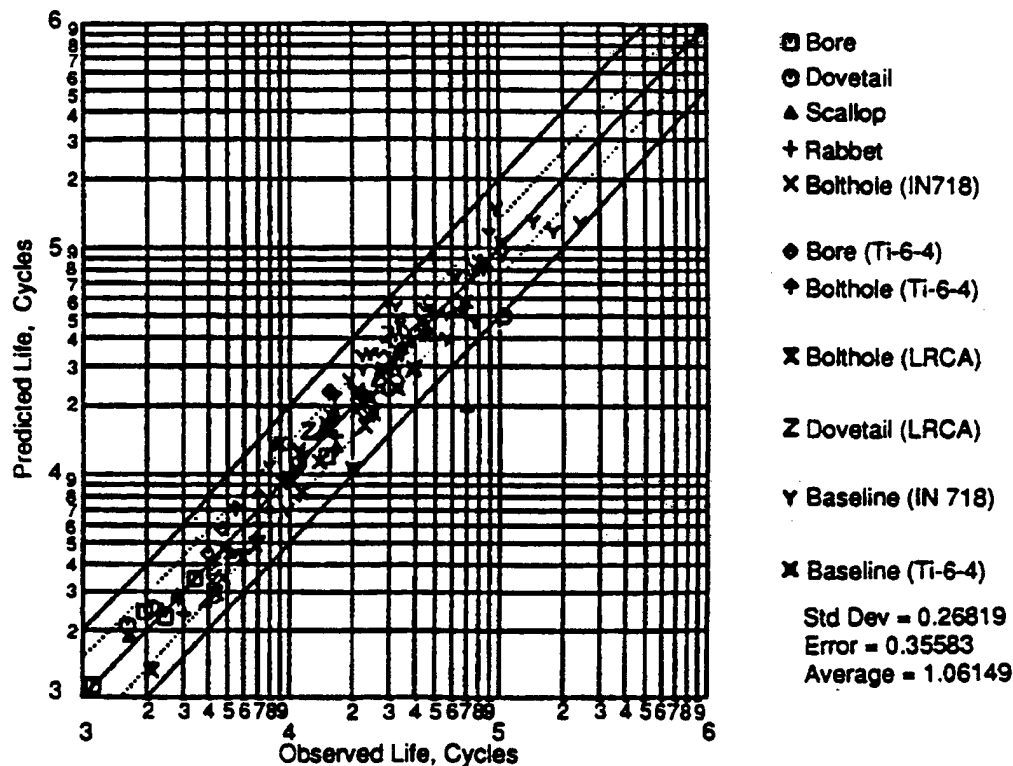


Figure 20. Fracture Mechanics Analysis – Model Comparison to Experiment (Two Materials, Multiple Specimen Geometries).

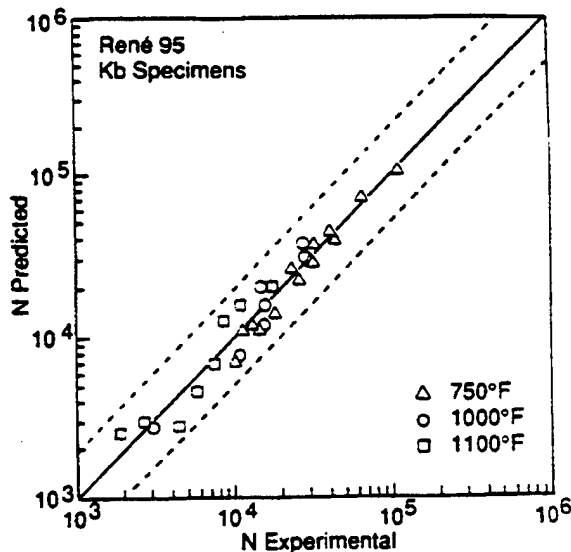


Figure 21. Fracture Mechanics Analysis - Model Comparison to Experiment (As-HIP PM René 95 Kb Bars).

Table 7. Threshold Stress Intensity Range, ksi in^{1/2}

Specimen	Shed			
	1	2	3	4
K1062	7.20	6.90	6.85	7.00
K1063	7.10	6.90	6.55	6.70
K1064	7.00	6.75	6.45	6.55
K1065	6.90	6.85	6.85	6.90
K1074	6.90	7.90	7.05	7.40

growth rate versus stress intensity are presented in *Figures 22-26*.

The maximum observed spread of thresholds within a single specimen is 1 ksi√in (Specimen K1066). The over-all spread is 1.45 ksi√in, but much of this appears to be artifactual. *Figures 27-30* show the crack growth rate curves superimposed for the first sheds of all the specimens, the second sheds, the third and the fourth. Clearly the specimen to specimen scatter in-

creases. The spread in the 5 first shed thresholds is only 0.3 ksi√in. This increases reasonably monotonically to 0.85 ksi√in in the five fourth sheds (though it is the second shed of specimen K1064 which is the real outlier).

This observation is not understood. The threshold stress intensity factor depends only on the load at which crack growth ceases and the corresponding crack size, both of which are accurately determinable. There is no suggestion that bending was present in the tests. The cracks remained planar, and their progression remained essentially uniform across the specimen.

Finally, referring to *Figures 22-26*, it should be noted that there is some internal correlation. Specimens with low thresholds tend to have high growth rates in the Paris regime.

To better assess the variability in crack growth rates within a single forging which was first reported in *Reference 34*, ten specimens were machined from a single HPT disk of DA Inconel 718, all at the same radial position, five from the top of the forging (A-series), five from the bottom (B-series). Nine of these were tested before the program was stopped.

The crack growth rate scatter in these wrought alloy specimens appears to be considerably greater than in the As-HIP PM specimens. Some of this increase might be accounted for by the fact that the crack fronts showed much greater deviations from uniformity (*Figure 31*). The Inconel data did, however, exhibit the same trends identified in the René 95 data. *Figures 32-35* do show the same increase in scatter from the first to the fourth sheds, and the same internal correlations between threshold and Paris regimes.

Summarizing, GEAE's sharp crack fracture mechanics methodology well predicts residual life on average, but there are deviations. It is likely that both model approximations and variability in material properties contribute to the

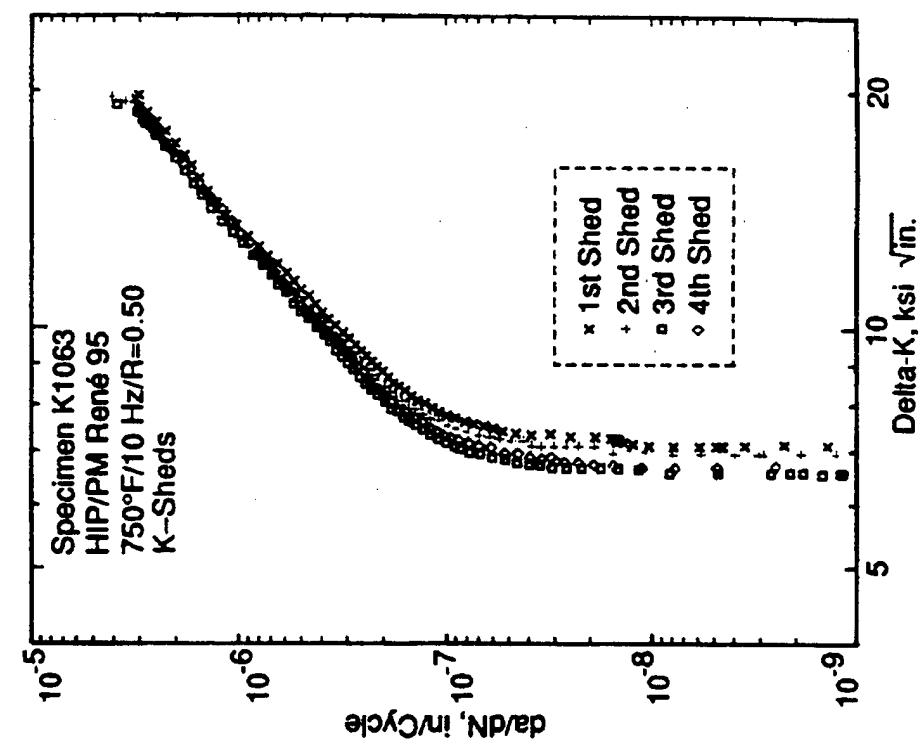


Figure 22. Crack Growth Rate Data for Specimen K1062
(As-HIP PM René 95, Four Load Sheds).

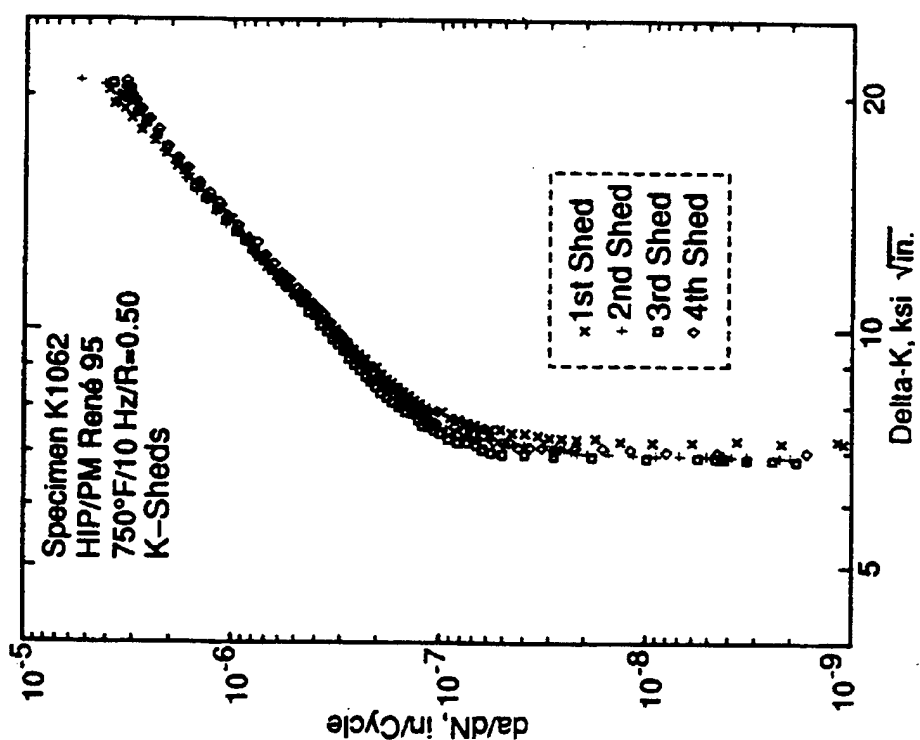


Figure 23. Crack Growth Rate Data for Specimen K1063
(As-HIP PM René 95, Four Load Sheds).

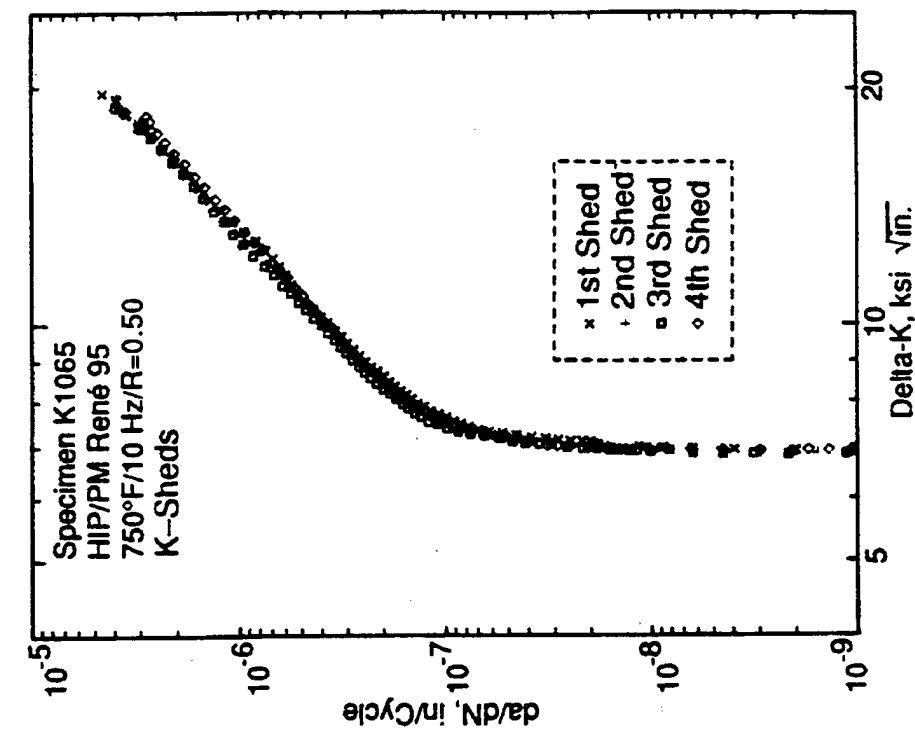


Figure 24. Crack Growth Rate Data for Specimen K1064
(As-HIP PM René 95, Four Load Sheds).

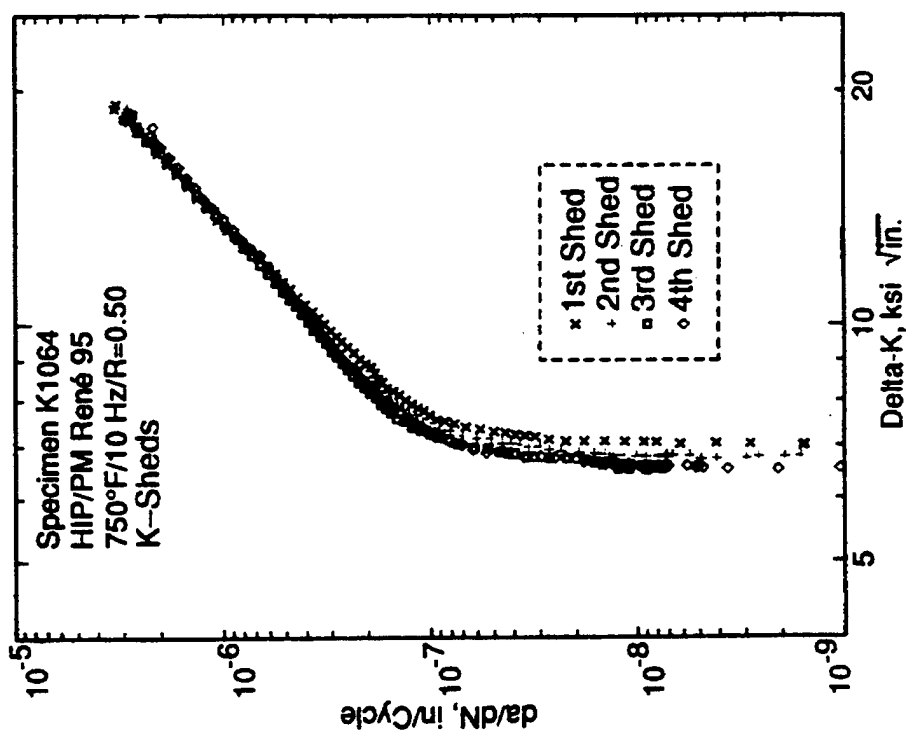


Figure 25. Crack Growth Rate Data for Specimen K1065
(As-HIP PM René 95, Four Load Sheds).

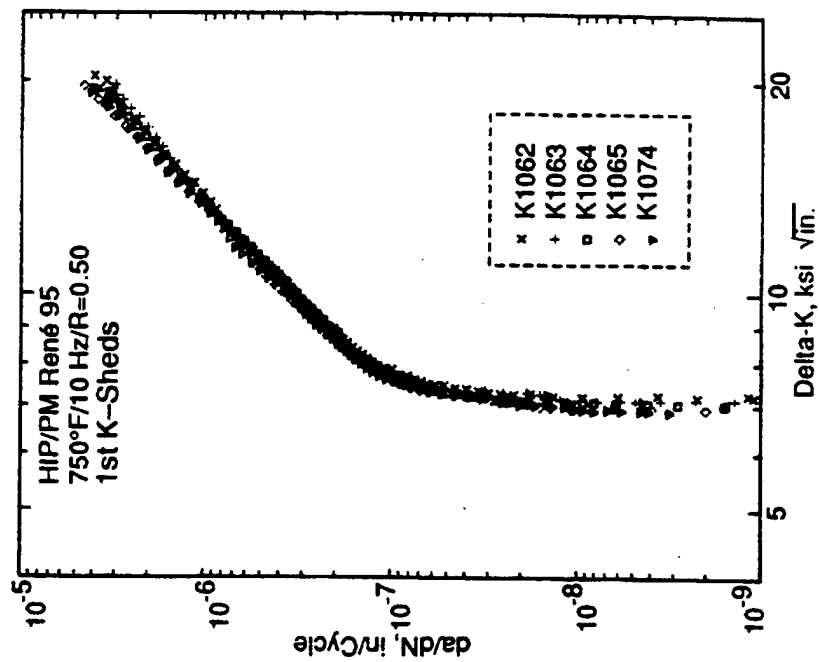


Figure 26. Crack Growth Rate Data for Specimen K1066
(As-HIP PM Rene 95, Four Load Sheds).

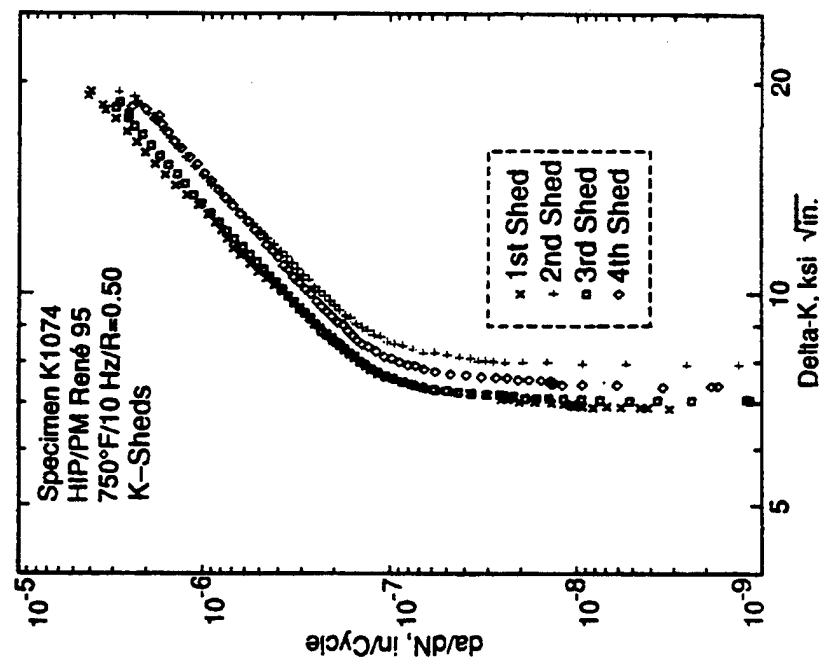


Figure 27. Crack Growth Rate Data for Specimen K1067
(As-HIP PM Rene 95, Four Load Sheds).

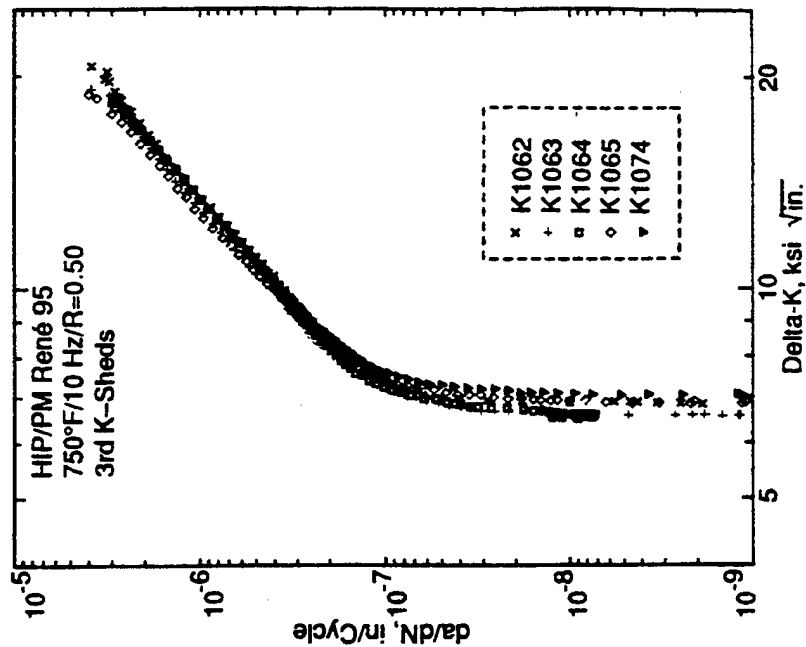


Figure 28. Second Load Sheds Compared
(As-HIP PM René 95 Specimens).

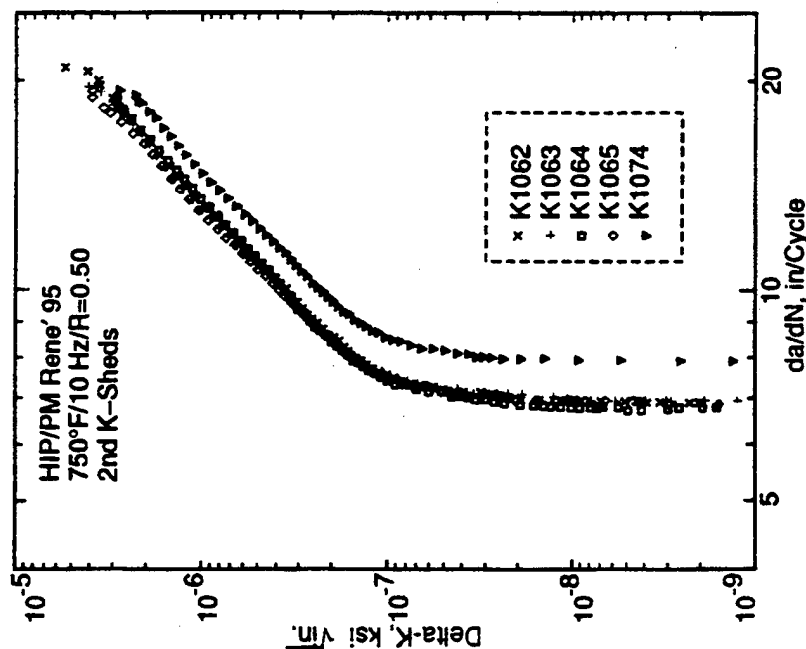


Figure 29. Third Load Sheds Compared
(As-HIP PM René 95 Specimens).

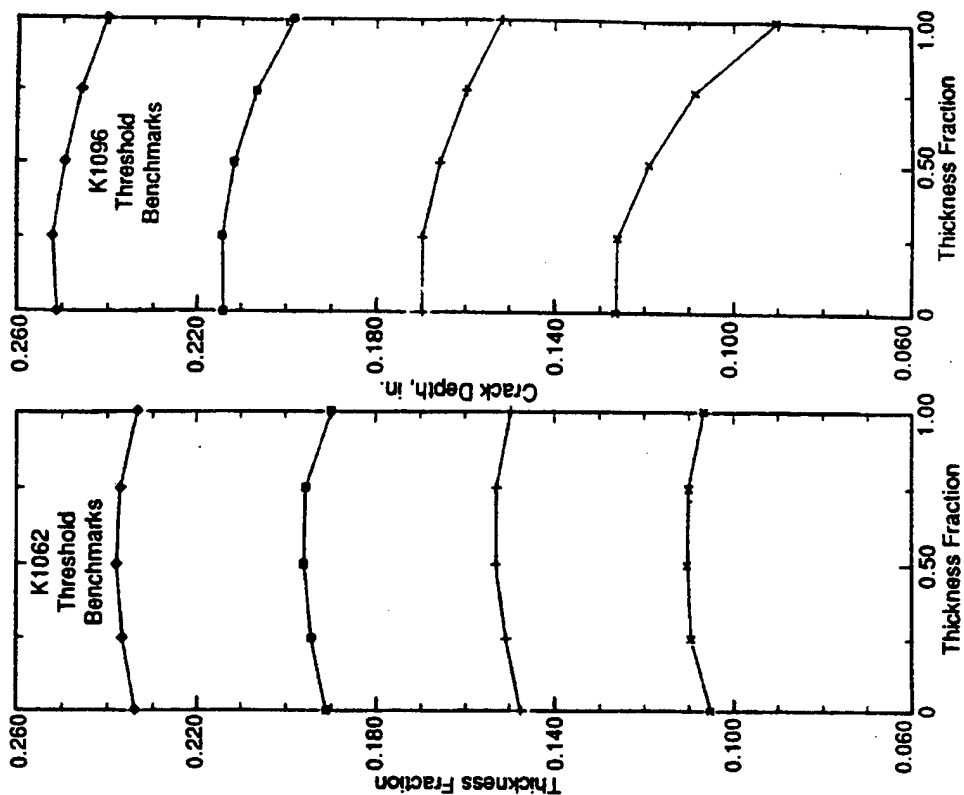


Figure 31. Threshold Benchmarks – Comparison of Typical As-HIP PM Rene 95 Specimen (K102) to Typical DA Inconel 718 Specimen (K1096)

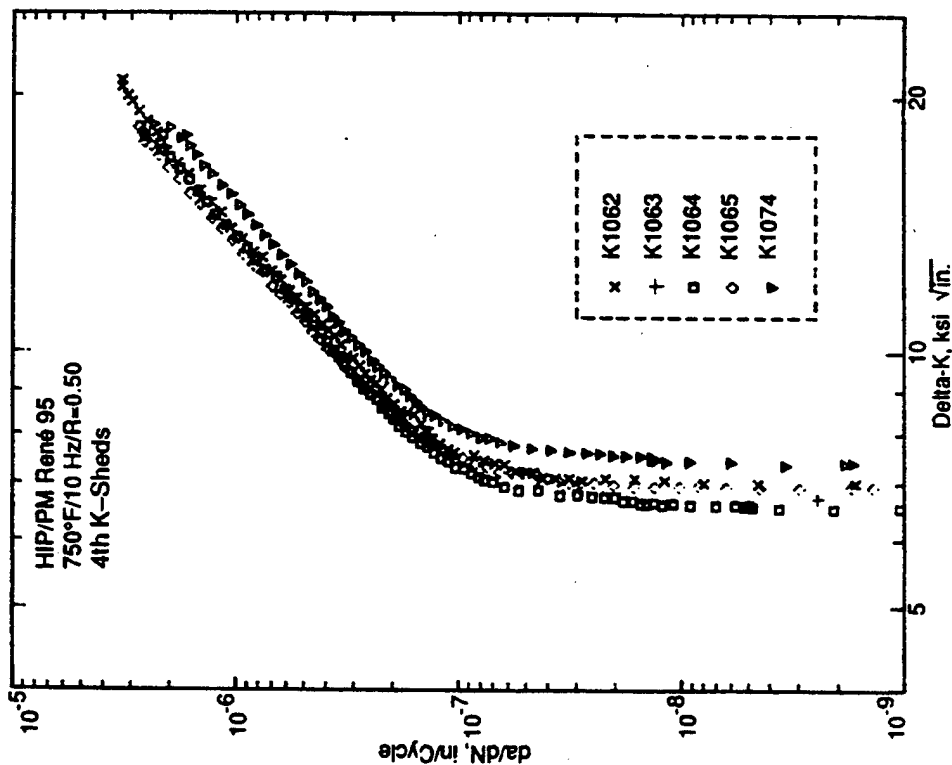


Figure 30. Fourth Load Sheds Compared (As-HIP PM Rene 95 Specimens).

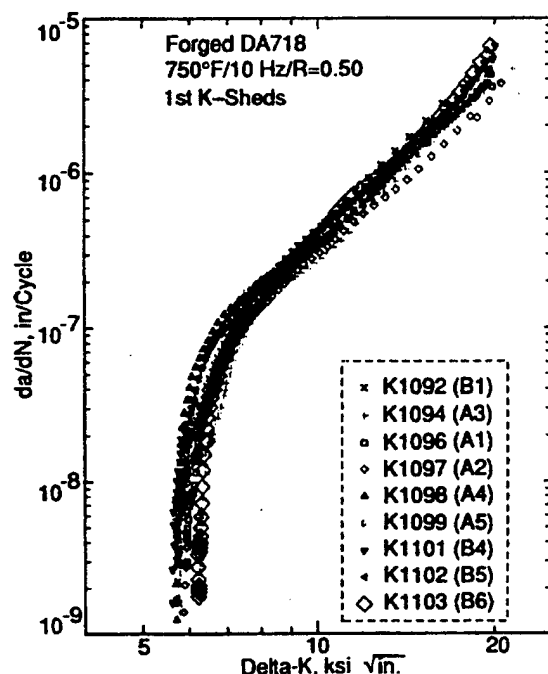


Figure 32. First Load Sheds Compared (DA Inconel 718 Specimens).

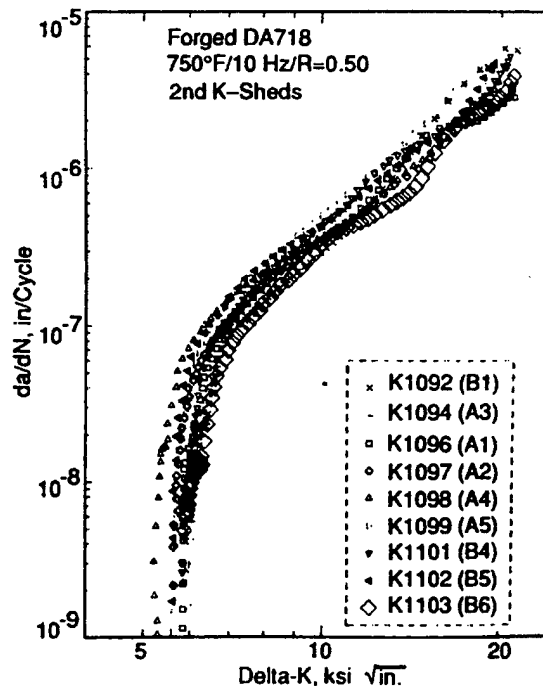


Figure 33. Second Load Sheds Compared (DA Inconel 718 Specimens).

deviations; considerable additional work will be necessary to assess their relative importance.

Traditionally a factor of 2 is applied to fracture mechanics calculations to provide a level of conservatism. In PRDS we will eliminate the factor and apply material variability as a direct contributor to risk probability.

The fracture mechanics models will be assumed correct. While better models are possible, material scatter must be lived with.

3.6 Probabilistic Fracture Mechanics Prediction

The acceptance of GEAE's MISSYDD probabilistic fracture mechanics methodology (*Reference 35*) has generally been based on its conceptual structure: Logically, given a distribu-

tion of flaws, and given that flaws fracture and initiate sharp cracks, and given that the growth of sharp cracks is accurately described by fracture mechanics, then MISSYDD should adequately predict a failure distribution.

The experimental validation program described here provides significant support. Fifty hourglass fatigue specimens manufactured from carefully seeded HIPped PM René 95 were continuously load cycled to failure at room temperature. Twenty-six of the fifty specimens failed at seeded flaws, the remainder by natural causes. Individual seeded flaws were found to last longer than anticipated based on linear elastic fracture mechanics. (This is attributed to crack initiation from the blocky seeded flaws.) The deviations were consistent,

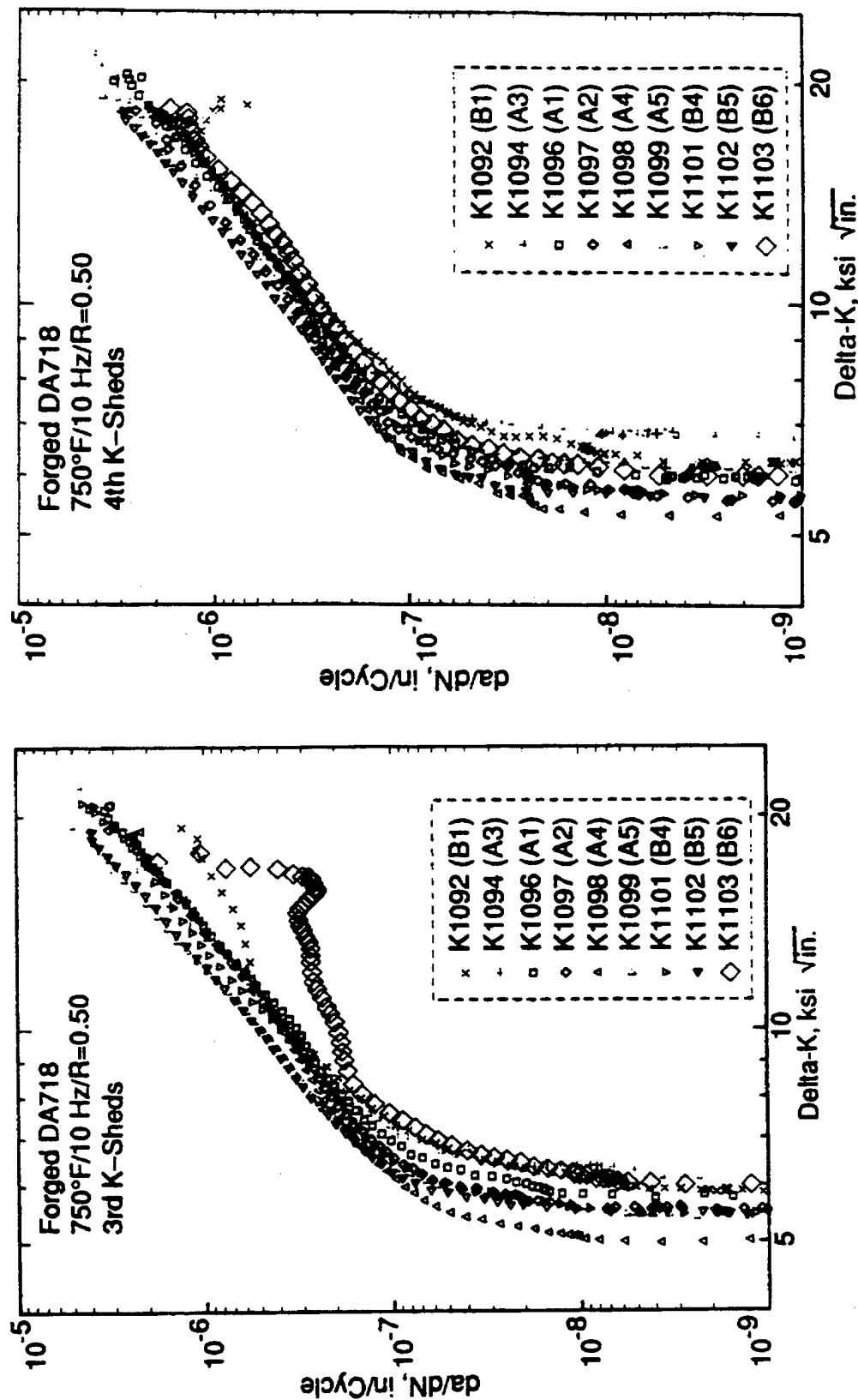


Figure 34. Third Load Sheds Compared
(DA Inconel 718 Specimens).

Figure 35. Fourth Load Sheds Compared
(DA Inconel 718 Specimens).

however, suggesting correction by a simple scale factor.

The MISSYDD prediction is shown in **Figure 36** superimposed on the observed failure distribution. The prediction was based on:

1. CYANIDE analysis of stress distribution.
2. Sharp crack fracture mechanics with a multiplicative correction for initiation.
3. Flaw size distribution based on known seeding.
4. Flaw density (volume rate of occurrence) based on ultrasonic inspection of specimen blanks.

Very good agreement resulted. Two points can be made:

- The matrix fatigue life of the specimens was found to be about 20,000 cycles. **Figure 37** is a magnified window of the failure distribution containing all twenty-four

tests which avoided the seeded aluminas. These failures serve to censor the MISSYDD prediction which, at the time, could only address the threat of the seeded flaws.

LCF continues to compete as an active failure mechanism and would be recognized by the proposed PRDS methodology.

- The large scatter observed in the test results is adequately reflected in the MISSYDD prediction. Moreover, there are steps observed in the prediction which result from the discrete nature of the seeding distribution (nominally five flaw sizes). The data suggests the same steps.

Work is continuing in other programs to develop better flaw distributions, better understanding of flaw behavior, and better general understanding of competitive cyclic failure mechanisms. The results presented here are encouraging: Given the right inputs, MISSYDD does seem to work.

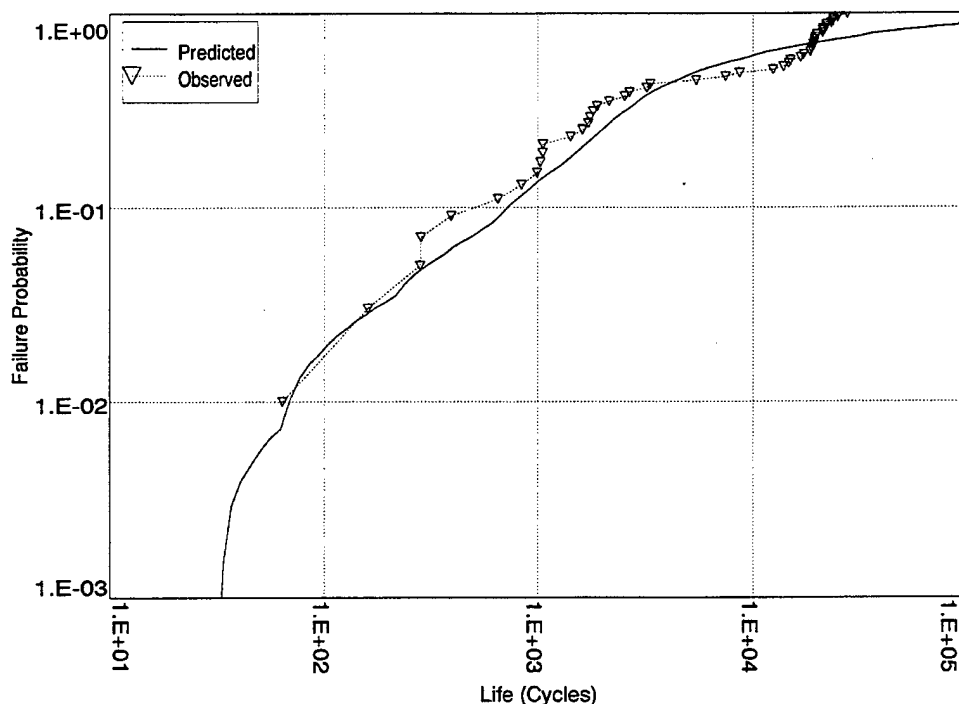


Figure 36. MISSYDD Validation Study – Predicted Defect Failure Distribution Compared to Data.

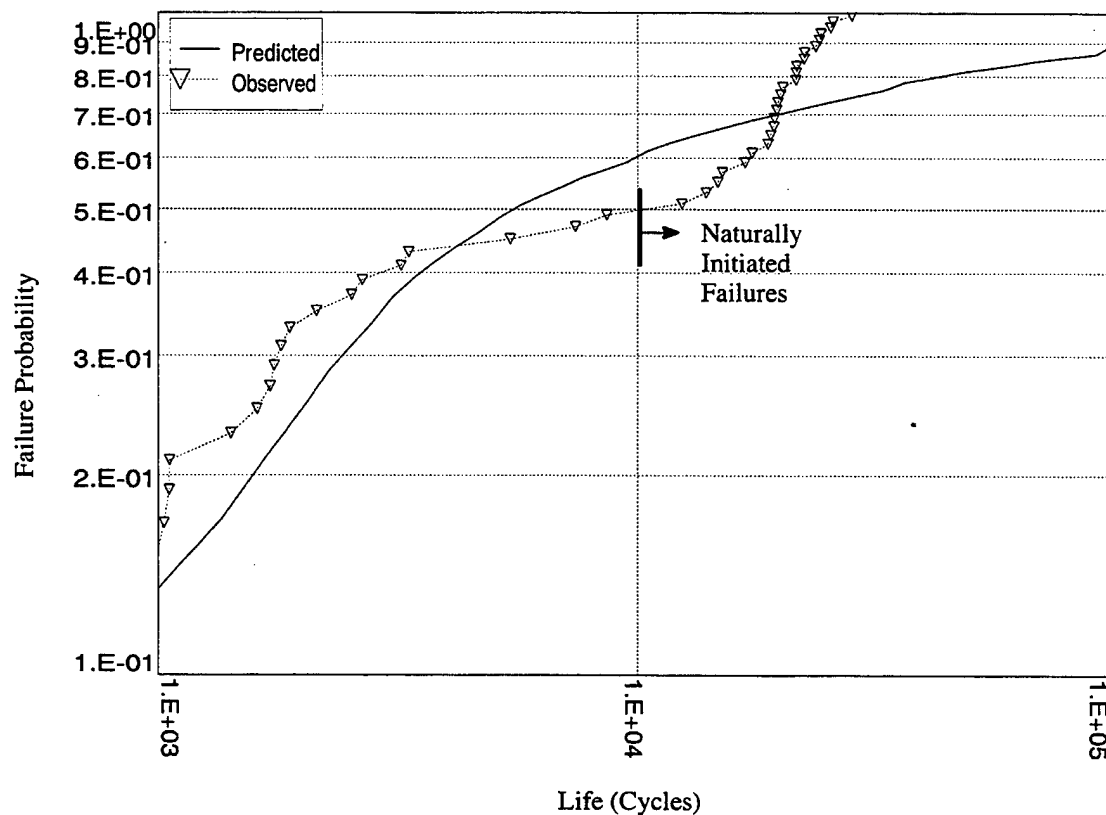


Figure 37. MISSYDD Validation Study – Natural Fatigue Competes with Seeds.

3.7 Statistical Competition

Failure mechanisms may or may not be independent. In the MISSYDD validation study (Section 3.6), crack initiating seeds were in competition with natural fatigue. We believe these mechanisms to be independent (the presence or absence of the seeds does not influence the natural fatigue mechanism). The assumption of independence yields the following equation for net failure probability:

$$F_{\text{net}} = 1 - (1 - F_{\text{flaws}})(1 - F_{\text{lcf}})$$

F_{flaws} is the seed-induced failure distribution calculated by MISSYDD (Figure 36). F_{lcf} is the natural fatigue failure distribution (Figure 38). F_{net} is shown in Figure 39 compared to the data. The agreement is excellent.

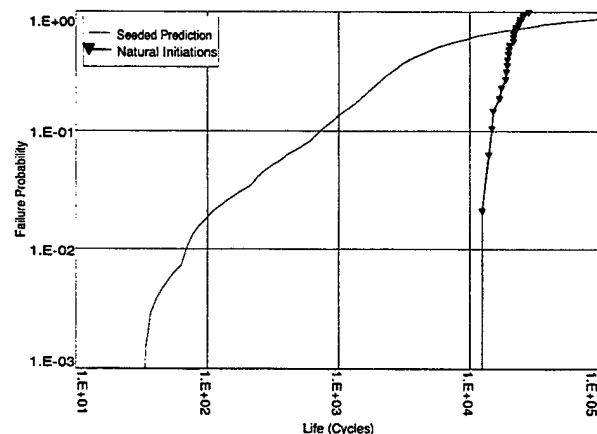


Figure 38. MISSYDD Validation Study – Natural Fatigue Failure Distribution Compared to Data.

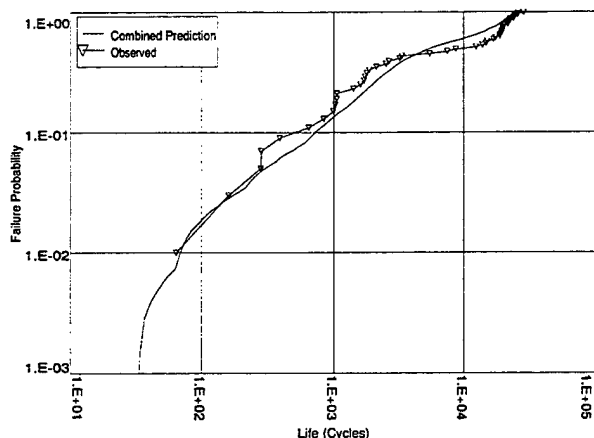


Figure 39. MISSYDD Validation Study- Predicted Defect Failure Distribution Combined with Natural Fatigue Distribution Compared to Data.

3.8 Quality Control and NDE Prediction

Although components are manufactured and assembled with great care, it is recognized that deviations do sometimes occur. Quality controls address this reality. Inspection techniques seem to be divided into two classes:

1. Some are direct and quantifiable. Alloy compositions, for example, are checked by standard chemistry techniques; steps are taken to ensure that the personnel performing the tests are properly trained, but their results are accepted without question. Similarly, the mechanics of measuring part dimensions are so well understood that the results are accepted essentially as absolute.
2. Others are indirect and resist quantification. FPI (Fluorescent Penetrant Inspection), ECI (Eddy Current Inspection) and USI (UltraSonic Inspection) all assess a part's integrity; they are designed to detect cracks or crack-inducing flaws. Each, however, requires the interpretation of subtle shadings of complex and only imperfectly understood physical phenomena.

Each of the second class of techniques is quite complicated, and none produce results which are as convincing as those from the first class of compositional or dimensional analyses. Doubts arise based on experience; flaws have been known to elude inspection.

Given that NDE measurement of part integrity is not absolute, it cannot be said with certainty that a part is clean of (or dirty with) flaws. It may be possible, however, to probabilistically assess cleanliness; two approaches have been tried. The first attempts to characterize a population of flaws inherent to the material. The second attempts instead to characterize the Probabilities Of Detection (POD's) of flaws when they do exist.

This section will summarize and comment on the POD methodology developed by PW Hovey and AP Berens of the University of Dayton Research Institute (*Reference 36 and 37*).

3.8.1 Background

It has always been assumed (but never experimentally confirmed) that the probability of detecting a single crack is a constant and that individual inspections are independent. It follows from the assumption that the number of times a crack is detected is binomially distributed. This is summarized in *Figures 40-41*. *Figure 40a* presents a binomial simulation of 30 inspections of a single crack; it was found 25 times. If 30 more inspections were to be made of the same crack, it might be found 25 times, or 27 times, or 20 times, and so on.

Figure 40b presents the results (the number of finds) for 1000 such simulations. The number 28 appears most frequently (220 times in the 1000 simulations). It very rarely occurred that the crack was observed less than 22 times in 30 inspections (less than 50 instances). A histogram of the results is presented in *Figure 41a*.

This empirical distribution of results closely approximates the theoretical binomial distribu-

Results of 30 Inspections of a Single Crack

Inspection	Outcome
1	1
2	1
3	1
4	1
5	1
6	1
7	0
8	1
9	1
10	1
11	1
12	1
13	1
14	1

Found Crack in 24 of the 30 Inspections

(a)

Repeat this Experiment Once Each Day
for 1000 Days

Day	Number of Finds
1	28
2	27
3	27
4	27
5	28
6	28
7	27
8	28
9	28
10	27
11	26
12	28
13	28
14	30
15	28
16	25
17	26
18	26
19	26

(b)

Figure 40. (a) Binomial Simulation of 30 Inspections of a Single Crack, (b) Simulation Repeated 1000 Times.

tion shown in *Figure 41b* which assumes a POD of 0.90. Given the data from 1000 simulations, one might be inclined to estimate the POD in this fashion, but there is in practice never such a surfeit of data (a total of 30,000 points). More realistically, a single set of 30 inspections might be hoped for; assume that the results of *Figure 40a* have been provided.

A simple estimate of the POD based on this data would be the ratio 25/30 (0.833); this is conservative (since the true POD is 0.90). It is very likely, however, that a different sample would yield a nonconservative estimate.

The binomial probability $b(\text{POD}, N, n)$ of detecting a crack in n of N inspections is given by:

$$N!/(N-n)!n! \text{ POD}^n (1 - \text{POD})^{N-n}$$

The related probability that 0, or 1, or 2, or anywhere up to n finds occur is denoted by $B(\text{POD}, N, n)$:

$$\begin{aligned} B(\text{POD}, N, n) &= b(\text{POD}, N, 0) \\ &+ b(\text{POD}, N, 1) + b(\text{POD}, N, 2) \\ &+ \dots + b(\text{POD}, N, n) \end{aligned}$$

Assume that N inspections result in n finds. There exists a unique value L such that

$$B(L, N, n) = \alpha$$

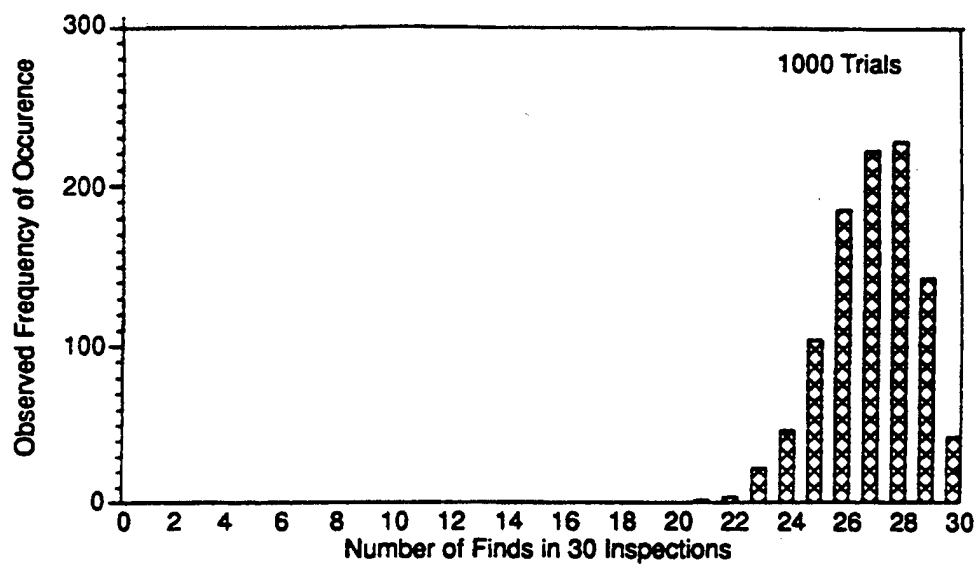
If n decreases, then L decreases.

Let τ be the smallest integer such that the following inequality holds true:

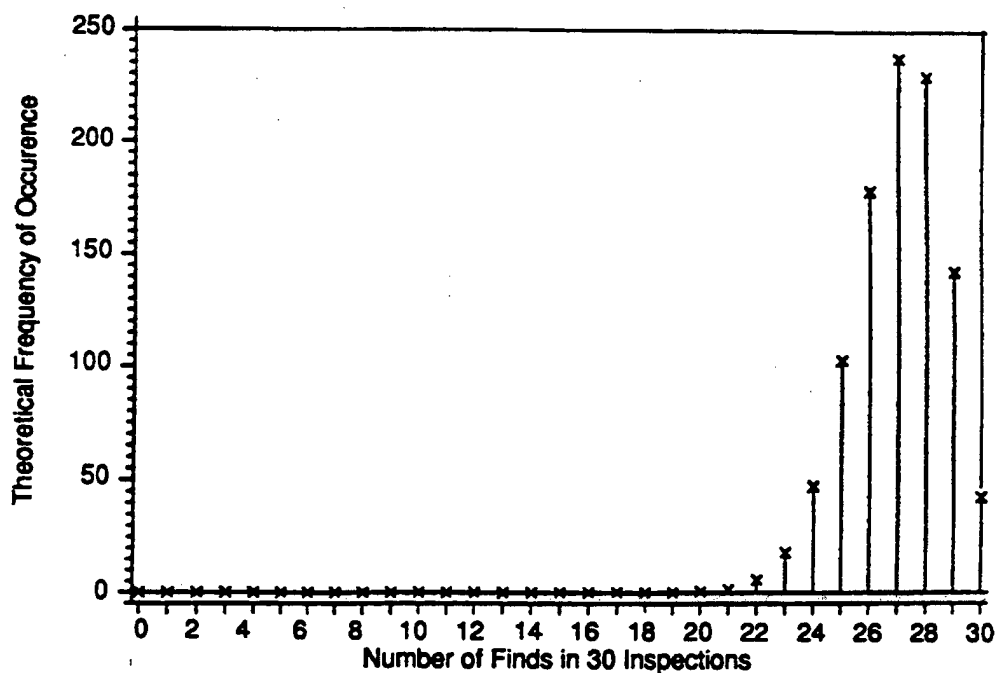
$$B(\text{POD}, N, \tau) > \alpha$$

The probability that L is less than or equal to POD equals the probability that n , the observed number of finds, is less than or equal to τ . This probability is $B(\text{POD}, N, \tau)$ which is greater than or equal to α .

L is, then, a low estimate of POD with probability not less than α . If the probability is high, then it is felt to be a conservative estimate. L is said to be a lower confidence bound on the detection probability with confidence α , or (more simply) an α lower confidence bound. (A common choice for α is 0.95.)



(a)



(b)

Figure 41. (a) Histogram of Simulation Results. (b) Theoretical Binomial Distribution Function (Binomial Parameter is 0.90).

3.8.2 The Log-Logistic Prior Model

Statistical analyses prior to 1980 assumed detection probability to be an explicit function of crack size, and that detection probability increases with size in a continuous fashion. With these assumptions, it was possible to generate lower confidence limits on detection probability for any crack size by inspecting a crack of that size a number of times and applying the above definition. Equivalently, given the assumption, multiple cracks could be inspected over a range of lengths. These could be grouped together into intervals such that the cracks within each interval have approximately equal detection probabilities.

Numerous variations on this interval method were formulated, but the resulting curves tended to be poorly behaved. The erratic behavior was thought to be due to the extreme sensitivity of binomial confidence limits for small samples, and each variation on the interval method was somehow designed to compensate for this. Berens and Hovey argued that a more fundamental problem existed, that the model was itself basically wrong.

FPI, ECI and USI all apply sophisticated physical principles to the problem of detecting cracks. The response of each technique is sensitive to numerous factors, only one of which is crack size. They therefore felt it unreasonable to assume that the simple binomial model could fully capture the statistics of crack detection.

This was supported by a massive data program generated by the Air Force, colloquially known as Have-Cracks-Will-Travel (*Reference 38*). Each of 174 cracks was subjected to a number of inspection techniques by as many as 107 inspectors. For each crack, the proportion of finds was plotted against its length. (*Figure 42* shows two of the data sets.) The scatter observed could not be reasonably attributed to binomial fluctuations.

Berens and Hovey developed an alternative model which recognizes that all cracks of a given size are not equally detectable, but which does maintain that detectability is correlated with crack size, and that it tends to increase as crack size increases.

They retained the assumption that detection of a single crack inspected under rigorously controlled conditions is binomially distributed, but proposed that a distribution of detectabilities exists for each crack size (see *Figure 43*). They suggested that the distribution should account for “the non-reproducibility of all factors other than crack length” (see p. 17 of *Reference 36*); these are factors such as differences “due to operators, environments, and crack orientation, geometry or location”.

This is an example of a Bayesian Model, which is mentioned only in order to introduce the Bayesian term *Prior Distribution* that is applied to the distributions of detectabilities.

The simulation presented in *Figure 44* demonstrates the concept of a prior distribution. 1000 cracks of a fixed size are chosen at random; the detectability of each is assumed accurately measured (this would, of course, entail a very large number of inspections for each crack). *Figure 44a* is a partial tabulation of the results; *Figure 44b* summarizes the simulation as a histogram. (This data was generated assuming a Beta Distribution as prior.)

To assess the probability that a crack of some given size might be missed by an inspection, it is necessary to compound the binomial variability discussed earlier with the variability in the detectability parameter described by the prior distribution. If it is assumed that 30 cracks of a fixed size are chosen at random from the beta prior distribution and that each is inspected once, then the number of finds is distributed as shown in *Figure 45*. (This, in the language of Bayesian statistics, is a Posterior Distribution of the model.)

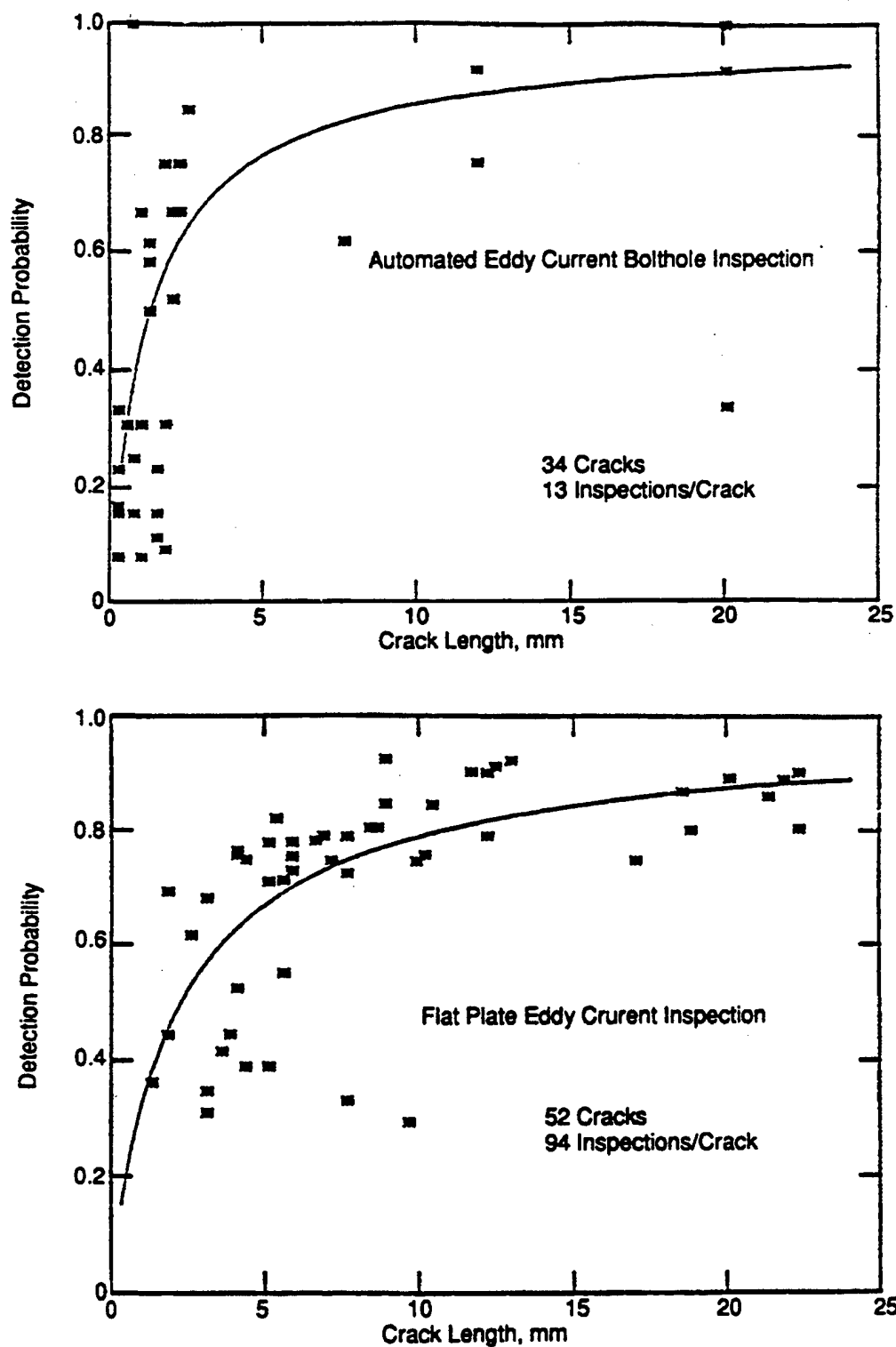


Figure 42. Two Data Sets from the Have-Cracks-Will-Travel Study and Log-Logistic Fits.

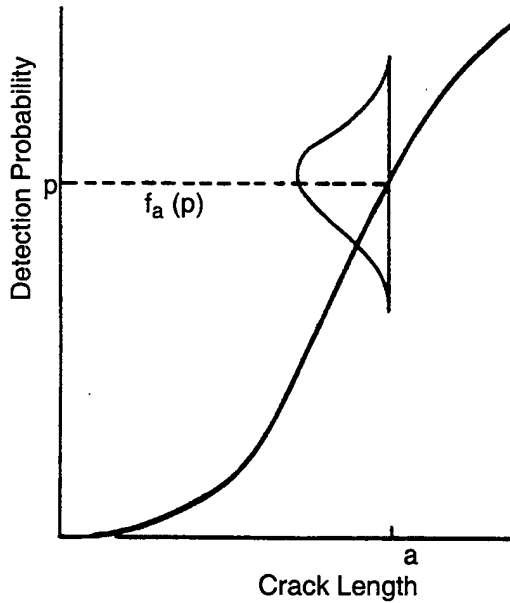


Figure 43. Average POD Curve with Distribution of Detectability.

Berens and Hovey further assumed that a transformation could be found under which the prior distribution becomes a Normal Distribution at each crack size with one standard deviation for all, and with the mean depending linearly on the transformed variant of the crack length. Seven candidate transformations were selected for comparison on the basis of the Have-Cracks-Will-Travel data set. The criteria used for the comparison were: goodness of fit, normality of deviations from the fit, and constancy of the standard deviation. The best of the seven was judged to be the Log-Odds Model:

$$\ln[\text{POD}/(1 - \text{POD})] = \alpha + \beta \ln(\text{length}) + \text{Normal}(0, \sigma)$$

Regression analysis is only applicable to the problem of fitting the log-logistic form if a fairly large number of cracks have each been inspected a very large number of times so that their individual detection probabilities are accurately estimated. GEAE has adopted the somewhat more economical approach of inspecting each of a number of cracks one time. This is possible given the provision by Berens and Hovey of an alternative scheme for analy-

sis, Maximum Likelihood Estimation, which had been developed by Cox (*Reference 39*). This approach is now outlined.

The likelihood that a crack of size a will be detected is the log-logistic probability:

$$\frac{\exp(\alpha + \beta \ln(a))}{[1 + \exp(\alpha + \beta \ln(a))]}$$

denoted by $p(a)$. The likelihood that it is not found is $1 - p(a)$. A sample of cracks is assumed, the sizes of which are a_i . Each crack is inspected once; if it is found, an indicator Z_i is set equal to 1; if it is not found the indicator is set equal to 0. The joint probability that all of the cracks that were found should have been found and that all of the cracks that were not found should not have been found is the product of all of the individual likelihoods $p(a_i)$ or $(1 - p(a_i))$. This product is called the likelihood function; the values of α and β which maximize the likelihood function (if, in fact, such values exist) are called the Maximum Likelihood Estimates of the parameters. The likelihood function is maximized if and only if its logarithm is maximized, the log-likelihood function is denoted by $L(\alpha, \beta)$ and has the following convenient expression:

$$\sum_{i=1}^n Z_i \ln(p(a_i)) + (1 - Z_i) \ln(1 - p(a_i))$$

L is maximized only if its partial derivatives with respect to the parameters α and β vanish. The partials have the following expressions:

$$L_{\alpha} = \sum_{i=1}^n [Z_i - p(a_i)]$$

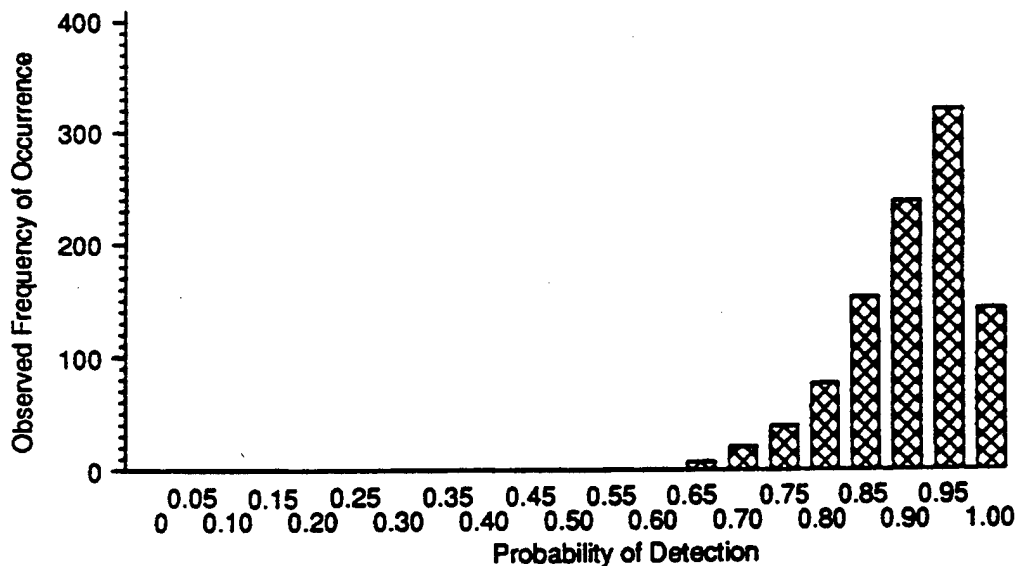
$$L_{\beta} = \sum_{i=1}^n \ln(a_i) [Z_i - p(a_i)]$$

Setting the partials equal to 0 and solving numerically for the critical points will lead to the maximum likelihood estimates.

Select 1000 Cracks at Random. Each
Will Have Its Own Characteristic
Probability of Detection

Crack #	P.O.D.
1	0.88
2	0.93
3	0.84
4	0.85
5	0.93
6	0.88
7	0.77
8	0.87
9	0.80
10	0.83
11	0.92
12	0.86
13	0.99
14	0.83
15	0.91
16	0.88
17	0.97
18	0.89
19	0.98
20	0.90

(a)



(b)

Figure 44. (a) Beta Simulation of 1000 Cracks. (b) Histogram of Detectabilities.

We feel that the insights which led to the log-logistic model were revolutionary, and that Cox's maximum-likelihood approach is a very clever way to define a best fit. There are, however, several points which we would like to make:

1. The Have-Cracks-Will-Travel database was divided into 13 sets for evaluation of the seven candidate transformations; 5 of these data sets were judged by Berens and Hovey to be too small to be statistically useful. They applied the Shapiro-Wilks W-Test (*Reference 40*) to evaluate the normality assumption. The model was rejected for 2 of the data sets at significance levels between 0.05 and 0.1; the remaining sets supported the model at a 0.1 level of significance.

The meaning of the significance level is crucial. To test the validity of a model by an experiment, the probability is calculated that the result of the experiment is reason-

able given the hypothesis. If the model is good, the probability should be large; if, on the other hand, the probability is small, the model should be questioned. This probability that the observations are reasonable is called the *Significance Level* of the test.

If there are very good reasons to accept the model (perhaps it is derived from a fundamental physical theory, such as the kinetic theory of gases), then very convincing evidence is necessary to reject it. That is, only a very unlikely result (yielding a small value of the significance level) would be considered far enough afield of the expected to warrant rejection of the hypothesis.

To base acceptance of a hypothesis on a 0.1 level of significance for rejection indicates a very strong disposition to believe the hypothesis regardless of experimental evidence. Given that there is no theoretical ba-

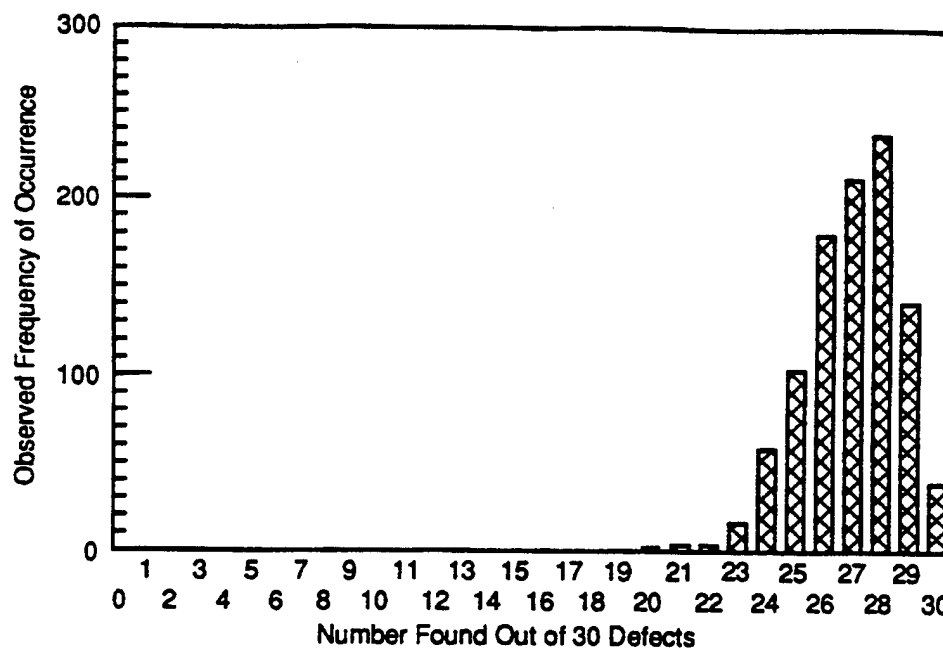


Figure 45. Beta Simulation of Crack Detectability Combined with Binomial Simulation of Inspections.

sis for the Berens-Hovey model, no such disposition is justified.

Provided that the distribution is fairly tight and that only values near the average are significant, the normality assumption is not particularly bad, but the fact that it is only an approximation should be kept in mind.

2. The prior distribution should account for "the non-reproducibility of all factors other than crack length." The analysis of GEAE data tacitly recognizes that there are factors which are not statistically distributed. Different curves have been provided for different materials, for different part geometries and for different inspection techniques. Other sources of variability (such as crack closure and surface condition) which seem equally unlikely to be statistically distributed are treated as if they are. The following hypothetical example demonstrates the potential problem:

POD curves are generated from inspections of sharp fatigue cracks generated in flat plate or bolthole specimens. The cyclic loading which drives the crack growth produces minimal residual compressive stress; consequently, provided forging and machining residual stresses are also minimal, there is little tendency for crack closure.

Highly stressed disk locations (where cracking is most likely and of critical concern) are often compressively stressed upon engine shutdown; cracks in such locations are always tightly closed during inspection and (it is believed) therefore always less detectable than comparably sized cracks in the POD specimens.

3. The regression approach was used to fit the candidate models to the Have-Cracks-Will-Travel data. The database was di-

vided into sets, each set corresponding to a different inspection technique. Each crack in each set was inspected once by multiple inspectors. The proportion of finds was used as an estimate of the crack's detectability. This estimate along with the crack length comprised one point of input to the regression analysis. The true POD of a single crack, however, is theoretically measured under fixed conditions; the variability between inspectors (felt to be quite significant) is assumed to be part of the prior distribution. The use of a simple proportion violates this intent by averaging their capabilities in front of the analysis.

4. The application by Berens and Hovey of Cox's methodology is felt to be inconsistent with their basic model. The inconsistency is that this analysis assumes there to be a single detectability associated with each crack size, but it has been carefully pointed out that this is unrealistic.
5. Given a crack of size a , Berens and Hovey show that its detection probability is the integral of $f_a(p)$ dp (the probability that it has a given detectability) times the detectability p , the integral being from 0 to 1:

$$\int_0^1 p f_a(p) dp$$

They therefore claim that "the true POD function is the curve through the averages (means) of the individual density functions of detectability. Such a curve is also the traditional regression equation of POD as a function of crack length." (*p. 21 of Reference 36*). Given, however, that their regression approach involves a logistic transformation of p , the regression average that they refer to is not the same as the stated integral.

6. Inspection probabilities are usually stated in terms like: 90/95 — 90% POD at 95%

confidence. The confidence concept is unambiguous in the context in which it was introduced in Section 3.8.1. It provides a conservative estimate of the single binomial parameter assumed to define detectability of a crack of a given size.

In the same spirit, confidence bounds are calculable to provide conservative estimates of the log-logistic parameters α and β . It should be noted, however, that 90/95 does not mean that 95% of all cracks of a given length have detectabilities greater than or equal to 90%, though this interpretation would really be more significant given that the spread is sometimes large. While Berens and Hovey recognize the difference and suggest that “another name should be given to this type of more conservative characterization” (p. 29 of Reference 36), the misinterpretation is quite common.

7. Berens and Hovey calculate confidence bounds for the maximum likelihood estimated log-logistic parameters as suggested by Cox (Reference 39). We do not believe that this is appropriate since α and β are not distributional parameters in the normal sense, but rather express the relationship between distributional parameters and crack size.

3.8.3 The \hat{a} versus a Model

The response of eddy current and ultrasonic inspection systems is a quantifiable signal which is designed to remain essentially constant until a discontinuity is encountered. If a change in the signal occurs which exceeds a set threshold, a rejectable flaw is assumed to exist, and the part is removed for further evaluation. It was recognized by Berens and Hovey that considerable information was being lost in the analysis of detectability data by reducing results from such systems to a pass/fail classification. They have consequently developed an

alternative approach, documented in *References 36 and 37*, which compares the sizes a of sample cracks to their response amplitudes \hat{a} .

The probability that a crack of size a will be rejected by an inspection is the probability that \hat{a} exceeds the threshold. Berens and Hovey assumed that \hat{a} is normally distributed about an average value which has a known functional relationship $f(a)$ to a . *Figure 46*, which is excerpted from their report, depicts the basics of the model. *Figure 47*, also from their report, demonstrates the construction of a probability of detection curve based on the relationship $f(a)$ and the distribution of the deviations. For each crack size, the detectability is quantified as the probability that the response of a crack of that size will exceed the threshold.

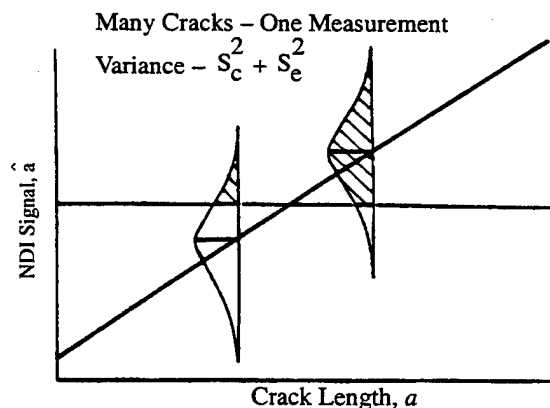


Figure 46. Berens-Hovey \hat{a} -versus- a NDE Response Model – POD at a is the Probability that \hat{a} Exceeds a Threshold.

We feel that the insights are accurate, that response amplitude and hence detectability are not uniquely determined by crack size. We urge discretion, however, in applying statistical methods to analyze the scatter. The assumption of randomness and the ensuing dependence on statistical analysis can discourage fruitful basic research. *Figures 48 and 49* are pertinent....

For measuring the lengths of known cracks, replication techniques are generally judged superior to optical methods. *Figure 48* shows \hat{a}

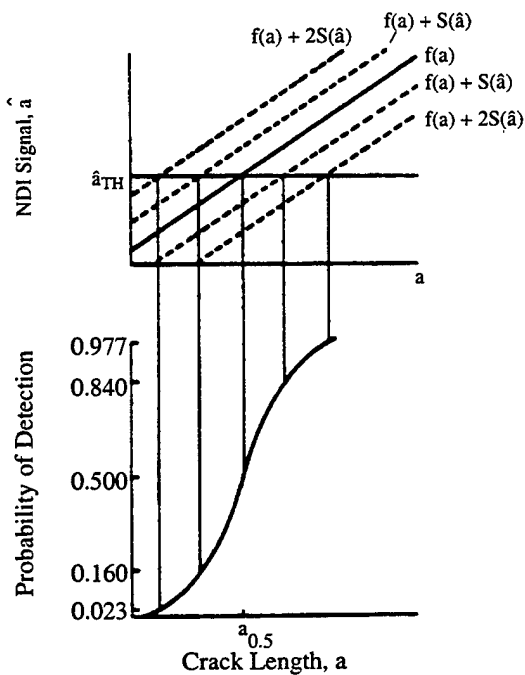


Figure 47. Berens-Hovey \hat{a} -versus- a NDE Response Model - POD Curve Construction.

vs. a data for eddy current inspection of bolt-hole cracks as originally plotted. The crack lengths were measured optically; areas were calculated by assuming that the crack dimensions interior to the boltholes equalled those measured on the specimen surfaces.

The cracks were subsequently remeasured by replication, both on the specimen surfaces and interior to the boltholes. The areas were recalculated and the results plotted in **Figure 49**. The apparent scatter is noticeably decreased.

Also, it is speculated that nicks may be more detectable by eddy current inspection than the sharp cracks used to calibrate NDE capability. A coupon of Ti6-4 was prepared with a sequence of hardness indentations on one surface to simulate nicks. The plate was scanned with standard eddy current equipment. Replicas of the indents were taken for dimensional measurement. The data is summarized in **Table 8**:

If the threshold is set at 20% full scale, it appears that a nick as small as 3 by 16 mils may be detectable. The POD for a 5 by 16 mil sharp crack is only 0.33.

Statistics is useful, but statistical analysis should usually be sought only to supplement mechanistic understanding, not as a replacement. Therefore, we hold that proper and accurate recognition of POD in risk analysis calls for better understanding of the physical processes of NDE.

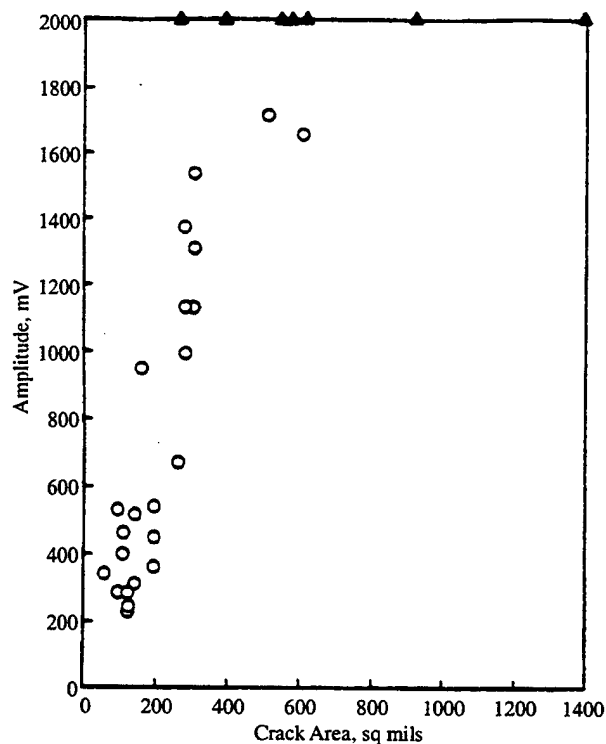


Figure 48. Eddy Current Amplitude Plotted against Crack Area – Area Inferred from Optical Measurement.

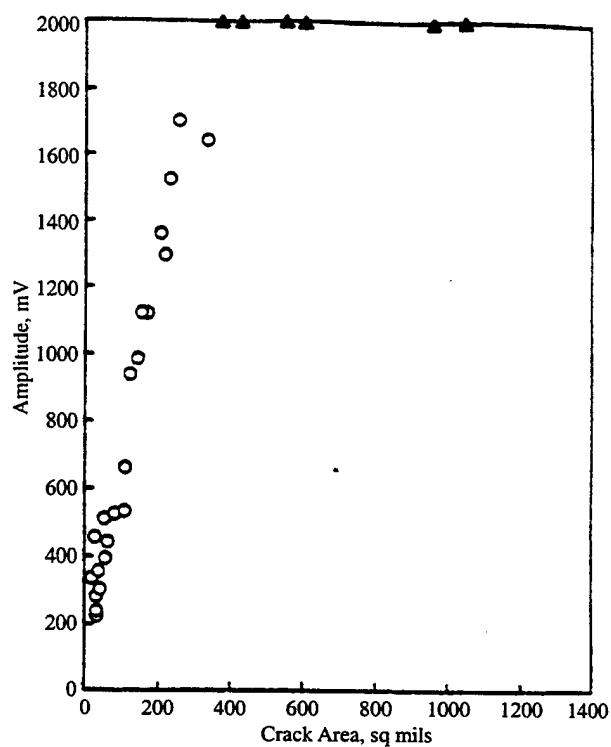


Figure 49. Eddy Current Amplitude Plotted against Crack Area – Area Inferred from Replica Measurement – The Scatter Decreases.

Table 8. Dimensions of Simulated Cracks Measured by Eddy Current.

Indenter Load (kg)	Diameter (mils)	Depth (mils)	Eddy Current Amplitude (% full scale)
150	29.2	4.04	82
150	28.8	2.16	82
100	24.0	4.64	46
100	24.0	5.20	46
60	18.4	3.76	28
60	18.4	3.44	28
45	16.8	3.36	28
45	17.2	3.48	28
30	14.4	2.76	16
30	14.8	2.88	16
Baseline	---	---	8

4.0 Probabilistic Rotor Design System Parameters

On the basis of our review of field and laboratory experience, the following failure mechanisms will be considered:

- LCF – Damage in a region of uniform microstructure cyclically accumulated during major load excursions.
- Flaw Induced Cracking – Distinguished from LCF in that damage is exacerbated by stress concentrating flaws not associated with the material microstructure (e.g. refractory inclusions, porosity, machining marks).
- Yield – Loss of function or integrity due to excessive stable deformation.
- Ultimate Strength – Fundamental inability of a sound structure to support required mechanical loads. Distinguished from final failure following stable crack growth.

Historically, the first two are considered major mechanisms, the second two minor. In the future it will be desirable to add creep to the list (loss of function or integrity due to excessive time dependent deformation). While this mechanism is becoming more of a concern in our newer, hotter-running engines, our understanding of its statistical dimension is too immature for inclusion at this time.

Potential causes to be evaluated are:

- *Part-to-Part Interactions* – Lack of proper recognition of connecting parts resulting in inappropriate analysis boundary conditions.
- *Operating Temperature, Analysis* – Poor thermal analysis resulting from inadequate engine cycle data or computational inaccuracy leading to compromised material capability.
- *Operating Stress, Dimensional Variability* – Extreme sensitivity of a stress concentration to dimensional deviations coupled with hard-to-achieve manufacturing tolerances.
- *Engine Build Variability* – Significant engine-to-engine variability in operating pressures, temperatures or speeds.
- *Basic Properties* – Variability in basic material mechanical properties (e.g. fatigue resistance).
- *Material Flaws (Process Related)* – Flaws, such as refractory inclusions, introduced during material processing.
- *Manufacturing Damage* – Nicks, gouges or otherwise damaged material resulting from tool breakage or abusive machining.
- *Handling/Assembly Damage* – Nicks, gouges, prestrains, etc. introduced following component manufacture.

5.0 Algorithm Flowcharting and Development

GEAE has been developing probabilistic life methods for about a decade and a half. The product of this continuing effort is the MIS-SYDD program which provides a flexible tool for estimating risk of component failure given the presence of randomly distributed flaws. Since the release of Version 1 in 1982, MIS-SYDD has been used for ENSIP embedded flaw tolerance calculations on the F101, F110-100, F110-129, CF6-80C2 (Air Force 1 application) and YF120 engines. It also has had commercial engine applications, notably evaluations of CF6-6 and CF6-50 fan disks, and of the CFM56-5 high pressure turbine disks.

The PRDS tool will be derived from MIS-SYDD. The new software will be known as PDAS for Probabilistic Design Analysis System, recognizing its expanded capability and purpose.

5.1 Response Surface Formulation of Risk Calculation

The basic assumption of PDAS is that the object parameters, risk and weight, are smooth functions of part geometry and material properties. Smoothness allows approximation by low order response surfaces which simplifies evaluation of basic integrals of conditional probability which define risk:

$$\int F(\mathbf{p}) f(\mathbf{p}) d\mathbf{p}$$

$F(\mathbf{p})$ is the failure probability given the parameter vector \mathbf{p} ; $f(\mathbf{p})$ is the joint probability density function of \mathbf{p} .

Example: As web thickness varies from part to part, stresses vary. For any given thickness (hence stress distribution) there is a probability calculated for failure from fatigue, flaw-induced cracking, etc. $F(t)$ is the functional

dependence of failure probability on thickness t . Web thickness will likely populate a truncated normal distribution with density function $f(t)$.

Continuing: the probability that t lies in some small interval $[t, t + dt]$ approximately equals $f(t)dt$. If the interval is small enough, $F(t)$ is nearly constant. The combined probability that t lies in the interval and failure occurs is approximately:

$$F(t) f(t) dt$$

Summing over the disjoint intervals

$$[t_0, t_1), [t_1, t_2), \dots, [t_{n-1}, t_n]$$

on which $f(t)$ is significant, the probability of failure is approximated by the Riemann sum:

$$\sum F(t_i) f(t_i) (t_i - t_{i-1})$$

Letting the interval size decrease and taking the limit yields the risk integral formulation:

$$\int F(t) f(t) dt$$

The density function $f(t)$ in this example is based on data; it is assumed known. The conditional probability $F(t)$, however, must be calculated for any given t , and the computation is often expensive. The risk integral can be evaluated numerically by simple quadrature algorithms, but these require many evaluations of the integrand. Enormous savings are recognized if $F(t)$ can be approximated by a readily evaluable function (*References 41 and 42*).

5.2 Program Organization

PDAS will be built from software elements already available at GEAE. Modularization of our system will allow future upgrades which are beyond the scope of the current contract.

The PDAS flowchart is shown in *Figure 50*.

- Execution is controlled by a design decision function having the following responsibilities:
 - Definition of the shape parameters and constraints (e.g. a particular disk must fit a given flowpath, must have a given number of blade attachment points, must have a web composed of a fixed number of straight line segments blended by circular arcs, etc.).
 - Specification of basic finite element structure (2-D or 3-D, axisymmetric or planar, shells or quads, master regions, mesh density and biasing).
 - Assignment of material properties (thermal, constitutive, fatigue, fracture mechanics, NDE response, flaw distribution).
- Organization of the dimensional, operational and properties response surfaces (identification of the relevant degrees of freedom: shape parameters, operating temperature, engine speed, etc.).
- Optimization direction (shape change to affect computed risk and weight).
- Each point of the dimensional response surface is a design that requires analysis. Finite element models are created.
- Material properties and operational conditions for thermal, stress, displacement, and life analyses are assigned according to the appropriate response surfaces.
- The response of the model is integrated with the statistical distributions of the analysis variables to yield calculated risk at

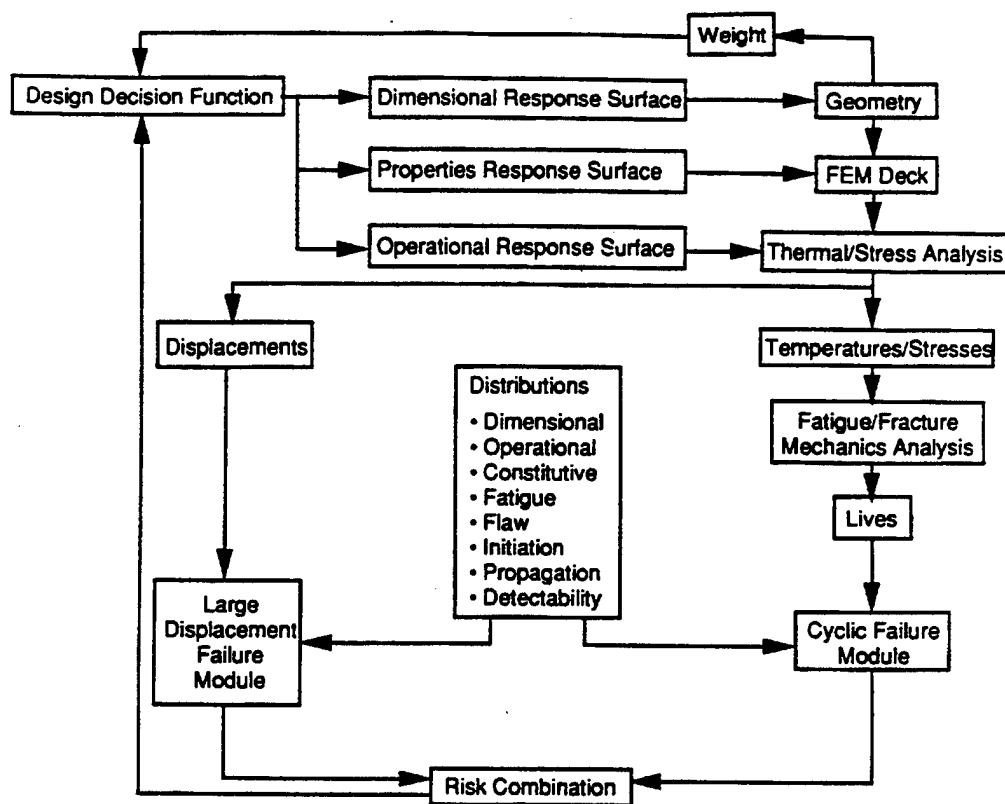


Figure 50. PDAS (Probabilistic Design Analysis System).

each design point of the dimensional response surface.

- The risk and weight response surface dependencies are returned to the design decision function for initiation of the next iteration.

Specific elements of PDAS will be outlined in the following sections.

5.3 Database Architectures

The PDAS database will be derived from the existing MISSYDD structure.

The database index is summarized in *Figure 51*. The nodes of this diagram are referred to as text entries. Some text entries are generated by MISSYDD in response to user requests:

- DOCUMENT
- MATERIAL LIBRARY
 - FRACTURE MECHANICS DATA
 - FLAW DISTRIBUTION DATA
- MODEL LIBRARY
 - INPUT LIBRARY
 - HISTORICAL RECORD
 - MISSION LIBRARY
 - LOAD CASE DOCUMENTATION
 - COMPUTATION LIBRARY

Other text entries which lie under these nodes are input by the user:

- MATR n – Material Designation
- FRCT n – Fracture Mechanics Dataset Designation
- FLAW n – Flaw Distribution Dataset Designation
- MODL n – Component Model Designation
- UIF – SIESTA Unified Input Filename
- UOF n – SIESTA Unified Output Filename

- MSSN n – Mission Designation
- LOAD n – Documentation for Individual Load Case
- COMP n – Computation Designation

Database nodes are created as necessary, either by branching or by growing an existing branch as suggested by *Figure 51*.

New classes of nodes will be added for PRDS. These will include nodes defining the response surfaces for each iteration and nodes for new classes of material data (e.g. constitutive constants, fatigue distributions, NDE POD curves).

5.4 ANSYS Parametric Modeling and Analysis

The modeling function of ANSYS will serve as the principal geometry interface. This package provides good 2-D construction capability and flexible mesh generation.

Both construction and meshing in ANSYS can be driven by Macro programming which will facilitate setting up the individual finite element models of the dimensional response surface. Node definition and elemental connectivity can be exported for external analysis. It should be emphasized that ANSYS appears to offer the best current capabilities for parametric definition. It could be replaced by other geometry packages as they become available (e.g. Unigraphics).

Figure 52 shows a baseline model disk design and eight perturbations (minus the meshes) comprising a full factorial design on the three parameters: bore width, web transition width and web transition radius (*Reference 43*). In total, 17 parameters are needed to define the model which includes an axisymmetric bore and web and plane stress rim.

ANSYS will also be called on for all thermal/stress/displacement analyses.

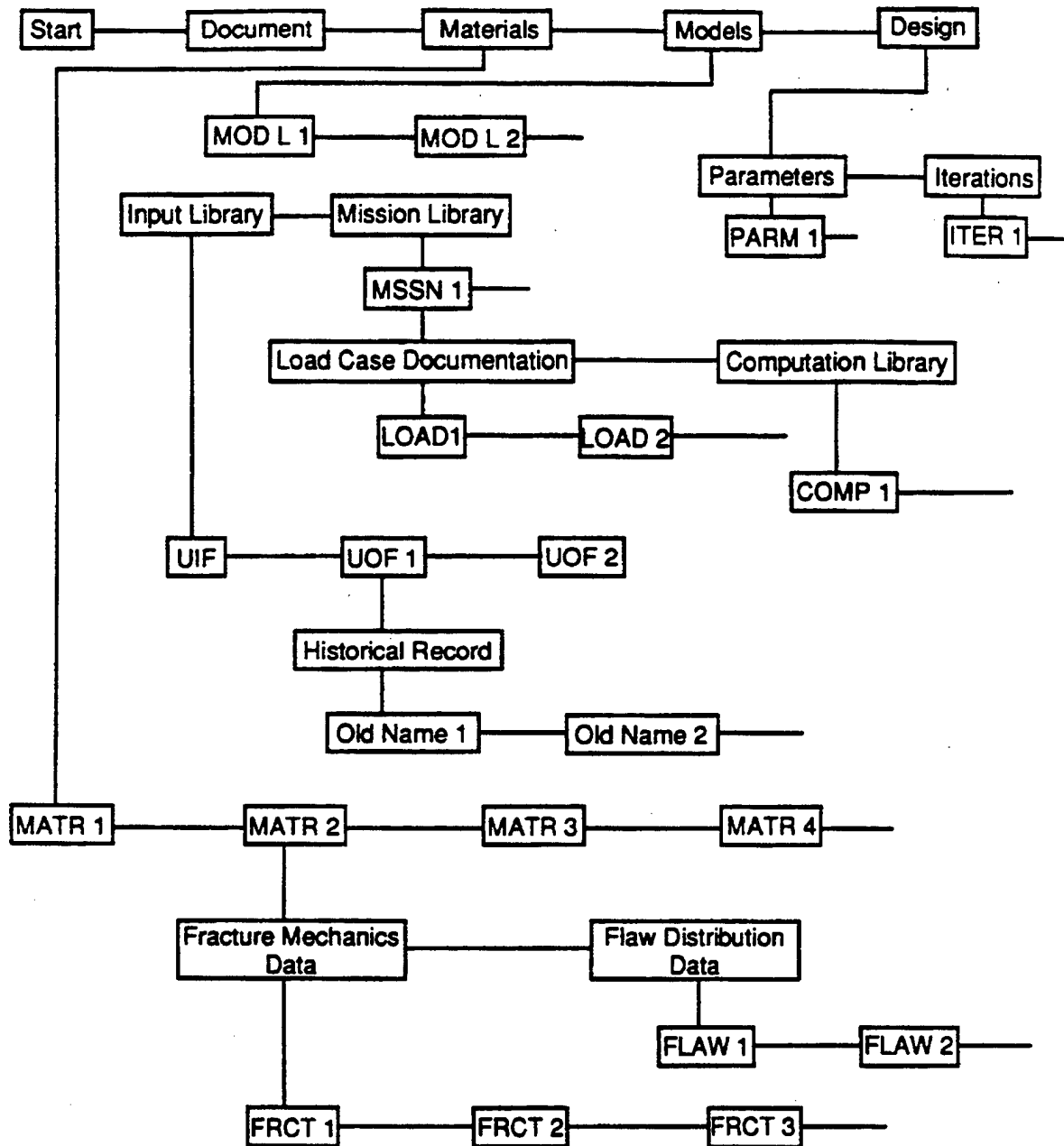


Figure 51. MISSYDD Data Base Index.

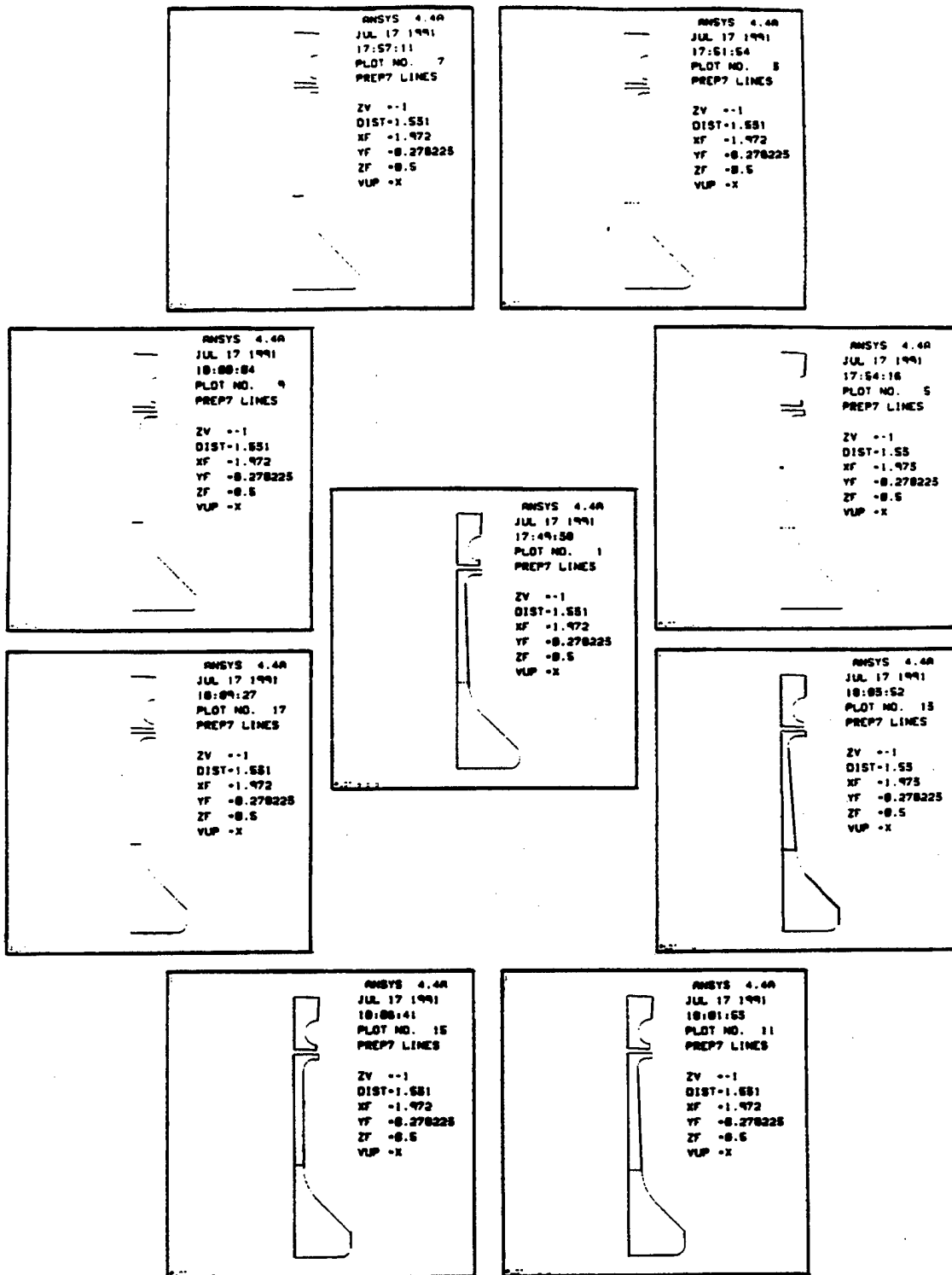


Figure 52. Baseline ANSYS Disk Model (Center) Plus Eight Parametric Perturbations.

5.5 SIESTA (System for Integrated Engineering STructural Analysis)

Interface of component thermal/stress/displacement analyses to MISSYDD is moderated by SIESTA (System for Integrated Engineering STructural Analysis) which has been developed to coordinate the variety of tools used at GEAE. For PDAS, SIESTA will track model geometry, boundary conditions and material property assignments, and serve to postprocess ANSYS output.

5.6 MISSYDD Fracture Mechanics and Fatigue

MISSYDD integrates the probability of failure if a flaw is present (determined by the spatial stress/temperature distribution of the component) with the probability that the flaw is present (the flaw distribution). Details will be provided in Section 5.7.2.

Earlier releases employed an approximate fracture mechanics algorithm which left its application restricted to embedded flaws. MISSYDD.v4 offers the option of more realistic calculations which erase the line between surface and subsurface. Algorithms have been developed for an enhanced fracture mechanics module which enable recognition of the geometry of each flaw location relative to free surfaces, and necessary stress gradient information.

As shown in Section 3.6, the accuracy of MISSYDD predictions has been validated given the proper inputs.

5.7 Statistical Combination

In what follows, F_{lcf} , F_{flaws} , F_{yield} and F_{burst} will denote failure probabilities associated with the four failure mechanisms being addressed. The evaluation of these failure probabilities depends on the nature of the relevant statistical models.

5.7.1 F_{lcf}

To calculate F_{lcf} , the challenge remains to translate small specimen fatigue distributions to complex components. As was shown in Section 3.4.1, incorrect scaling of fatigue distributions for size effect can result in grossly conservative predictions. The following two hypothetical examples further explore this concern.

Example 1 – Assume that disk life is controlled by a single axisymmetric zone having volume n . Fatigue scatter within this zone of a given disk is characterized by a unit volume survival probability function $S(N)$. A carefully designed data program determines that part-to-part variability can be modeled by a finite number of such functions ($S_1, S_2, S_3, \dots, S_m$) where S_i occurs with probability f_i .

The fleet survival probability is correctly calculated as follows:

$$S_{fleet} = \sum f_i S_i^n$$

If the data stratification is ignored and the data averaged prior to the size effect translation, a conservative prediction results:

$$\left\{ \sum f_i S_i \right\}^n \leq \sum f_i S_i^n$$

(This follows from Jensen's inequality for convex sums (*Reference 44*).)

Here, inappropriate averaging of data is conservative. This is not always true as the second example shows.

Example 2 – Assume that disk life is controlled by m competing zones having unit volume survival probability functions $S_1, S_2, S_3, \dots, S_m$. Each zone has volume n . The stratification between the zones is attributed to large differences in cooling rates following forging, but part-to-part variability is found to be minimal.

Correct calculation of fleet survival probability:

$$S_{\text{fleet}} = \prod S_i$$

In this case, ignoring the data stratification is non-conservative:

$$\left\{ \frac{1}{m} \sum S_i \right\}^m \geq \prod S_i$$

(This also follows from Jensen's inequality.)

Current design practice at GEAE applies fatigue data differently. Design Life is defined as the minimum -3σ life (that is, the minimum of all component locations). This does not recognize that a disk with a hundred holes will fail sooner than a specimen with a single hole (assuming that the holes are critical locations), but the non-conservatism is probably well offset by the fact that the σ reflects significant non-statistical scatter.

We are proposing changes in the design and application of material data programs to take advantage of our developing understanding of stratification, but our proposals are aimed at the future. Distributional assumptions will have to be made for Phase III and IV PDAS applications.

5.7.2 F_{flaws}

Calculation of F_{flaws} follows a three step procedure (illustrated by **Figure 53**):

1. Calculation of $G(N, a)$, the probability of failure by life N given a single flaw of a fixed size a occurring randomly in the model. This probability is geometric in that it involves the spatial distribution of stress and temperature. In principle, each point of the model has a well defined life dependent on the precise mission conditions, geometric constraints and material properties in the vicinity of the point. Given random placement of the flaw, the probability of failure by a life N is the volume of material having

life less than or equal to this value ratioed to the total volume.

2. Calculation of $R(N)$, the probability of failure given a single flaw the size of which is a random variable having density function $r(a)$.

$$R(N) = \int G(N, a) r(a) da$$

3. Assuming that there is no interaction between individual flaws, a component survives n flaws with probability $(1 - R(N))^n$. The Poisson distribution is a simple model for the probability that exactly n flaws are present.

$$\begin{aligned} F_{\text{flaws}} &= \sum (e^{-\lambda} \lambda^n / n!) [1 - (1 - R(N))^n] \\ &= 1 - e^{-\lambda R(N)} \end{aligned}$$

In this expression λ is the average number of flaws for the volume of the component. It is more common to replace this parameter by λV where λ now represents the average number of flaws in a unit volume and V is the volume of the component.

5.7.3 F_{burst} and F_{yield}

Calculation of F_{burst} also follows three steps (**Figure 54**):

1. Approximation by $B(\mathbf{p})$ of the burst speed response surface (i.e. $B(\mathbf{p})$ is the approximate dependence of burst speed on the parameters \mathbf{p}).
2. Calculation of $E(s)$, burst probability as a function of speed:

$$\begin{aligned} E(s) &= \text{Prob}(B(\mathbf{p}) > s) \\ &= \int_{B(\mathbf{p}) > s} f(\mathbf{p}) \end{aligned}$$



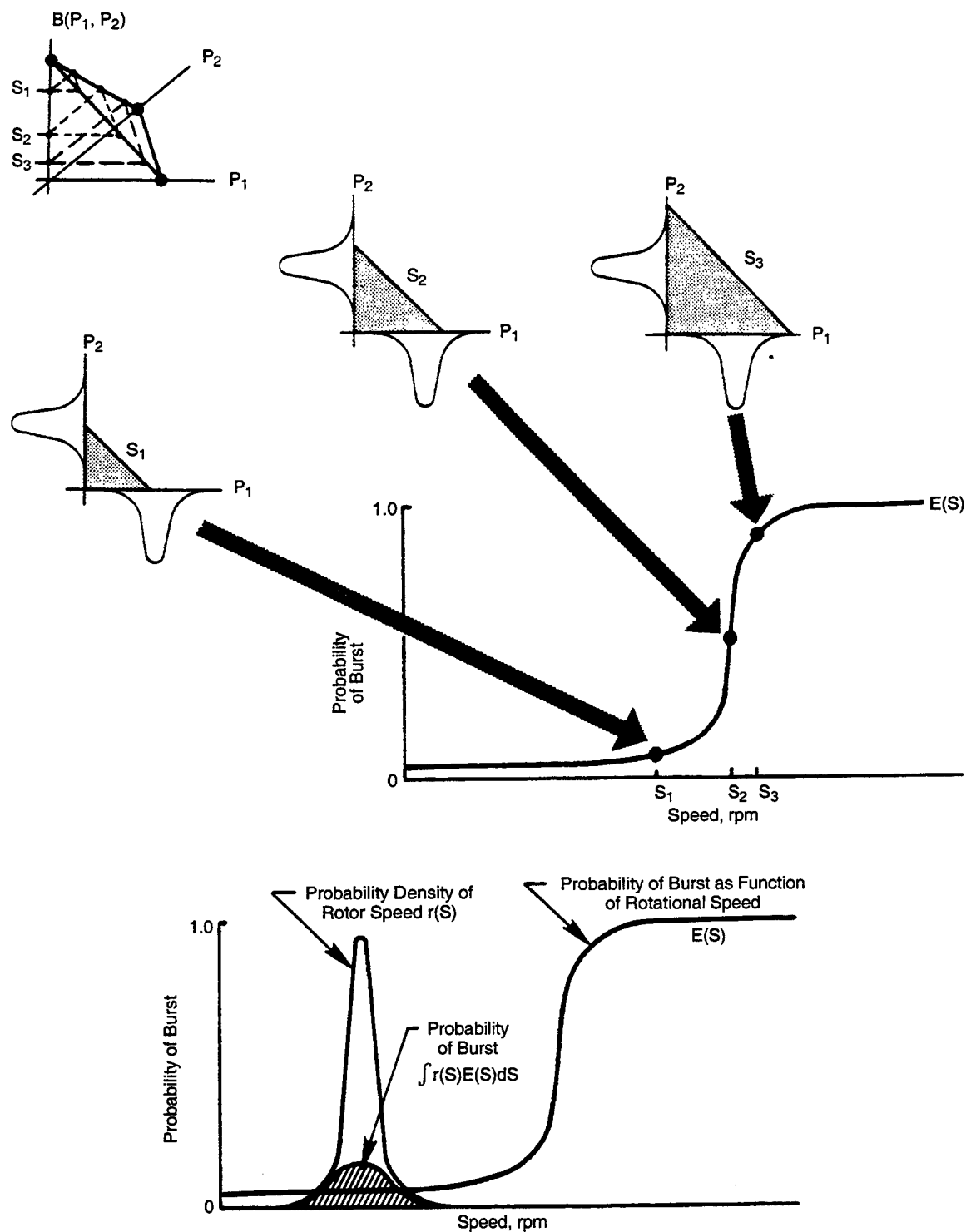


Figure 54. Computation of F_{burst} .

3. Integration of $E(s)$ with $r(s)$, the probability density function of rotational speeds:

$$F_{\text{burst}} = \int E(s)r(s) ds$$

F_{yield} is similarly calculated.

5.7.4 Competition between Mechanisms

In Section 3.7 it was shown that the simple expression:

$$F_{\text{net}} = 1 - (1 - F_{\text{lcf}})(1 - F_{\text{flaws}})$$

adequately reflected the apparent competition between LCF and flaw induced cracking in the MISSYDD validation study.

If, for example, F_{lcf} and F_{flaws} had been impacted by significant loading variability, the above expression would probably not have worked very well; the flaw and LCF failure mechanisms would have been correlated by stress, and its effect would have to be factored out:

$$F_{\text{net}} = 1 - \int (1 - F_{\text{lcf}}(p)) (1 - F_{\text{flaws}}(p)) f(p) dp$$

where $f(p)$ is the probability density function of the loading p . PDAS will allow for both independent and dependent statistical combinations.

5.8 Nondestructive Evaluation

The following approach has been developed to incorporate NDE POD into MISSYDD probabilistic fracture mechanics calculations.

It is assumed that the flaw content of a material is Poissonly distributed with average density λ (referenced to 1 cubic inch). That is, the probability that n flaws will be found in 1 cubic inch of material is given by:

$$\exp(-\lambda) \lambda^n / n!$$

Furthermore, it is assumed that the flaws have a distribution of sizes described by a density function $f(a)$. Note that this presupposes some rather simple notion of flaw geometry for which a single parameter suffices. Flaws will be pictured as ellipsoidal. Any planar cross section of an ellipsoid is elliptical; and in a cyclic, uniform, uniaxial stress field, it is not unreasonable to assume that a flaw will crack through the maximum-area elliptical cross section normal to the stress axis. The maximum cross-sectional area will be taken as the parameter a which describes the flaw population.

The cumulative probability distribution function associated with $f(a)$ is denoted by $F(A)$.

$$F(A) = \int_0^A f(a) da$$

Summarizing To This Point: The flaws are characterized by their maximum cross-sectional area. The Poisson distribution characterizes the overall frequency of flaws; the function $f(a)$ describes their relative distribution of sizes.

The probability that a volume of material contains flaws having size greater than or equal to some size has been termed its Dirtiness. The functional relationship $D(A)$ denotes the probability that 1 cubic inch is dirty with flaws of size A or larger. It has been shown that $D(A)$ is related to the density λ and the size distribution $F(A)$ as follows:

$$D(A) = 1 - \exp[-\lambda (1 - F(A))]$$

Given that a flaw is present, the probability that it is larger than A and not caught by NDE is given by:

$$\int_A^\infty f(a) \text{POD}(a_1) \text{POD}(a_2) \dots \text{POD}(a_p) da$$

where the integration is with respect to the initial flaw size a , a_i is the size of this flaw at the

i 'th inspection, $\widetilde{POD}(a_i)$ denotes the probability that the flaw is missed at the i 'th inspection, p inspections have occurred.

Note that it has tacitly been assumed that the crack is growing and that its size is known (or may be calculated) at each inspection point. It has also been assumed that the probability of detection is known at each point and that the individual inspections are statistically independent (allowing us to multiply the factors \widetilde{POD}).

The above integral may be approximated by the sum:

$$\sum [F(x_{j+1}) - F(x_j)] \widetilde{POD}(x_{j1}) \widetilde{POD}(x_{j2}) \dots \widetilde{POD}(x_{jp})$$

where $x_0 < x_1 < x_2 < \dots$; the sum begins at x_0 ($x = A$) and terminates when no additional, significant probability can accrue. Denote the sum by Φ .

The probability that there are flaws bigger than A which are not caught by inspection is approximated by:

$$\sum_{n=1}^{\infty} \exp(-\lambda) \lambda^n / n! \left\{ \sum_{i=1}^n (n, i) \Phi^i (1-\Phi)^{n-i} \right\}$$

where (n, i) denotes the binomial coefficient.

$$\begin{aligned} &= \exp(-\lambda) \sum_{n=1}^{\infty} \exp(-\lambda) \lambda^n / n! \{1 - (1-\Phi)^n\} \\ &= \exp(-\lambda) \{(\exp(\lambda) - 1) - (\exp(\lambda(1-\Phi)) - 1)\} \\ &= 1 - \exp(-\lambda\Phi) \end{aligned}$$

It may be that the dirtiness distribution $D(A)$ can be estimated without recourse to the Poisson model. If it is assumed that the model still underlies the distribution, then:

$$F(A) = 1 + (1/\lambda) \ln[1 - D(A)]$$

λ remains unknown. Note that $\Phi = \tau/\lambda$ where

$$\tau = \sum_{j=1}^{\infty} \{ \ln [1 - D(x_{j+1})] - \ln [1 - D(x_j)] \} \widetilde{POD}(x_{j1}) \widetilde{POD}(x_{j2}) \dots \widetilde{POD}(x_{jp})$$

It follows that the probability that there are flaws of size greater than or equal to A which elude inspection assumes the simple approximate form:

$$1 - \exp(-\tau)$$

5.9 Optimization

PDAS will provide the capability of optimizing the design of a selected disk to minimize weight while maintaining low net failure probability. Two optimization options are being considered: ADS (Automated Design Synthesis, *Reference 45*) and the Downhill Simplex Method (*Reference 46*).

Shown in *Figure 55* is an example of a design optimization for burst generated using ADS (*Reference 47*). Burst calculation was based on the empirical model (see Section 3.3) using elastic stresses computed by a simple stacked ring disk program.

5.10 Distributed Processing

We are investigating the possibility of distributed processing using our workstation network. Each point on the response surface will require the same sequence of calculations: thermal/stress/displacement/life. Each sequence can conveniently be performed on a single Unix workstation without significant drain on disk-space. Software is available to control simultaneous execution on multiple units. Ideally, an entire response surface could be evaluated in a single day, though it is more likely that two to three days may be required. Given the response surface, the risk integration is fairly straightforward. Response gradients will identify the next iteration.

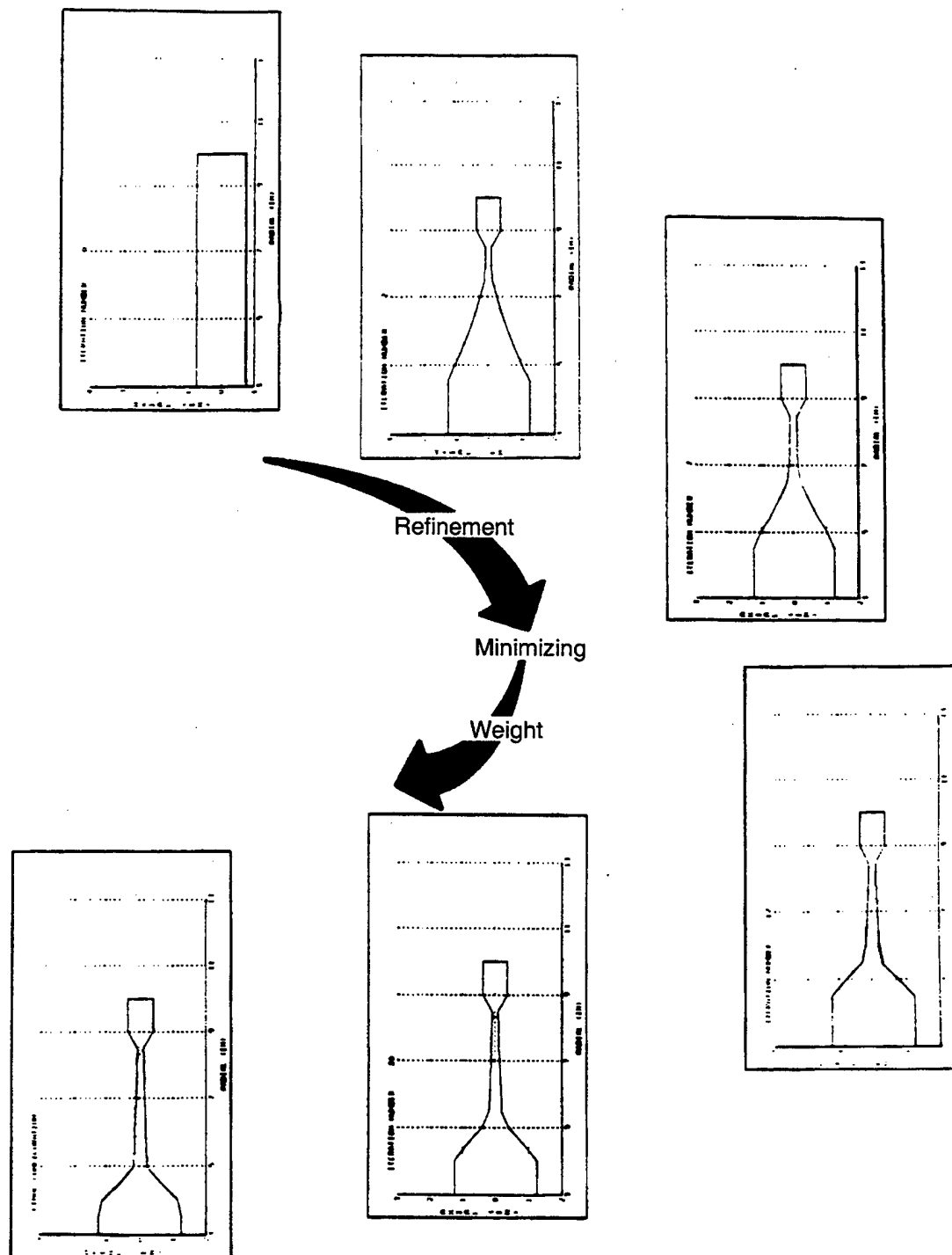


Figure 55. ADS Design Optimization.

6.0 Development of Acceptable (or Appropriate) Risk Criteria

In this section we propose an appropriate level of risk based on the historical FAA/NAPC data discussed in Section 2.1. Analysis of the data was easy; clarifying what is meant by 'appropriate' was not. The clarification constructed below includes an examination of the nature of risk calculations: the need for extrapolation, the wisdom of validation and the question of interpretation. The point is made that risk is a necessary companion of survival, and that requiring exceedingly low risks (e.g. $1/10^6$ over a 30 year life) is neither supportable nor productive.

It is concluded that the recommendation of a design limit on failure rate of 7.2/1,000 per engine lifetime is supportable based on commercial experience. To be accepted for engine certification, the risk calculation must, to the satisfaction of the certifying agency, be demonstrated to be methodologically sound and adequately supported by data. Believing that these conditions can be reasonably met, we argue that risk-based design is preferable to design based on safety factors.

6.1 Analysis of FAA/ NAPC Data

A number of tables were constructed from the FAA/NAPC reports (*References 3-18*) and serve as the basis for the following discussion. Summarizing their contents:

- Table 1 - The number of engine failures from 1972 to 1987 by model and by failure type (blade, seal, disk, rim, none, other).
- Table 2 - The number of disk/rim failures from 1972 to 1987 by model and by cause code (design and life prediction problems, secondary causes, foreign object damage, quality control, operational exceedance, assembly and inspection error, unknown).

Includes breakdown by component type (fan, compressor, turbine).

- Table 3 - The number of disk/rim failures from 1972 to 1987 by model and by flight condition (Inspection/Maintenance, Taxi/Ground Handling, Takeoff, Climb, Cruise, Descent, Approach, Landing, Hovering, Unknown).
- Table 9 - The average number of large engines in service by model and by year from 1972 to 1987.
- Table 10 - The number of disk failures (combining the FAA disk and rim classifications) by model and by year from 1972 to 1987.
- Table 11 - Failure rates (numbers of disk failures per 1000 engines) by model and by year from 1972 to 1987. Calculated from Tables 10 and 11.
- Table 12 - Hours of operation by model and by year from 1981 to 1987.
- Table 13 - Average hours per engine by model and by year from 1981 to 1987. Calculated from Tables 10 and 13.
- Table 14 - Hours of operation by model and by year from 1972 to 1987. Entries for the years 1972 through 1980 were estimated by applying the average of the average hours per engine for each model (the bottom line of Table 14) to the average numbers of engines in service from Table 10. Entries for the years 1981 through 1987 are taken directly from Table 13.
- Table 15 - Failure rates (number of disk failures per million engine hours) by model and by year from 1972 to 1987. Calculated from Tables 10 and 14. The bottom line of this table is the average failure rate of each

model over the covered 16-year period. It is calculated from the total numbers of failures for each model (*Table 11*, bottom line) and the estimated total operating hours for each model (*Table 14*, bottom line).

The 1972–1987 time period covered by the FAA/NAPC reports is interesting in that it embraces such a range of engine lines at different points of their life cycles. The failure rates do not necessarily reflect the intrinsic reliability of the engines since failure rates can be reduced by frequent inspections and periodic replacement of suspect parts. These details are highly proprietary.

The JT8 is particularly interesting. Its fleet is already mature at the beginning of the sixteen year reporting period, the number of engines growing from about 3,000 to nearly 6,000, many times the number of the closest competitor. (Note: The figure reported in *Table 10* of 4,000 engines for the year 1972 is suspicious

given the decrease to 3,104 for the following year.) The failure rates seem low, but reasonably constant (*Tables 12* and *15*). It is certainly not known whether this reflects a small number of recurring problems or the occasional appearance of a new problem, but it does provide a standard for comparison.

Tables 10 and *11* provide yearly breakdowns of the average numbers of engines in operation from year to year and the number of disk failures. Since the individual histories are not provided, it is not possible to assess failure probabilities as a function of engine life, but it does serve to demonstrate the general levels of safety provided by the airlines.

During the late 70's and early 80's the young CF6 family of engines suffered a rash of failures (*Table 11*). The problems were fixed, with no additional failures from 1983 to 1987. 8.9 million hours were logged over this time (*Table 15*). At the 1.2/million failure rate experienced during the problem period, 10 to 11 additional

Table 9. Average Number of Engines in Operation.

Year	JT3	JT4	JT8	JT9	PWA2037	CF6	CFM56	RB-211	ALL
1972	2,376	314	4,000	422	--	111	--	20	7,243
1973	2,192	272	3,104	464	--	210	--	112	6,354
1974	1,992	172	3,200	470	--	252	--	220	6,306
1975	1,892	212	3,276	470	--	297	--	283	6,430
1976	1,684	217	3,385	486	--	103	--	312	6,187
1977	1,632	209	3,548	386	--	312	--	235	6,322
1978	1,514	120	3,809	513	--	338	--	239	6,533
1979	1,427	103	4,134	554	--	366	--	254	6,838
1980	1,188	84	4,380	632	--	420	--	275	6,979
1981	950	73	4,484	621	--	451	--	298	6,877
1982	717	--	5,061	641	--	488	--	344	7,251
1983	492	--	4,646	654	--	455	--	332	6,579
1984	379	--	4,834	690	--	529	--	311	6,743
1985	195	6	5,051	672	29	563	362	307	7,185
1986	223	--	5,483	731	67	644	512	361	8,021
1987	280	--	5,854	751	111	630	626	416	8,668

Table 10. Number of Disk/Rim Failures.

Year	JT3	JT4	JT8	JT9	PWA2037	CF6	CFM56	RB-211	ALL
1972	1	1	1	0	--	1	--	1	5
1973	2	0	2	1	--	0	--	0	5
1974	1	1	0	0	--	1	--	0	3
1975	0	0	2	3	--	0	--	0	5
1976	1	0	1	0	--	0	--	0	2
1977	0	0	0	0	--	3	--	1	4
1978	0	0	1	0	--	1	--	1	3
1979	1	0	0	0	--	1	--	0	2
1980	0	0	4	2	--	2	--	1	9
1981	0	0	1	0	--	2	--	0	3
1982	0	--	2	0	--	1	--	0	3
1983	2	--	2	0	--	0	--	0	4
1984	0	--	3	1	--	0	--	0	4
1985	0	0	1	0	0	0	0	0	1
1986	0	--	0	0	0	0	0	0	0
1987	0	--	1	10	0	0	0	0	1
ALL	8	2	21	7	0	12	0	4	54

Table 11. Failure Rates - Disk/Rim Failures per 1000 Engines.

Year	JT3	JT4	JT8	JT9	PWA2037	CF6	CFM56	RB-211	ALL
1972	0.42	3.18	0.25	0	--	9.01	--	50.00	0.69
1973	0.91	0	0.64	2.16	--	0	--	0	0.79
1974	0.50	5.81	0	0	--	3.97	--	0	0.48
1975	0	0	0.61	6.38	--	0	--	0	0.78
1976	0.59	0	0.30	0	--	0	--	0	0.32
1977	0	0	0	0	--	9.62	--	4.26	0.63
1978	0	0	0.26	0	--	2.96	--	4.18	0.46
1979	0.70	0	0	0	--	2.73	--	0	0.29
1980	0	0	0.91	3.16	--	4.76	--	3.64	1.29
1981	0	0	0.22	0	--	4.43	--	0	0.44
1982	0	--	0.40	0	--	2.05	--	0	0.41
1983	4.07	--	0.43	0	--	0	--	0	0.61
1984	0	--	0.62	1.45	--	0	--	0	0.59
1985	0	0	0.20	0	0	0	0	0	0.14
1986	0	--	0	0	0	0	0	0	
1987	0	--	0.17	0	0	0	0	0	0.12

Table 12. Engine Hours Accrued (Millions).

Year	JT3	JT4	JT8	JT9	PWA2037	CF6	CFM56	RB-211	ALL
1981	1.640	0.035	11.500	2.130	--	1.340	--	0.944	17.59
1982	1.256	--	11.740	2.199	--	1.399	--	1.052	17.65
1983	0.785	--	11.365	2.260	--	1.299	--	0.923	16.6
1984	0.560	--	12.775	2.415	--	1.634	--	0.893	18.28
1985	0.200	0.002	13.574	2.304	0.077	1.765	0.848	0.932	19.70
1986	0.275	--	14.369	2.582	0.192	1.998	1.384	1.094	21.39
1987	0.419	--	15.352	2.731	0.321	2.186	1.794	1.335	24.14
ALL	5.135	0.037	90.675	16.621	0.590	11.621	4.026	7.173	135.9

(Statistics not available prior to 1981)

Table 13. Hours Accrued per Engine.

Year	JT3	JT4	JT8	JT9	PWA2037	CF6	CFM56	RB-211
1981	1,726	481	2,565	3,430	--	2,971	--	3,168
1982	1,752	--	2,320	3,431	--	2,867	--	3,058
1983	1,596	--	2,446	3,456	--	2,855	--	2,780
1984	1,478	--	2,643	3,500	--	3,089	--	2,871
1985	1,026	333	2,687	3,429	2,655	3,135	2,343	3,036
1986	1,233	--	2,621	3,532	2,866	3,102	2,703	3,030
1987	1,496	--	2,622	3,636	2,892	3,470	2,866	3,209
AVG.	1,472	407	2,558	3,488	2,804	3,070	2,637	3,022

(Statistics not available prior to 1981)

Table 14. Engine Hours Accrued (Millions).

Year	JT3	JT4	JT8	JT9	PWA2037	CF6	CFM56	RB-211	ALL
1972	3.500	0.128	10.232	1.472	--	0.341	--	0.060	15.73
1973	3.227	0.111	7.940	1.618	--	0.645	--	0.338	13.88
1974	2.932	0.070	8.186	1.639	--	0.774	--	0.665	14.27
1975	2.785	0.086	8.380	1.639	--	0.912	--	0.855	14.66
1976	2.479	0.088	8.C59	1.695	--	0.316	--	0.943	14.18
1977	2.402	0.085	9.076	1.346	--	0.958	--	0.710	14.56
1978	2.229	0.049	9.743	1.789	--	1.038	--	0.722	15.57
1979	2.101	0.042	10.575	1.932	--	1.124	--	0.7C8	16.54
1980	1.749	0.034	11.204	2.204	--	1.289	--	0.831	17.31
1981	1.640	0.035	11.500	2.130	--	1.340	--	0.944	17.59
1982	1.256	--	11.740	2.199	--	1.399	--	1.052	17.65
1983	0.785	--	11.365	2.260	--	1.299	--	0.923	16.63
1984	0.560	--	12.775	2.415	--	1.634	--	0.893	18.28
1985	0.200	0.002	13.574	2.304	0.077	1.765	0.848	0.932	19.70
1986	0.275	--	14.369	2.582	0.192	1.998	1.384	1.094	21.89
1987	0.419	--	15.352	2.731	0.321	2.186	1.794	1.335	24.14
ALL	28.539	0.730	174.670	31.955	0.590	19.018	4.026	13.065	272.6

Table 15. Failure Rates - Disk/Rim Failures (Number per Million Engine Flight Hours).

Year	JT3	JT4	JT8	JT9	PWA2037	CF6	CFM56	RB-211	ALL
1972	0.286	7.813	0.098	0	--	2.933	--	16.667	0.318
1973	0.620	0	0.252	0.618	--	0	--	0	0.360
1974	0.341	14.286	0	0	--	1.292	--	0	0.210
1975	0	0	0.239	1.830	--	0	--	0	0.341
1976	0.403	0	0.11S	0	--	0	--	0	0.141
1977	0	0	0	0	--	3.132	--	1.408	0.274
1978	0	0	0.103	0	--	0.963	--	1.385	0.193
1979	0.476	0	0	0	--	0.890	--	0	0.121
1980	0	0	0.357	0.907	--	1.552	--	1.203	0.520
1981	0	0	0.087	0	--	1.493	--	0	0.17
1982	0	--	0.170	0	--	0.715	--	0	0.170
1983	2.548	--	0.176	0	--	0	--	0	0.241
1984	0	--	0.235	0.414	--	0	--	0	0.219
1985	0	0	0.074	0	0	0	0	0	0.051
1986	0	--	0		0	0	0	0	0
1987	0	--	0.065	0	0	0	0	0	0.04
ALL	0.280	2.740	0.120	0.219	0	0.631	0	0.306	

failures would have been expected. If failures occur at 0.12/million rate estimated from the JT8 experience, 1 additional failure would have been expected. The CF6 fleet may have stabilized, but it will take time to tell.

Similar trends are noted for the RB-211 which was introduced at about the same time as the CF6 and for the JT9 which was introduced somewhat earlier. While disconcerting, it is not unexpected that engines must push their way through a break-in barrier.

Summarizing, a large commercial fleet of multiple engine aircraft was managed for 270 million engine hours of operation with only 54 disk failures. This failure rate has not had a crippling impact on schedule commitments, manufacturing and maintenance requirements, or life cycle cost. Certainly, improving this rate would be desirable, but **Table 2** shows that only 13 of the 54 failures were directly attributable to inadequate design. The most stringent design practices probably would not reduce failure rates by more than a factor of 2.

Still, given continuing improvements in all aspects of engine design, analysis, testing, manufacturing, inspection and life management, we expect that newer engines should suffer fewer break-in problems. **Table 15** does suggest that this may be true.

6.2 Application of Probabilistic Methods

Based on the JT8 experience, an acceptable rate of disk failure might be set at 0.12 per million engine hours. The average risk per flight (assuming an average time per flight of 3 hours) is 3.6×10^{-7} . The risk per engine lifetime, given a 20,000 cycle (flight) engine, is a surprising 7.2/1,000 – not far from 1 in a 100. (Section 6.4 discusses translation to individual disks.)

What does this number 7.2/1,000 really mean? Qualitatively, risk is a condition of uncertainty with undesirable potential results. In attempt-

ing to quantify risk, probability theory is called on. This assumes that there is predictability even in randomness which is sometimes true; we refer to physics and chemistry and the success of statistical and quantum mechanics, or to genetics and gambling where much simpler combinatoric predictions work on average. In these applications, populations may be sampled repeatedly and repeatably (the populations are open). Their statistical distributions can be derived from basic principles or inferred by preliminary sampling, and then applied to predict the results of subsequent sampling.

A population of engines is closed rather than open; a few thousand will be made over a span of several years. It is closed and probably not even stable. During production, design revisions may be made; melting and forging practices may be modified; subcomponent suppliers may change. Consequently, computed risks, while stated as probabilities, are usually not verifiable. A predicted 1/1,000 risk of failure can be disputed if enough fail, but can not be verified, and while 1/10,000 may be lower risk than 1/1,000, the difference can not be demonstrated. Decisions are qualitative despite the quantitative language.

It is necessary to discuss three activities: Extrapolation, Validation, Interpretation

Extrapolation

Stating design limits in terms of small probabilities of failure (say 1/10,000) demonstrates recognition that failures are very serious and should never willingly be allowed to happen. To go beyond this simple interpretation, however, requires deeper understanding of the origins of the numbers.

The failure probability of a jet powerplant is inferred from that of a critical component (or interactions of critical components) which in turn are inferred from small LCF specimens.

At this lowest level (the LCF data programs) it is almost unheard of that the number of tests is large enough to confidently estimate the 1/10,000 failure probability without considerable extrapolation. Considerably more remote failure probabilities are required if a size effect translation is necessary to scale the failure distribution. For example, the 1/10,000 life for an array of 100 boltholes is very nearly the 1/1,000,000 life for a single bolthole.

Thus, the basic desire that design risk be so low as to be unverifiable makes the need for extrapolation unavoidable. Estimation of extreme distributional quantiles presupposes that they have meaning, but there are limits in any physical application. As is the case with all models of the real world, statistical models are approximations.

In *Reference 48*, W Weibull makes the following comments:

"The number of specimens . . . depends on the information wanted. The mean or median of the fatigue lives may be sufficiently accurately estimated from 6 or 10 specimens. The scatter measured for instance by the standard deviation may demand 20, but the distribution function will not be too accurately determined with 100 specimens. The decision between two adjacent functions may increase the necessary number to several thousands."

"The latter statement may be illustrated by comparing the logarithmic normal distribution with the function $F(x) = 1 - \exp(-(x-x_u/x_0)^m)$." [The distribution function $F(x)$ is, of course, known by the name Weibull.]

"In fact, a significant experimental decision between these two distribution functions on the basis of the chi-square test would require something like 10,000 observed values and is thus practically excluded, in spite of the fact that the lower limit of the

former function is $-\infty$ and of the latter is -3.218 ."

DM Neal, WT Matthews and MG Vangel have recently published a study showing how minute contamination of assumed statistical models can result in real failure probabilities of 1/1,000 vs. calculated 1/100,000 (*Reference 49*). In their paper they recalled a couple of quotable quotes:

"When dealing with probabilities a clear distinction should be made between conditions arising in design of inexpensive mass products in which the probability figures are derived by statistical interpretation of actual observations or measurements (since sufficiently large number of observations are actually obtainable), and conditions arising in design of structures or complex systems. In the latter, probability figures are used simply as a scale or measure of reliability that permits the comparison of alternative designs. The figures can never be checked by observations or measurement since they are obtained by extrapolations so far beyond any possible range of observation that such extrapolation can no longer be based on statistical arguments but could only be justified by relevant physical reasoning. Under these conditions the absolute probability figures have no real significance ..." [A.M. Freudenthal, *Reference 50*]

"The probability of failure $P_f = 1 \times 10^{-6}$ has an Alice in Wonderland flavor and should be banned from non-fiction literature." [L. Breiman, *Reference 51*]

In the end, extrapolation is a leap of faith conditioned by experience.

Modeling should begin with identifying the sources of variability and isolating those which truly are statistical. The importance of this can not be overemphasized. Reasonable extrapolations are possible given tight distributions, and

experience suggests that disk alloy processing can be controlled to keep distributions tight. Property distributions may in fact be truncated by quality checks, effectively defining minimum capabilities. If for a material the real, uncontrollable scatter is uncomfortably large relative to its desired average, it might be suggested that the material not be used where safety is a concern.

Validation

Probabilistic design methodology must be validated. Given that extrapolations are acceptable, it is important that the assumptions made in putting them together are correct. It was shown in Section 3.4.1 that terrible errors can arise with even simple size effect translations. This will only be exacerbated given complicated systems with many competing failure mechanisms.

For all practical purposes validation must be done within the range of probabilities 0.01 to 0.99. The MISSYDD verification study was, for example, rigorously designed to judge adequacy of the model over a large range of life, but a small range of probability. (Section 3.6) To achieve this, the specimens were prepared from seeded powder metal. Given that real rates of flaw occurrence are orders of magnitude lower than the seeding density, it is entirely reasonable to accept that the failure probabilities are proportionately lower. More traditional accelerated testing strategies (e.g. proof tests at 20% overstress) are similarly defended.

Interpretation

The FAA data supports the belief that disk failures are rare, but also points out that they do occur. Safety factors do not prevent them; neither will PRDS (again, recognize from *Table 2* that a large number of disk failures have nothing to do with design or analysis). Premature failures very often mean that something has

been overlooked. If assumptions are wrong, reducing the design level may or may not affect the real risk.

PRDS will produce a quantitative tool validatable under controlled conditions. All analysis techniques are defended in this way. Finite element methods, for example, can seldom be directly validated for real parts under real operating conditions, but they can be shown to work well for simple geometries for which analytical solutions are available and for more complicated geometries when measurements can be made under simple loading conditions.

Safety factors are not, by contrast, quantitative in this sense. Experience tells us that we have been successful when we apply maximum stresses to minimum properties and divide by 3. We don't have a lot of failures, but maybe we could have skipped the division and still had enough conservatism; we just don't know.

6.3 Appropriate Risk

There have been many books written under the general classification: *Risk and Society*. Six titles are included as *References 52-57*. Five are edited collections of papers. The sixth, a collaboration by five authors, is more systematic in its development. With the exception of one chapter of one book (*Reference 58*), the contributions are all essentially historical and/or philosophical.

It is not possible to set an appropriate level of risk that everyone will accept (or that anyone will accept all of the time). People take the risks that they want to take, usually denying that the risk is real. People rail against risks that they do not want to take, sometimes in the face of considerable evidence that the risk is quantifiably insignificant.

Many risks are required for the survival and advancement of humanity. There is risk in agriculture, in manufacturing, in power generation and distribution, in transportation,

in medicine – risk which impacts everyone to a greater or lesser extent.

It is not possible to set a universally acceptable level of risk. The ENSIP MIL-STD-1783 (*Reference 48*) was written requiring for intrinsic defects that “Assumed defect size will encompass 99.9% (using a scatter factor of 2 on residual life) of the distribution.” The adjectives “maximum” and “minimum” are often interpreted as plus and minus 3σ (99.865% and 0.135%).

We propose that the 7.2/1,000 failure rate suggested by the FAA statistics is an appropriate level of risk for design. It is what people are currently willing to accept (albeit unconsciously). It may be reasonable, given the fuzziness of such a number, to reduce this slightly to the more traditional 1/1,000, but there is no compelling reason to add lots of zeroes for the sake of comfort, unless they can be added at little or no cost. In reality, adding zeroes probably has no impact on real risk. More planes are lost by pilot error, weather conditions and terrorism than by engine failure. Moreover, adding zeroes with current technology does decrease engine efficiency which wastes natural resources and increases operating costs (two negative impacts on society).

There does appear to be some legal precedence to this position. The following case is interesting. It is not known whether the ruling is either unique or in contrast to other decisions. The account is excerpted from *Reference 59*.

“In 1978 the Occupational Safety and Health Administration (OSHA) promulgated a new standard lowering the permissible exposure limit (PEL) to benzene from 10 ppm to 1 ppm. The revised standard was challenged in court, and ultimately the Supreme Court ruled against the agency (*Reference 60*). The Court rejected OSHA’s contention that the applicable law

permitted the Administrator to reduce the standard simply because benzene is a carcinogen and there is no proven safe level of exposure. The agency had to show that exposure at current levels creates a significant risk that would be significantly reduced by the new standard. OSHA’s failure to do this meant that it had not met its statutorily-imposed burden of showing that the lower standard is ‘reasonably necessary and appropriate’ (*Reference 61*).”

Given a mandated level of risk, engine manufacturers must be able to demonstrate prior to certification the validity of the analysis backing their risk estimates. The methodology must be sound, and its application supported by adequate data. Given the subjectivity in accepting any extrapolation (they are always on the fringe of demonstration), it doesn’t make particular sense to define adequate, but rather it is the responsibility of the reviewing agency to be convinced.

This position is a “bootstrapping approach” as described in *Reference 57*. The following is the lead-in paragraph to the relevant chapter in this book (p. 79):

“Both the professional-judgement and formal-analysis approaches assume that we can think our way to sensible acceptable-risk decisions. With a little computational help, one can accommodate all relevant points of view and achieve a balance that acknowledges political and technical realities. Proponents of the bootstrapping approach reject this assumption, arguing that risks cannot be analyzed adequately in any short period of time. Rather, society achieves an acceptable trade-off between risks and benefits only through a protracted period of hands-on experience that allows for trial-and-error learning.”

Today's designs probably are safer. Many of the design problems which have bitten in the past are unlikely to recur. Materials are better; processes have improved. Still, there is little data to support the contention. The FAA reports have not caught up to the explosion of usage of the CFM56, our newest engine line, although internal data suggests that it has a remarkably low rate of problems of any kind. It is an evolving story. 7.2/1,000 is appropriate for today.

The above discussion has been in the context of commercial aviation. Still, the basic points apply equally to the military:

- Risk based on probabilistic analysis is quantifiable ... risk based on safety factors is not.
- An appropriate level of risk must be set by Command weighing the needs of the many against those of the individual. War is a national recognition of necessary personal risk. Limits must be set which include thrust-to-weight and life cycle cost. Risk to the pilot must certainly be considered and is not necessarily in conflict with other variables in the risk equation. For example: high individual risk probably means low reliability and high life cycle cost. On the other hand, over-conservative design means only death from another direction.
- For peacetime application, a design level any lower than 7.2/1,000 is difficult to justify.
- Designing to that level will not prevent surprises.

6.4 System Risk versus Component Risk and Some Final Considerations

Analysis of the FAA data, supplemented by some assumptions, led to a suggested appropriate level of risk for design stated per engine

lifetime. Other assumptions would be needed to translate this level of risk to the individual disks. Rather than make the assumptions, a few possible scenarios are presented:

- A set of n disks (call it an engine) each with a failure probability of F has a combined failure probability of $1 - (1 - F)^n$, approximately nF if nF is a small number (less than 1/10). Given that engines have on the order of 10 disks, F must be on the order of 0.72/1,000 to yield the acceptable level of 7.2/1,000 for the engine.

This is certainly an oversimplification. *Table 2* suggests that engines are not so evenly balanced. Fan disks probably have lower failure probabilities than compressor or turbine disks, and compressor disks probably have lower failure probabilities than turbine disks (while the number of reported compressor and turbine failures are approximately equal, compressors have more disks than turbines).

- There are 1 or 2 problem disks in an engine, say 2; their failure probabilities are comparable and considerably greater than the failure probabilities of the other disks. Then F must be on the order of 3.3/1,000 to yield the acceptable level of 7.2/1,000 for the engine.
- There is 1 problem disk in an engine. It is so much a problem that it is planned to replace it at half the engine life. Let F be the failure probability of this disk (that is, the failure probability at the disk life which is half the engine life). Again, F must be on the order of 3.3/1,000 to yield the 7.2/1,000 level for the engine.

These last scenarios are more realistic, but still miss important points. Consider the calculation which led to the number 7.2/1,000:

Based on the JT8 experience, an acceptable rate of disk failure might be set at 0.12 per million engine hours. The average risk per flight (assuming an average time per flight

of 3 hours) is 3.6×10^{-7} . The risk per engine lifetime, given a 20,000 cycle (flight) engine, is a surprising 7.2/1,000 – not far from 1 in a 100.

Failure probability is not constant over the life of an engine; ideally it increases monotonically as cycles are accrued. While we don't know the age distribution of the JT8 fleet, we do know that the average engine adds only 2,558 hours or about 853 cycles per year (*Table 14*), and conclude that most engines are far short of the assumed 20,000 cycle design life. It must follow then that the actual failure probability at 20,000 is considerably higher than 7.2/1,000.

A fleet of engines is not, however, a collection of specimens which are all tested to failure. A fleet grows gradually, and as problems are detected they are fixed (design changes are implemented ... retrofits are made); thereby, failure probabilities are controlled. At GEAE, a Life Management Programs section provides this assurance.

Summarizing, 7.2/1,000 per engine is an appropriate level of risk for design. Appropriate levels for individual disks, levels which are necessarily lower, can be readily calculated. The actual level of risk per engine for today's commercial fleet projected forward in time is much higher, which is not to say that thousands of engines will be expected to fail. The risk will be managed.

Phase I - References

1. Nessus, Southwest Research Institute, San Antonio, TX, 78228-0510.
2. SIESTA (System for Integrated Structural Analysis), GE Aircraft Engines.
3. DeLucia, R.A. and Mangano, G.J., "Rotor Burst Protection Program: Statistics on Aircraft Gas Turbine Engine Rotor Failures that Occurred in U.S. Commercial Aviation during 1972," NAPTC-PE-40, Naval Air Propulsion Test Center, Trenton, NJ 08628, (March 1974).
4. DeLucia, R.A. and Mangano, G.J., "Rotor Burst Protection Program: Statistics on Aircraft Gas Turbine Engine Rotor Failures that Occurred in U.S. Commercial Aviation during 1973," NAPTC-PE-61, Naval Air Propulsion Test Center, Trenton, NJ 08628, (August 1975).
5. DeLucia, R.A. and Mangano, G.J., "Rotor Burst Protection Program: Statistics on Aircraft Gas Turbine Engine Rotor Failures that Occurred in U.S. Commercial Aviation during 1974," NAPTC-PE-67, Naval Air Propulsion Test Center, Trenton, NJ 08628, (September 1975).
6. DeLucia, R.A. and Mangano, G.J., "Rotor Burst Protection Program: Statistics on Aircraft Gas Turbine Engine Rotor Failures that Occurred in U.S. Commercial Aviation during 1975," NAPTC-PE-106, Naval Air Propulsion Test Center, Trenton, NJ 08628, (May 1977).
7. DeLucia, R.A. and Salvino, J.T., "Rotor Fragment Protection Program: Statistics on Aircraft Gas Turbine Engine Rotor Failures that Occurred in U.S. Commercial Aviation during 1976," NAPC-PE-9, Naval Air Propulsion Center, Trenton, NJ 08628, (July 1978).
8. DeLucia, R.A. and Salvino, J.T., "Rotor Fragment Protection Program: Statistics on Aircraft Gas Turbine Engine Rotor Failures that Occurred in U.S. Commercial Aviation during 1977," NAPC-PE-23, Naval Air Propulsion Center, Trenton, NJ 08628, (July 1979).
9. DeLucia, R.A. and Salvino, J.T., "Rotor Fragment Protection Program: Statistics on Aircraft Gas Turbine Engine Rotor Failures that Occurred in U.S. Commercial Aviation during 1978," NAPC-PE-23, Naval Air Propulsion Center, Trenton, NJ 08628, (September 1981).
10. DeLucia, R.A. and Salvino, J.T., "Rotor Fragment Protection Program: Statistics on Aircraft Gas Turbine Engine Rotor Failures that Occurred in U.S. Commercial Aviation during 1979," NAPC-PE-80, Naval Air Propulsion Center, Trenton, NJ 08628, (October 1982).
11. DeLucia, R.A., Salvino, J.T., Gagliardi, L.J., "Rotor Fragment Protection Program: Statistics on Aircraft Gas Turbine Engine Rotor Failures that Occurred in U.S. Commercial Aviation during 1980," NAPC-PE-84, Naval Air Propulsion Center, Trenton, NJ 08628, (September 1984).
12. DeLucia, R.A., Salvino, J.T., and Russo, T., "Statistics on Aircraft Gas Turbine Engine Rotor Failures that Occurred in U.S. Commercial Aviation during 1981," DOT/FAA/CT-86/42, FAA Technical Center, Atlantic City International Airport, NJ 08405, (March 1987).
13. DeLucia, R.A. and Salvino, J.T., "Statistics on Aircraft Gas Turbine Engine Rotor Failures that Occurred in U.S. Commercial Aviation during 1982," DOT/FAA/CT-88/23, FAA Technical Center, Atlantic

- City International Airport, NJ 08405, (July 1988).
14. DeLucia, R.A. and Salvino, J.T., "Statistics on Aircraft Gas Turbine Engine Rotor Failures that Occurred in U.S. Commercial Aviation during 1983," DOT/FAA/CT-89/5, FAA Technical Center, Atlantic City International Airport, NJ 08405, (March 1989).
 15. DeLucia, R.A., Salvino, J.T., and Fenton, B.C., "Statistics on Aircraft Gas Turbine Engine Rotor Failures that Occurred in U.S. Commercial Aviation during 1984," DOT/FAA/CT-89/6, FAA Technical Center, Atlantic City International Airport, NJ 08405, (June 1989).
 16. DeLucia, R.A., Salvino, J.T., and Fenton, B.C., "Statistics on Aircraft Gas Turbine Engine Rotor Failures that Occurred in U.S. Commercial Aviation during 1985," DOT/FAA/CT-89/7, FAA Technical Center, Atlantic City International Airport, NJ 08405, (July 1989).
 17. DeLucia, R.A., Salvino, J.T., and Fenton, B.C., "Statistics on Aircraft Gas Turbine Engine Rotor Failures that Occurred in U.S. Commercial Aviation during 1986," DOT/FAA/CT-89/30, FAA Technical Center, Atlantic City International Airport, NJ 08405, (January 1990).
 18. DeLucia, R.A., Salvino, J.T., and Blake, J., "Statistics on Aircraft Gas Turbine Engine Rotor Failures that Occurred in U.S. Commercial Aviation during 1987," DOT/FAA/CT-90/19, FAA Technical Center, Atlantic City International Airport, NJ 08405, (January 1991).
 19. ANSYS, Swanson Analysis Systems, Inc., P.O. Box 65, Houston, PA, 15342.
 20. Analysis by KE Seitzer, GE Aircraft Engines (4/6/89).
 21. CLASS/MASS, GE Aircraft Engines.
 22. McKnight, R.L., Brown, JF, Holt, R.V. and Chen, P.C., "CYANIDE — Cyclic Analysis of Inelastic Deformation," R79AEG578, GE Aircraft Engines (October 1979).
 23. Hodge, P.E. and White, S.H., "A Quantitative Comparison of Flow and Deformation Theories of Plasticity," J of Applied Mechanics, 17, pp. 180-4 (1950).
 24. Bathe, K.J., ADINA (Automatic Dynamic Incremental Nonlinear Analysis), MIT Report 82448-1, Massachusetts Institute of Technology, Cambridge, MA 02139 (December 1978).
 25. Storrs, CT, and Coffin, L.F. "Fatigue at High Temperature," presented at the 1972 Symposium on Fatigue at Elevated Temperatures, University of Connecticut, June 18-23, 1972.
 26. Monzel, F.J. "Rotor Overspeed Integrity (Burst)," Design Practice 3210, GE Aircraft Engines (February 1983).
 27. Hallinan, M., "The Design of Rotating Disks to Avoid Burst at Overspeed," TIS R60SE94, GE Aircraft Engines (1960).
 28. Presentation by RH Weisgerber, GE Aircraft Engines (2/20/84).
 29. Analysis by McClintick, B. GE Aircraft Engines (9/14/78).
 30. Model by Coomer, J.T., GE Aircraft Engines (6/10/91)
 31. Gibbons, J.D., Nonparametric Statistical Inference, McGraw-Hill, Inc. (1971).
 32. Yau, J.F., Laflen, J.H., and Gooden, O. C., "A New Stress Intensity Factor Solution of Surface Cracks for Fatigue Crack Growth Analysis and Residual Life Prediction," R83AEB404, GE Aircraft Engines (1983).
 33. "FSD F110-GE-100 ENSIP Structural Durability and Damage Tolerance Analysis Final Report," Book 2, R84AEB386, GE Aircraft Engines (1984).

34. "On the Effect of Orientation and Forging Thru-Thickness Position of Fatigue Crack Propagation Rates In DA718 - Part 1," MF Henry, General Electric Company Memo Report MOR-82-102 (1982).
35. MISSYDD (MISSion SYNthesis given Defect Distribution), GE Aircraft Engines.
36. Berens, A.P. and Hovey, P.W., "Evaluation of NDE Reliability Characterization", AFWAL-TR-81-4160, Air Force Wright Aeronautical Laboratories, Wright-Paterson Air Force Base, OH 45433 (December 1981).
37. Berens, A.P. and Hovey, P.W., "Flaw Detection Reliability Criteria, Volume I - Methods and Results", AFWAL-TR-84-4022, Air Force Wright Aeronautical Laboratories, Wright-Paterson Air Force Base, OH 45433 (April 1984).
38. Lewis, W.H., Dodd, B.D., Sproat, W.H., and Hamilton, J.K., "Reliability of Nondestructive Inspections - Final Report", Report No. SA-ALC/MEE 76-6-38-1, USAF San Antonio Air Logistics Center, Kelly AFB, Texas, (1978).
39. Cox, D.R., The Analysis of Binary Data, Methuen and Co., LTD, London, (1970).
40. Shapiro, S.S., "How to Test Normality and Other Distributional Assumptions," ASQC Basic References in Quality Control: Statistical Techniques, 3, ASQC, 161 W. Wisconsin Avenue, Milwaukee (1980).
41. McLean, R.A. and Anderson, V.L. Applied Factorial and Fractional Designs, Volume 55 of the series Statistics: Textbooks and Monographs, ASQC Quality Press, 310 W. Wisconsin Avenue, Milwaukee (1987).
42. Khuri, A.I. and Cornell, J.A., Response Surfaces, Designs and Analyses, Volume 81 of the series Statistics: Textbooks and Monographs, ASQC Quality Press, 310 W. Wisconsin Avenue, Milwaukee (1987).
43. Austin, N.K., Programming, GE Aircraft Engines.
44. Royden, H.L., Real Analysis, 2nd Edition, MacMillan Publishing Co. (1968).
45. ADS (Automated Design Synthesis), Engineering Design Optimization, Inc., 1275 Camino Rio Verde, Santa Barbara, CA 93111.
46. Nelder, J.A. and Mead, R., "Downhill Simplex Method," Computer Journal, 7, p. 308 (1965).
47. McClain, R., Application, GE Aircraft Engines.
48. Weibull, W. and Freudenthal, A.M., Written discussion submitted following the presentation: "Planning and Interpretation of Fatigue Tests," ASTM STP 121, pp. 3-22 (June 1951).
49. Neal, D.M., Matthews, W.T., and Vangel, M.G., "Model Sensitivity in Stress-Strength Reliability Computations," MTL TR 91-3, Army Materials Technology Laboratory, Watertown, MA 02172-0001 (January 1991).
50. Freudenthal, A.F., "Fatigue Sensitivity and Reliability of Mechanical Systems, Especially Aircraft Structures," WADD Technical Report 61-53, Wright-Paterson Air Force Base, OH 45433 (1961).
51. Breiman, L. and Stone, C., "Broad Spectrum Estimates and Confidence Intervals for Tail Quantiles," Technical Report No. 46, Statistics Department, U. of California, Berkeley, CA (1985). (Also to be published in Journal of Statistical Computation and Simulation.)
52. Singleton, W.T. and Hovden, J. Wiley, John & Sons, Risk and Decisions, Eds. (1987)

-
53. Risk Assessment and Management, Ed. LB Lave, Plenum Press (1987).
 54. Risk and Society, Ed. L Sjoberg, Allen and Unwin (1987).
 55. Hadden, S.G. Risk Analysis, Institutions and Public Policy, Ed. Associated Faculty Press (1984).
 56. Johnson, B.B. and Covello, V.T., The Social and Cultural Construction of Risk, Eds. D Reidel Publishing Co. (1987)
 57. Fischhoff, B., Lichtenstein, S., Slovic, P., Derby, S.L., and Keeney, R.L., Acceptable Risk, Cambridge University Press (1981).
 58. Spjotvoll, E., Singleton, W.T., and Hovden, J., Wiley, John & Sons, "Probability – Interpretations and Estimation," Risk and Decisions, Ed. pp. 13–24 (1987)
 59. Swanson, Steven M. and DeLong, James V., "Regulatory Negotiation: Lessons from Benzene," Risk Assessment and Management, Ed. LB Lave, Plenum Press, pp. 609–617 (1987).
 60. Industrial Union Department, AFL/CIO v. American Petroleum Institute, 448 U.S. 607 (1980).
 61. Occupational Safety and Health Act, 29 U.S.C. #652(8).

Phase II – Method Development

7.0 Introduction to Probabilistic Design Analysis

Science (hence, science-based engineering) builds upon the conviction that the world works by cause and effect; actions are predictable functions of initial conditions given the right equations and adequate computational power.

If inputs can be accurately measured, and outcomes are not overly sensitive to allowable deviations, this ideal is achievable. A gearbox predictably converts rotation of the input shaft into rotation of the output shaft. A hydraulic actuator translates electric potential into ram force with relatively little deviation from a governing empirical equation.

Often, however, it is the case that controlling parameters are poorly characterized and widely variable, and/or that response is sensitive to small parameter changes, and/or that response exhibits a degree of randomness which cannot be tied to identified parameters. Fatigue life is correlated to grain size, but grain size is only an approximate measure and the correlation is not perfect – scatter is observed. Cause and effect works on average, but the deviations can not be dismissed.

Variability is an annoying fact of life for all designers and manufacturers. Products from ball bats to bridges do not always perform as advertised with failures ranging from partial and of little consequence to total and catastrophic. The options available to prevent failures are sometimes limited, may be counter-productive and in some cases may simply not be worth the trouble.

Baseball bats sometimes crack; the result is most often not life-threatening and, therefore, little has been done to redesign the concept to reduce the occurrence. Bridges sometimes collapse; the result is often loss of life and usually disruption of commerce and mobility. Civil engineering practices consequently opt for overdesign of such structures. Critical support

elements may be sized to handle two or three times the maximum foreseeable service load.

There are situations when overdesign is not practical, for example where added bulk defeats the purpose of a system. Excess weight hinders performance in flight for birds, for aircraft, and for space systems. Aerodynamic forces of weight and drag can be overcome by thrust, but thrust requires energy, depletion of natural resources, and increase in pollution. In military applications, increasing weight decreases survivability when maneuverability is critical.

A design may be adjusted by rules of thumb and the risk of failure subsequently ignored as extremely (or, at least, adequately) remote, or the likelihood of failure may be recognized, quantified and controlled. Probabilistic design analysis methods attempt the latter. In the simplest case:

1. System response is completely determined by parameters p_1, p_2, \dots, p_n which are statistically distributed with distribution $D(p_1, p_2, \dots, p_n)$.
2. The response can be quantified as a function of the parameters: $R(p_1, p_2, \dots, p_n)$.
3. A failure region can be specified: $\{p_1, p_2, \dots, p_n : R(p_1, p_2, \dots, p_n) \text{ represents failure}\}$.

In theory, this information is sufficient to determine a failure probability, a measure of risk. The design can be adjusted and/or the parameter distributions controlled to hold failure probability below an appropriate limit.

Much published research focuses on tools used to estimate failure probability (see *Reference 1* for a summary of current approaches). In the next two sections, three algorithms will be evaluated: Direct Numerical Integration, Monte Carlo Integration, and the First Order Reliability Approximation.

7.1 An Example

The following scenario, while admittedly contrived, is easily stated yet challenging.

Problem Statement

Assume that there are identical pressure waves incident on a target produced by two simultaneous detonations separated by a distance $2v$. The midpoint of the detonations is related to the target by coordinates (x, y) relative to axes centered at the midpoint (**Figure 56**). Targeting is not precise. The point (x, y) is symmetrically binormally distributed about a nominal center (x_0, y_0) with standard deviation σ . Failure of the site occurs if the total pressure exceeds an ultimate value ρ . What is the failure probability?

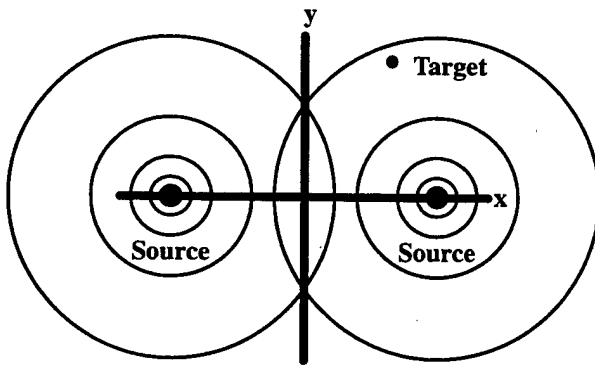
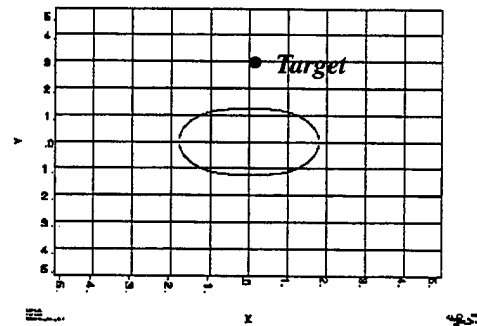


Figure 56. Dual Pressure Waves Hitting a Target.

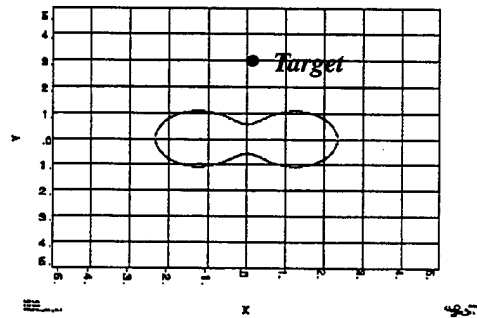
Peak pressure from each detonation varies inversely with the square of the distance from the center. Total peak pressure will be approximated by the sum of the individual peaks:

$$P(x, y) = p \cdot [(x - v)^2 + y^2]^{-1} + p \cdot [(x + v)^2 + y^2]^{-1}$$

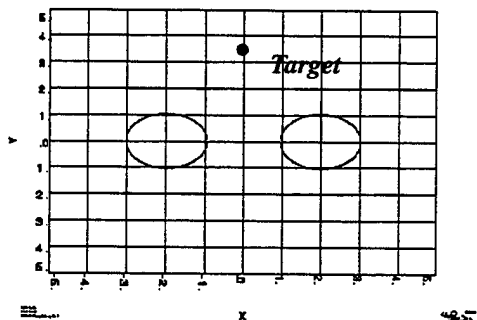
The failure region $\{(x, y) : P(x, y) > \rho\}$ can have a variety of shapes as shown in **Figure 57** for the specific choices $(x_0, y_0) = (0, 3)$, $\rho = 1$ and three values of v : 0.7, 1.3 and 2.0. With σ set to 1, estimates are made of the probability F associated with each failure region:



$v = 0.7$



$v = 1.3$



$v = 2.0$

Figure 57. Failure Regions.

Direct Numerical Integration

$$F = \frac{1}{2}\pi \int_{y_{\min}(x)}^{y_{\max}(x)} \exp\left[-\frac{(x-x_0)^2}{2\sigma^2}\right] \int \exp\left[-\frac{(y-y_0)^2}{2\sigma^2}\right] dy dx$$

where:

$y_{\min}(x)$ and $y_{\max}(x)$ solve the equation $P(x,y)=\rho$

Monte Carlo Integration

A random sample of points is generated from the binormal distribution: $\{(x_i, y_i) : i=1, 10^6\}$.

F =fraction of points satisfying $P(x_i, y_i) > \rho$

First Order Reliability Approximation

The failure regions are simply bounded as in **Figure 58**.

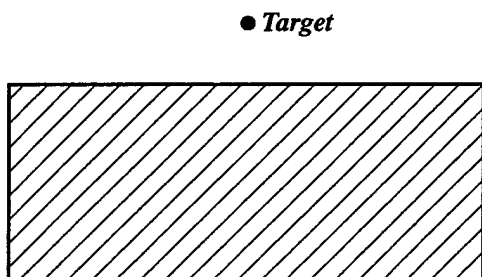


Figure 58. First Order Approximation to Failure Region.

$$F=N(-D/\sigma)$$

where: D is the distance of the point (x_0, y_0) from the shaded half-plane, and $N(z)$ is the standard normal distribution.

The results are compared in **Table 16**. Direct numerical integration and Monte Carlo integration yield essentially identical estimates for all three values of v ; the first order reliability method, as implemented, is uniformly conservative. The latter estimate could be improved by choosing different bounding regions (e.g. the polyhedral region shown in **Figure 59**), but evaluation of the probabilities associated with

the more complex regions is generally no easier than executing the exact numerical integrations.

Table 16. Failure Results Comparison.

V	Direct Numerical Integration	Monte Carlo Integration	First Order Reliability Method
0.7	0.0295	0.0297	0.0387
1.3	0.0169	0.0171	0.0266
2.0	0.0054	0.0050	0.0244

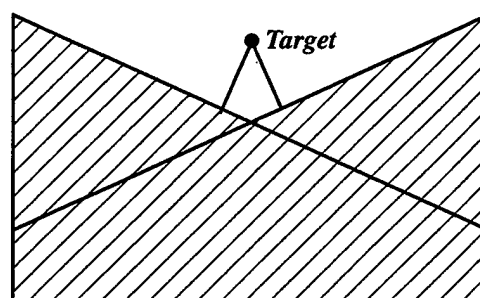


Figure 59. Polyhedral Approximation to Failure Region.

7.2 Discussion of the Estimation Algorithms

Realism could be added to the example of the preceding section by correctly modeling the propagation of the wavefronts and by adding probabilistic dimensions. For example, the following could be treated as random variables:

- The critical pressure ρ sustainable by the target.
- The spatial separation of the detonations.
- The angular orientation about the midpoint of the detonations.
- The magnitudes of the detonations.
- The time between detonations.

Both direct numerical integration and first order reliability approaches become less feasible as the dimension of the problem increases. Both suffer from the necessity to clearly specify failure regions; the latter requires additional effort to define bounding polyhedra which are themselves not easily integrated.

By contrast, the performance of Monte Carlo integration does not intrinsically depend on problem dimension. The coefficient of variation of the estimator (a measure of convergence) is $[(1 - \theta)/\theta n]^{1/2}$, depending only on the probability being estimated, θ ; and the number of iterations, n . While Monte Carlo is more robust than the other two approaches, in this respect there are issues which must be addressed:

Convergence

The number of iterations required to estimate a small probability is very large. The number of iterations required to maintain a given coefficient of variation, R , is approximately inversely proportional to the probability being estimated:

$$n = (1 - \theta) / \theta R^2$$

$$n \cong 1/\theta R^2 \text{ for small values of } \theta$$

(Confident estimation to within a factor of 2 of the true value of a probability on the order of 1/10,000 requires roughly 10,000 trials.)

Fortunately, it is often possible to modify Monte Carlo by effective acceleration techniques, significantly improving convergence rates (see *Reference 2* for discussions of stratified sampling, importance sampling and Latin hypercube sampling).

Cost

Even the fastest Monte Carlo algorithm may be prohibitive in applications where each iteration is computation intensive (requiring, for example, refined finite element analysis).

Given sufficient continuity (or smoothness), a system can be approximated by a response sur-

face constructed to interpolate analyses run at a selected grid of parameter points. With a response surface set, millions (even hundreds of millions) of Monte Carlo trials can be run at little additional cost. It may be countered that too many points are required to fit a high dimension response surface, but lacking the requisite system analysis, meaningful probabilistic estimates are simply not possible.

(It is emphasized that the above definition of "response surface" allows for more than a single linear or quadratic functional approximation.)

Numerical Traps

Good pseudorandom number generators are required for Monte Carlo.

While this seems a simple requirement, research has shown that common, older algorithms can generate sequences which cycle with very short periods. For example, an algorithm provided in *Reference 3* based on the Multiplicative Linear Congruential (MLC) Method (*Reference 4*) can produce sequences with periods as short as 8,192 (*Reference 5*). Newer algorithms have been developed based on the Lagged Fibonacci (LF) Method with periods exceeding 10^{40} (*Reference 6*).

Also of concern are correlations between dimensions when points are generated by pulling $x_1(i)$ from the generator, then $x_2(i)$, and so on. Correlations invalidate the assumption of independence. Four examples of correlated sequences generated by the referenced MLC algorithm are shown in *Figure 60*. The LF algorithms seem not to suffer this problem.

Much effort has been spent developing algorithms derived from the first order and related second order reliability approximations and three commercially available computer programs are reviewed in *Reference 7*: NESSUS, PROBAN and CALREL (*References 8-10*). The comment is often made that there is no

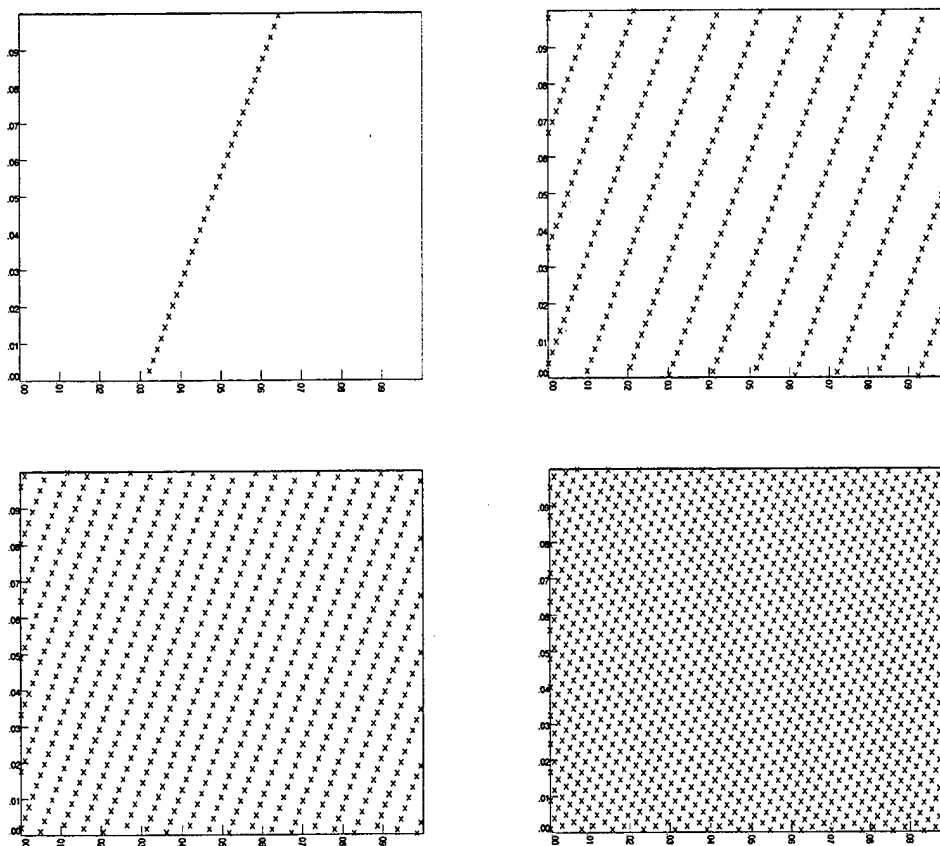


Figure 60. Correlated (x,y) Sequences Generated by MLC Algorithm.

alternative when problems involve hundreds of random variables.

Approximation techniques can be effective. It is easy to calculate the probability, P , of a hypercube whose sides are independent random variables having known distributions. If it can be shown that the hypercube avoids the failure region, then $1-P$ upper bounds the failure probability. When this is an acceptable estimate, why do more?

Approximation techniques are not always good. First and second order reliability algorithms can be applied blindly since it is easy to assume a failure region to be bounded by a hyperplane even if it is not. Given the Section 7.1 example demonstrating that even simple phenomena can yield complex failure regions,

caution should be exercised when computing a problem involving hundreds of random variables, even if there are no alternatives.

7.3 Probabilistic Design Analysis System (PDAS)

The algorithms reviewed in Sections 7.1 and 7.2 could be presented briefly given that the example involved a simple algebraic response function. A probabilistic analysis of a complex structure works conceptually the same. Controlling parameters are identified. These are varied and the response observed. A failure region is identified and its probability volume estimated.

Simplicity vanishes, however. All probabilistic algorithms require multiple analyses, and each analysis of a complex structure tends to be, for

lack of a better word, complex. A typical turbine engine disk analysis requires geometric definition, finite element meshing, thermal and stress solutions, and life calculations. This must be preceded by a cycle definition: rotor speeds, gas temperatures, pressures and flow rates, requiring additional analysis. The analyses all require data: measured engine parameters, heat transfer coefficients, coefficients of expansion, tensile curves, fatigue curves, and crack growth rate curves.

PDAS was developed to:

- Manage multiple executions of the user's choice of analysis process, facilitating its application to design perturbations as needed to map a structure's response.
- Provide a range of integration approaches for estimating the structure's failure probability given its response to statistically distributed controlling parameters.

- Enable the structure's design to be optimized subject to a constraint on failure probability.

The mix of required analysis tools can vary and it is not currently practical to hard wire all mixes into a single computer code. Accepting the need for flexibility, PDAS was designed to be more like a language than a program – it does not define an analysis but provides words and concepts so that the user can define the analysis. There are core GEAE-developed modules for selected functions such as spreadsheet management, distributional handling, finite element model interfacing, and life calculations. There are also links to external functions such as Uni-graphics, Patran, and ANSYS, ensuring the best tools can be applied to a given problem.

PDAS will be described in detail in Section 11. Appendix C will provide examples of three PDAS programs used for the calculations summarized in Section 7.1.

8.0 Probabilistic Fracture Mechanics

Traditional fatigue life approaches focus on limited numbers of critical component locations, estimating minimum lives at those locations based on calculated temperatures and stresses, lower bounds on material fatigue capability based on laboratory testing of carefully prepared, simple geometry specimens, and a mechanistic model to relate the generally multiaxial, complex-cycle stresses of the part to the generally uniaxial, simple-cycle stresses of the specimens. Damage tolerance approaches (e.g. ENSIP, *Reference 11*) depart from this theme only in that they set criteria based on residual life from cracks assumed placed at the same component locations.

The methods which are used work to yield the best possible accuracy at the focused critical locations: 3-D models are used to calibrate stress concentration factors. Mission simulation programs generate local temperature/stress histories that may contain many thousands of partial cycles. K_t corrected missions enter into life algorithms where they are integrated with material data to yield a predicted number of cycles to failure.

The introduction of powder metal (PM) alloys into disk applications led GEAE, Pratt & Whitney, SNECMA and others to question the validity of traditional lifing methodology. Early PM alloys (René 95, Inconel 100, N° 18) were recognized to be life-limited by inherent process-related inclusions. Unless suppressed by a surface treatment such as shot peening, a 50 sq mil inclusion falling on the surface of a part at a high stress location significantly impacts life. Efforts have been made through the years to improve the powder process, and more recent alloy development programs have produced materials such as René 88 DT which are more tolerant of inclusions. Even so, inclusions must remain a concern.

When inclusions play a dominant role, a statistical size effect is clearly implied. Large volumes are more likely to hold limiting inclusions than small volumes. Given this observation, GEAE resolved to pursue a new lifing methodology with a more solidly probabilistic basis. The Probabilistic Fracture Mechanics (PFM) program MISSYDD (MISSION SYNthesis given Defect Distribution) was begun and is now in its seventh generation. MISSYDD serves as a foundation for the PDAS development.

8.1 Outline of the PFM Risk Calculation

While many approaches can be considered for calculating a component's failure probability from its inherent inclusions, the following three step division of the procedure has advantages:

1. Calculation of the probability of failure by given a single inclusion of a fixed size occurring randomly in the component. This probability is geometric in that it involves the spatial distribution of stress and temperature. In principle, each point of the model has a well defined life dependent on the precise mission conditions, geometric constraints and material properties in the vicinity of the point. Clearly, none of these factors are firmly fixed by design. The mission may be variable so that stresses and temperatures fluctuate randomly. Free surfaces may vary within drawing tolerances. Material properties influencing life may differ from point to point and part to part. These factors must be recognized and, ideally, should be incorporated into the analysis. Given random placement of the inclusion, the probability of failure by a life N is the volume of material having life less than or equal to this N divided by the total volume.

2. Calculation of the probability of failure given a single inclusion from a distribution of sizes. The geometric failure distribution is integrated with the relative inclusion size distribution.
3. Calculation of the probability of failure given more than one inclusion. This is like flipping a coin:

The probability of one head is 0.5. The probability of two heads is $(0.5)^2$. The probability of n heads is $(0.5)^n$, a very small number for n large.

A component may survive a single inclusion with high probability, say 0.999999 (since the probability that the inclusion is large and in the wrong place is small). But there are many inclusions in powder alloy parts, all competing for failure. The survival probability given 100 inclusions is $(0.999999)^{100} \approx 0.9999$.

If F is the failure probability given a single inclusion, then $(1-F)$ is the corresponding survival probability. The survival probability given n independently competing inclusions is $(1-F)^n$; the failure probability is $1-(1-F)^n$. This simple expression is integrated with the probability that there are n inclusions to yield net failure probability. This last step depends on the average rate of occurrence (number per cubic inch) of inclusions in a part times the part volume.

Summarizing the risk equations

Let $G(N, a)$ denote the geometric failure probability, the probability of failure by life N given a single inclusion of size a . Let $s(a)$ denote the probability density function of the inclusion size distribution. $G(N, a)$ and $s(a)$ are integrated to yield $R(N)$, the probability of failure given a single inclusion, randomly sized.

$$R(N) = \int_0^{\infty} G(N, a) s(a) da$$

To calculate the failure probability given competing inclusions, $F(N)$; the Poisson model for inclusion occurrence will be assumed:

The probability that there are n inclusions in a component volume is $e^{-V\lambda} (V\lambda)^n/n!$ where λ the average inclusion frequency (number per cubic inch) and V is the volume.

$$F(N) = \text{Prob (1 defect present – it fails by } N)$$

$$+ \text{Prob(2 defects present – one or both fail by } N)$$

$$+ \text{Prob(3 defects present – one or more fails by } N)$$

$$+ \dots$$

$$= \frac{e^{-\lambda V} (\lambda V)^1}{1!} (1 - (1-R(N))^1)$$

$$+ \frac{e^{-\lambda V} (\lambda V)^2}{2!} (1 - (1-R(N))^2)$$

$$+ \frac{e^{-\lambda V} (\lambda V)^3}{3!} (1 - (1-R(N))^3) + \dots$$

$$= e^{-\lambda V} (e^{\lambda V} - 1 - e^{\lambda V(1-R(N))} + 1)$$

$$F(N) = 1 - e^{-\lambda V R(N)}$$

8.2 Note on the Statistical Size Effect

The size effect concept has broader application. All materials initiate failure at limiting microstructural features (grains, carbides, nitrides). The confluence of microstructure and stress is to some extent statistical. Disks with 80 bolt holes will have a lower minimum life than specimens with single bolt holes (assuming the two geometries can be equivalently stressed).

Detailed studies of the size effect in wrought Inconel 718 have concluded that it is overwhelmed by non-statistical stratification of data between parts and between part locations (*Reference 12* or Section 3.4.1). Statistical size effect is inconsequential if life distributions are narrow within the volumes of the stress-concentrated regions, but powder alloy life distributions can be very broad given the distributions of inclusion sizes, locations and behaviors.

9.0 Dealing with Variability: The Probabilistics Target

Figure 61 shows the comparisons among PFM-predicted and observed failure distributions for five specimen sets: cylindrical and hourglass, unseeded baseline, large and small seeded ... all peened and all tested at the same conditions of strain and temperature. The comparisons demonstrate the capability of the PFM model over the range of probabilities 0.01 to 0.99 when provided the right inputs of inclusion distribution and behavior. It is easily accepted that were the rate of inclusion occurrence orders of magnitude lower than the selected seeding densities (more like the real world), the failure probabilities would be proportionately lower in the absence of other failure mechanisms.

Significant efforts are being made to ensure the right inputs for design application of PFM. For example, Heavy Liquid Separation (HLS)

analysis has been developed to quantify and control inclusion content. This work was presented at the 1994 Toronto meeting of the Metal Powder Industries Federation and published in the proceedings with the vision that HLS (or something like it) will become an industry standard (*Reference 13*). Also, an intensive seeded fatigue program providing a model for crack initiation at inclusions is ongoing. Some of the details of this work will be presented at the September 1996 Seven Springs Superalloys Conference.

Accepting that the technology is available and sufficiently mature to be applied to hardware, two challenges remain: an appropriate risk design level must be accepted and surprises must be avoided.

Conventional deterministic design methods yield products having nonzero risk of failure,

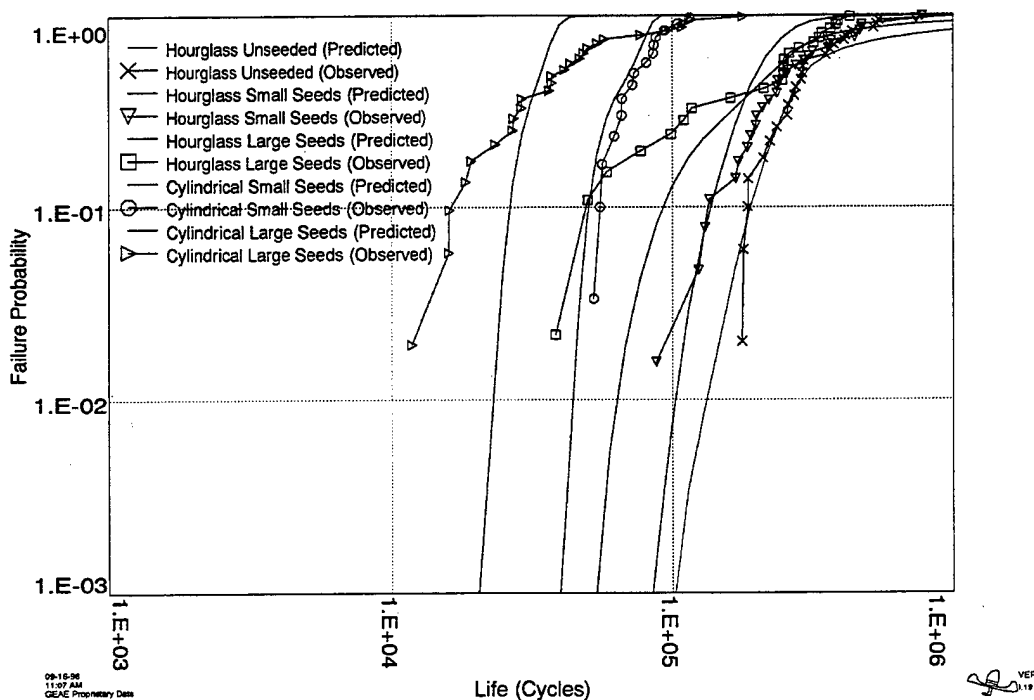


Figure 61. Peened Specimens Tested at One Temperature/Strain Condition.

but the risks are hidden. Given a design based on minimum properties (-3σ), it is seldom noted that failure might occur 1.35 times out of 1000. In practice, conservatism is usually compounded and safety factors applied, but there is always some risk, and there can be failures. By contrast, PFM quantifies risk; risk becomes a characteristic to be controlled and kept below an accepted level. In Reference 1, FAA statistics are used to support 1/1,000 or 1/10,000 probabilities at full life as appropriate for fatigue failure.

Given the right inputs, the seeded validation testing supports the capability of PFM to correctly predict risk. The second challenge addresses our ability to define the right inputs. Each failure distribution in **Figure 62** corresponds to a perturbation in part geometry (the nine perturbations overlaid as shown). Designing to a low failure probability on the nominal curve ignores the fact that it may be the wrong curve for any given part. Many other factors

can move PFM calculated failure curves and create similar concerns.

An aircraft engine component design analysis is based on many knowns: basic geometry is well defined as is the envelope of speeds and gas temperatures defining the cycle for a given application. Metal stresses and temperatures can be calculated with reasonable precision using finite element and finite difference methods. For PFM calculations, the average inclusion distribution can be determined, as can the average incubation behavior of the inclusions (cycles to crack initiation) and the average crack growth properties (growth from initiation to failure).

But the example of **Figure 62** illustrates the need to recognize sensitivities to deviations from nominal values of design parameters. The example (though admittedly extreme) demonstrates the potential impact of manufacturing tolerances. The effect of variations in other parameters may be as significant or more so:

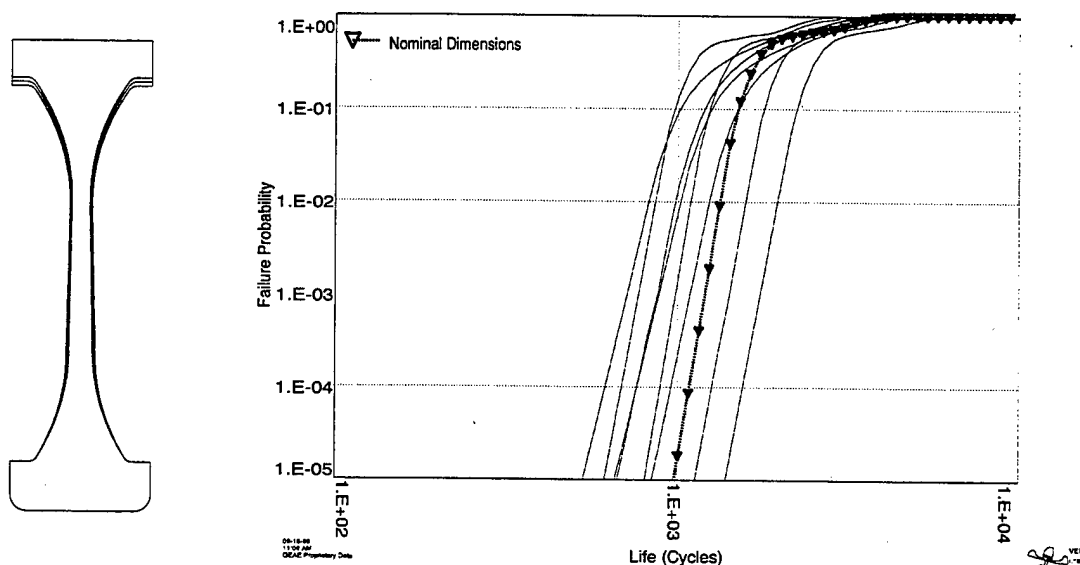


Figure 62. Predicted Failure Distributions for Nine Disk Perturbations.

Actual engine usage will vary from flight to flight, from base to base, or from pilot to pilot. Stresses and temperatures may be reasonably calculated, but not exactly (temperatures within $\pm 25^\circ\text{F}$ at steady state conditions, within $\pm 50^\circ\text{F}$ for transients; critical material properties can vary significantly over 50°). There is variability in inclusion distribution and in inclusion behavior.

There will also be surprises: deviations from manufacturing tolerances, unexpected applications, analysis oversights, methodology shortfalls, and material anomalies.

The target in **Figure 63** suggests a strategy:

1. *The Bull's-eye* – Apply what we know as well as we know how to. PFM does provide a measure of product capability given nominal assumptions.
2. *The Middle Ring* – Evaluate sensitivities to known deviations and bound the results: Assume the left-most curve in **Figure 62**.
3. *The Outer Ring* – Back off from the calculations until accumulated experience justifies doing otherwise: Apply a safety factor on computed minimum life.

The relative proportions of the target circles can vary as a fleet matures and as probabilistic methodology improves. Middle ring sensitivities may be pushed into the bull's-eye if the variability can be statistically defined and properly incorporated. The outer ring may shrink given experience and/or implementation of production controls aimed at preventing surprises.

9.1 Example – Factoring In Dimensional Variability

The risk curves in **Figure 62** define a response surface dependent on part dimensions X_1 , X_2 and X_3 . Assume that manufacturing deviations in these parameters can be modeled as random variables with joint density $\rho(x_1, x_2, x_3) = u(x_1) v(x_2) w(x_3)$ (**Figure 64**). Let $F(N : x_1, x_2, x_3)$ denote the conditional probability of failure given geometry defined by x_1 , x_2 and x_3 , and integrate against the joint density:

$$\int F(N : x_1, x_2, x_3) \rho(x_1, x_2, x_3) dx_1 dx_2 dx_3$$

This yields an average distribution, the Integrated Result indicated in **Figure 65**. Designing to this distribution captures the variability, but removes the arbitrary conservatism entailed in designing to the minimum (left-most) curve.

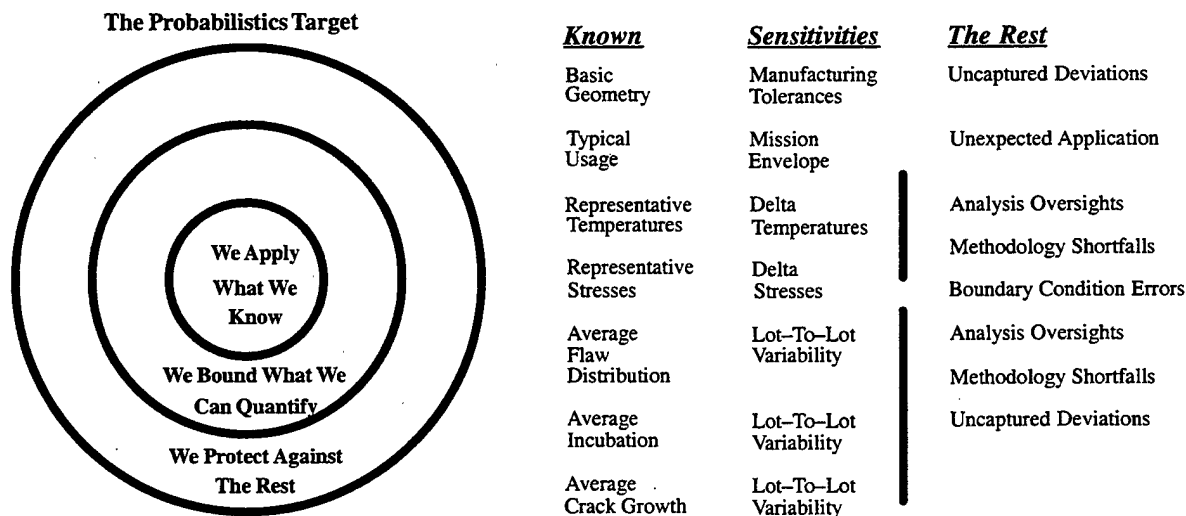


Figure 63. Strategy for Implementation of Probabilistics.

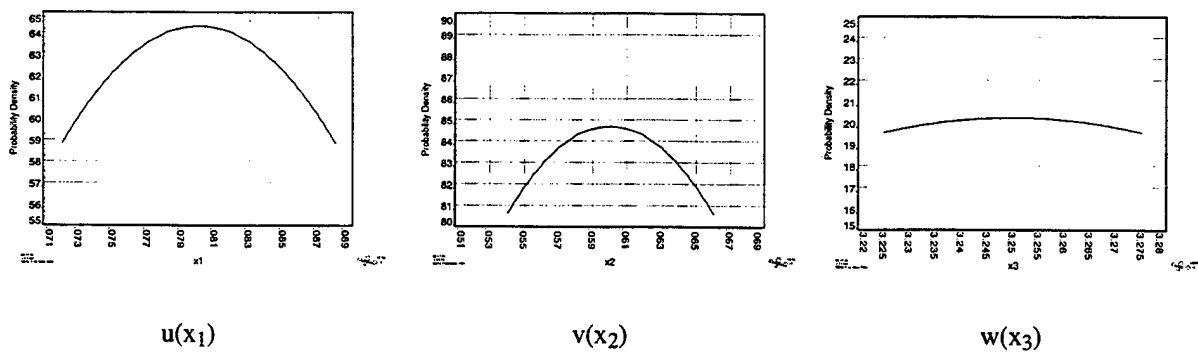


Figure 64. Dimensional Distribution Probability Density Functions.

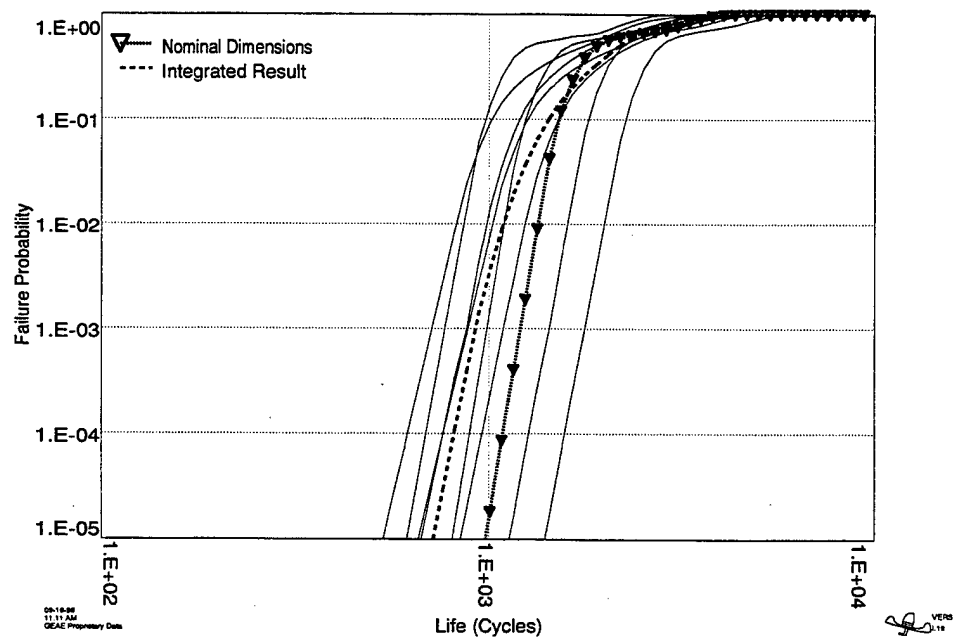


Figure 65. Risk Response Surface Integrated against Dimensional Distributions.

9.2 Example – Factoring in Variability in Inclusion Distribution

As was discussed in (*Reference 13*), Heavy Liquid Separation (HLS) is a PM cleanliness evaluation technique which has been developed by GE Aircraft Engines and Wyman-Gordon. A high density liquid is used to float ceramic inclusions from a PM sample for characterization by automated SEM/EDAX analysis. The number, size distribution, and chemistries of the recovered inclusions can be used for statistical process control (SPC) monitoring and improvement of PM lot cleanliness, and as a quality control screen to help ensure an acceptable level of cleanliness for PM used in critical applications.

Inclusion distributional models are core to the evolving risk analysis methodology. For any given material, MISSYDD assumes a homogeneous inclusion distribution (a single distribution which can be generically applied to all pro-

duction lots). Sufficient data exists to demonstrate the inadequacy of this assumption.

HLS analysis of a large number of powder lots yielded considerable scatter between samples (*Figure 66*). A conservative (middle ring) application of this data would use an upper bound distribution for PFM calculations. Design life would be based on the acceptable risk level assuming the part was manufactured from the dirtiest powder likely to be encountered.

Conservatism can be reduced (movement towards the bull's-eye) if the observed scatter can be integrated into the risk calculation. Assume that lot variations can be modeled as a random vector \mathbf{x} with joint density $\rho(\mathbf{x})$. Let $F(N : \mathbf{x})$ denote the conditional probability of failure given the inclusion distribution defined by \mathbf{x} , and integrate against the joint density:

$$\int F(N : \mathbf{x}) \rho(\mathbf{x}) d\mathbf{x}$$

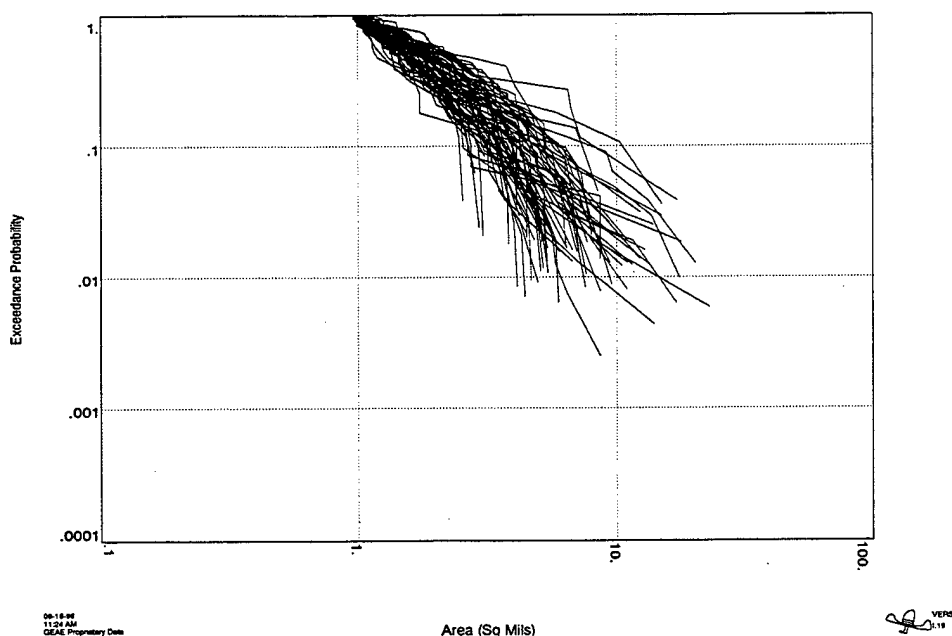


Figure 66. Lot-to-Lot Variability in Inclusion Distribution.

This would yield the desired refinement. Unfortunately, the parametrization is not available, much less the joint density $\rho(\mathbf{x})$. Fortunately, it can be shown that:

$$\begin{aligned} & \int F(N : \mathbf{x}) \rho(\mathbf{x}) d\mathbf{x} \\ & \leq 1 - \exp \left[-\lambda V \int R(N : \mathbf{x}) \rho(\mathbf{x}) d\mathbf{x} \right] \\ & = 1 - \exp \left[-\lambda V \int G(N, a) \int s_x(a) \rho(\mathbf{x}) d\mathbf{x} da \right] \end{aligned}$$

(Jensen's Inequality for the exponential function, *Reference 14*). The integral $\int s_x(a) \rho(\mathbf{x}) d\mathbf{x}$ is an average inclusion distribution estimated by combining all data into a single distribution having density $s(a)$ (see *Figure 66*). The inequality is rewritten:

$$\begin{aligned} & \int F(N : \mathbf{x}) \rho(\mathbf{x}) d\mathbf{x} \\ & \leq 1 - \exp \left[-\lambda V \int G(N, a) s(a) da \right] \end{aligned}$$

Thus, it is sometimes possible to factor in lot-to-lot scatter without actually quantifying it. Using the average distribution produces an estimate of failure probability which is conservative, but not as conservative as would result from assuming a worst-case distribution.

9.3 Example – Factoring in Variability in Inclusion Behavior

The PFM risk algorithm as presented in Section 8 assumes that the life of any given inclusion at any component location can be predicted exactly. In reality, there is scatter about the pre-

dicted life due to many factors including variability in inclusion shape, variability in matrix properties, and variability in actual loading.

Because this scatter has not been integrated into the calculations, the *Figure 61* peened data predictions capture the average behavior of the observed distributions but not their breadth. The following model is a simple correction:

1. Assume that the scatter can be modelled by a distribution of life multipliers: Let μ denote the ratio of predicted to observed life for a single inclusion, and let $m(\mu)$ denote the probability density function of the μ distribution.
2. Assume also that the distribution of μ predominantly represents testing variability (i.e. specimen-to-specimen rather than inclusion-to-inclusion).

The distribution of life is derived from the basic PFM risk algorithm as a kind of convolution:

$$\int [1 - e^{-\lambda V \cdot R(N\mu)}] m(\mu) d\mu$$

Figure 67 shows that a Weibull distribution can be found for μ which fits the predicted/observed ratios of the cylindrical large and small seeded data sets of *Figure 61*. Convolution of this distribution with the calculations in *Figure 61* yields better agreements between predictions and observations (see *Figure 68*). *Figure 69* shows comparisons for other data sets. Note that the calculations for the unpeened data sets in *Figure 69* appear to capture the competition between surface and subsurface initiated failures (surface initiated failures have shorter lives but occur with lower probability).

Additional details and further refinements will be offered Section 15.

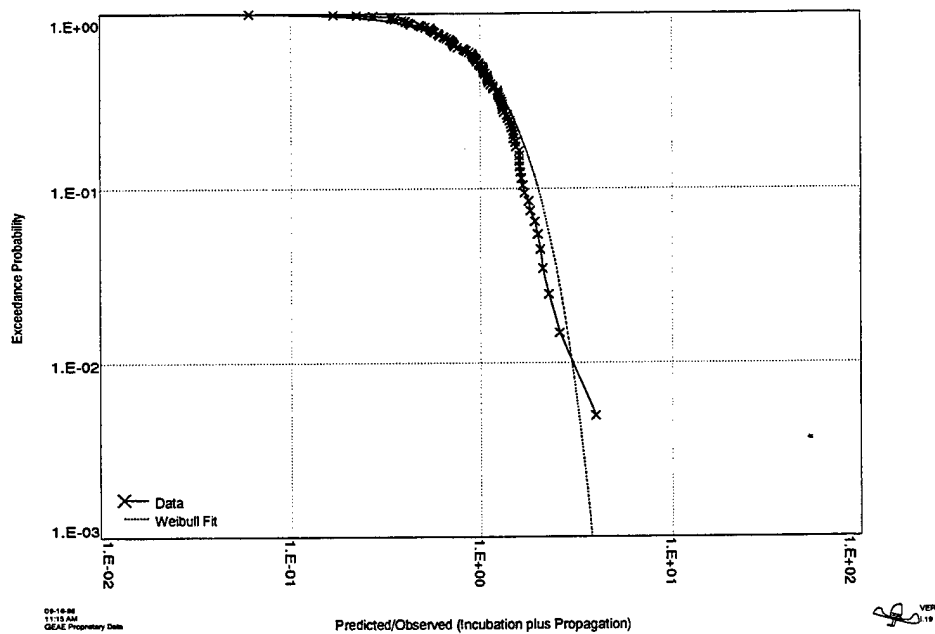


Figure 67. Weibull Fit to Predicted/Observed Distribution.

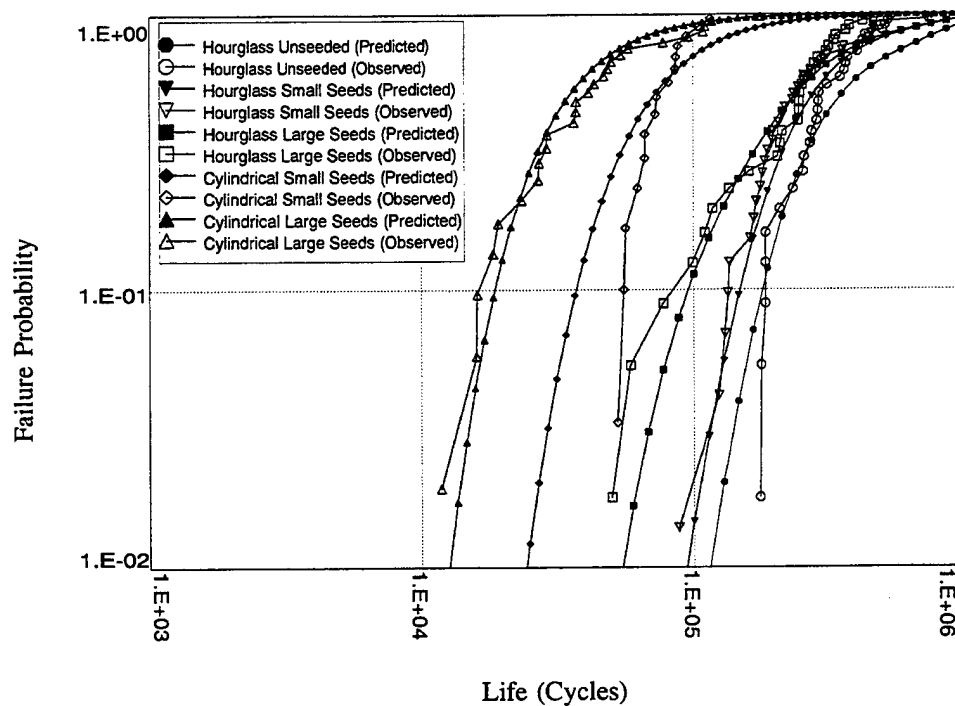


Figure 68. Material Variability Integrated into Specimen Predictions of Figure 61.

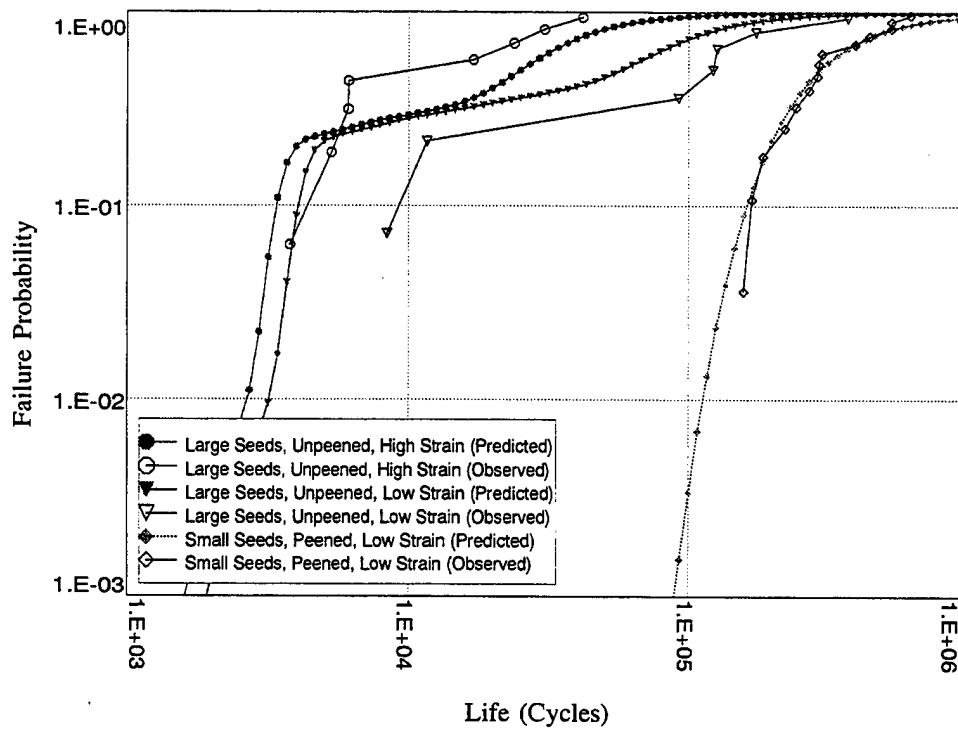


Figure 69. Material Variability Integrated into Other Cylindrical Specimen Data Sheets.

10.0 Statistical or Not?

Improvements as described in the last three examples can provide better analysis of middle-ring sensitivities, but only if the sensitivities can be properly modeled statistically. Probabilistics are often sought as cures for all variability, but they are strictly useful only in situations where randomness is well defined.

Qualitatively, risk is a condition of uncertainty the potential result being undesirable. In attempting to quantify risk, probability theory is called on.

Probability and statistics deal with variables (measurable quantities) which are random for individual samples, but which are predictable (on the average) for larger samples - quantities for which the empirical distributions converge for large samples to fixed forms which may be parametric (binomial, normal, Weibull) or non-parametric. Statistical samples are generated under controlled conditions and analyzed to infer the underlying distribution; probabilistic theory is applied to predict the effects of the randomness under more complex circumstances.

We point to physics and chemistry and the success of statistical and quantum mechanics, or to genetics and gambling where much simpler combinatoric predictions work on average. In these applications, populations may be sampled repeatedly and repeatably (the populations are open). Their statistical distributions can be derived from basic principles or inferred by preliminary sampling, and then applied to predict the results of subsequent sampling.

A population of aircraft engines is closed rather than open; a few thousand will be made over a span of several years. It is closed and probably not even stable. During production, design revisions may be made, melting and forging practices may be modified, subcomponent sup-

pliers may change. Consequently, computed risks, while stated as probabilities, are usually not verifiable. A predicted 1/1,000 risk of failure can be disputed if enough fail, but can not be verified, and while 1/10,000 may be lower risk than 1/1,000, the difference can not be demonstrated. Decisions are qualitative despite the quantitative language.

Component integrity is dependent on many factors, some of which are at least approximately statistical (inclusion distribution), but many of which are inherently non-statistical. For example, a design modification in a derivative engine may be mistakenly assumed benign based on its ancestry, and no further analysis performed. In another example, a stress concentration may be underestimated based on an oversimplified textbook solution or on a poorly refined finite element model. While a probabilistic design framework can sometimes facilitate evaluation of sensitivities by quantifying risk as a function of the potential error, such errors can probably not be usefully accommodated by statistical analysis.

Safety factors may be applied to computed minimum component lives upon launch of new designs or design revisions as a hedge against analysis errors and oversights. The factors may be essentially arbitrary, or they may be tied to some qualitative judgement of analysis goodness or based on field inspection intervals. In any case they need not remain fixed. Analysis refinements and improvements in material understanding can be counted on, and while operating experience may uncover problems, it will also support a good design's fundamental integrity. In most cases, factors will increase with time.

Probabilistics work if properly applied. They can produce designs which are robust against failure since risks and sensitivities are quanti-

fied. In some cases they may yield economies in weight or manufacturing requirements. In other cases weight may be added or manufacturing requirements stiffened to lower risk to an accepted appropriate level.

The probabilistic tools do work, but must be applied at a proper level. Some parameter sensitivities cannot be incorporated probabilistically (at least not at the outset) and must be bounded. Some allowance must also be made for oversights. Thus, conservatism should not be abandoned, but may be reduced in time given dedicated efforts. While it is prudent that caution be exercised in reducing conservatism, it is equally prudent to pare away unnecessary conservatism which wastes resources and impedes society's growth into the future.

10.1 Application Strategies

It is given that some components cannot be designed for the largest possible defect or the worst possible material properties, and risk based design provides a reasonable alternative. The examples of integrated risk analyses in Section 9 cover situations which could be different.

As demonstrated in Section 9, variability in part dimensions yields parts with a range of failure distributions, and while dimensional variability can only be controlled within limits, it can be quantified for all parts produced. Similarly, variability in inclusion distribution from powder lot to powder lot yields a range of failure distributions; it cannot be controlled, but can be quantified within the limits of sampling variability.

There is a difference between fielding 10,000 parts, expecting (based on an estimated failure probability of 1/10,000) that 1 will fail, and fielding 10,000 parts, expecting (based on an inspection) that 1 particular part will fail. The latter would clearly be unethical. The distinction is less clear if an inspection can quantify a

parameter which might indicate higher risks for some parts and lower risks for others.

Consider the following alternative strategies:

- Retire parts at the 1/10,000 life for the absolute *worst* component where *worst* covers all parameters which can be measured.

Of course *worst* never really means *worst*. *Worst* means somewhere on the edge of a sharply defined process window. It is tacitly assumed that the measurements are exact and that a point inside the window is always better than a point outside. It is also assumed, tacitly, that parts are rejected if they fall outside the window.

When the assumptions are met, this middle ring solution of the probabilistic target has merit from the point of view of safety. It is wasteful, however, if there is a large difference between the worst part and one that is likely to be made.

- Retire parts at the 1/10,000 life predicted by a fully integrated risk analysis. This yields an average 1/10,000 failure probability, but individual parts will have risks higher or lower than 1/10,000.

This second strategy may be acceptable if the assumptions behind the first strategy are in question. For example, HLS is useful as a quality control tool. It can detect trends, and can detect a process gone out of control. Given samples from many powder lots, it also provides an average picture of the inclusion distribution which can be used for PFM calculations. However, HLS cannot be used to collect enough data for individual lots to confidently define a window; the measurement is not exact. (Sampling variability is demonstrated in Appendix B.)

This second strategy may be acceptable if it is judged that there is adequate conservatism built elsewhere into the analysis. For example, it was demonstrated in Section 9.2 that applying the full breadth of the average inclusion distribution overestimates failure probability.

This second strategy may be essential to managing a field problem. For example: A fillet radius is found to be a critical dimension only after several hundred engines have been fielded. A badly undersized radius would be expected to lead to cracking long before the first planned shop visit. Earlier inspections may be needed to assure that offending parts are weeded out for rework. Assuming that all fillet radii are undersized would call for immediate grounding of the fleet. Based on a measured distribution of fillet radii, an inspection interval may be set which holds the risk below 1/10,000.

- Retire parts at the 1/10,000 life predicted by a fully integrated risk analysis, but reject parts having failure probabilities exceeding 1/10,000 at this life.

This third strategy is less conservative than the first, but addresses a concern with the second strategy by holding risk at an acceptable level for all components. Given a robust design, very few parts will be rejected.

- Retire parts at individually calculated 1/10,000 life limits.

This strategy seems to be optimal. It holds risk at a uniform level for all components, and also utilizes full part life.

It will be argued that it is too complicated, but parts are already tracked by cycles and hours flown. Adding another number onto a spreadsheet is not a major burden and seems completely consistent with the USAF interest in life monitoring. Balancing engines so that tear-downs are efficiently managed will be necessary, but the net cost savings must be tremendous if there are large part-to-part differences.

11.0 PDAS Template Programming

MISSYDD was developed to perform only very specific analysis functions. Other programs were needed for concurrent tasks of data analysis, algebraic manipulations and simulation studies. While commercially available packages were sometimes available, they were often found wanting, and special programming had to be developed.

Local analysis programs are generally written in languages such as Fortran or C++.. Large portions of the programs are generally very similar from one to another. There may be blocks of input/output code, a sorting routine, random number generators, and so on. Much of the overlap can be eliminated by linking programs with libraries of standard subroutines; this requires careful attention to assure that calling sequences be exactly right. Arrays must be dimensioned, files opened and closed. Often the lines dedicated to actual computations are outnumbered many times by the wrapping.

Two developments at GEAE suggested an alternative: First, the SIESTA development team refined the concept of keyword defined input and output (SIESTA – System for Integrated Engineering Structural and Thermal Analysis). Second, Greg Blanc developed an expression evaluator package which interprets Fortran-like algebraic expressions. Using these concepts (and many of the routines) as a starting point, a new programming language has been developed which greatly simplifies many analysis tasks. Simple commands replace blocks of code. For example:

```
table 1 input  
x.dat
```

causes the file x.dat to be opened and the keyword-defined data to be entered into a table identified as 1.

```
table 1 set y = EXP(LOG(X) + SIN(X**2))
```

creates a y-column in table 1 by transforming the x-column by the expression following the equal sign.

```
distribution make Y (table) 1 x
```

produces an empirical distribution, labeled Y, from the x-column data in table 1.

```
x = (random) Y
```

assigns to parameter x a random value from the Y-distribution.

Other commands enable manipulation of a MISSYDD database. Models, missions, and computations can be defined and operated on as directed by simple template programs.

External functions are also significantly assisted by GEAE's SIESTA software. Component designs generally require many analysis steps for accurate deterministic predictions: parametric geometry definition, finite element thermal/stress/displacement analysis (both elastic and plastic (up to burst)), fatigue, and fracture mechanics calculations. The best deterministic tools are required to maximize accuracy in a probabilistic analysis.

SIESTA provides unified access to a range of disciplines. For example, ANSYS may be chosen for geometry definition and thermal/stress/displacement analysis, or it may be decided to call Unigraphics and Patran for modeling and meshing followed by ANSYS for the solution. This flexibility allows concentration on the leading edge of development needs.

The following is a brief summary of the template language.

11.1 Keywords

Keywords control program flow. They can be entered in any case, and only the first four characters are significant (TABLE, table, Table, TABL, tabl, Tabl are all equivalent). The following are the supported primary keys:

TABL	Table Manipulation	
TEXT	Text Entries	
EXPR	Expression Definition	
ALGE	Algebraic Operations	
DIST	Distribution Handling	
REGR	Regression Functions	
LOOP	Loops	
OPTI	Optimization	
PLOT	Plotting	} Probabilistic Fracture Mechanics Management
MODL	Model Library	
MSSN	Mission Library	
COMP	Computation Library	
LIFE	Life Calculations	
RISK	Risk Calculations	

Entering a primary keyword changes control to its menu of secondary keywords. Secondary keywords can follow on the same line or on following lines. For example:

```
table 1 input
x.dat
table 1 set y = EXP(LOG(X) + SIN(X**2))
```

is equivalent to

```
table 1
input
x.dat
set y = EXP(LOG(X) + SIN(X**2))
```

A few secondary keywords lead to menus of tertiary keywords.

11.2 Table Manipulation

A table is an array of numbers. Each column is a parameter. The rows are individual values. Example:

Row No.	...	X	Y	Z
1	...	2	1	21
2	...	1	2	12
3	...	2	2	22
4	...	2	1	21
5	...	1	1	11
6	...	2	1	21
7	...	1	1	11
8	...	1	2	12
9	...	2	2	22

Tables are identified by integer labels from 1 to 100 specified by the user after the primary keyword. For example:

```
table 10
```

Subsequent commands will look for direction from the TABLE menu and will address table 10 until the next occurrence of a primary key.

Tables may be referenced to define digitized functions or parameter distributions, and as data sets for regression analysis or plotting functions.

Tables may be defined by ASCII files or built by the template program. Columns may be defined or redefined by functional transformations. For example:

```
set U = exp(X + Y + Z)
```

Column U is defined by the expression to the right of the equal sign where X, Y and Z are constants or other table columns.

Rows may be flagged on or off for subsequent operations based on general lists of conditions. For example:

```
flag X .gt. 100 X .le. Y .le. Z
```

where X, Y and Z are constants, parameters, expression (identified by the keyword (EXPR)), local response surfaces (identified by the keyword (RESP)) or subroutines (identified by the keyword (SUBR)). Rows satisfying the multiple inequalities are turned on.

Tables may be sorted or grouped by column values. Tables (or specified table columns) may be output to ASCII files.

11.3 Text Entries

A number of functions requiring alphameric entry can use the keyword (text) to reference the contents of an 80 character text buffer. For example:

table 10 input/output
(text)

uses the current value of the text buffer as the filename for input/output

Text entries are stored in tables created and managed for this purpose. Text tables are identified by integer labels following the lead of numeric data tables for example:

text 10

Subsequent commands will look for direction from the TEXT menu and will address text table 10 until the next occurrence of a primary key.

11.4 Equalities

Equalities have the following forms:

A = value	Initialization.
A = (EXP) {expression ID}	Expression evaluation.
A = (RESP) {response surface ID}	Response surface evaluation.
A = (SUBR) {subroutine ID}	Subroutine evaluation.
A = Expression	Expression evaluation.
Examples:	
A = 1	
expr A : X + Y + Z	
A = (exp) A	
A = X + Y + Z	
A = (dig) (table) 1 Y X (pol)	
A = (DIG) {expression ID}	Digitized function evaluation.
Example:	
A = (dig) (table) 1 Y X (pol)	
A = (MIN) list	List minimum
A = (MAX) list	List maximum
Examples:	
A = (min) X Y Z	
A = (max) A 1	
A = (TABLE) ID (MIN) column	Column minimum
A = (TABLE) ID (MAX) column	Column maximum
A = (TABLE) ID (SUM) column	Column sum

Examples:

X	Y	Z
2	1	21
1	2	12
2	2	22
2	1	21
1	1	11
2	1	21
1	1	11
1	2	12
2	2	22

A = (table) 1 (min) X

yields: 1

A = (table) 1 (max) Y

yields: 2

A = (table) 1 (sum) Z

yields: 153

A = (DER) (EXPR) {ID} WRT list

A = (DER) (RESP) {ID} WRT list

A = (DER) (SUBR) {ID} WRT list

Derivative of the expression, response surface or subroutine function with respect to the list variables.

A = (INT) (EXPR) {ID} WRT list

A = (INT) (RESP) {ID} WRT list

A = (INT) (SUBR) {ID} WRT list

Integral of the expression, response surface or subroutine with respect to the list variables.

A = (RAN) parameter

Random value from a previously entered parameter distribution.

A = (RAN) (EXP) {expression ID}

Random expression evaluation, some or all of the expression parameters being random variables.

A = (MODL) parameter

Model data such as volumes or surface areas, stress components, or temperatures at specific locations or averaged over model sections.

A = (LIF)

Life calculation at specific model locations.

A = (QUA) *quantile*

Survival or failure probability
quantile following risk
calculations

11.5 Expressions

Expression evaluation routines have been incorporated into PDAS, enabling the application of algebraic functions for a variety of purposes. Digitized functions can also be defined with up to three independent variables.

Expressions play a part in parameter definitions, as integrands, as constraints and as regression models. Incubation in the life calculation module is also defined by expressions in terms of stress, temperature, inclusion area and inclusion depth. In the future it is planned to enable user definition of other material properties by expressions (e.g. crack growth rate curves, probability of detection curves, inclusion distributions).

The following is the basic format used for expression definition:

EXPR {*expression ID*}:*Expression*

EXPR is the primary keyword which initiates definition. The *ID* is an optional four character case-insensitive label. The colon points to the beginning of the expression. If the *ID* is included, the expression is stored in an expression table initialized at the start of template execution (up to 100 expressions can be so entered). If the *ID* is omitted, the expression is processed and held as the current expression for subsequent operations.

Expression is either an algebraic function (in capitals) or a digitized function defined by a previously input file. The rules for definition follow.

11.5.1 Algebraic Functions

Expression has the form of a Fortran expression using the operator set {+, -, *, / and **} and the function set {sin, asin, cos, acos, tan, atan, cosh, sinh, tanh, log, log10, exp, sqrt, abs, int, and unsf} (unsf is the unit step function: $\text{unsf}(x) = 0$ for $x \leq 0$, $\text{unsf}(x) = 1$ for $x > 0$).

Parentheses within an expression are used to determine precedence of operation. The parentheses in the expression must balance – there must be as many right parentheses as left parentheses.

The equality symbol = is used to define relations to be fit in regression analyses.

11.5.2 Digitized Functions

Expression has the form:

(DIG) (TABLE) {*ID*} {*dep. var*} [*format*] {*ind. var 1*} [*format*] ...

Up to three independent variables can be considered.

[*format*] is optional. The following are recognized: (LIN), (LOG), (POW) and (POL). The default is (LIN).

(LIN) treats the variable as linear in the interpolation, (LOG) as logarithmic.

(POL) treats the variable as an angle in radians for a polar interpolation.

(PWR) does a power function interpolation (i.e. $dep = a \cdot ind^{**b}$).

Only (LIN) and (LOG) are applicable to the dependent variable.

The interpolation begins with the last independent variable. Independent variables are assumed to be layered in the following sense: Each combination of the first p variables must be adequately represented in the $p+1$ variable to enable interpolation.

Example:

table 1 input

inputs the following data file:

RAVG	RMIN	THETA	TEMP
169.4	165.5	0	1200
94.7	75.7	0.24498	1200
55.8	44.6	0.59031	1200
48.1	38.5	0.7854	1200
44.3	35.4	1.5708	1200
109	103.6	0	1400
87.2	69.8	0.24498	1400
57.3	45.9	0.59031	1400
50.9	40.7	0.7854	1400
45.1	36.1	1.5708	1400
77.9	70.3	0	1600
76.1	60.9	0.24498	1600
54.3	43.4	0.59031	1600
46.7	37.3	0.7854	1600
43.4	34.7	1.5708	1600
41	33.8	0	1800
31.8	25.4	0.24498	1800
27.9	22.3	0.59031	1800
26.9	21.5	0.7854	1800
33.8	27.1	1.5708	1800
16.6	13.8	0	2000
15.6	12.5	0.24498	2000
15.3	12.2	0.59031	2000
14.9	11.9	0.7854	2000
19.1	15.3	1.5708	2000
12.2	10.5	0	2050
11.5	9.2	0.24498	2050
10.8	8.9	0.59031	2050
11.3	9	0.7854	2050
14.4	11.5	1.5708	2050
8.9	7.2	0	2100
7.8	6.3	0.24498	2100
7.4	5.9	0.59031	2100
7.4	5.9	0.7854	2100
11	8.8	1.5708	2100
4.1	3	0	2200
3.3	2.6	0.24498	2200
3.1	2.4	0.59031	2200
3	2.4	0.7854	2200
4.8	3.8	1.5708	2200

EXPR EX1 : (DIG) (TABLE) 1 RMIN TH (POLAR) TEMP

When evaluated, new values of RMIN are calculated for each TH by linearly interpolating with respect to TEMP. The new values of RMIN are then polar interpolated with respect to TH (see *Figure 70*)

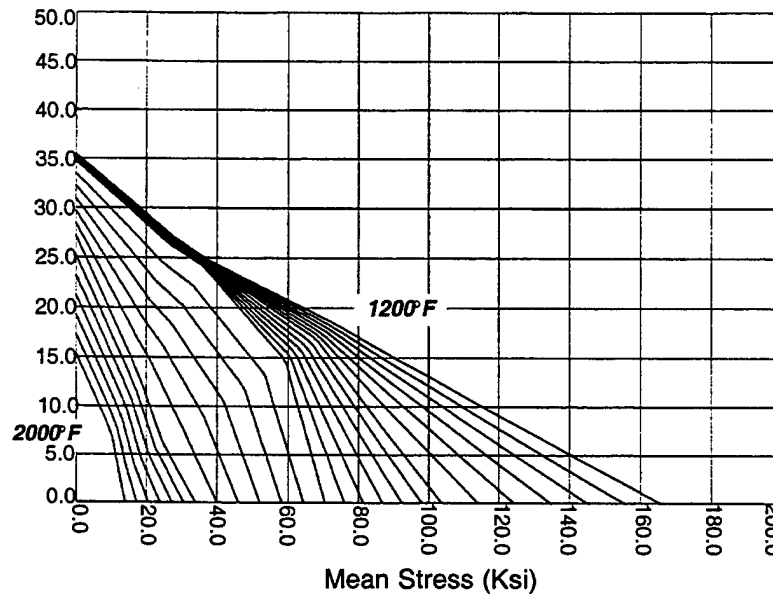


Figure 70. Digitized Goodman Curves: Polar in Theta . . . Linear in Temperature.

11.6 Response Surfaces

Digitized functions as structured in Section 11.5.2 are often useful when there is a single independent variable; but since the number of points required for their definition tends to increase exponentially with dimension, they can be most inefficient given two or three independent variable. (While $f(x)$ might be reasonably represented with 100 points, $g(x, y)$ might require 10,000 points, and $h(x, y, z)$ might require 1,000,000 points). The PDAS response surface algorithm controls the density of points in a digitization based on the rate of change of the function being digitized.

Examples:

```
expr FUNC : (1 + ((X + 2*X**2) * (Y + 4*Y**2))**3)/1000
response fit LRS (expr) FUNC Z X Y.
```

The function FUNC is digitized yield a patchwork labeled LRS of local response surfaces. X and Y are the independent variables of the patchwork; Z is the dependent variable. *Figure 71* displays the digitization. *Figure 72* presents a clearer picture of the points (X,Y) required. At the level of precision requested, the digitization could have generated up to 1,024 rectangular cells; only the 212 shown were required.

While this example does demonstrate the selective digitization produced by the PDAS algorithm, the expression, being algebraic, can be more easily evaluated directly without resorting to the

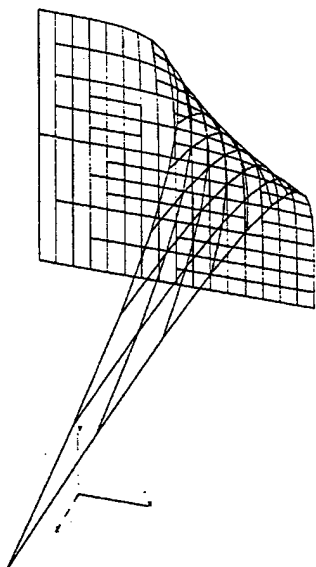


Figure 71. Response Surface Example.

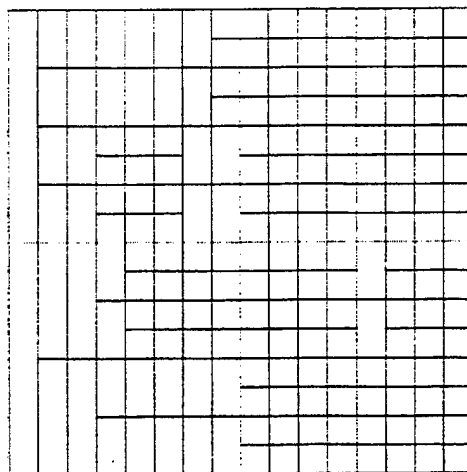


Figure 72. Response Surface Example - Grid Required for Interpolation.

digitization. In other cases, however, each function evaluation requires significant computation (e.g. a Monte Carlo simulation, see **Figure 73**, or a finite element stress intensity calculation).

Weibull Distribution for X:

expr WEIB : $\exp(-(X/ALPHA)**BETA)$

Error Expression:

expr ERROR : $10000*X**2 - X**6$

Monte Carlo Estimation of Error Probability:

table 1 rand X # 1000

table 1 set F = (expr) ERROR

table 1 flag F .le. 1000

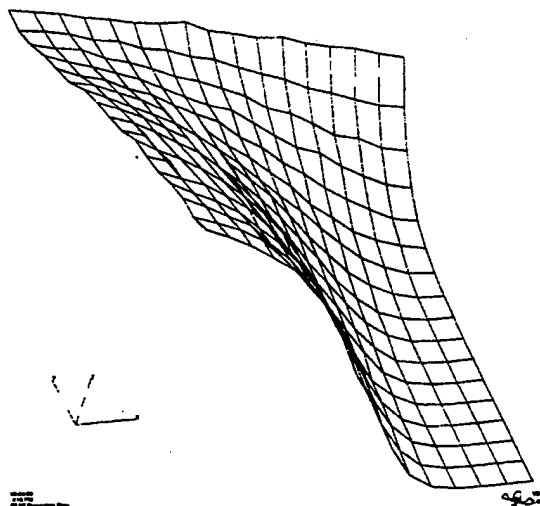


Figure 73. Response Surface of Monte Carlo Estimate (Z) as Function of Alpha (X) and Beta (Y).

11.7 Algebraic Operations

Expressions may be rearranged symbolically.

(This operation is performed internally prior to an integration of an algebraic function.)

Examples:

```
expr aaaa : X*(X*(X*(X*(X+1)+1)+1)+1
```

```
expr prep aaaa
```

```
expr write aaaa
```

produces:

```
X*X*X*X*X+X*X*X*X*1+X*X*X*1+X*X*1+X*1+1
```

```
expr bbbb : exp((sin(A) + B + C)*(sin(A) + B + C))
```

```
expr prep bbbb
```

```
expr write bbbb
```

produces:

```
exp((sin(A)*sin(A)+sin(A)*B+sin(A)*C+B*sin(A)+B*B+B*C &
+C*sin(A)+C*B+C*C))
```

Expression variables may be replaced with current parameter values.

Example:

```
expr cccc : A*(B + SIN(C + D))
```

```
B = 11
```

```
D = 22
```

```
expr replace B D
```

```
expr write cccc
```

produces:

```
A*(11.0000000+SIN(C+22.0000000))
```

Limited matrix operations may be performed (currently, only symmetric matrix diagonalization). Let X be the matrix key and n be the matrix order. The matrix is defined by the n^2 parameters:

```

X11      ...   X1n
X21  X22
X31  X32  X33
. . .
Xn1  Xn2  Xn3  ...   Xnn

```

The current values of the super-diagonal elements determine the symmetric matrix to be diagonalized. The eigenvalues determined by the operation are placed in the parameters EIG1, EIG2, ..., EIGN. The eigenvectors are placed in the column parameters X1i, X2i, X3i, ..., Xni (i from 1 to n).

11.8 Distribution Handling

A good many PDAS operations involve statistical distributions of one type or another: Inclusion distributions feed into risk calculations. Functions are integrated against various parameter distributions.

Distributions are stored in one of three digitized formats (X is a random variable):

1. Cumulative Format

As ordered pairs (x, C(x)) where $C(x) = \text{Probability}(X \leq x)$.

2. Exceedance Format

As ordered pairs (x, E(x)) where $E(x) = \text{Probability}(X \geq x)$.

3. Density Format

As ordered pairs (x, r(x)) where $r(x) = dC(x)/dx = -dE(x)/dx$.

$$C(x) = \int_{-\infty}^x r(u) du$$

$$E(x) = \int_x^{\infty} r(u) du$$

There are also specialized statistical models: The Poisson or Dirtiness models for material inclusion distribution are examples (*Reference 13*).

11.9 Loops

One of the most powerful features of any programming language is the loop, the ability to repeat the same sequence of operations a specified number of times. Loops (and nested loops) can be incorporated into PDAS templates in a number of ways:

Programs can loop over a numerical range.

Example:

```
loop from 1 to 10 by 0.5
```

Executes the loop for the following values of a counter: 1, 1.5, 2, 2.5, 3, 3.5, 4, 4.5, 5, 5.5, 6, 6.5, 7, 7.5, 8, 8.5, 9, 9.5, 10.

Programs can loop over the active rows of a table.

Example:

```
loop over (table) 1
```

Executes the loop once for each active row of table 1.

Programs can loop until a general list of conditions is met.

Example:

```
loop until U .le. 2 (expr) A .ge. (expr) B
```

Executes the loop until the parameter U is less than or equal to 2 and expression A is greater than or equal to expression B.

Programs can loop while a general list of conditions is met.

Example:

```
loop if U .le. 2 (expr) A .ge. (expr) B
```

Executes the loop if the parameter U is less than or equal to 2 and expression A is greater than or equal to expression B.

While template loops are useful, it must be emphasized that they are not efficiently compiled. PDAS cycles through loop blocks interpreting and executing the instructions one by one. While working analyses have been made with millions of loop iterations, they can take days to run. PDAS template programming is a good tool for many simple everyday applications, for some complex once-only analyses and for general development prototyping. It can not compete with dedicated programs targeting single tasks.

11.10 Subroutines

Blocks of code may be separated as subroutines:

Example:

```
subr start ERR
table 1 set WEIB = exp (-(AREA/ALPHA)**BETA)
table 1 set DIFF = (log (PROB) - log(WEIB)) **2 &
                  + (log (1-PROB) - log(1-WEIB))**2
ERR = (table) 1 (sum) DIFF
```

```
subr stop
```

Table 1 holds a column AREA of observations and a column PROB of empirical probabilities. The subroutine ERR creates a column WEIB of computed Weibull probabilities assuming the parameters ALPHA and BETA. Next a column of squared logarithmic differences is constructed reflecting differences between the empirical and computed probabilities; this column is summed to yield an integrated error.

The subroutine is referenced by an optimizer in the body of a template program to locate values ALPHA and BETA minimizing the summed squared error. The following is the line of code making the reference:

```
opti init
minimize (subr) ERR wrt ALPHA BETA
```

11.11 Regression Functions

Parametric models defined by Fortran-like equations can be least squares fit to data. A model is referenced by its expression ID and the data held in a table. The regression can include all active rows of the table or it can proceed iteratively over groups of rows. The resulting parameter estimates can be written to a table.

Example: (*Reference 16.*)

The data was generated from the equation: $y = 1.0 - x + 0.2*(x**2)$ and random errors added:

X	Y
0.050	0.956
0.110	0.890
0.150	0.832
0.310	0.717
0.460	0.571
0.520	0.539
0.700	0.378
0.740	0.370
0.820	0.306
0.980	0.242
1.170	0.104

```
expr aaaa : y = a + b*x + c*(x**2)
```

```
regr fit (expr) aaaa to (table) 1
```

yields:

A : .9979684E+00

B : -.1018042E+01

C : .2246821E+00

11.12 Optimization

A flexible optimization module was developed based on commercially available ADS and IMSL algorithms (*References 16-18*). Definitions of constraints and bounds can be made with greater freedom than allowed by the conventions of either commercial package.

Secondary Keys:

INIT Initializes an optimization.

ALGO Specifies the algorithm: ADS (the default) or IMSL. The ADS selection allows optional specification of strategy, optimizer, one dimensional search and print options as controlled by the respective secondary modifiers ISTRAT, IOPT, IONED and IPRINT as described in the ADS user manual.

Usage: ALGO ADS ISTR *option* IOPT *option* IONE *option* IPRI
option

or: ALGO IMSL

Secondary Modifiers:

ISTR Strategy. Default is 8 – Sequential Quadratic Programming.

IOPT Optimizer. Default is 5 — Modified Method of Feasible Directions for constrained minimization.

IONE One dimensional search. Default is 7 – Determination of bounds followed by polynomial interpolation.

IPRI Print control. Default is 0 – No output printed. (Also recommended is 3120.)

MINI Specifies minimization or maximization.

MAXI

Usage: MINI/MAXI (EXPR) {Expression ID} WRT *list*

or: MINI/MAXI (RESP) WRT LIST

or: MINI/MAXI (SUBR) {Subroutine ID} WRT *list*

CONS Constraint specification.

Usage: CONS *constraint*₁ *constraint*₂ ...

The constraints have the forms:

X = Y

X .EQ. Y

X .LE. Y

X .LT. Y

X .GT. Y

X .GE. Y

where X and Y are constants, parameters or expressions (identified by the keyword (EXPR)), local response surfaces (identified by the keyword (RESP)) or subroutines (identified by the keyword (SUBR)).

Examples:

constraint u .le. 2

constraint u .le. v

constraint (expr) a .ge. 0

constraint (expr)a .ge. (expr)b

Note that .LE. and .LT. are both interpreted as .LE., and that .GE. and .GT. are both interpreted as .GE.

Note also that multiple constraints may be combined in a single string.

Example:

```
constraint (expr) a .ge. 0
constraint (expr)b .ge. (expr)a
can be rewritten as:
constraint (expr) b .ge. (expr) a .ge. 0
```

BOUN Boundary specification.

Usage: BOUN *bound₁* *bound₂*...

The bounds have the forms:

```
X = Y
X .EQ. Y
X .LE. Y
X .LT. Y
X .GT. Y
X .GE. Y
```

where X and Y are constants, parameters or expressions (identified by the keyword (EXPR)), local response surfaces (identified by the keyword (RESP)) or subroutines (identified by the keyword (SUBR)).

Examples:

```
bound u .le. 2
bound u .le. v
bound (expr) a .ge. 0
bound (expr) a .ge. (expr) b
```

Note that .LE. and .LT. are both interpreted as .LE. and that .GE. and .GT. are both interpreted as .GE.

Note also that multiple bounds may be combined in a single string.

Example:

```
bound (expr) a .ge. 0
bound (expr) b .ge. (expr) a
can be rewritten as:
bound (expr) b .ge. (expr) a .ge. 0
```

EXEC Executes the optimization.

Example (ADS test case):

```
expr a : 2*sqrt(2)*X + Y
expr b : (2*X + sqrt(2)*Y) / (2*X*(X + sqrt(2)*Y))
expr c : 1/(2*(X + sqrt(2)*Y))
X = 1
Y = 1
opti init
opti algo ads istrat 0 iopt 5 ioned 7
minimize (expr) a wrt x y
constraint (expr) b .le. 1
constraint (expr) c .le. 1
bound 0.01 .le. x .le. 1e20
bound 0.01 .le. y .le. 1e20
execute
A = (expr) a
B = (expr) b
C = (expr) c
display X Y
display A B C
```

The results follow:

```
X : .7826923E+00 Y : .4152020E+00
A : .2628990E+01 B : .1003817E+01 C : .3649964E+00
```

11.12.1 Optimization Notes

The gradient based algorithms called by this optimization module are reasonably robust when the functions being minimized or maximized and the imposed constraints are algebraic expressions, but problems can arise when the functions and constraints are generated by more complex analyses. Consider, for example, the following sequence of steps:

- 1) Part geometry defined by ANSYS for parameter vector $(\alpha_0, \beta_0, \gamma_0)$.
- 2) Geometry meshed in ANSYS and thermal/stress analysis executed
- 3) Volume V_0 calculated based on (2)
- 4) Probabilistic fracture mechanics calculation set up and executed based on (2).
- 5) Life L_0 corresponding to a 0.001 failure probability calculated based on (4).
- 6) Part geometry defined by ANSYS for perturbed parameter vector $(\alpha_1, \beta_0, \gamma_0)$.
- 7) Steps (1) through (5) repeated for new geometry yielding volume V_1 and life L_1 .

- 8) Partial derivative estimated: $\partial(V, L)/\partial\alpha = (V_1 - V_0, L_1 - L_0)/(\alpha_1 - \alpha_0)$
- 9) Steps repeated as necessary to estimate $\partial(V, L)/\partial\beta$ and $\partial(V, L)/\partial\gamma$.

The first problem concerns the estimation of the partials of V. The volume calculations for small perturbations of a model geometry can be compromised by differences in the automatically generated meshes. A small change in parameter α may yield a larger part volume in principle, but the differences in meshing between the two perturbations may yield a smaller estimated part volume. In this case, the estimate of $\partial V/\partial\alpha$ would have the wrong sign. While this can be overcome by iterative mesh refinement, doing so adds significant computational overhead.

The second problem affects the estimation of the partials of L and is more subtle. There is an element of statistical sampling in the probabilistic fracture mechanics calculations of step (4). Sampling variations can overwhelm theoretical differences in failure probability between close geometric perturbations which in turn affects the estimate of $L_1 - L_0$. Again, brute force can be applied to overcome this problem: Convergence can be approached by increasing sampling in the relevant Monte Carlo algorithm. The penalty is longer execution time.

The following was felt to be a better solution:

- A small region about the initial guess is defined. V and L are calculated at design points within and on the boundary of the region.
- Local response surfaces $V(\alpha, \beta, \gamma)$ and $L(\alpha, \beta, \gamma)$ are fit to the calculations.
- V is minimized in the region subject to the constraint that L remain above a specified value.
- The solution defines a new local region, and the process continues until a convergence criterion is satisfied.

This approach relies on larger perturbations in model geometry which are designed to result in larger (and less easily masked) differences in V and L; it also tends to average out the noise inherent in the meshing and lifing operations.

11.13 Plotting

PDAS links into a powerful keyword-driven plotting library developed as part of SIESTA. Blocks of plotting commands are embedded into template programs by the PLOT primary keyword. An added PDAS capability: Lines can be defined by pointing to table columns.

Example:

```
tdata (table) 10 X Y Z
line nlin 1 Y X
line nlin 2 Z X
```

Produces two lines, one determined by the points (X_i, Y_i) defined by the the X and Y columns of table 10, the second by the points (X_i, Z_i) defined by the X and Z columns. If TABL FLAG is called prior to TDAT, only active rows of the table are considered.

11.14 Model, Mission and Calculation Libraries

Engines are broken down to components; components may be modeled in pieces (e.g. axisymmetric shells and quads for disk bores, webs, flanges, etc.; plane stress, plane strain quads or 3-D bricks

for stress concentrated details such as bolt holes and dovetail slots. Each model may have several relevant missions (e.g. Air Combat, Air to Surface). Each mission may require more than one life calculation (e.g. multiple material assignments, differing sets of calculation points).

MISSYDD organizes models, missions and calculations, as well as material data, within a flexible database architecture. The program is driven by menus which are closely tied to the database index, and these menus are echoed by PDAS template commands.

There are many menu items, and many possible paths through an analysis. There are, however, eight basic steps:

1. Create a material library
 - Incubation models
 - Fracture mechanics constants
 - Inclusion distributions
2. Assemble a model
 - Geometric interfacing via SIESTA
 - Stress/thermal analysis interfacing via SIESTA
 - Material data assignments
 - Subsets
3. Define a mission
 - Load cases sequences
 - Scaled sequences
 - Superpositions
4. Initialize a computation
 - Material data assignments
 - Subsets
5. Initialize a life calculation
 - Incubation and fracture mechanics options
 - Crack area selection
6. Calculate fracture mechanics lives
7. Compute risk estimates
 - Fracture mechanics calculations and elemental volumes yield geometric failure distributions
 - Integrated with assigned defect distributions
 - Multiple model/mission/computations combined
8. Output
 - Elemental mission stresses/temperatures
 - Fracture mechanics lives
 - Risk estimates

These activities are driven with the primary keywords MODL, MSSN, COMP, LIFE and RISK and subtiered secondary and tertiary keywords.

11.15 General Commands

SUBM Submits user entered Unix commands.

Usage: SUBM

command

command

command

...

DONE

DISP Displays current values of specified parameters.

Usage: DISP *parameter parameter parameter ...*

GLOB Sets global options:

QUIE Suppresses echoing of template.

ECHO Enables echoing of template.

(LIF Sets the argument list for life calculations.

EDIT Edits a file, changing lines of the form:

parameter =

to:

parameter = current value

Usage: EDIT

filename

WAIT (Followed by FILE) Holds template execution until a specified file appears.

Usage: WAIT FILE

filename

11.16 Response Surfaces

Overlaid in *Figure 62* are the failure distributions for nine design perturbations of a seeded model disk geometry. The significance is that these analyses (including geometry definition, finite element stress analysis, mission definition, property assignments, and probabilistic fracture mechanics analysis) were generated with a single PDAS template.

Summarizing:

- A response surface is defined to be a set of analysis nodes (geometry, thermal, stress, ...). Each node is tied to a vector of parameters (part dimensions, rotor speeds, ...), the variables of the analyses. Typically a response node involves a model (the subject), a mission (the action), and a computation (the result).
- A response surface is created by a template which is a set of keyword commands such as `MODL INIT` for Model Initialize, `MSSN COPY` for Mission Copy or `RISK EXEC` for Risk Execute. There are currently more than 200 distinct commands referring specifically to PDAS functions which can be used to build a template in addition to any other system recognized commands (Unix or program executables).
- The first step in execution generates copies of a master template, one for each response surface node included in the current run. Each copy is edited to name certain node-unique entries. For example, a parameter file (named `diskbase.prm`) used by ANSYS to define model geometry is copied into node-named files (`disk1.prm`, `disk2.prm`, `disk3.prm`, ...).
- PDAS cycles through each template copy, executing commands one at a time. If there is a hold up at some line, the program moves to the next node template. If all nodes are held up, the program goes to sleep. After predetermined length of time, it wakes up to check whether execution can resume.
- For example, the ANSYS parameter file `disk1.prm` is edited to assign parameter values (part dimensions, loading conditions). The geometry definition and finite element job is submitted via a distributed processing scheduler. At the end of the ANSYS execution, SIESTA functions are called to post-process the output file to create a SIESTA Random Data Base (RDB). PDAS looks for the node-named RDB files (`disk1.37` and `disk1.38`). Since the ANSYS job was just submitted, they will not be found, and PDAS proceeds onto the next node, editing `disk2.prm`, and so on.
- When `disk1.37` and `disk1.38` do show up, PDAS copies model, mission and computation formats, creating new MIS-SYDD database entries for response node 1. The new model entry references the RDB files for geometry information; it includes all required elemental material property assignments (incubation, fracture mechanics and inclusion distribution data). The new mission entry also references the RDB files; the mission is defined as a scaled sequence of load cases or superpositions of load cases. The computation entry includes specification of incubation and fracture mechanics options (e.g. gradients vs. no-gradients) and requested inclusion sizes.
- PDAS next performs fracture mechanics calculations yielding the life response of the model as a function of crack size, and integrates this response with the inclusion distribution to produce one of the failure distributions shown in *Figure 62*.

The PDAS architecture enables control of an enormous array of computations (it would have been as easy to execute 90 response surface nodes as it was to execute 9). While simple rules of logic must be obeyed in constructing the templates (computation definition must follow mission definition, which must follow model definition), there is great freedom in terms of organizing both internal and external program functions.

Phase III – Validation

12.0 Probabilistic Fracture Mechanics (PFM)

12.1 Probabilistic Fracture Mechanics (PFM)

Algorithm 1

Let $G(N, a)$ denote the geometric failure probability . . . the probability of failure by life N given a single flaw of size a . Let $s(a)$ denote the probability density function of the flaw size distribution. $G(N, a)$ and $s(a)$ are integrated to yield $R(N)$. . . the probability of failure given a single randomly sized flaw.

$$R(N) = \int_0^{\infty} G(N, a) s(a) da$$

To calculate $F(N)$. . . the failure probability given competing flaws . . . the Poisson model for flaw occurrence will be assumed:

The probability that there are n flaws in a component volume is $e^{-V\lambda} (V\lambda)^n/n!$ where λ the average flaw frequency (number per cubic inch) and V is the volume.

$$\begin{aligned} F(N) &= \text{Prob}(1 \text{ defect present} \text{ -- it fails by } N) \\ &+ \text{Prob}(2 \text{ defects present} \text{ -- one or both fail by } N) \\ &+ \text{Prob}(3 \text{ defects present} \text{ -- one or more fails by } N) \\ &+ \dots \\ &= e^{-\lambda V} (\lambda V)^1/1! (1 - (1 - R(N))^1) \\ &+ e^{-\lambda V} (\lambda V)^2/2! (1 - (1 - R(N))^2) \\ &+ e^{-\lambda V} (\lambda V)^3/3! (1 - (1 - R(N))^3) + \dots \\ &= e^{-\lambda V} (e^{\lambda V} - 1 - e^{\lambda V} (1 - R(N)) + 1) \\ &= 1 - e^{-\lambda V R(N)} \\ F(N) &= 1 - e^{-\lambda V R(N)} \end{aligned}$$

Additional detail can be found in Section 8.1.

Algorithm 2

Algorithm 1 assumes that the life of any given flaw at any component location can be predicted exactly. In reality, there is scatter about the predicted life due to many factors (variability in flaw shape, variability in matrix properties, variability in actual loading, etc.). If this scatter is not integrated into the calculations, predictions capture the average behaviors of the observed distributions but not their breadth. The following model is a simple correction:

1. Assume that the scatter can be modelled by a distribution of life multipliers: Let μ denote the ratio of predicted to observed life for a single inclusion, and let $m(\mu)$ denote the probability density function of the μ distribution.
2. Assume also that the distribution of μ predominantly represents testing variability (i.e. specimen-to-specimen rather than inclusion-to-inclusion). The distribution of life is derived from the basic PFM risk algorithm as a kind of convolution:

$$\int [1 - e^{-\lambda V \cdot R(N\mu)}] m(\mu) d\mu$$

Figure 74 shows a Weibull distribution of Predicted/Observed ratios for the basic René 88 DT life model used for the calculations presented in this report (*Reference 1* or Section 15.1).

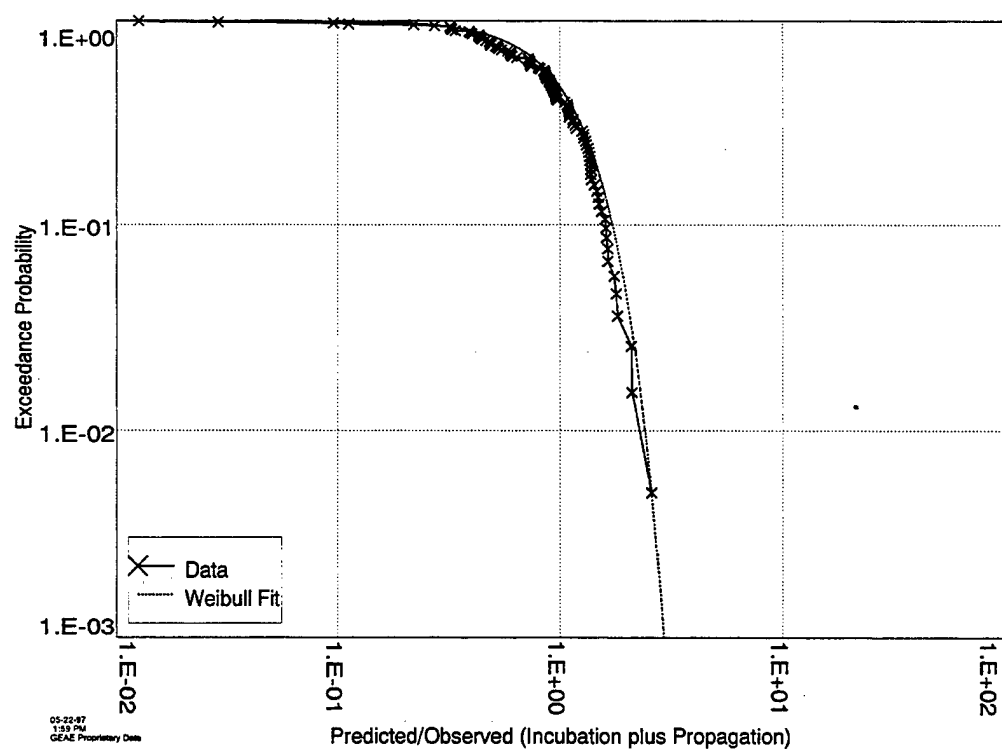


Figure 74. Weibull Fit to Predicted/Observed Distribution.

13.0 An Early PFM Validation Study

For all practical purposes PFM validation must be done within the range of probabilities 0.01 to 0.99. The following validation study was rigorously designed to judge adequacy of the model over this small range of probability but over a large range of life (3 orders of magnitude). To achieve this, the specimens were prepared from seeded PM René 95. Given that rates of flaw occurrence in production hardware are orders of magnitude lower than seeding rates, it is entirely reasonable to accept that the failure probabilities are proportionately lower.

The study covered in this section was initiated in 1984, and was shaped by limitations of the MISSYDD Version 3 release. In particular the fracture mechanics module at that time incorporated only an approximate fracture mechanics algorithm which limited applications to:

1. Situations where surface initiations could be assumed to be suppressed.
2. Situations where critical surface flaws could be discounted given inspections.
3. Situations where surface and buried flaws could be assumed equivalent.

Given the desire to employ specimens seeded with a broad size distribution of ceramics, and given the resulting likelihood that many (if not most) failures would be surface initiated, it was necessary to pick test conditions which minimized the differences between surface and buried flaws. Based on the belief that vacuum and air crack growth rate curves are approximately the same at room temperature, it was decided to run the tests cold.

Unfortunately, room temperature material properties were not (and still are not) available. Also, the seeding distribution appeared to be non-uniform; segregation during can filling

was suspected. These problems led to assumptions being made which left the accuracy of the data analyses in some doubt. Still, the results strikingly supported MISSYDD's validity, and all subsequent GEAE seeded LCF programs have been patterned after this study.

13.1 Background

The acceptance of MISSYDD as GEAE's PFM methodology has generally been based on its conceptual structure: Logically, given a distribution of flaws, and given that flaws fracture and initiate sharp cracks, and given that the growth of sharp cracks is accurately described by fracture mechanics, then MISSYDD should adequately predict a failure distribution. The experimental validation program described in this section offers important lessons:

1. Flaw distributions are hard to come by, even under very controlled conditions.
2. Sharp crack fracture mechanics can be conservative when applied to flaws.
3. Other fatigue mechanisms actively compete with flaws.

Work is continuing to develop better flaw distributions, better understanding of flaw behavior, and better general understanding of competitive cyclic failure mechanisms. The results presented here are significant and encouraging: Given the right inputs, MISSYDD does seem to work.

13.2 Specimen Preparation

In late 1984, -150 mesh powder metal René 95 was seeded as summarized in *Table 17* and hot isostatically pressed into bar stock by Special Metals (Princeton, KY). The seeds were drawn from sieved fractions of Exolon SP&C alumina grit provided by Carborundum Abrasives Co. (Niagara Falls, NY). In 1985, sixty cylindrical

Table 17. Seeding Definition.

Nominal Grit Number	Nominal Diameter (Mils)	Area (Sq Mils)	Density (Particles/Pound)
40	36	530	16.8
36	36.2	1030	13.5
24	50.4	1995	10.1
16	74	4303	6.7
12	93.7	6896	3.4

specimen centersections were machined from the bars by Low Stress Grind (Cincinnati, OH) and returned to GEAE for nondestructive examination.

Following the inspections, end tabs were inertia welded to the centersections by MTI (Indianapolis, IN), after which fifty-seven of the welded blanks were machined by Metcut (Cincinnati, OH) into MV2 hourglass specimens (see *Figure 75*).

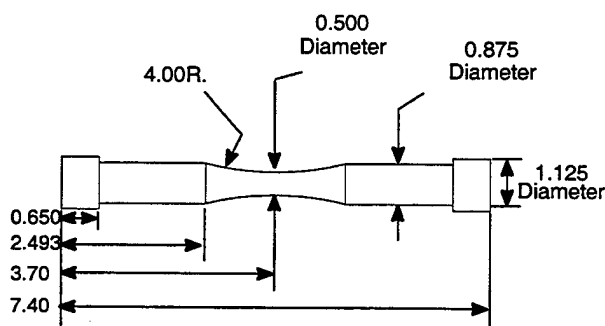


Figure 75. MV2 Specimen Design.

13.3 Evaluation of Seeding Practice

Each of the centersections was visually inspected and the numbers of flaws observed on the ground surfaces recorded. It was sometimes difficult to obtain truly definitive counts, and so minimum and maximum estimates were reported. Following visual inspection, forty of the centersections were

examined ultrasonically (longitudinal immersion ultrasonics). The estimated locations of each indication was recorded; if two indications were reported at approximately the same location, they were assumed to correspond to the same flaw. The results of both inspections are included in *Table 2*. (The results of a final visual inspection of the finish machined specimens is also included, as well as the observed life and failure location of each specimen tested.)

The visual and ultrasonic data are highly correlated. Specimens which appeared relatively clean of flaws as judged by visual inspection also appeared clean when examined ultrasonically. Specimens which appeared visually to be dirty with flaws also appeared dirty ultrasonically. There are exceptions, but the trend is supported by a calculated Spearman coefficient of 0.76 between the first round of visual inspections and the subsequent ultrasonic inspections (*Reference 2*). The visual and ultrasonic examinations both exhibit a disturbing trend. In manufacturing the bar stock, stainless steel tubular cans were filled with seeded powder metal and then hot isostatically pressed. Each can was long enough to yield three specimen centersections. The centersections were labeled sequentially, preserving the order in which the cans were filled. Centersections 1, 2 and 3 were cut from the top, middle and bottom of the first

can; centersections 4, 5 and 6 were similarly cut from the second can, and so on. A few of the cans were partially damaged, and so the labeling of the centersections extends beyond 60, as is apparent from *Table 18*. It appears, based on the data, that the density of flaws in the first ten or so cans may be less than that in the second ten filled. There was no particular order to the inspections; hence this trend can not be attributed to a learning curve on the part of the inspectors.

Prior to the production of the bar stock, a study had been performed to assure that the procedure to be used in filling the cans would result in a uniform distribution of the seeded flaws. Five hundred large and five hundred small ceramic particles were blended into five hundred pounds of the powder metal. Fifty ten pound samples were withdrawn from the bottom of the blend and resieved through -140 mesh screen to recover the flaws. Before drawing each sample, the mixture was tumbled four times, attempting to minimize segregation.

Table 19 tabulates the number of seeds found in each of the fifty samples. It must be noted that a total of 502 large seeds were found (a possible counting error) and 480 small ones (some may have been passed by the screen). Also, the sample weights were never exactly ten pounds. Still, no trends were observed, and the empirical distributions of the seeds recovered sensibly agree with the expected Poisson distribution (see *Figure 76*).

It is noted that the Kolmogorov-Smirnov distances of the small and large empirical distributions from the Poisson hypothesis are 0.08345 and 0.1449 respectively. The approximate significance level of the difference between the small seed distribution and the Poisson hypothesis is 0.85 based on the Kolmogorov-Smirnov one sample test (*Reference 3*).

(This is the probability that a sample from the assumed distribution will yield a Kolmogorov-Smirnov distance of 0.08345 or larger. If the

probability were very small, it would be concluded the data was not likely sampled from a Poisson population. If the probability were very large, it would be concluded the data fit the Poisson model too well, and that the variability was not statistical but somehow deterministic. While a good significance level is a matter of taste and conviction, the author is typically satisfied with values lying between 0.1 and 0.9.)

The significance level of the difference between the large seed distribution and the Poisson hypothesis is 0.22.

The preliminary study was witnessed; the actual filling of the cans was not. It is possible, therefore, that the supplier deviated from the approved process. It may be that the seeded blend was not tumbled between cans. Or it may be that the first ten cans were filled too slowly, increasing the likelihood of seed segregation.

In any case, the assumption will have to be made that the relative size distribution of the seeds is constant from can to can. The average seeding density is estimated based on the ultrasonic finds:

There were a total of 151 ultrasonic indications in the 40 inspected centersections (about 96 cubic inches total), yielding an average density of 1.57 seeds per cubic inch.

The intended seeding density was 15 per cubic inch, nearly 10 times larger (*Table 17*). A similar disparity was observed in a 1988 program studying electron beam (EB) melt flotation as a method for separating ceramic flaws from metallic samples (*Reference 4*). Electrodes were machined from seeded -150 mesh René 95 powder HIPped in tubular cans, and individually drip melted in an EB furnace. Ceramics floating on the surfaces of the resulting buttons were counted and characterized via SEM image analysis. The size distributions of the recovered seeds agreed with the initial distributions, but the numbers recovered were generally lower than expected.

Table 18. Inspection Comparisons.

Blank ID	First Visual Count (Blanks)	Ultrasonic Count (Blanks)	Second Visual Count (Specimens)	Cycles To Failure	Initiation Site (Surface or Internal) Flaw Location
1	3	--	0	--	--
2	1 to 2	--	4	1,417	S
3	4 to 5	7	1	8,627	I
4	1 to 4	0	0	--	--
5	1 to 2	--	--	19,820	S
6	1	0	1	19,578	S
7	0 to 1	0	0	--	--
8	1	0	0	13,881	S
9	1	2	0	14,674	S
10	2	7	1	--	--
11	1 to 2	1	0	17,285	S
12	1	1	0	24,079	S
13	1	0	1	--	--
14	1	0	0	25,488	S
15	1	0	0	22,201	S
16	2 to 3	3	0	--	--
17	1 to 3	0	0	25,235	S
18	1	0	1	19,193	S
19	1 to 3	1	0	--	--
20	0	--	0	21,359	S
21	0	0	0	12,360	S
22	0 to 1	0	0	16,720	S
23	0 to 2	--	--	--	--
24	1 to 3	0	0	22,279	S
25	3 to 4	0	0	835	I
26	2	1	1	20,032	S
27	2	--	1	1,027	S
28	5 to 7	--	1	23,910	S
29	3 to 5	3	4	19,476	S
30	--	--	--	--	--
31	4 to 7	19	6	281	S
32	3 to 6	--	3	5,435	S
33	3 to 4	12	2	64	S
34	2	4	2	1,055	S

Table 18. Inspection Comparisons. (Concluded)

Blank ID	First Visual Count (Blanks)	Ultrasonic Count (Blanks)	Second Visual Count (Specimens)	Cycles To Failure	Initiation Site (Surface or Internal) Flaw Location
35	2 to 3	8	1	18,891	S
36	4	10	3	160	S
37	2	4	0	27,875	S
38	4 to 7	9	1	1,607	S
39	3 to 4	6	1	2,528	S
40	1	--	--	--	--
41	1	2	0	3,331	I
42	--	--	--	--	--
43	1 to 4	1	4	1,880	S
44	4	2	0	1,743	I
45	2	7	2	7,436	I
46	3	6	3	990	I
47	2	--	2	642	S
48	4 to 7	--	--	--	--
49	3 to 5	--	0	2,134	I
50	2 to 4	--	0	19,241	S
51	1	--	2	1,712	S
52	1 to 3	--	1	387	S
53	4 to 6	5	3	3,214	S
54	4 to 6	11	7	279	S
55	--	--	--	--	--
56	2 to 6	11	3	1,053	S
57	--	--	--	--	--
58	4 to 7	8	1	1,801	I
59	4 to 8	--	4	2,660	S
60	--	--	--	--	--
61	0 to 1	--	0	21,385	S
62	0 to 1	0	0	23,469	S
63	0 to 1	--	0	21,426	S
64	2	--	2	18,465	S
65	2	--	2	14,979	S

Table 19. Blending Study.

Sample Number	Small Seeds Recovered	Large Seeds Recovered	Sample Number	Small Seeds Recovered	Large Seeds Recovered
1	14	14	26	8	18
2	15	13	27	15	10
3	8	8	28	10	7
4	10	9	29	11	7
5	6	14	30	7	9
6	7	8	31	5	11
7	7	8	32	8	11
8	14	8	33	11	9
9	11	4	34	6	13
10	15	10	35	13	10
11	12	8	36	15	15
12	8	8	37	12	13
13	8	10	38	6	8
14	12	16	39	7	10
15	9	9	40	9	9
16	8	11	41	11	15
17	10	11	42	9	5
18	16	7	43	7	9
19	9	7	44	5	13
20	10	3	45	16	7
21	11	8	46	9	12
22	5	6	47	6	14
23	8	7	48	12	15
24	10	10	49	7	8
25	10	14	50	12	13

It was hypothesized that the powder had formed conical mounds during can filling, and that many seeds had rolled to the can walls and been subsequently lost during machining. This possibility was demonstrated. A can was filled with seeded -150 mesh powder, a thin-walled tube inserted so as to divide the can into two concentric regions, and the inner and outer fractions separately sieved to recover the seeds. It was found that the density of 388 sq mil seeds in the outer fraction was 2.65 times that in the inner fraction. This ratio decreased to 2.30 for the 100 sq mil seeds and to 1.80 for the 16 sq mil seeds.

Given that the seeds in the MISSYDD verification material were very large, the losses may well have been greater. The estimated average

density of 1.57 seeds per cubic inch has been used for the MISSYDD calculations.

(There is, it should be noted, evidence that seeded -270 mesh powder is less prone to such segregation. See Section 14.2)

13.4 Fatigue Testing

It was planned to test the specimens in load control at room temperature. A triangular waveform from 0 to 50 ksi in the shank (0 to 150 ksi at the neck of the hourglass) was chosen; the frequency: 30 cycles per minute. An average life of 4000 cycles was expected based on an elastic stress analysis MISSYDD calculation; the scatter about this average, it was realized, would be large.

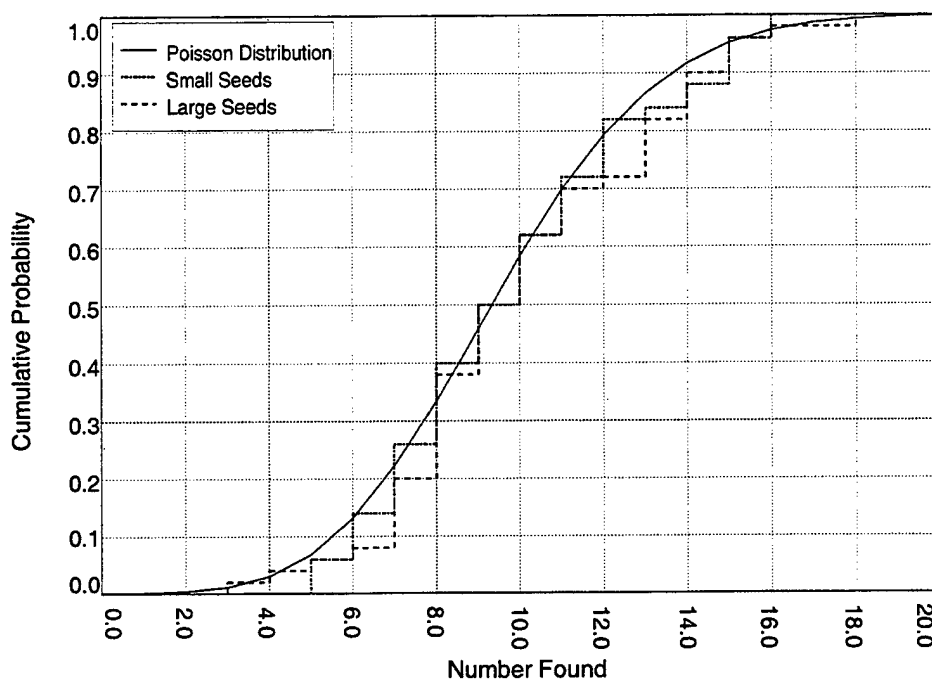


Figure 76. SMC Blending Study - Evaluation Based on Poisson Model.

A single machine was dedicated to the program, and the specimens were tested in the order specified in **Table 20** (MBRC, Cincinnati, OH). Scribe marks identifying one end of each specimen were always oriented to the front of the test stand; some specimens were loaded with their mark up, some with their mark down — refer again to **Table 20**.

All tests were instrumented with a diametral extensometer monitor; the maximum and minimum strains were to be recorded by a computer data acquisition system at each cycle, and the data transmitted to GEAE on IBM PC readable floppy discs.

The first five specimens tested exhibited the following lifetimes:

MV2-1	39,927 (cycles)
MV2-4	40,290
MV2-7	34,293
MV2-10	29,940
MV2-13	71,335

Only one of these (MV2-10) failed from a seeded flaw, a large one located near the highly stressed minimum cross-section of the hour-glass. The fact that only one failure was seed initiated, though frustrating, was understandable given the apparent lower density of seeds in the low numbered specimens. That one seed made a respectable showing in life was encouraging on the one hand; on the other hand, it was apparent that the testing costs might rise by an order of magnitude. The decision was made to raise the stresses.

New parameters were fixed by the eighth test (MV2-22). Fifty specimens were tested at a 1.0% computed axial strain (constant strain amplitude); the waveform was triangular and the frequency, 30 cycles per minute.

An attempt was made to simulate this loading with an ANSYS finite element stress analysis. Elastic-plastic calculations were made using a five point cyclic stress-strain curve defined by Ramberg-Osgood constants for As-HIP PM René 95 ($K = 214.4$, $N = 0.03732$). The analysis was iterated with changes to boundary

conditions until a total strain of 1% was attained at the min-section surface node. The procedure was then repeated to push the strain at this node back to 0%.

The first try yielded stresses much higher than had been observed in the tests: -130 ksi in

compression to 161 ksi in tension. The differences are probably the result of nonuniform strain through the specimen min-section — strain at the surface does not equal average crosssectional strain, the quantity measured by a diametral extensometer.

Table 20. Test Orientations.

Test	Specimen ID	Orientation	Test	Specimen ID	Orientation
1	MV2-1	Up	30	MV2-32	Up
2	MV2-4	Down	31	MV2-35	Down
3	MV2-7	Up	32	MV2-38	Up
4	MV2-10	Down	33	MV2-41	Down
5	MV2-13	Up	34	MV2-44	Down
6	MV2-16	Down	35	MV2-47	Up
7	MV2-19	Up	36	MV2-50	Down
8	MV2-22	Down	37	MV2-53	Up
9	MV2-25	Up	38	MV2-56	Up
10	MV2-28	Down	39	MV2-59	Down
11	MV2-31	Up	40	MV2-62	Up
12	MV2-34	Down	41	MV2-65	Down
13	MV2-37	Up	42	MV2-3	Up
14	MV2-43	Down	43	MV2-6	Down
15	MV2-46	Up	44	MV2-9	Up
16	MV2-49	Down	45	MV2-12	Down
17	MV2-52	Up	46	MV2-15	Up
18	MV2-58	Down	47	MV2-18	Down
19	MV2-61	Up	48	MV2-21	Up
20	MV2-64	Down	49	MV2-24	Down
21	MV2-2	Up	50	MV2-27	Up
22	MV2-5	Down	51	MV2-33	Up
23	MV2-8	Up	52	MV2-36	Down
24	MV2-11	Down	53	MV2-39	Up
25	MV2 14	Up	54	MV2-45	Down
26	MV2-17	Down	55	MV2-51	Down
27	MV2-20	Up	56	MV2-54	Up
28	MV2-26	Up	57	MV2-63	Up
29	MV2-29	Down			

A second attempt was made using a reduced target tensile strain of 0.92%. While the results were better (see *Figure 77*), the stresses were still a bit off. It was decided to proceed by scaling the tensile load case by 0.9070702 and the compressive load case by 1.161684.

13.5 Fracture Mechanics Analysis

Referring to *Table 21*, it is seen that twenty-six of the fifty specimens failed at seeded flaws (the remaining twenty-four failed, presumably, at much smaller, naturally occurring inclusions or at grain facets). As the alumina seeds were not particularly ellipsoidal, their fracture cross sections were not particularly elliptical; and, consequently, the accuracy of their fracture mechanics treatment could be de-

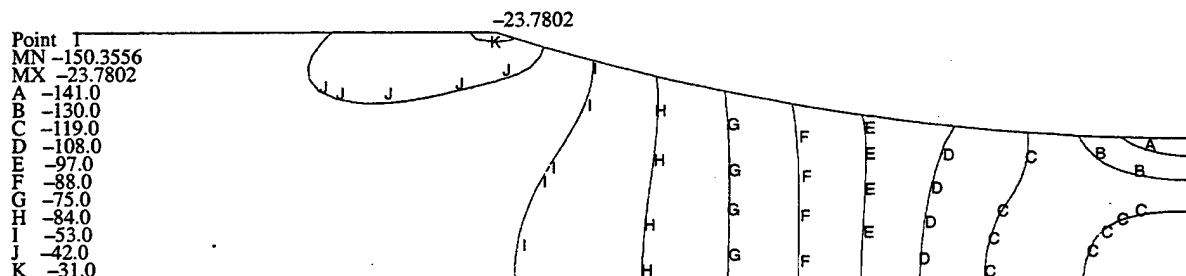
bated. The specimens were viewed optically at low magnification (20X); rectangles similar in appearance to the flaws were visualized, and their locations and dimensions measured.

Residual lives were calculated using a PDAS Template accessing the scaled ANSYS analysis. Buried flaws were translated into circular cracks of equal area. Surface intersecting flaws were translated into semicircular cracks of equal area (requiring that the areas reported in *Table 21* be doubled for the calculations).

Extruded+Forged (E+F) -150 mesh PM René 95 750° F (482° C) vacuum crack growth sigmoidal shape constants were chosen for the initial fracture mechanics calculations. This choice was felt to be consistent with the accepted practice of using room temperature air

MISSYDD NODAL PROJECTED MISSION STRESS DATA

Compressive Load Case



MISSYDD NODAL PROJECTED MISSION STRESS DATA

Tensile Load Case

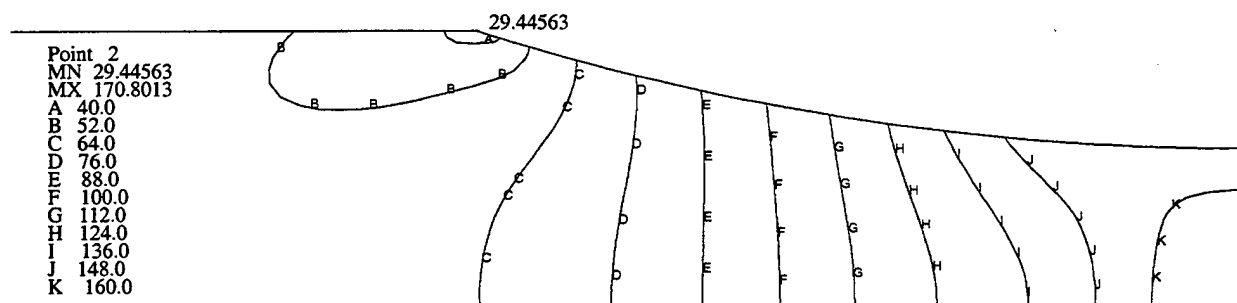


Figure 77. MV2 Elastic/Plastic Stress Distribution.

Table 21. Test Results Summary.

Obsd. Cycles To Failure	Predicted Cycles To Failure	Flaw Loc.	Calculated Specimen Diameter At Crack (inches)	Flaw a (inches)	Flaw 2c (inches)	Flaw Area (2ac) (Sq Mils)	Surface To Flaw Center (inches)	Max Stress (ksi)	Min Stress (ksi)	Spec. ID (MV2-XX)
64	12	S	0.500133	0.0745	0.1125	8381.25	0.03725	152	-150	33
160	85	S	0.528367	0.0678	0.0564	3823.92	0.03390	152	-114	36
279	97	S	0.507425	0.0353	0.0728	2569.84	0.01765	157	-134	54
281	328	S	0.500102	0.0290	0.0338	980.20	0.01450	152	-150	31
387	394	S	0.505125	0.0272	0.0363	987.36	0.01360	156	-138	52
642	644	S	0.500453	0.0194	0.0337	653.78	0.00970	152	-149	47
835	3880	I	0.508515	0.0179	0.0260	465.40	0.08800	156	-124	25
990	1156	I	0.510792	0.0310	0.0700	2170.00	0.05000	155	-125	46
1,027	1093	S	0.501811	0.0210	0.0225	472.50	0.01050	154	-146	27
1,053	814	S	0.500017	0.0138	0.0404	557.52	0.00690	152	-150	56
1,055	1181	S	0.507761	0.0180	0.0288	518.40	0.00900	157	-133	34
1,417	521	S	0.516594	0.0240	0.0422	1012.80	0.01200	157	-122	2
607	2076	S	0.502952	0.0175	0.0186	325.50	0.00875	155	-143	38
1,712	2446	S	0.536077	0.0140	0.0347	485.80	0.00700	148	-110	51
1,743	2138	I	0.502401	0.0330	0.0400	1320.00	0.09250	161	-125	44
1,801	2560	I	0.500035	0.0250	0.0339	847.50	0.09700	163	-125	58
1,880	1093	S	0.524365	0.0154	0.0445	685.30	0.00770	154	-116	43
2,134	2395	I	0.500280	0.0225	0.0350	787.50	0.05800	159	-134	49
2,528	2466	S	0.513438	0.0113	0.0187	211.31	0.00565	157	-125	39
2,660	90	S	0.577717	0.0802	0.0807	6472.14	0.04010	125	-99	59
3,214	3141	S	0.535915	0.0154	0.0265	408.10	0.00770	148	-111	53
3,331	1948	I	0.500640	0.0245	0.0390	955.50	0.04800	158	-136	41
5,435	26274	S	0.511292	0.0050	0.0150	75.00	0.00250	158	-128	32
7,436	3139	I	0.508281	0.0175	0.0239	418.25	0.04300	157	-128	45
8,627	2083	I	0.514503	0.0250	0.0370	925.00	0.04400	154	-123	3

crack growth rate curves for subsurface calculations at higher temperatures. The rationale behind this is that the acceleration of crack growth rate at higher temperatures is environmentally induced. The impact of the environment on René 95 crack growth is minimal at room temperature. Also, crack growth rates in vacuum are found to be relatively insensitive to temperature.

Figure 78 compares predicted and observed specimen lives. Referring to the plot, it is seen

that the predicted lives are off by a factor of about 2,000 for the surface failures and by a factor of 30 for the subsurface failures.

In the Paris regime, crack growth rate is log-linearly related to stress intensity, and for circular buried cracks or semicircular surface cracks in a uniform stress field, stress intensity is, in turn, approximately log-linearly related to radius. The differential equation in this regime has the simplified form:

$$da/dN = \alpha \cdot a^{\beta}$$

Table 21. Test Results Summary (Concluded).

Obsd. Cycles To Failure	Predicted Cycles To Failure	Flaw Loc.	Calculated Specimen Diameter At Crack (inches)	Flaw a (inches)	Flaw 2c (inches)	Flaw Area (2ac) (Sq Mils)	Surface To Flaw Center (inches)	Max Stress (ksi)	Min Stress (ksi)	Spec. ID (MV2-XX)
12,360	-	S	0.502096	-	-	-	-	154	-145	21
13,881	-	S	0.500142	-	-	-	-	152	-150	8
14,674	-	S	0.502064	-	-	-	-	154	-145	9
14,979	-	S	0.500002	-	-	-	-	152	-150	65
16,720	-	S	0.501365	-	-	-	-	153	-147	22
17,285	-	S	0.500614	-	-	-	-	153	-149	11
18,645	-	S	0.500024	-	-	-	-	152	-150	64
18,891	-	S	0.500847	-	-	-	-	153	-148	35
19,193	-	S	0.501332	-	-	-	-	153	-147	18
19,241	-	S	0.501197	-	-	-	-	153	-147	50
19,476	425	S	0.589997	0.0400	0.0670	2680.00	0.02000	119	-95	29
19,578	-	S	0.501182	-	-	-	-	153	-147	6
19,820	-	S	0.506572	-	-	-	-	157	-135	5
20,032	-	S	0.500433	-	-	-	-	152	-149	26
21,359	-	S	0.500492	-	-	-	-	153	-149	20
21,385	-	S	0.500825	-	-	-	-	153	-148	61
21,426	-	S	0.500016	-	-	-	-	152	-150	63
22,201	-	S	0.500034	-	-	-	-	152	-150	15
22,279	-	S	0.500634	-	-	-	-	153	-148	24
23,469	-	S	0.500120	-	-	-	-	152	-150	62
23,910	-	S	0.500864	-	-	-	-	153	-148	28
24,079	-	S	0.500094	-	-	-	-	152	-150	12
25,235	-	S	0.500704	-	-	-	-	153	-148	17
25,488	-	S	0.500588	-	-	-	-	153	-149	14
27,875	-	S	0.502209	-	-	-	-	154	-145	37

where a is crack radius and N is time (typically measured in cycles). Solving this equation yields that:

$$N = N_i + [a_c^{(1-\beta)} - a_i^{(1-\beta)}] / [\alpha \cdot (1-\beta)]$$

where N_i is an incubation period prior to sharp crack initiation, a_i is the initial radius of the crack, and a_c is the critical radius at which growth becomes unstable.

It is emphasized that the differences between surface and subsurface crack growth should be slight excepting for the environmental effects. The stress intensity factors for a semicircular surface crack and a circular subsurface crack of the same radius are very nearly identical.

Sharp crack calculated life is inversely proportional to the growth rate constant α . Multiplying the Paris curve used for surface crack

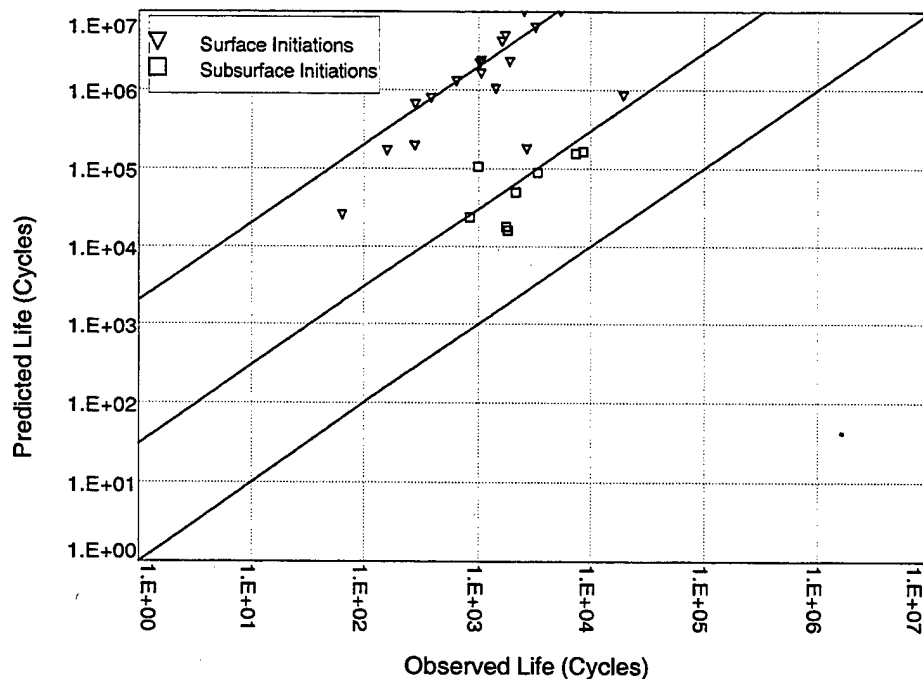


Figure 78. Fracture Mechanics Comparisons Using 750° F Vacuum Data.

growth by 2,000 and repeating the fracture mechanics calculations yields the revised comparisons shown in **Figure 79**. Note that this single change pulled not only the surface into line but also the subsurface.

There is evidence that the two long life outliers might be reconciled by incubation. Flaws exercised at low stresses are expected to lie dormant longer than at high stresses. The specimen numbers in **Figure 79** identify the plotted points farthest from the central band. The failure planes of specimens 29 and 59 were found to be the lowest and next to lowest in stress out of fifty specimens.

13.6 MISSYDD Analysis

The MISSYDD predicted failure distribution is plotted in **Figure 80** superimposed on the observed failure distribution of the fifty tests.

The deviation of the MISSYDD prediction from the data is reasonably uniform suggesting either that crack growth rates should decrease

slightly (which would shift the prediction to the right), or that the assumed seeding rate should decrease slightly from 1.57 per cubic inch (which would shift the prediction downward). Attempting the latter (and reducing the rate by a factor of 2 to 0.785 per cubic inch) produces the comparison in **Figure 81**.

Two points are worth making:

1. The matrix fatigue life of the specimens was found to be about 20,000 cycles. **Figure 82** shows a magnified window of the failure distribution containing all twenty-six tests which avoided the seeded aluminas. These failures serve to censor the MISSYDD prediction which only addresses the threat of the seeded defects.
2. The large scatter observed in the test results is adequately reflected in the MISSYDD prediction. Moreover, there are steps observed in the prediction which result from the discrete nature of the seeding distribution (nominally five defect sizes). The data suggests the same steps (**Figure 81**).

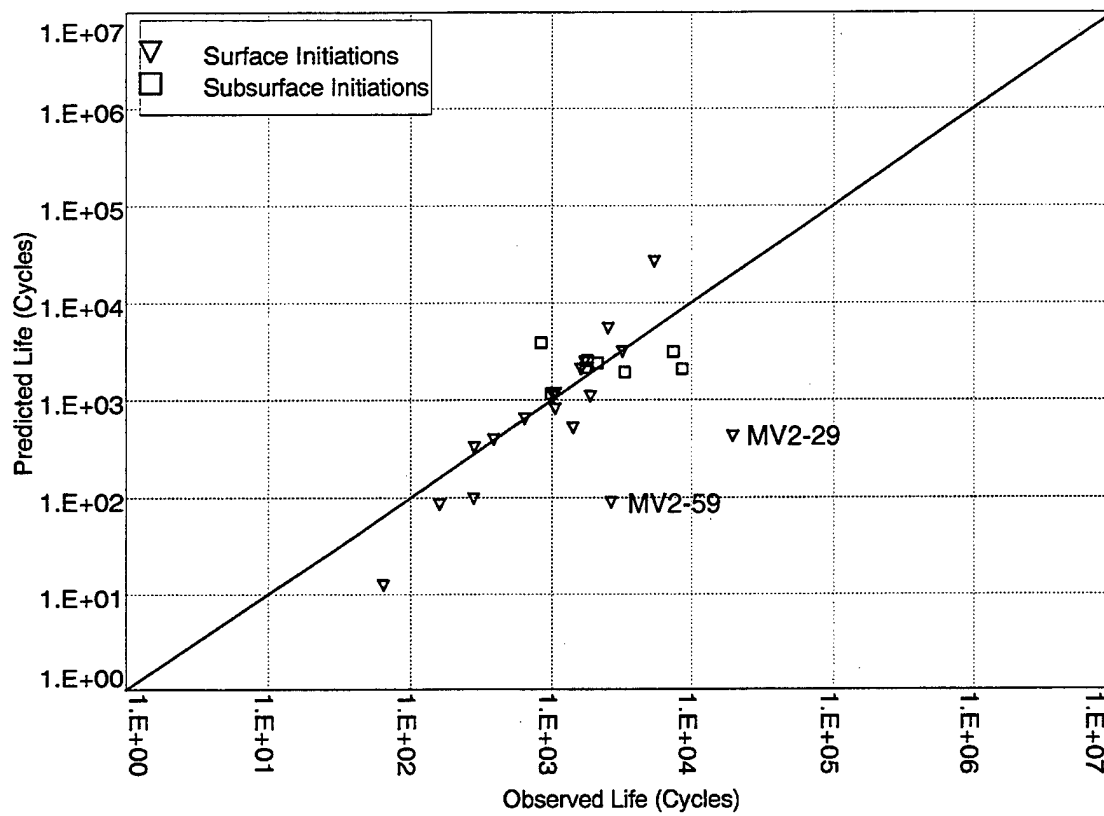


Figure 79. Revised Fracture Mechanics Comparisons.

While it is disappointing that agreement could not have been achieved without resorting to factoring of crack growth constants and seed-

ing rates, it is encouraging that the statistical aspects of the failure data are so well represented.

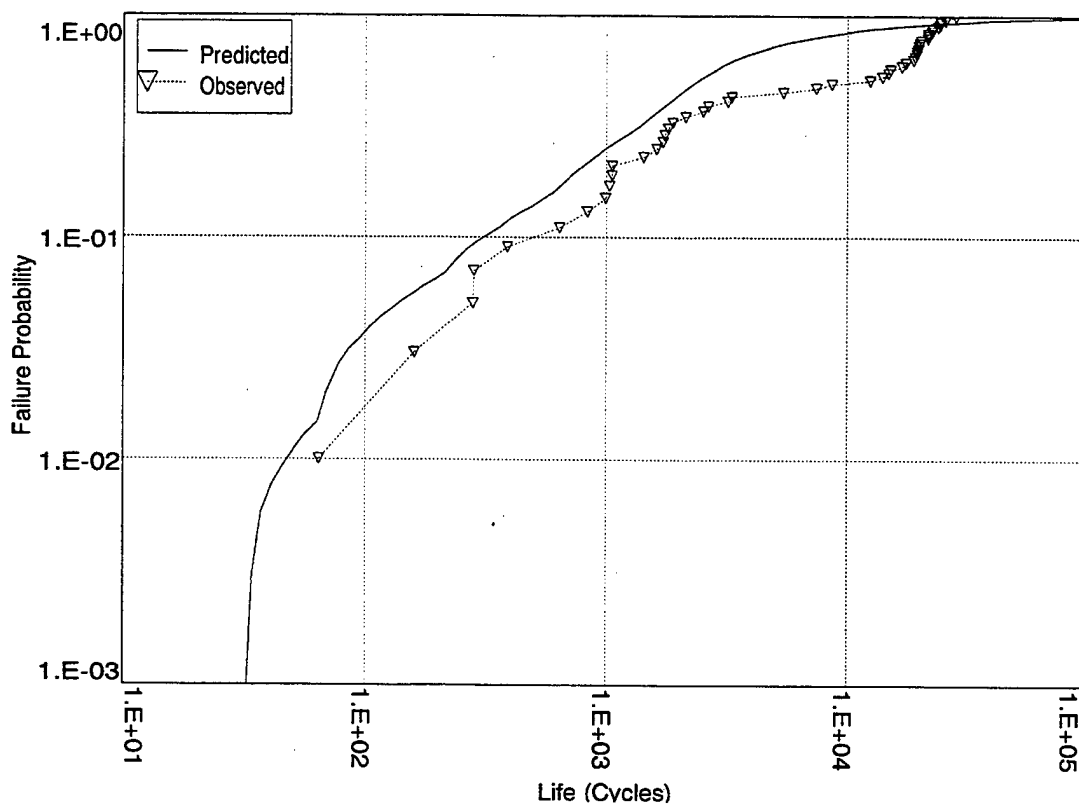


Figure 80. MV2 MISSYDD Analysis.

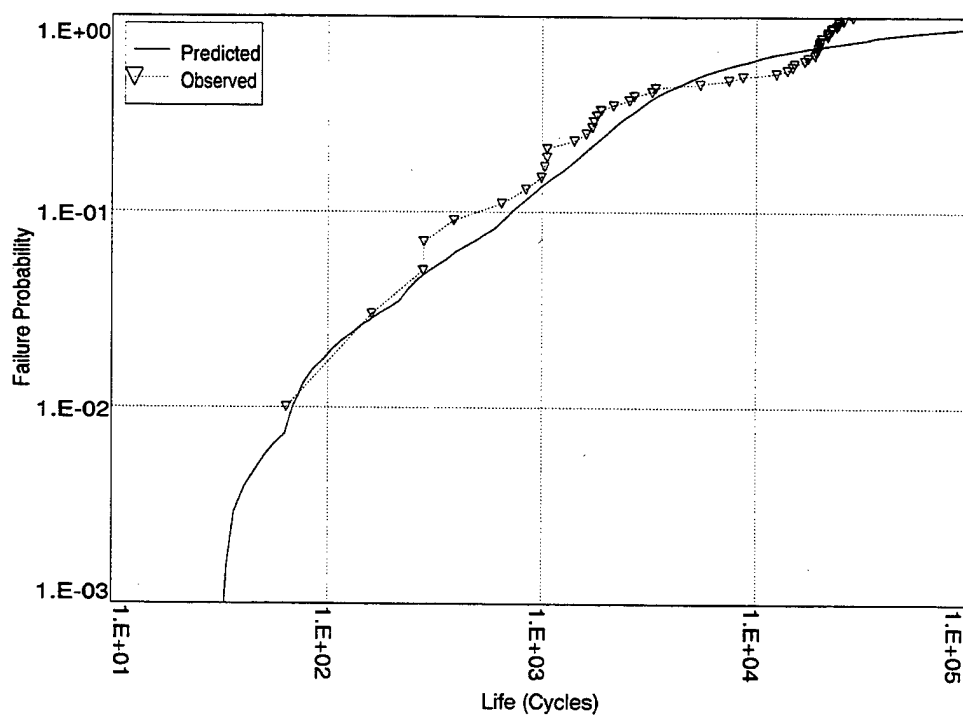


Figure 81. Revised MV2 MISSYDD Analysis.

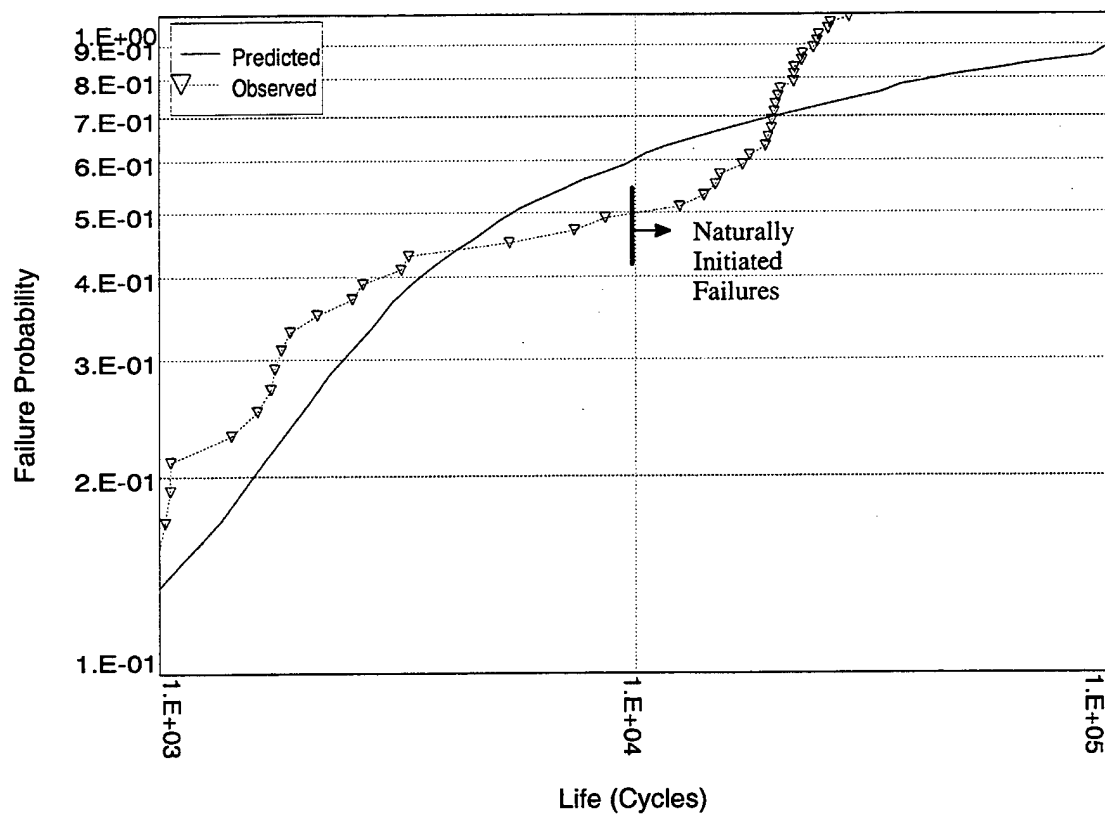


Figure 82. Revised MV2 MISSYDD Analysis -- Focus on Natural Initiations.

14.0 PRDS Validation Program

The PRDS PFM validation testing has included both hourglass push-pull specimens and small model disks. The hourglass concept was again chosen to simulate stress gradients present in real hardware while allowing adequate numbers of tests to enable proper statistical comparisons. The model disks more closely simulate real hardware: Machining conformed to production practices. The stress field is generally multiaxial. But given their much higher costs (both of manufacturing and of testing), far fewer could be run.

Most of the specimens were prepared from forgings seeded with controlled size distributions of alumina particles supplementing the inherent inclusion population. The following will describe this program.

14.1 Specimen Preparation

From 1992 to 1994, -270 mesh PM René 88 DT was seeded as summarized in *Table 22*, and extruded and forged into pancakes by Cameron Powder Systems (Brighton, MI) and Cameron

Forge (Houston, TX), both now part of Wyman-Gordon (Worcester, MA). The seeds were drawn from sieved fractions of ANSI 240 and FEPA 100 polycrystalline alumina grain provided by Norton Materials (Worcester, MA, a subsidiary of Saint-Gobain Industrial Ceramics).

Ten extrusions were prepared: 4 Large Seeded (S1), 4 Small Seeded (S2) and 2 Unseeded (S0). The weights, seeding conditions and extrusion ratios are recorded in *Table 23*. Extrusion temperature was 1920° F (1050° C).

The extrusions were cut into mulds (sequentially labelled AB, BC, ...) which then were forged at 1920° F (1050° C) into pancakes about 1.5 in. thick by about 8.7 in. diameter.

The forgings were heat treated through a 2100° F (1149° C) supersolvus solution followed by air cooling followed by a 1400° F (760° C) aging cycle followed, again, by air cooling.

Twenty-two pancakes were dedicated to push-pull LCF specimens as layed out in *Table 23*, yielding six specimens each. The HG1 and

Table 22. Seeding Definition.

Extrusion	Seeding Distribu.	Blend Weight	Fill Weight	50/+60 (FEPA 100)	-60/+80 (FEPA 100)	140+170 (FEPA 100)	270+230 (FEPA 100)	-270/+325 (ANSI 240)	Extrusion Ratio
-	Test Blend	-	-	-	50.3860	14.8120	-	-	-
-	Blend Study	198	-	-	50.3800	14.8126	-	-	-
E-666	S1B	203	201	16.2966	-	10.5485	-	-	5.7
E-675	S1C	221	201	16.2956	-	10.5463	-	-	5.3
E-721	S1E	104	104	9.3155	-	6.0243	-	-	5.2
E-722	S1F	166	166	14.0380	-	9.0734	-	-	5.2
E-667	S2A	208	199	-	-	-	2.2048	0.9782	5.7
E-668	S2B	205	203	-	-	-	2.2043	0.9786	5.7
E-669	S2C	209	200	-	-	-	2.2047	0.9785	5.7
E-670	S2D	203	200	-	-	-	2.2045	0.9778	5.7
E-663	S0	-	203	-	-	-	-	-	5.7
E-720	S0	-	251	-	-	-	-	-	5.2

Table 23. Forging Dispositions.

Extrusion	Seeding Distribution	Pancake AB	Pancake BC	Pancake CD	Pancake DE	Pancake EF	Pancake FG	Pancake GH
E-666	S1	scrap	HG1	HG1	HG1	HG2	MD902	
E-675	S1	scrap	HG1	HG1	MD1001	HG1	holding	
E-721	S1	MD1002	MD1003	MD1004	MDI005			
E-722	S1	MD1006	MD1007					
E-667	S2	scrap	HG2	HG2	HG2	HG2	MD910	
E-668	S2	scrap	HG2	HG2	MD911	HG2	MD912	
E-669	S2	scrap	HG1	HG1	MD913	MD903	MD904	
E-670	S2	scrap	MD905	MD906	MD907	MD908	MD909	
E-663	S0	scrap	HG1	MD901	HGI	HG2	holding	
E-720	S0	holding	HG1	holding	HGI	HGI	holding	holding

HG2 hourglass geometries are detailed in **Figures 83** and **84**. The cutup plan is shown in **Figures 85** and **86**. Cylindrical centersections machined from the pancakes were inertia welded to Inconel 718 end pieces and the

welded blanks low stress ground and polished by Metcut (Cincinnati, OH).

Twenty pancakes were machined into model disks (again, refer to **Table 23**). It was

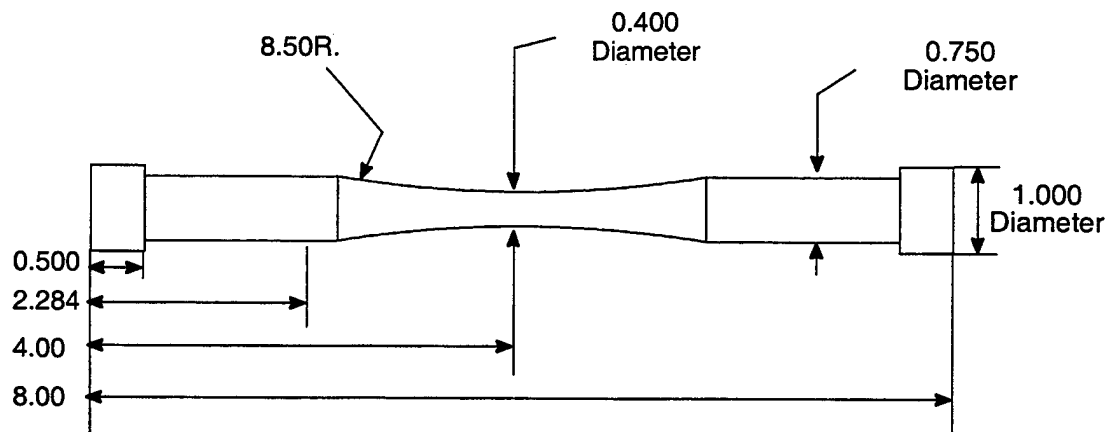


Figure 83. HG1 Hourglass Geometry.

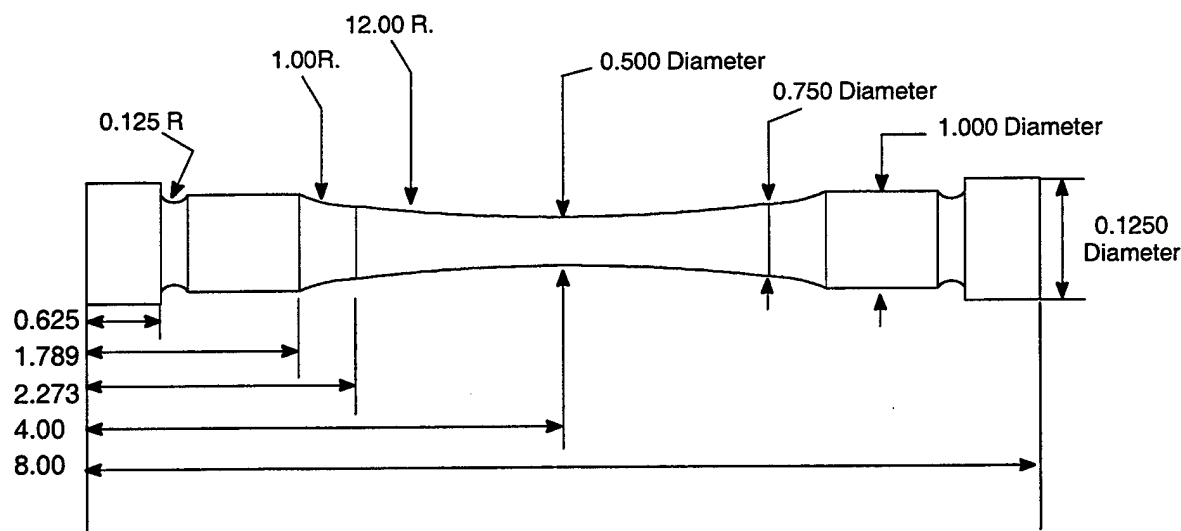


Figure 84. HG2 Hourglass Geometry.

Extruded and Isothermally Forged into Pancakes by Cameron at Texas Facility.

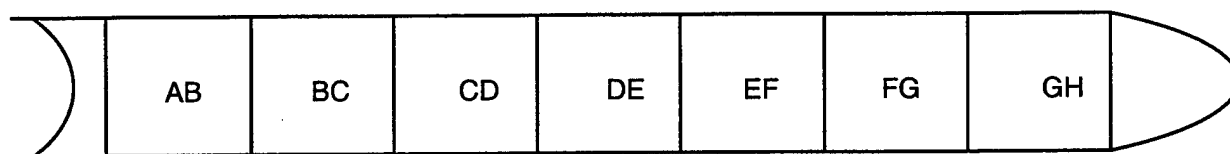


Figure 85. Forging Mult Coding.

originally intended that all twenty be of the MD-9 geometry shown in *Figure 87*. Unfortunately, several of the pancakes were excessively rounded at the peripheries requiring redesign of one block of seven model disks to the MD-10 geometry shown in *Figure 88*.

All specimens were shotpeened at GEAE using CCW 31 shot at 7A intensity and 125% coverage.

14.2 Evaluation of Seeding Practice

Segregation concerns from the first validation program needed dealing with. Prior to making the seeded material, another blending study was conducted, this time with -270 mesh powder.

Alumina seeds were blended into 198 pounds of powder: 50.3800 g of -60/+80 mesh fraction alumina (average mass of 0.0125952 g/seed)

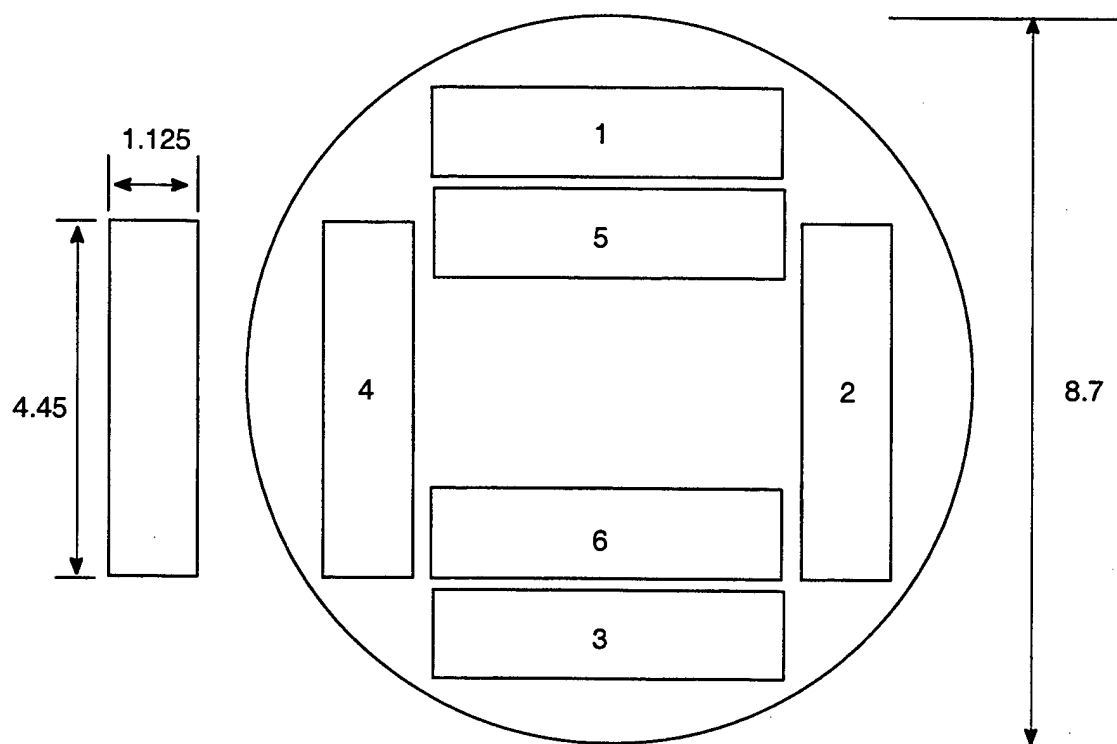


Figure 86. Forging Cutup.

and 14.8126 g of $-140/+170$ mesh fraction alumina (average mass of 0.0037040 g/seed) — approximately 4,000 of each mesh fraction. Blending proceeded for 4 hours. The blender shell was inverted and samples drawn: 22 roughly 1-pound samples at 9-pound intervals (i.e. a 1-pound sample followed by 9 pounds discarded; a second 1-pound sample followed by 9 pounds discarded; etc.). This procedure simulated can filling. The individual samples were sieved through a 230 mesh screen, and the collected particles counted.

The results are summarized in *Table 24*. The empirical distributions of the seeds recovered again sensibly agree with the expected Poisson distribution (see *Figure 89*). The Kolmogorov–Smirnov distances of the small and large empirical distributions from the Poisson hypothesis are 0.1668 and 0.1327 respectively. The significance level of the difference be-

tween the small seed distribution and the Poisson hypothesis is 0.52 based on the Kolmogorov–Smirnov one sample test (*Reference 3* – Refer to the discussion on significance in Section 13.3). The significance level of the difference between the large seed distribution and the Poisson hypothesis is 0.79.

As part of GEAE's IR&D incubation data program, the can filling experiment described in Section 13.3 was also refined and executed as follows: 3.5 grams of $-80/+100$ mesh alumina (Fisher Scientific) was blended with 1135 grams of -270 mesh PM René 88 DT, and the mixture poured into a 17.78 cm tall by 7.62 cm diameter can using a funnel having a neck diameter of 0.2 inches simulating the fill tube of an extrusion can. Following filling, an array of three concentric cylinders was pressed into the can, separating the powder into four zones (*Figure 90*). The material captured was

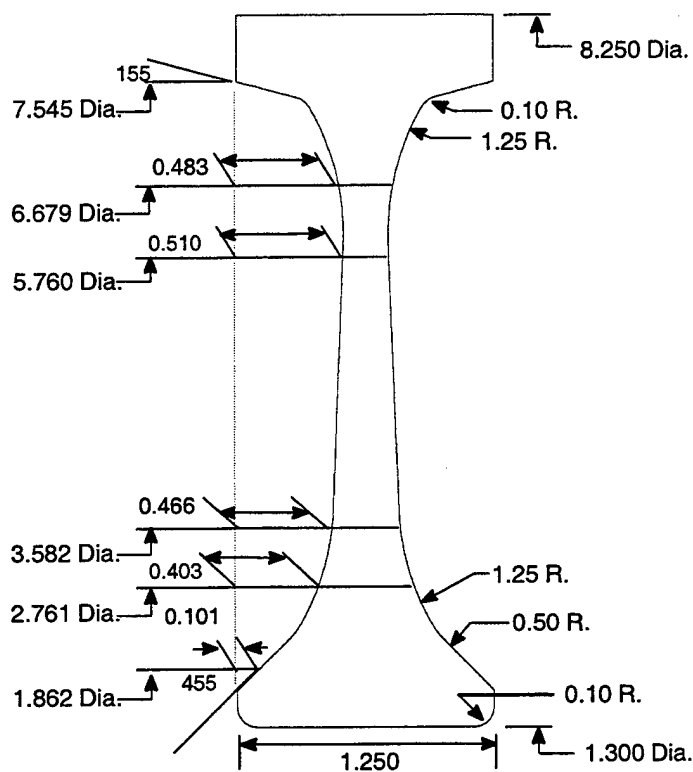


Figure 87. MD-9 Model Disk Geometry.

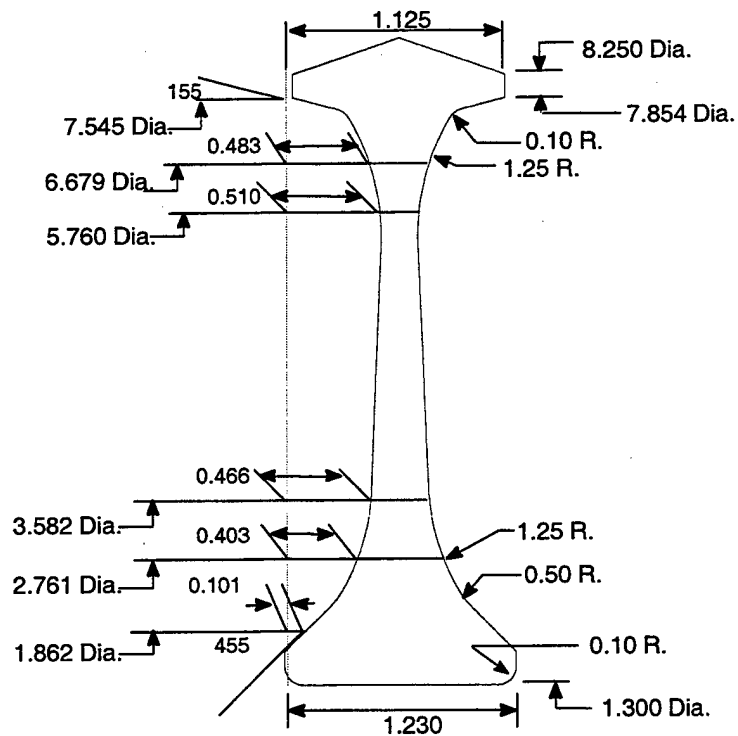


Figure 88. MD-10 Model Disk Geometry.

Table 24. Blending Study.

Sample Number	Sample Weight (grams)	Small Seeds Recovered	Large Seeds Recovered
1	501	18	20
2	536	23	24
3	536	23	26
4	512	29	28
5	444	17	17
6	520	28	26
7	506	22	25
8	482	22	18
9	505	23	24
10	507	19	25
11	546	19	25
12	537	13	19
13	523	25	21
14	457	25	21
15	555	17	18
16	506	21	26
17	524	24	14
18	478	18	23
19	536	20	21
20	540	41	21
21	516	17	28
22	562	20	18

Table 25. Can Fill Study.

Trial	Funnel	Zone	Alumina (grams)	Metal (grams)	Alumina/ Metal Fraction
1	Yes	1	1.40	382.5	0.003660
		2	0.58	189.7	0.003057
		3	0.42	148.0	0.002838
		4	1.24	399.5	0.003104
2	Yes	1	1.35	384.1	0.003515
		2	0.55	182.2	0.003019
		3	0.46	146.9	0.003131
		4	1.16	385.4	0.003010
3	No	1	1.27	383.5	0.003312
		2	0.62	189.8	0.003267
		3	0.47	144.0	0.003264
		4	1.22	383.1	0.003185
4	No	1	1.40	385.3	0.003634
		2	0.70	197.7	0.003541
		3	0.53	149.2	0.003552
		4	1.20	364.2	0.003295

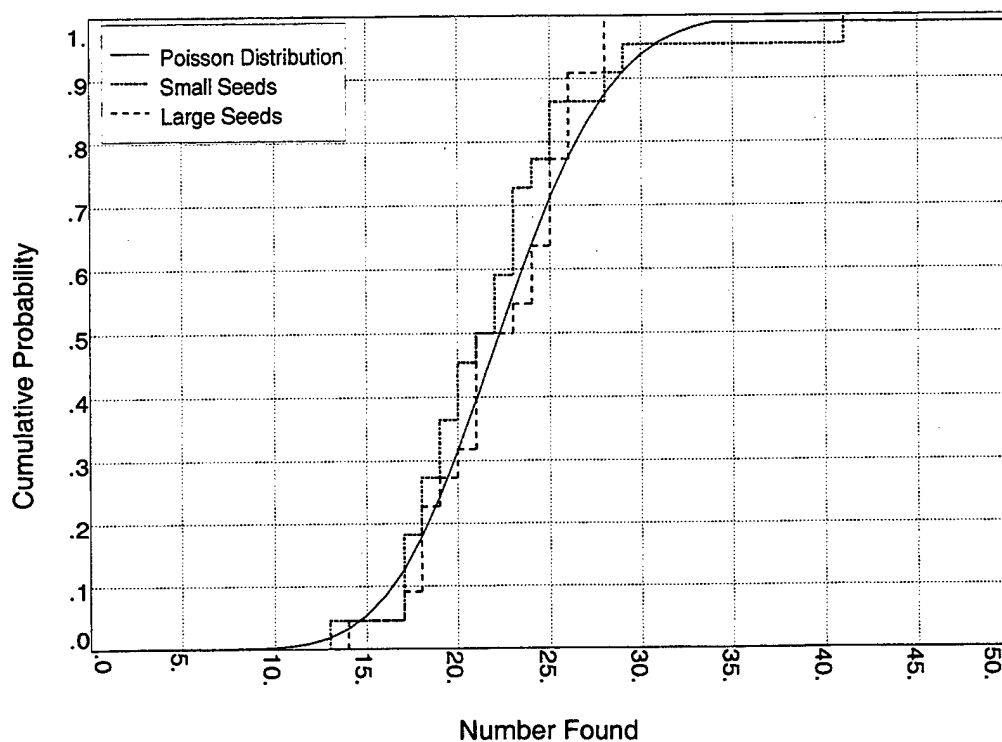


Figure 89. Cameron Blending Study - Evaluation Based on Poisson Model.

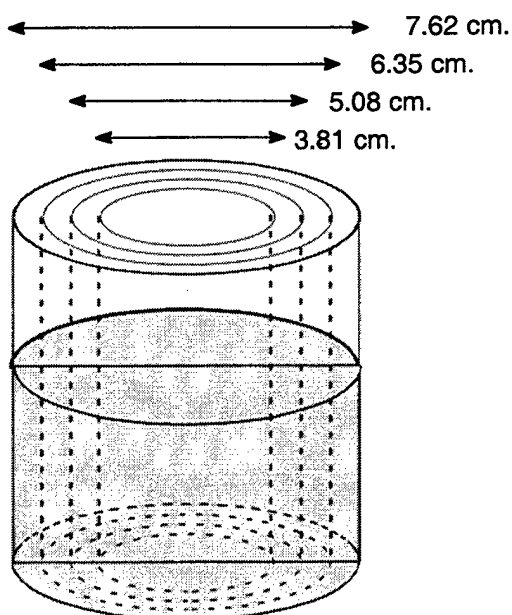


Figure 90. Schematic of Can Filling Experiment.

resieved, zone by zone, through a 150 mesh screen and the collected alumina weighed. This was repeated once with the funnel, and then twice without the funnel. The results, which are summarized in *Table 25*, along with those of the blending study, bolster confidence that segregation is not a concern.

14.3 Fatigue Testing

Diametrically strain-controlled push-pull LCF tests were performed at 1200° F (649° C) cycling between 0% and 0.78% (Metcut of Cincinnati). The first 100 cycles of the test were done using a procedure developed to minimize serrated yielding (*Reference 5*). This procedure utilized a triangular waveform in strain control at 1.5 cpm coupled with a 0.02% increase in strain range. After the first 100 cycles, the next 24 hours were run at the target strain range in strain control at 30 cpm, and any cycles beyond the first 24 hours (beyond about 42,000 cycles) were conducted in load control at 300 cpm.

Figure 91 shows the measured min and max stresses for the HG1 and HG2 specimen geometries at the computed axial strain of 0.78% plotted on the expected stress-strain curve at 1200° F. There is good agreement. After working out early problems and settling upon testing conditions, 115 specimens were successfully tested, divided as summarized in *Table 10*.

Push-pull fatigue testing is a well established and widely applied technology; spin pit fatigue testing is less so. Spin pit tests are challenging to run and expensive, but they can confer a valuable sense of realism to a methods validation program. The following discussion is included partly to provide a flavor of the problems which can be encountered, but also to document differences in two of the MD-10 tests which may or may not prove significant.

All model disks were tested by the Naval Air Warfare Center in Trenton, NJ in heated spin pits. Chamber temperatures were monitored by thermocouples. Aluminum (or Aluminum +

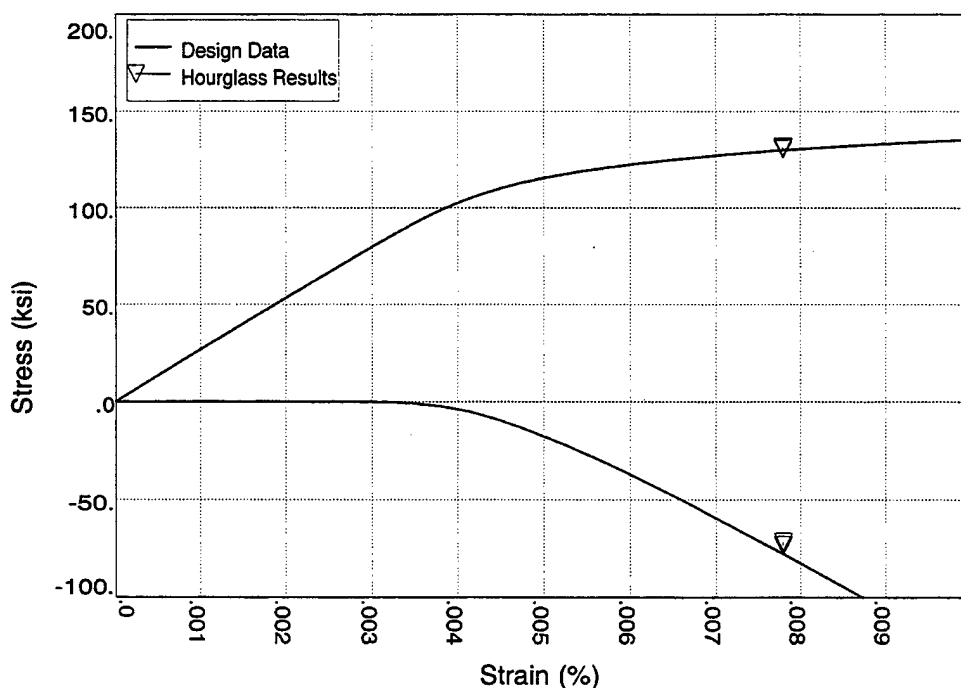


Figure 91. Comparison of Hourglass Test Stresses to René 88 DT Stress-Strain Curve.

Kevlar) containment barriers were provided to capture fragments without excessive distortion or break-up. The disks were fatigue cycled to fracture with speed-cycle marking every 4,000 LCF cycles. In speed cycle marking, the maximum speed of the LCF cycle is reduced to 90% of the maximum for 200 cycles. Test conditions are summarized in **Table 26**. Minimum speeds averaged about 3,200 rpm for the MD-9 tests and about 2,700 rpm for the MD-10 tests.

The first three disks were lost in testing for various reasons. The first disk (tested at 1200° F (649° C)) suffered a shaft bearing failure.

The disk was remounted and the test restarted with failure soon following. Post-test analysis found considerable secondary cracking which exhibited signs of hold time initiation and crack growth. In trying to provide realistically attainable test times, operating conditions had been selected outside of the recommended operating window for the alloy.

The second test was started at 1000° F (538° C) (low enough that hold time effects would not be pronounced), but another bearing failure occurred (this time on startup). The pit was reassembled, the disk remounted and restarted.

Table 26. Model Disk Test Matrix.

Test Sequence	Disk Serial Number	Seeding S0-Base S1-Large S2-Small	Extrusion/ Forging	Temp (°F)	Speed (rpm)	Observed Life
1	MD902	S1	E-666-FG	1200	48000	961
2	MD903	S2	E-669-EF	1000	48000	--
3	MD904	S2	E-669-FG	1000	48000	--
4	MD905	S2	E-670-BC	1000	48000	7530
5	MD906	S2	E-670-CD	1000	48000	7963
6	MD907	S2	E-670-DE	1000	48000	15481
7	MD908	S2	E-670-EF	1000	48000	9420
8	MD909	S2	E-670-FG	1000	48000	9890
9	MD910	S2	E-667-FG	1000	48000	12810
10	MD911	S2	E-668-DE	1000	48000	11586
11	MD912	S2	E-668-FG	1000	48000	8902
12	MD913	S2	E-669-DE	1000	48000	10258
13	MD1001	S1	E-675-DE	1000	49000	34360
14	MD1002	S1	E-721-AB	1000	49000	26883
15	MD1003	S1	E-721-BC	1000	49000	18563
16	MD1004	S1	E-721-CD	1000	49000	11455
17	MD1005	S1	E-721-DE	1000	49000	14002
18	MD1006	S1	E-722-AB	1000	49000	11587
19	MD1007	S1	E-722-BC	1000	49000	23433
20	MD901	S0	E-663-CD	1000	49000	10589

Disk failure soon followed. We believe that when the bearing froze on the first attempted start, the disk spun on its collet sustaining fretting damage until it seized and twisted the drive shaft off. Post-test analysis showed clear evidence of fretting damage in the bore of the disk. Cracks had initiated at many points around the bore, one of which led to disk fragmentation.

The third test suffered slippage of the shaft, moving the disk too close to the radiant heating element in the oven. This test could have been restarted, but any result would have been questionable. The slippage problem was solved by additional setscrews and the fourth test started. The next nine MD-9 disks were tested at 1000° F (538° C) without further mishap.

Problems began again with the first MD-10 disk (MD-1001) which slipped off its shaft after 630 cycles and suffered some minor damage in the rim as a result of bouncing around the spin pit. Given that 9 MD-9 disks had been successfully tested prior to this bad experience, the slippage was judged to be a fluke.

The second test (MD-1002) was successfully completed, but the third disk (MD-1003) suffered the same fate as the first, slipping off its

shaft after 2855 cycles. Close investigation concluded that steel set screws used to attach the colleted disk to the shaft had deformed and worked loose. The remaining tests either used Inconel 718 setscrews or avoided the problem altogether by using single-piece Inconel 718 shafts, and no further problems were encountered.

MD-1001 and MD-1003 were cleaned up, the damage polished out, re-peened and returned to testing.

Fatigue testing concluded with MD-901. This disk had been machined from an unseeded forging and allocated for burst testing. It was agreed that supplementing the MD-9 fatigue database would provide greater value than a single burst run. While the rest of the MD-9 block was seeded, failure probability is controlled by natural surface intersecting inclusions, and therefore adding an unseeded result was deemed statistically acceptable.

After testing, all specimens were evaluated by SEM/EDS. Inclusion and grain facet initiation sites were characterized for size, type, and location.

15.0 Analysis

15.1 Life Models

The most involved aspect of a MISSYDD PFM analysis is the calculation of the parametrized geometric failure distribution ($G(N, a)$ from Section 12.1, Algorithm 1). A Monte Carlo approach is employed to randomly place inclusions; the life is calculated for each placement (or *hit*) for a range of inclusion sizes and empirical distributions of the simulated results constructed.

The current life module recognizes both crack initiation and propagation; the latter is computed using linear elastic fracture mechanics, recognizing near surface and corner conditions, including polynomial stress gradients and plastic zone corrections, and allowing surface and subsurface temperature interpolated crack growth rate curves.

Crack initiation (or incubation) models were developed following recognition that buried ceramic inclusions in both E+F PM René 95 and E+F PM René 88 DT lead to sharp cracks only late in life. There are no cases of low life internal initiations from natural inclusions in either alloy's database, and even aggressive seeding in René 88 DT has yielded no low life internal initiations. Ignoring the incubation phenomenon results in unacceptably conservative PFM predictions given that the only other known benefit enjoyed by buried inclusions is protection from environmental acceleration of crack growth.

The author interprets incubation to be classical crack initiation in grains near stress concentrating inclusions, and therefore assumes that rain-flow counting, mean stress corrections and linear damage accumulation can be applied to calculate incubation for complex cycle missions given an empirical relationship for simple (min-max-min) cycling incubation life as a

function of inclusion size, temperature and stress. Details were presented at the 1996 Seven Springs Superalloys Conference (*Reference 1*).

The incubation model used for this report is based on seeded René 88 DT data at 400°, 750°, 1000° and 1200° F (399°, 482°, 538° 649° C).

15.2 Inclusion Distributions

15.2.1 Image Analysis

Both the size distribution of flaws and their rate of occurrence ($s(a)$ and λ from Section 12.1, Algorithm 1) can affect component life. Inclusions in fine mesh PM alloys are inherently small, too small to be of concern unless one falls at a very bad location (e.g. high stress). But PM alloys have a high rate of occurrence of such inclusions, and consequently the probability of an unfavorable location must be controlled by design.

The distribution of natural inclusions used for GEAE -270 mesh PM MISSYDD calculations (including those in this report) is currently supported by Heavy Liquid Separation (HLS) characterization of 76 lots of -270 mesh PM (mostly René 88 DT).

HLS is a powder metal (PM) cleanliness evaluation technique which has been developed by GE Aircraft Engines and Wyman-Gordon (*Reference 6*). A high density liquid is used to float ceramic inclusions from PM samples for characterization by automated SEM/EDAX analysis (*Figures 92 and 93*). The number, size distribution and chemistries of the recovered inclusions are tracked for statistical process monitoring and control of PM lot cleanliness.

The seeding distributions for this validation study were estimated by image analysis of

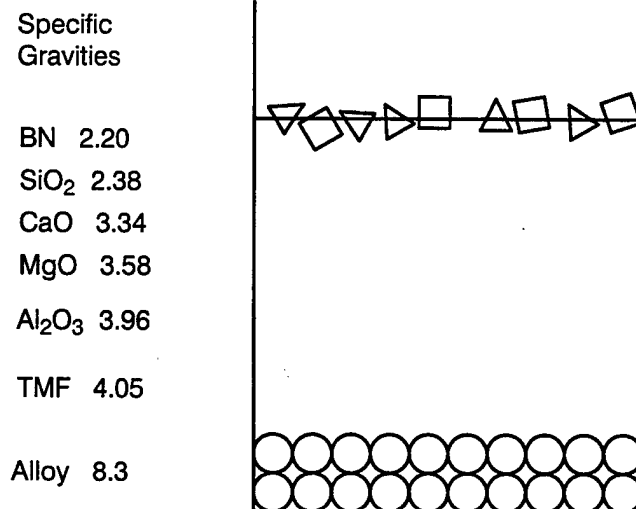


Figure 92. Heavy Liquid Separation.

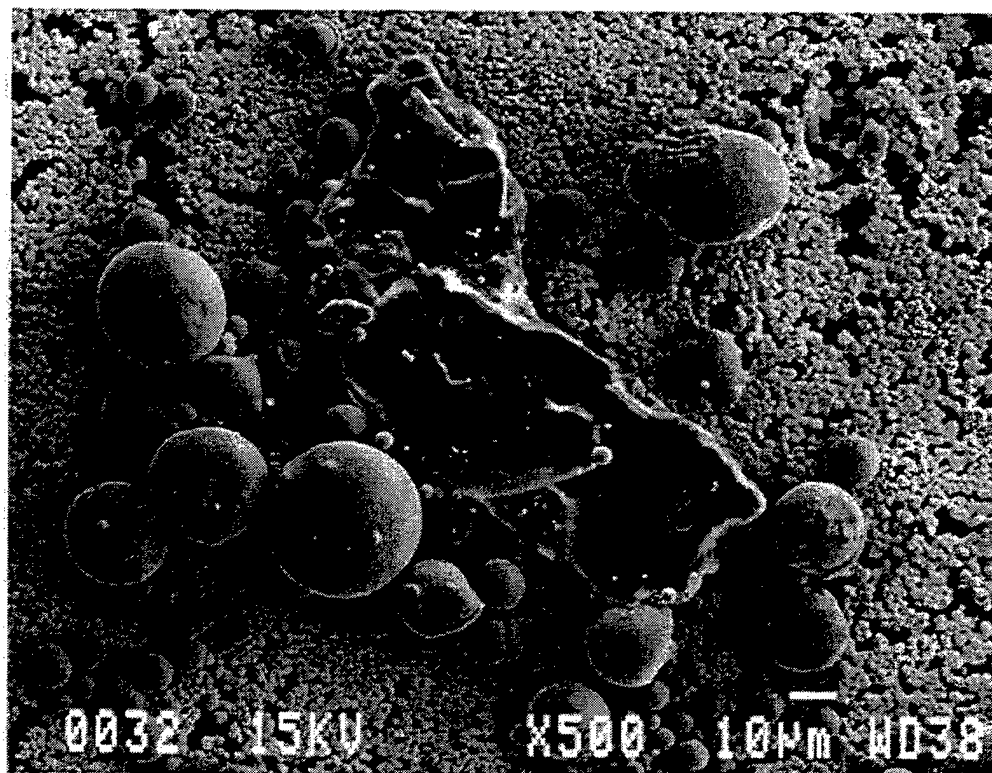


Figure 93. SEM Image of an HLS Recovered Inclusion.

random samples of 100-130 seeds of the four different mesh fraction constituents (-50,+60 mesh alumina, -140,+170 mesh alumina, -200,+230 mesh alumina and -270,+325 mesh alumina). Analytical microbalance measurements of the same samples yielded values of average mass per seed for each of the four fractions. **Table 27** summarizes these values and also states the rates of the fractions defining the S1 and S2 seeding mixes (refer also to **Table 22**).

Size and aspect ratio distributions of the natural inclusion population and the four seeding fractions are provided in **Figures 94 and 95**.

15.2.2 Dirtiness Distributions

A *dirtiness distribution* presents the probability of a given volume of material (usually 1 cubic inch) containing a flaw of a given size or larger. Physically, dirtiness distributions are related to the distributions sometimes inferred from fatigue or tensile data. Ideally a fatigue or tensile specimen should fail from the largest contained flaw. It follows that the probability that a volume of material contains a flaw of a given size or larger should equal the probability

that a test bar of that volume fails at that size flaw.

In general, this is a terrible oversimplification. Surface and subsurface flaws usually impact tests differently. Different flaw types (e.g. blocky vs. agglomerated) may have different effects. Other mechanisms may compete. Still, the simplification is useful for visualization, and in some cases is believed to be valid. The principal failure mechanism for René 88 DT at elevated temperatures is inclusion initiated cracking (**Reference 1**), and surface initiations can be suppressed by shotpeening at typical design stress levels. It is expected, therefore, that most bars *will* fail from the largest contained inclusion.

(Note: We usually take *flaw size* to mean *area* and ignore shape. In uniform stress fields, fracture mechanics calculations are reasonably insensitive to aspect ratio, justifying this simplification.)

The data of the last section (size distributions and occurrence rates) can be translated into dirtiness distributions and compared to the distributions of initiation areas for the S0, S1 and S2 PRDS program specimen sets. In the following derivations we will let A denote flaw size, D(A) the dirtiness probability at size A,

Table 27. Seed Weights and Seeding Rates.

Seed Fraction	Average Mass per Seed (mg/seed)	S1 Seeding (Number per Cu. Inch)	S2 Seeding (Number per Cu. Inch)
-50/+60 FEPA 100	0.011445	4	---
-60/+80 FEPA 100	0.003704	2	---
-200/+230 FEPA 100	0.001032	---	6
-270/+325 ANSI 240	0.000229	---	3

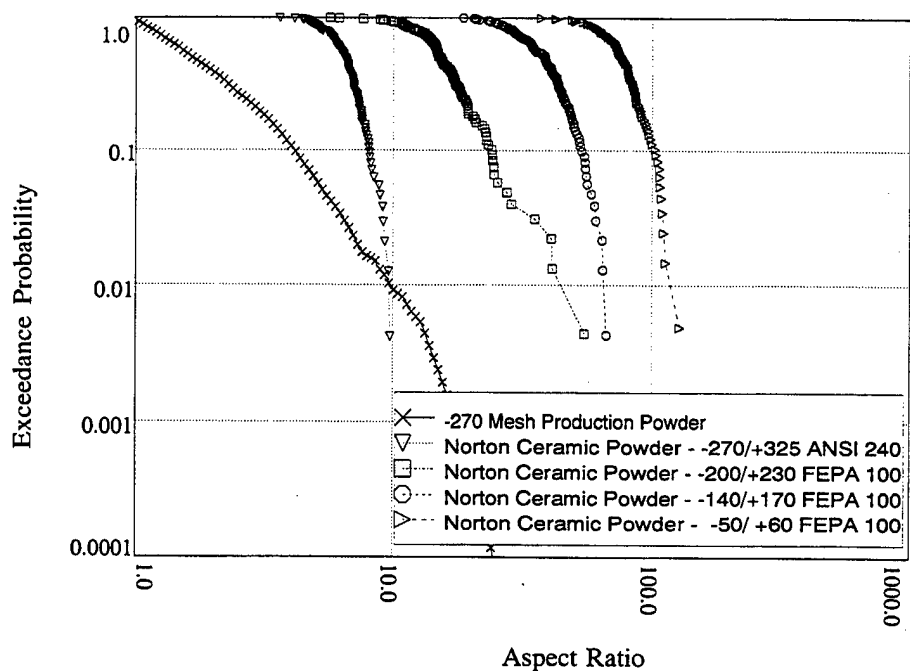


Figure 94. Size Distributions.

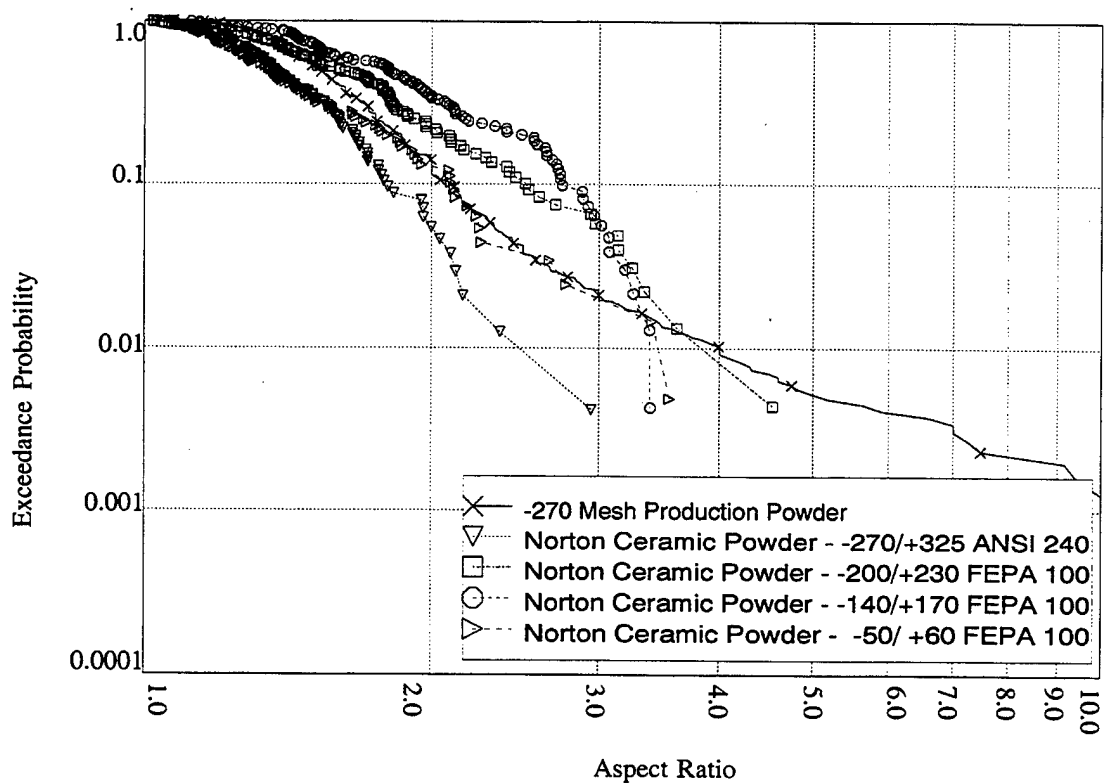


Figure 95. Aspect Ratio Distributions.

$S(A)$ the cumulative probability of the size distribution and λ the average flaw frequency per cubic inch. (Note that the plots in **Figure 94** are in exceedance probability format: $1 - S(A)$.)

The Poisson model for flaw occurrence will be assumed ... The probability that there are n flaws in a cubic inch is given by:

$$e^{-\lambda} \lambda^n / n!$$

Now, the derivations...

$$D(A) = 1 - \text{Prob(Any flaws present are smaller than } A)$$

$$= 1 - \text{Prob}(0 \text{ flaws present, any size})$$

$$- \text{Prob}(1 \text{ flaw present, size less than } A)$$

$$- \text{Prob}(2 \text{ flaws present, sizes less than } A)$$

$$- \text{Prob}(3 \text{ flaws present, size less than } A) - \dots$$

$$= e^{-\lambda} \lambda^0 / 0! S(A)^0 + e^{-\lambda} \lambda^1 / 1!$$

$$S(A)^1 + e^{-\lambda} \lambda^2 / 2! S(A)^2 +$$

$$e^{-\lambda} \lambda^3 / 3! S(A)^3 + \dots$$

$$= 1 - e^{-\lambda} e^{\lambda S(A)}$$

$$= 1 - e^{-\lambda (1 - S(A))}$$

$D(A)$, referenced to 1 cubic inch, can be translated to a volume v as follows:

$$D(A) = 1 - (1 - D(A))^v$$

Let $D_0(A)$ be the baseline dirtiness distribution of unseeded powder, and let $D_\alpha(A)$, $D_\beta(A)$, $D_\gamma(A)$ and $D_\delta(A)$ be the dirtiness distributions of the seeding fractions derived from the size distributions of **Figure 94** and the seeding rates of **Table 27** (α is the -50,+60 mesh fraction, β is the -140,+170 mesh fraction, γ is the -200,+230 mesh fraction, and δ is the -270,+325 mesh fraction).

The dirtiness distribution of the S1 (large) seed mix is computed as follows:

$$D_1(A) = 1 - (1 - D_0(A)) \cdot (1 - D_\alpha(A)) \cdot (1 - D_\beta(A))$$

The dirtiness distribution of the S2 (small) seed mix is computed as follows:

$$D_2(A) = 1 - (1 - D_0(A)) \cdot (1 - D_\gamma(A)) \cdot (1 - D_\delta(A))$$

Comparisons of $D_0(A)$, $D_1(A)$ and $D_2(A)$ to the observed distributions are made in **Figure 96**. $D_0(A)$ is seen to agree well with the unseeded finds, but $D_1(A)$ and $D_2(A)$ both overpredict the seeded finds. In fact, only 6 of the 43 small seeded tests failed at a seed, suggesting that the S2 seeding density may have missed the target. A better explanation is suggested in the next section.

15.2.3 Inclusion Orientation

As part of the René 88 DT incubation data program, GEAE executed a post-test metallographic study of ten seeded fatigue specimens looking for evidence of secondary cracking (**Reference 4**). Significant numbers of secondary grain-initiated cracks were observed in specimens tested at 400° F (399° C) and very little secondary cracking in specimens tested at 1200° F (649° C). A second significant observation was made: Inclusions were most often oriented tangentially in the pancake forgings if oriented at all (see **Table 28**). (Conventional wisdom held that they would be oriented radially.)

The implication of this observation is that the inclusion crosssections stressed in a tangentially oriented test specimen are smaller than the crosssections viewed by image analysis of loose samples of inclusions.

Given a distribution of inclusion areas, a distribution of aspect ratios, a seeding rate, the diameter and length of a cylinder, and the assumption of tangential orientation, the expected distribution of the largest inclusion

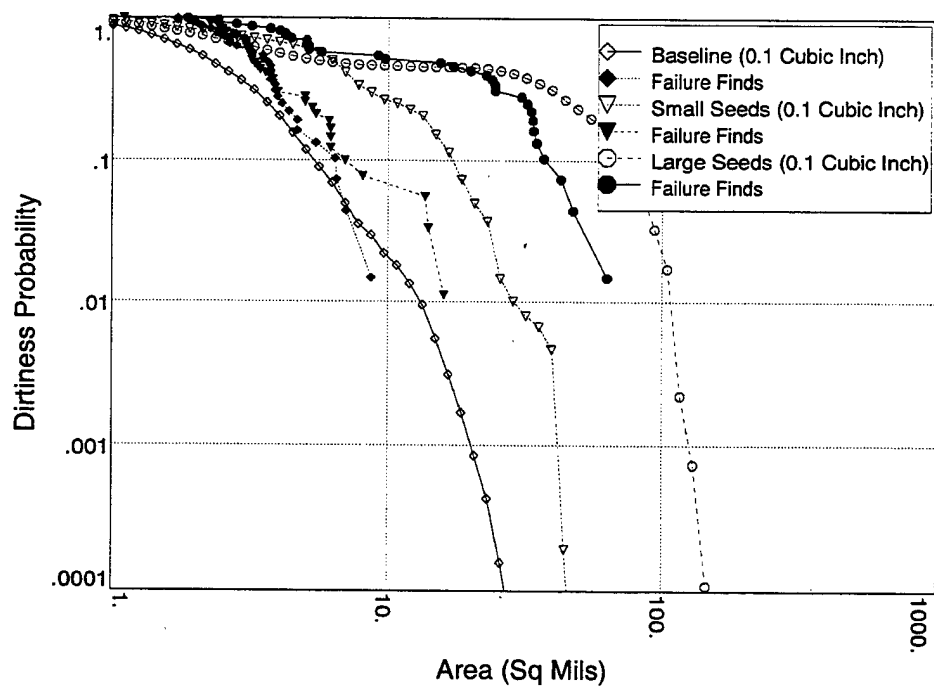


Figure 96. Predicted and Observed Distributions Compared.

Table 28. Inclusion Orientation Study.

Specimen	No Orientation	Tangential Orientation	Radial Orientation	Skewed Orientation	Totals
170AB-1	2	5	0	0	7
170BC-1	2	6	0	2	10
170CD-1	3	7	2	0	12
170DE-1	0	1	0	0	1
170EF-1	1	2	1	1	5
172AB-1	3	5	1	0	9
172BC-1	0	11	0	0	11
172CD-1	2	2	1	1	6
172DE-1	6	3	1	0	10
172EF-1	1	3	5	0	9
-----	-----	-----	-----	-----	-----
Totals	20	45	11	4	80
Fractions	0.25	0.56	0.14	0.05	1.00

area normal to the stress field in a test bar volume can be estimated by Monte Carlo simulation. **Figure 97** shows a single iteration of the simulation: there are 9 randomly sized inclusions; the largest clearly stands out.

New estimates of D_α , D_β , D_γ and D_δ were generated using this algorithm. D_0 was not altered given its good agreement with the observed distribution. Presumably the natural inclusions are also oriented, but the diminishment in size due to orientation is obscured by lot-to-lot variability in inclusion distribution (see **Figure 98**). Without knowing the inclusion distribution specific to the PM used for this study, there was no choice but to accept D_0 as derived from the pooled HLS data.

Figure 99 compares the expected oriented and unoriented dirtiness distributions for S1 and S2 seeding conditions, and **Figure 100** compares the oriented distributions with the observed distributions. Based on this comparison, the ori-

ented distributions will be used for the subsequent PFM analyses of the push-pull tests.

By contrast, the model disks all cracked circumferentially which implied that the original *unoriented* distributions were more appropriate for their analyses. Work has started to integrate forging orientation and deformation models into the PFM methodology.

15.3 MISSYDD Analysis

15.3.1 Hourglass Tests

Algorithm 1 in Section 12.1 computes failure distributions assuming that there is no variability in inclusion behavior. **Figure 101** compares Algorithm 1 predicted and observed failure distributions for the 35 HG1/S1 (large seed) tests, the 38 HG2/S2 (small seed) tests and the 29 baseline HG1/S0 (unseeded) tests. The results are encouraging, but clearly the prediction has not captured the full breadth of the first specimen set.

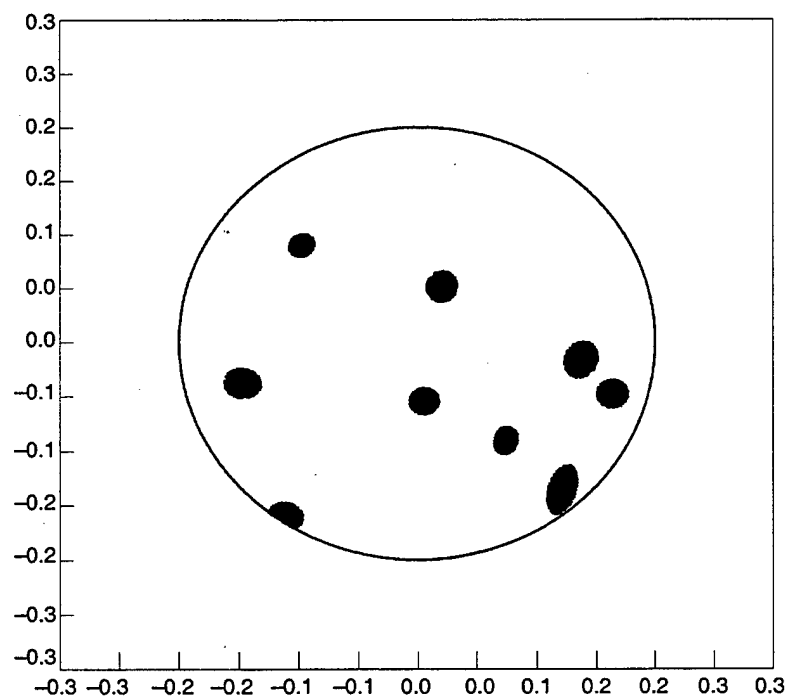


Figure 97. Simulation Example.

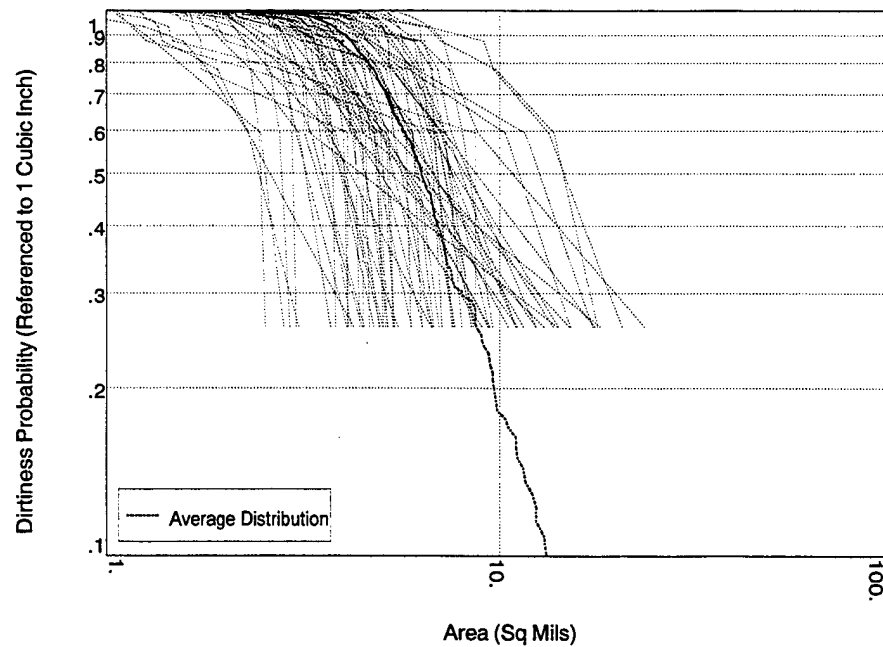


Figure 98. Lot-to-Lot Variability in Inclusion Distribution.

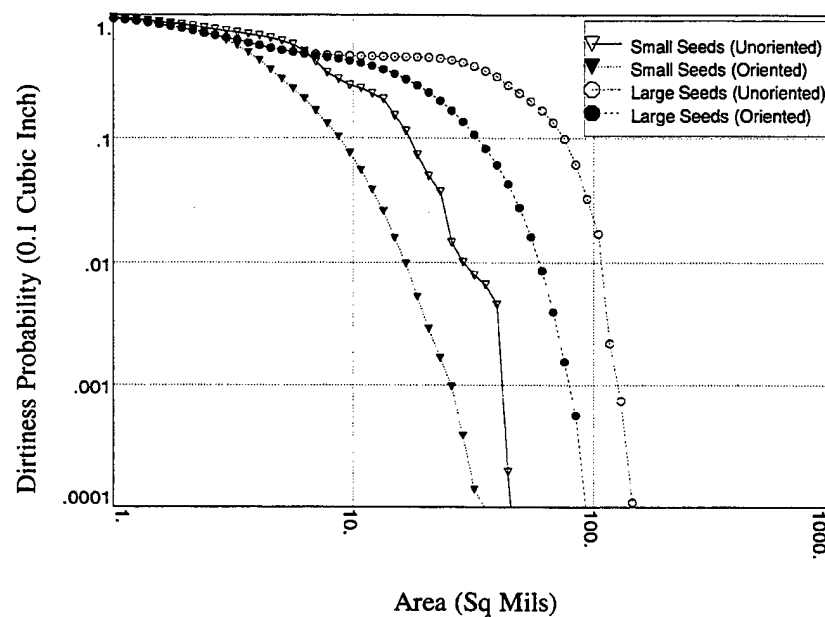


Figure 99. Oriented and Unoriented Distributions Compared.

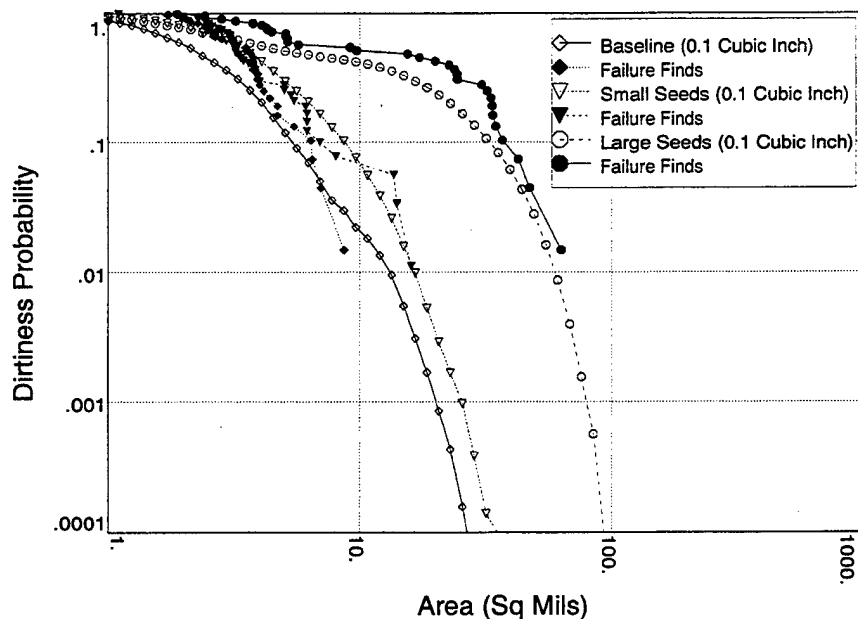


Figure 100. Predicted and Observed Distributions Compared Assuming Orientation.

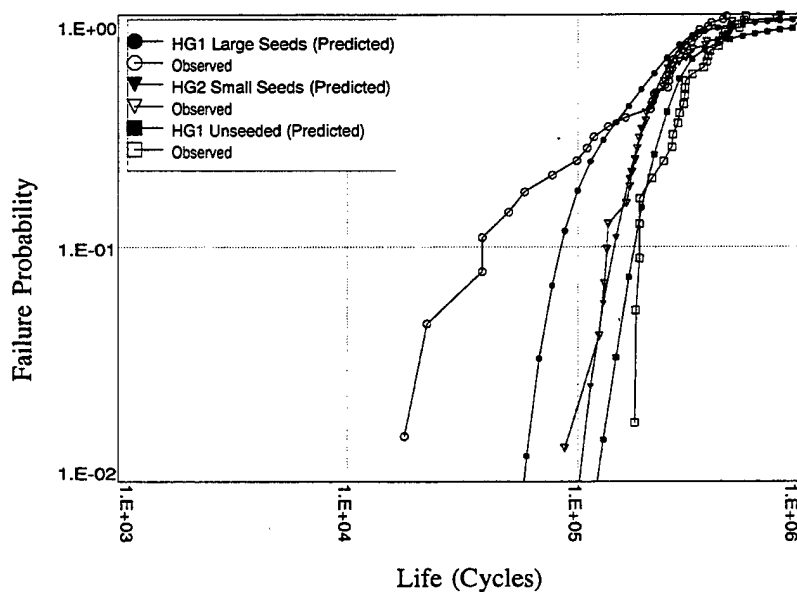


Figure 101. Algorithm 1 — Comparison of Predicted and Observed Distributions.

Algorithm 2 in Section 12.1 models material scatter as a distribution of life multipliers:

Let μ denote the ratio of predicted to observed life for a single inclusion, and let $m(\mu)$ denote the probability density function of the μ distribution.

Assuming that the distribution of μ predominantly represents testing variability (i.e. Specimen-to-Specimen rather than Inclusion-to-Inclusion), the scatter is integrated into the basic PFM (Probabilistic Fracture Mechanics) risk algorithm as a kind of convolution:

$$\int F(N \cdot \mu) m(\mu) d\mu$$

where $F(N)$ is the failure probability at life N computed without recognition of variability.

Figure 102 compares the empirical hourglass μ -distribution to the Weibull fit being used for René 88 DT PFM calculations (Reference 4); the two are different but not very different. The forgings for the PRDS program were produced by Cameron/Houston while those behind the

PFM life model were produced by SNECMA/France. Given the known differences between the Cameron and SNECMA forging sets (powder lots, extrusion conditions, forging conditions, forging sizes), minor differences in properties are not unexpected.

Four hourglass points appear to stand out from the general trend of the data. One specimen failing from a pair of nearby (and apparently interacting) inclusions contributed two of the outliers (one for each of the two inclusions). A third point is tied to an initiation from a large inclusion lying only 1.2 mils from the surface and very badly oriented. The fourth point is tied to the largest initiating inclusion in this data set, but the size is well captured by the SNECMA data and so does not explain the deviation. The third and fourth deviating points are tied to a common forging. **Figures 103** and **104** show significant stratification between the 21 forgings tested (note incidences of the clustering within forgings), and in **Figure 104** the E-Forging specimens lie farther to the right than do most other groups. Forging variability

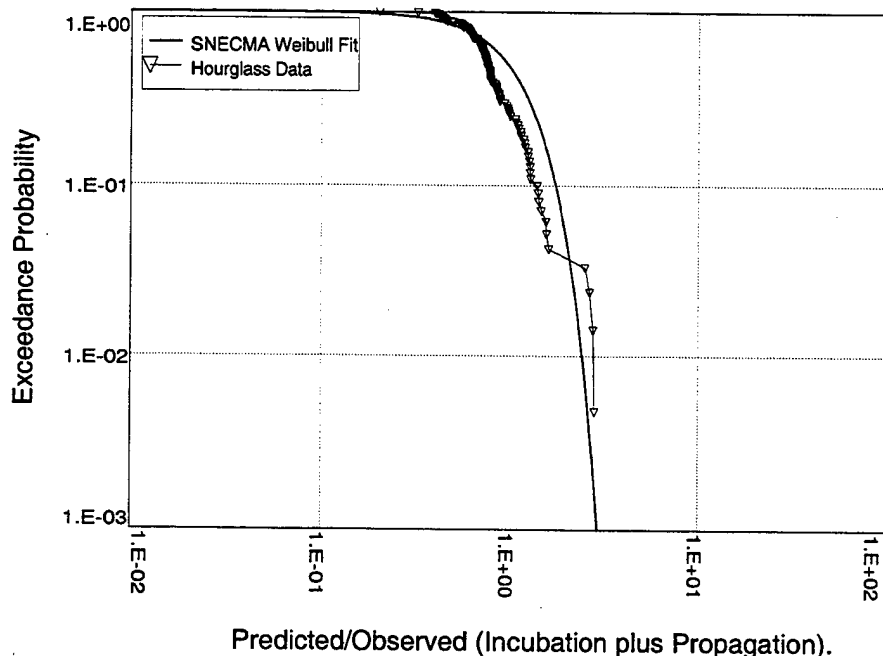


Figure 102. Comparison of Data Sets.

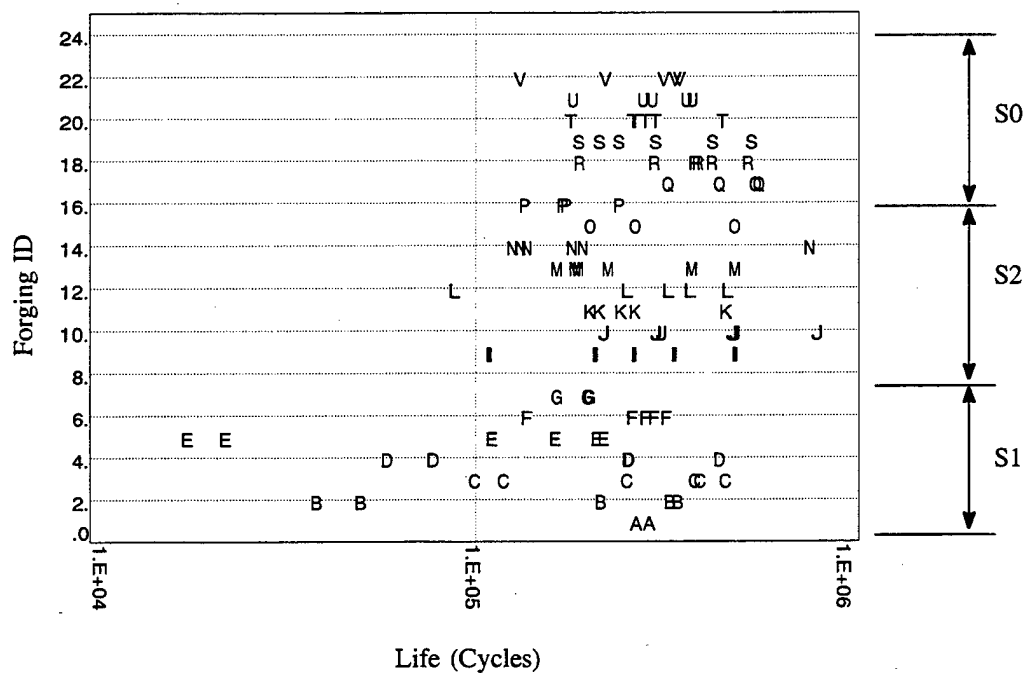


Figure 103. Stratification.

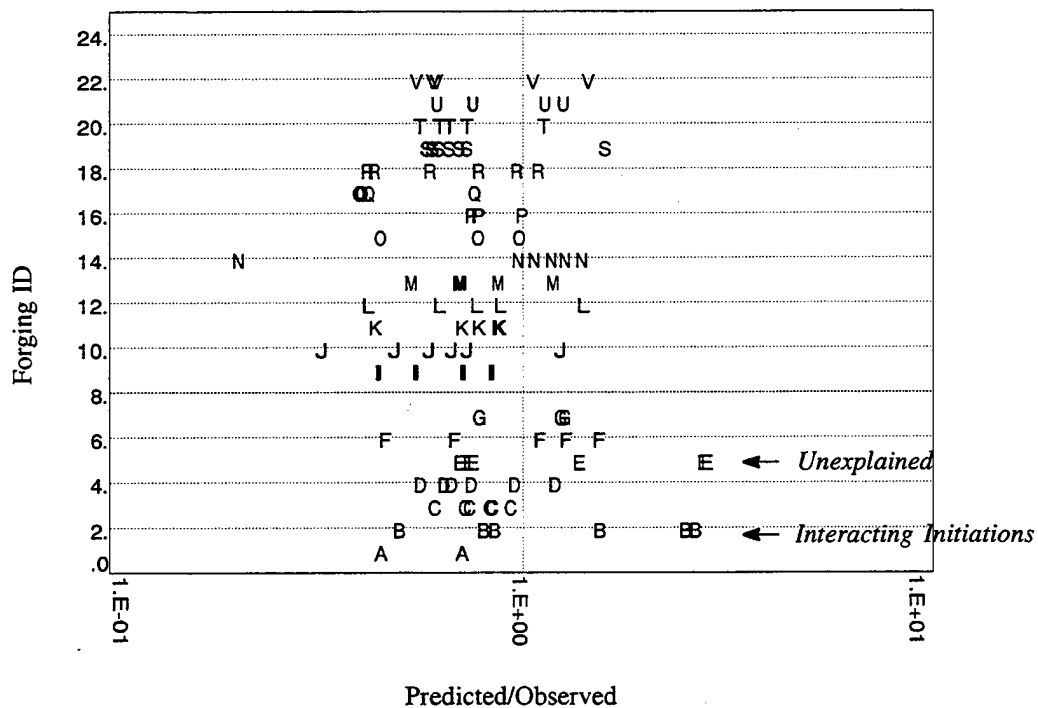


Figure 104. Stratification.

could therefore be suggested as a possible partial explanation for the deviations, but the weight of the evidence is hardly overwhelming.

The ideal PFM calculation should incorporate details of interacting initiations, surface influences, inclusion orientation, distributional stratification, and other refinements, some already recognized, some not. However, we do not at this time have adequate understanding of these effects to realistically incorporate them into the PFM life algorithm. Nor do we have adequate data to characterize the apparent distributional multimodality of the PRDS data sets.

Section 9 proposed a target for design analysis ... referring to **Figure 105**:

1. *The Bull's Eye* — Apply what we know as well as we know how.
2. *The Middle Ring* — Evaluate sensitivities to known deviations and bound the results.
3. *The Outer Ring* — Back off from the calculations until accumulated experience justifies doing otherwise.

In keeping with this philosophy, we need first to evaluate our ability to hit the Bull's Eye

given what we do know. The other sensitivities (interactions, surface influences, etc.) currently lie in the middle ring and must be dealt with differently. For example, for PFM design applications:

- It may be reasonably argued that initiation interactions are ignorably rare in unseeded production material.
- It may be conservatively assumed that surface (and near-surface) inclusions do not enjoy an incubation period prior to crack initiation.
- It may be conservatively assumed that the stress field always sees the maximum inclusion crosssections.

To more clearly assess the capabilities of the *current* PFM technology, the 3 specimens associated with the 4 points (deviating from the empirical μ -distribution) are set aside leaving 99 specimens for comparisons: 32 HG1/S1 (large seed) tests, 38 HG2/S2 (small seed) tests and 29 baseline HG1/S0 (unseeded) tests.

Figure 106 shows the empirical μ -distribution of the censored data. It is both slightly tighter than the SNECMA distribution and slightly shifted. **Figure 107** shows the Weibull fit to

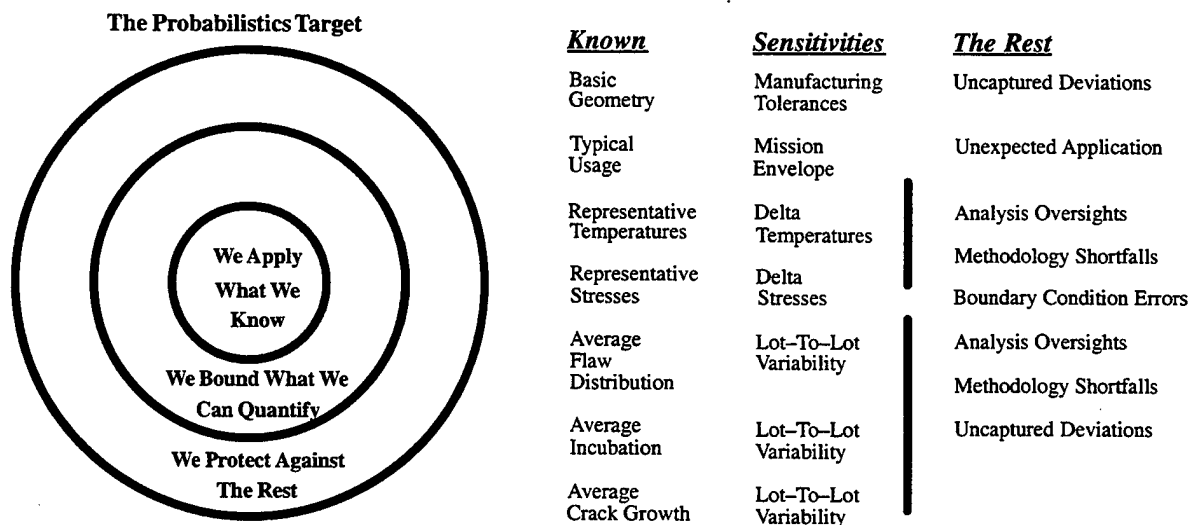


Figure 105. Strategy for Implementation of Probabilistics.

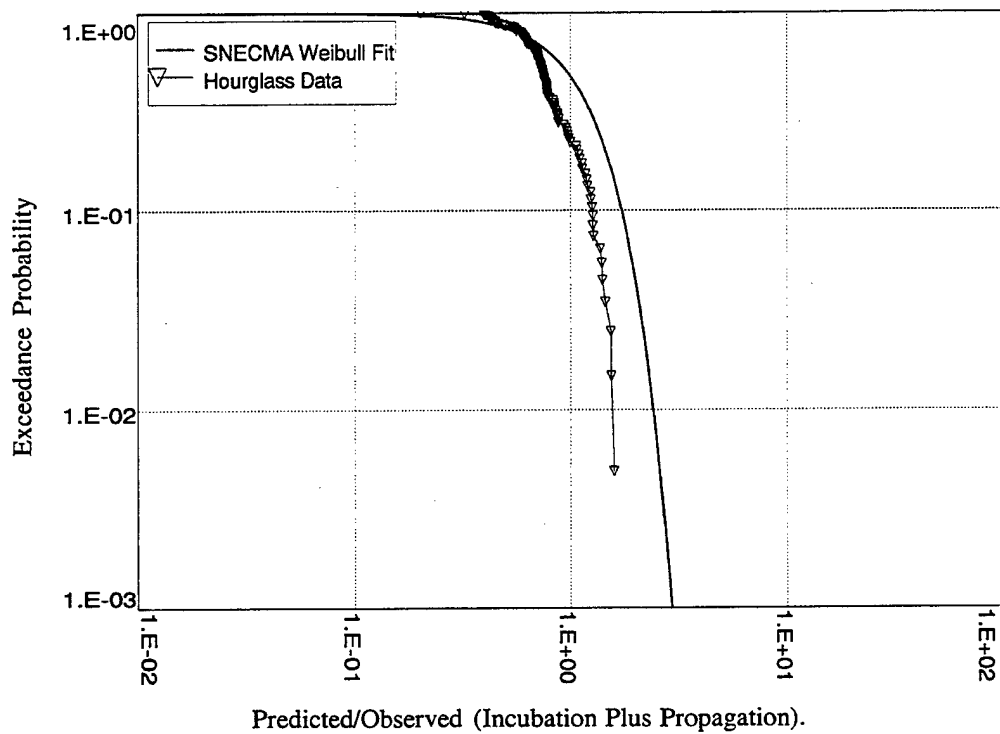


Figure 106. Censored Data Set Comparison.

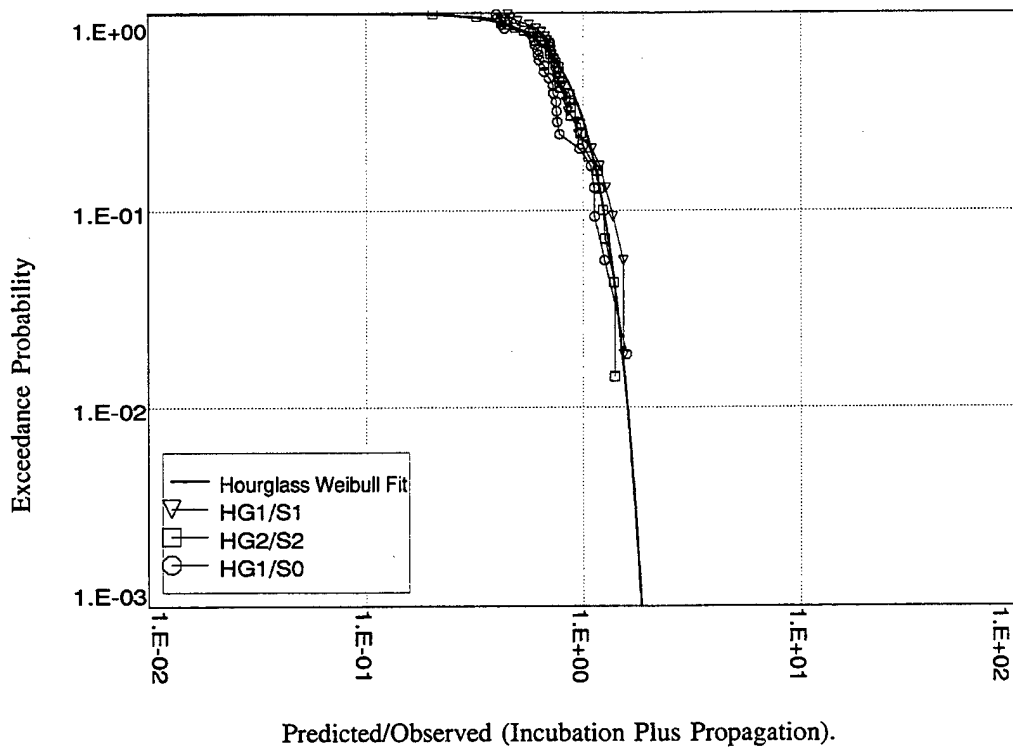


Figure 107. Censored Data Set Comparison.

this data compared to the separated HG1/S1, HG2/S2 and HG1/S0 data sets; all three sets are well described by the single fit. **Figures 108, 109 and 110** show good comparisons between PFM-predicted and observed failure distributions. Shown in each of **Figures 108–110** are an Algorithm 1 prediction assuming no material scatter, an Algorithm 2 prediction assuming the SNECMA material scatter, and an Algorithm 2 prediction assuming the Cameron material scatter. It is presumed that the last should be the best, but the differences between the last two are subtle, and the data sets too small for a clear decision.

15.3.2 Other Push-Pull Tests

Figure 111 shows PFM-predicted and observed comparisons for the three hourglass data sets plus two cylindrical specimen data sets from the René 88 DT incubation data program. The latter were machined from seeded pancakes, shotpeened, and tested at conditions

matching the hourglass tests (cycled between 0.00% and 0.78% strain at 1200° F, 649° C — see **Reference 1** for details).

It must be noted that the large seeded cylindrical data set has also been censored by removing 4 surface initiations, leaving 26 points. The effectiveness of shotpeening in suppressing crack initiation from surface intersecting inclusions is good but not absolute. The probability of surface initiation increases with stress, with seed size and with seeding density (**Reference 7**).

The censored comparisons support the capability of the PFM model over the range of probabilities 0.01 to 0.99 when inclusion distribution and behavior are understood.

Again, the surface can not be arbitrarily censored for PFM design applications, and an appropriate *Middle Ring* approach is suggested which assumes immediate sharp crack initiation from all surface intersecting inclusions. It is the author's opinion that this assumption is

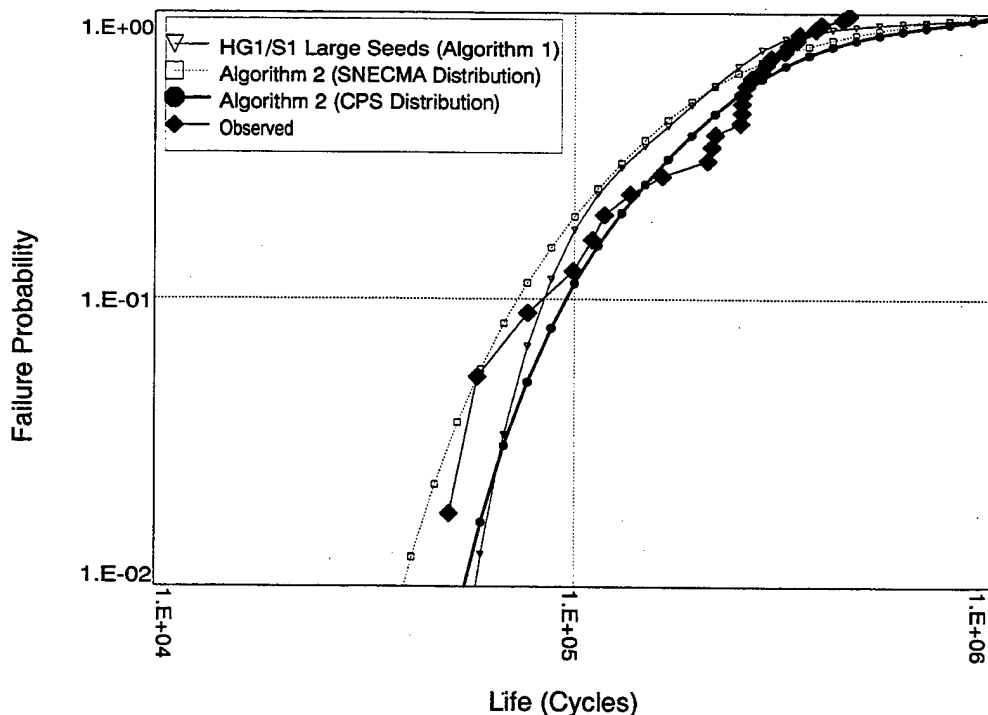


Figure 108. HG1/S1

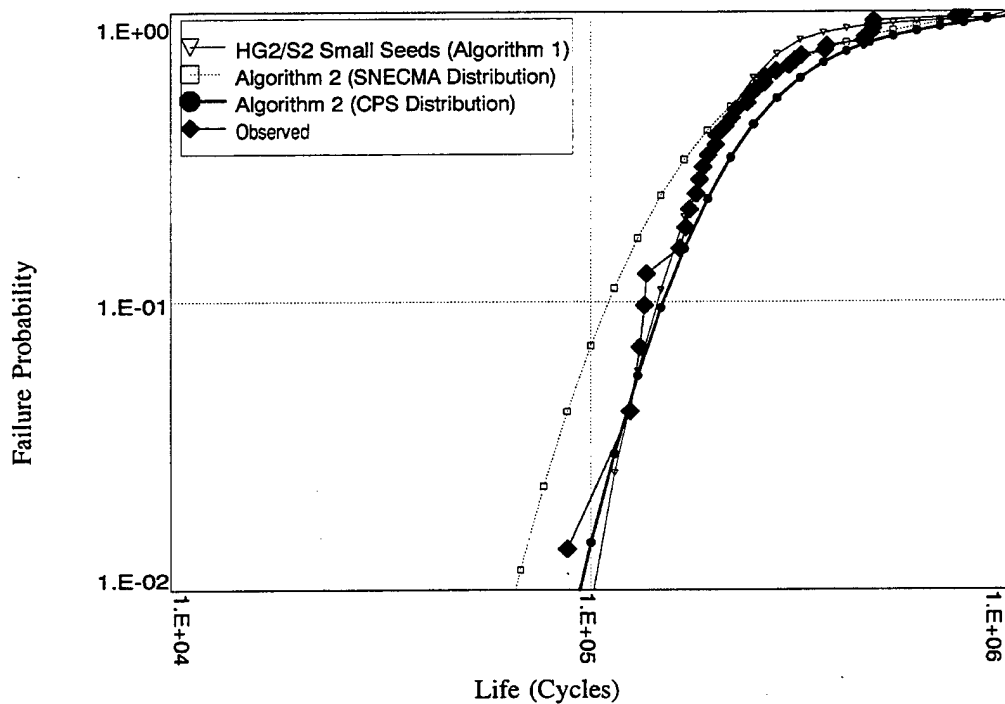


Figure 109. HG2/S2

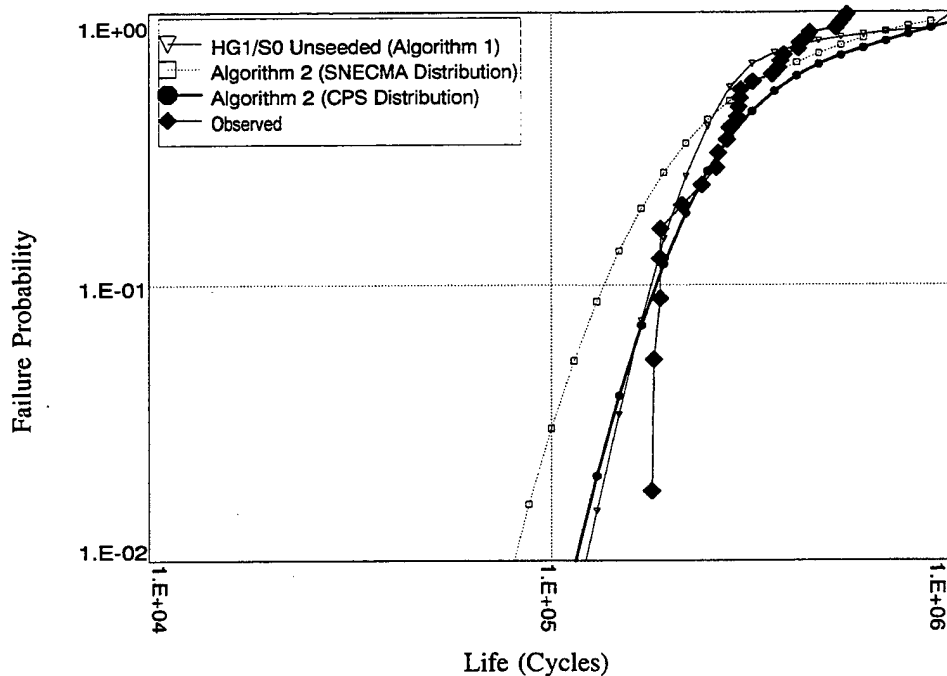


Figure 110. HG1/S0

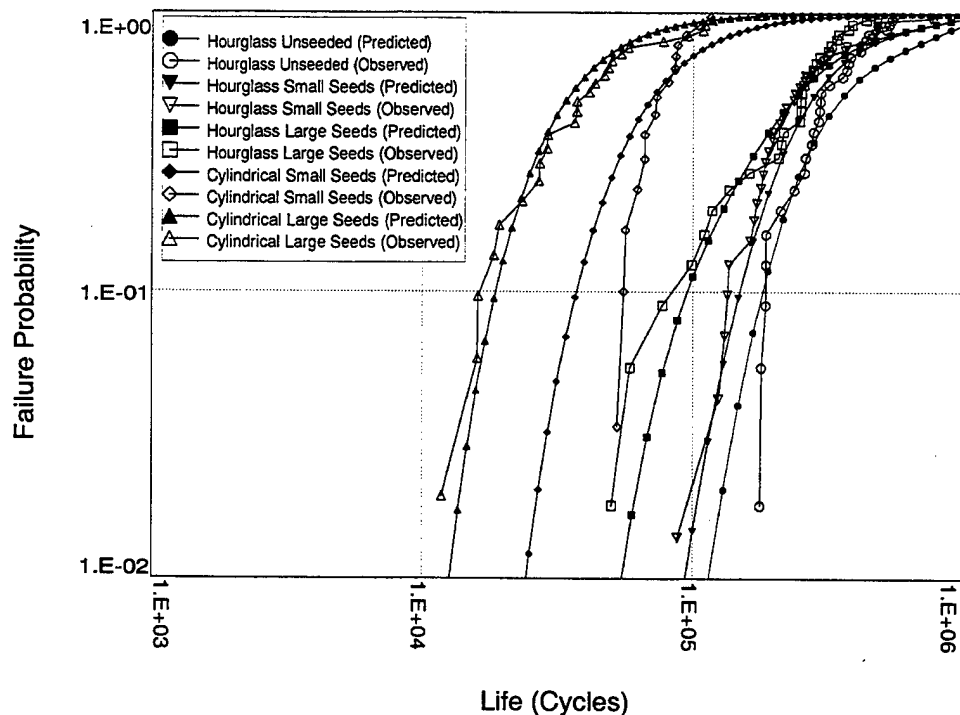


Figure 111. Algorithm 2 – Peened Specimens Tested at One Temperature/Strain Condition.

conservative and that a surface incubation model will eventually become part of a *Bull's Eye* solution.

One last refinement will be made to the predicted/observed comparisons. While the large seeded cylindrical data is very well predicted, the PFM estimated distribution for the small seeded cylindrical data set is significantly broader than the observed distribution. This is surprising given that the behaviors of individual inclusions seem to be distributed identically for both data sets. Refer to **Figure 112**: While the empirical μ -distributions are not expected to lie point for point one on top of the other, the differences are slight and readily ignorable in the absence of any contrary evidence. Contrary evidence will now be offered.

μ -values are computed by applying the life model (described briefly in Section 15.1) to each inclusion initiation; the area of the inclusion, its location in the specimen, and the mea-

sured Max and Min test stresses are entered into the calculation. There are actually three forging sets represented in the SNECMA data which will be called Phase 1 (small and large seeded), and Phases 2a and 2b (large seeded only). The three sets were observed to be stratified in their yielding behavior as indicated by **Figures 113** and **114** (all specimens cycled between 0.00% and 0.78% strain); there is about 5 ksi difference between the lowest and highest max stress distribution. Since μ is calculated with actual stresses, and given that the life model seems to work, the stratification is washed out — it is not reflected in the μ -distributions.

The specimen stress analyses used for the Algorithm 1 PFM calculations are, however, based on average properties; stress variabilities are not recognized. The Algorithm 2 integration of the μ -distribution into the calculation also ignores the stress variabilities given the discussion of the preceding paragraph. **Figure 115** shows revised μ -distributions based on stress

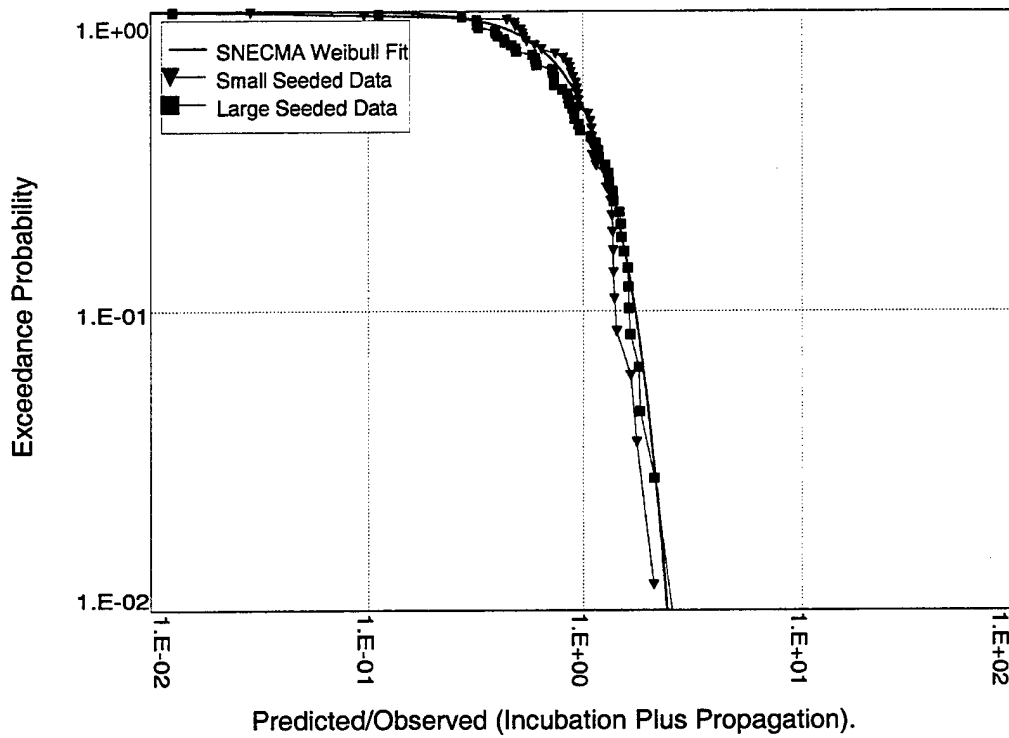


Figure 112. Comparison of Data Sets.

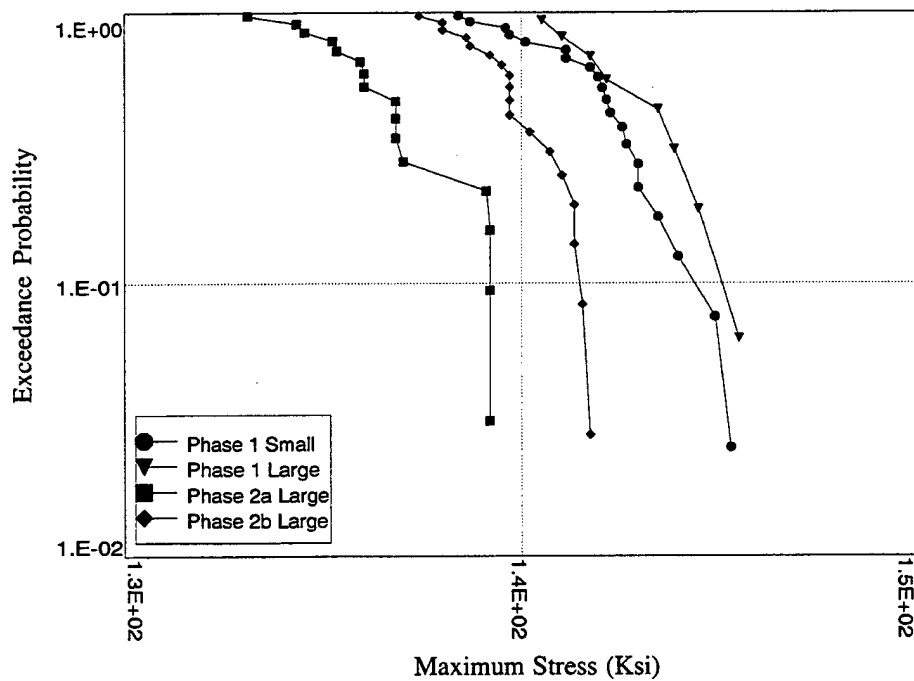


Figure 113. Distributions of Maximum Stresses.

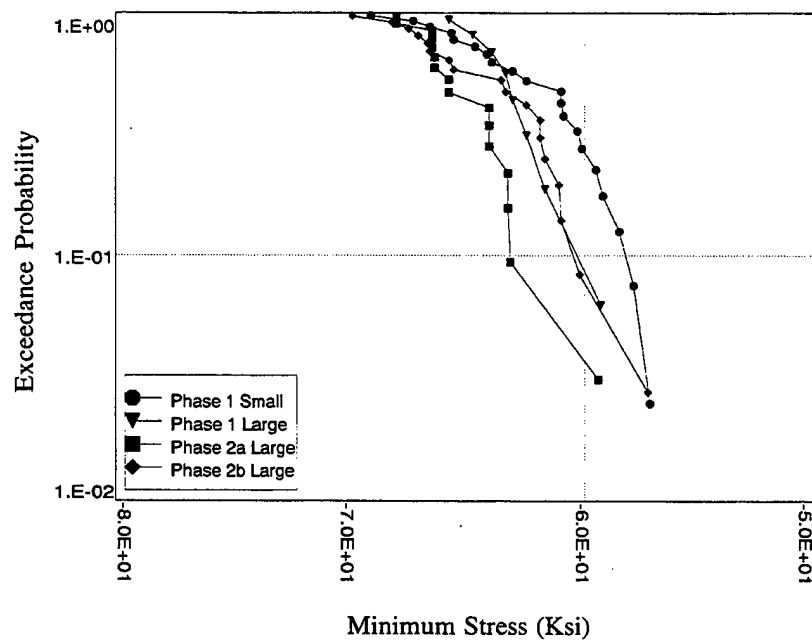


Figure 114. Distributions of Minimum Stresses.

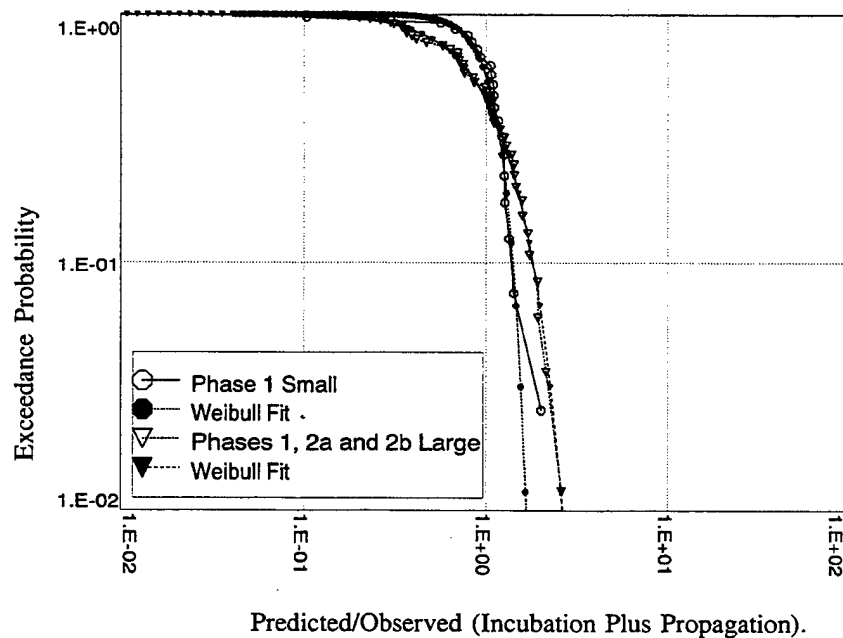


Figure 115. Distributions Broadened by Stress Variability.

analysis average stresses rather than measured test stresses; deviations from the average stresses are now reflected in the μ -values. The stress variabilities broaden the distributions, and a difference between large and small seeded data sets is clearer. If the separated Weibull fits are used for the Algorithm 2 calculations, the small seeded cylindrical data set comparison is much improved without affecting the quality of the large seeded data set comparison (see *Figure 116*).

Consolidating all material variability into a μ -distribution is a simple device which works for specimens given their relative simplicity; it is probably less appropriate for design applications. Specifically: Stress redistributions at plastically deforming features of complicated geometries are usually constrained by surrounding elastically deforming material, and the effect of yield strength variability on stresses may therefore only be quantifiable via elastic-plastic stress analysis. It seems likely,

therefore, that it will be some time before PFM design applications will incorporate this refinement.

To close this section, *Figure 117* shows predicted/observed comparisons for three other data sets from the René 88 DT incubation program (the high strain tests were cycled between 0.00% and 0.78% and the low strain tests were cycled between 0.00% and 0.64%, all at 1200° F, 649° C). Note that the calculations for the unpeened data sets appear to capture the competition between surface and subsurface initiated failures (surface initiated failures have shorter lives but occur with lower probability).

15.3.3 Model Disk Tests

Ideally maximum rotational speeds would have been chosen for the disk tests which were consistent with reasonable design limits, but doing so would have led to test times exceeding 10^6 cycles. The speed selected for the MD-9 geometry tests (48,000 rpm) was based on a

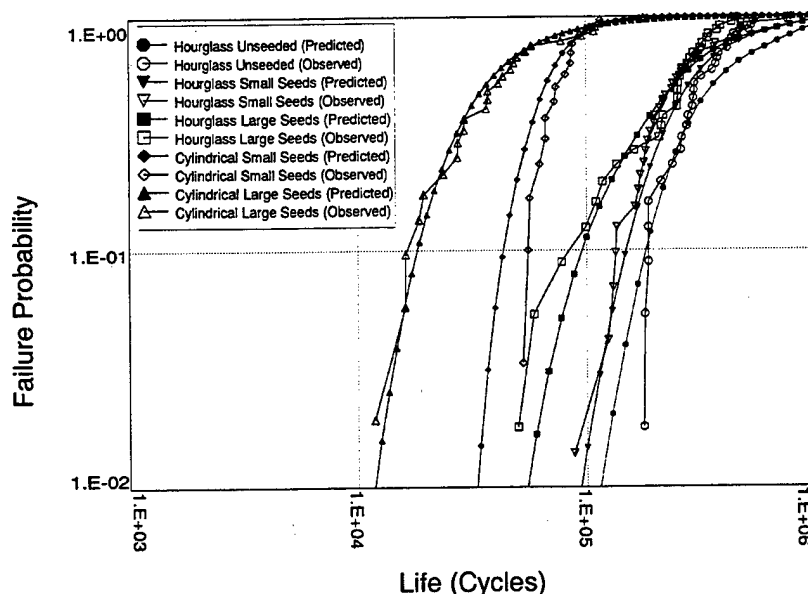


Figure 116. Stress Variability Factored into Cylindrical Data.

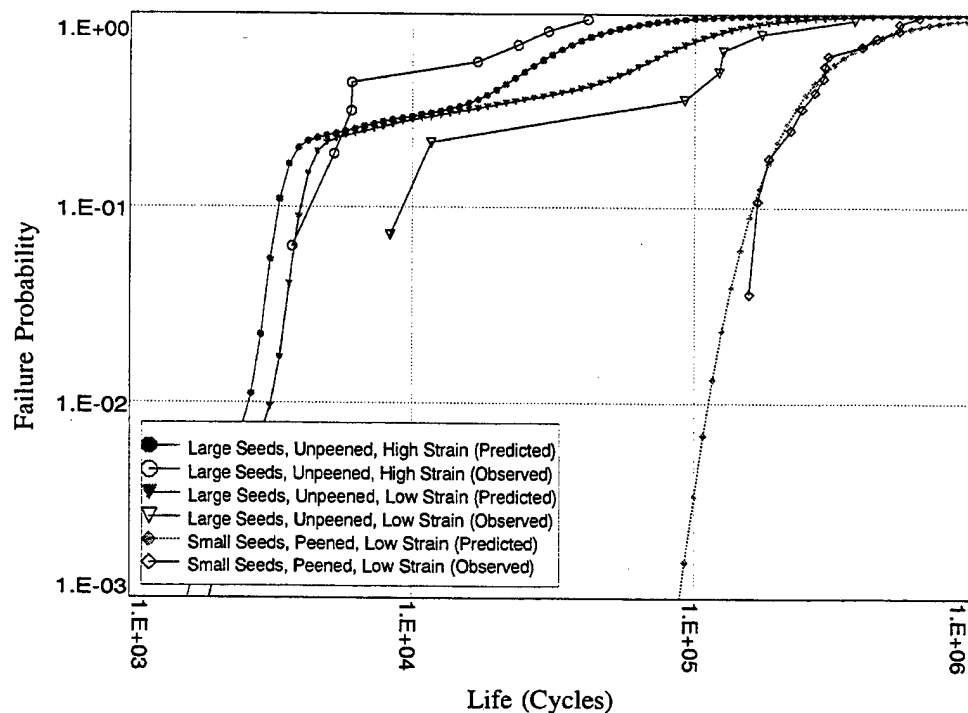


Figure 117. Other Cylindrical Specimen Data Sets.

target median life of 29,000 cycles predicted with the assumption that surface initiations would be suppressed despite high stresses (refer to *Figure 118*). The tests (and subsequent residual stress measurements) showed, however, that web stresses wiped out all peening benefit; all 10 failures probably initiated at the surface (fractography could definitively trace 8 of the 10 to natural surface intersecting inclusions — see *Table 29*). The observed failure distribution does agree very well with the PFM prediction made assuming that surface inclusions act as sharp cracks (see *Figure 118*). *Figure 119* provides a direct comparison of calculated and observed lives for the individual failure initiating inclusions.

Stresses were lowered for the MD-10 tests (cycled to 49,000 rpm) to yield a predicted 63,000 cycle median life assuming surface suppression and a predicted 7,300 cycle median life assuming the surface is active (refer to *Figure 120*). Note that the stresses are lower due

to the redesigned rim, but are still higher than typical design limits.

Referring to *Figure 120*, the observed failure distribution is lower than the PFM prediction assuming surface suppression, but much higher than the prediction assuming surface activity. Fractographic analysis of 7 MD-10 disks found 1 initiation at a peening dimple, 2 initiations at surface intersecting grains, 2 initiations at natural surface intersecting inclusions and 2 initiations at buried seeds, the latter being MD-1001 and MD-1003.

Given that MD-1001 and MD-1003 were reworked and repeened (see Section 14.3); it could be suggested that the double peening was responsible for forcing the subsurface initiations. This makes sense if one accepts that plastic deformation during the first cycle can reduce or even reverse the residual stress profile imparted by shotpeening (*Reference 8*). Disks MD-1003 yielded at start up, were repeened, and then restarted without further plastic de-

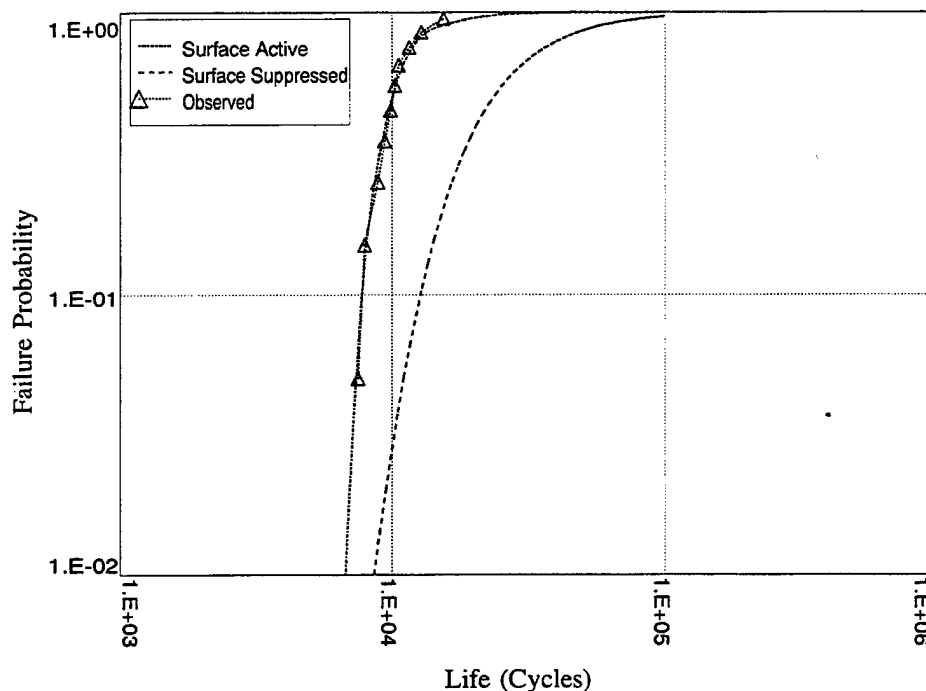


Figure 118. MD-9 Comparison of Predicted and Observed Failure Distributions.

Table 29. Model Disk Test Results Summary.

Test Sequence	Disk Serial Number	Seeding S0-Base S1-Large S2-Small	Cameron Forging	Initiation Type	Initiation Length Dimension (mils)	Initiation Depth Dimension (mils)	Distance From Centerline (inches)	Observed Life
1	MD902	S1	24	--	--	--	--	961
2	MD903	S2	41	--	--	--	--	--
3	MD904	S2	42	--	--	--	--	--
4	MD905	S2	44	Type 2, Surf.	3.9	1.8	2.21	7530
5	MD906	S2	45	Type 2, Surf.	2.8	1.7	1.97	7963
6	MD907	S2	46	Type 2, Surf.	1.0	0.8	2.23	15481
7	MD908	S2	47	Type 2, Surf.	3.8	1.9	2.55	9420
8	MD909	S2	48	Type 2, Surf.	2.4	1.4	2.16	9890
9	MD910	S2	30	--	--	--	--	12810
10	MD911	S2	34	--	--	--	--	11586
11	MD912	S2	36	Type 2, Surf.	1.3	1.0	2.22	8902
12	MD913	S2	40	Type 2, Surf.	1.4	0.7	2.08	10258
13	MD1001	S1	51	Type 1, Int.	10.0	17.0	1.82	34360
14	MD1002	S1	61	Peen Dimple	--	--	1.90	26883
15	MD1003	S1	62	Type 1, Int.	11.0	23.3	2.80	18563
16	MD1004	S1	63	Type 2, Surf.	2.8	1.6	1.84	11455
17	MD1005	S1	64	Type 1, Surf.	4.3	5.9	2.59	14002
18	MD1006	S1	65	Grain, Surf.	--	--	1.64	11587
19	MD1007	S1	66	Grain, Surf.	--	--	1.88	23433
20	MD901	S0	3	Type 2, Surf.	3.9	2.0	2.01	10589

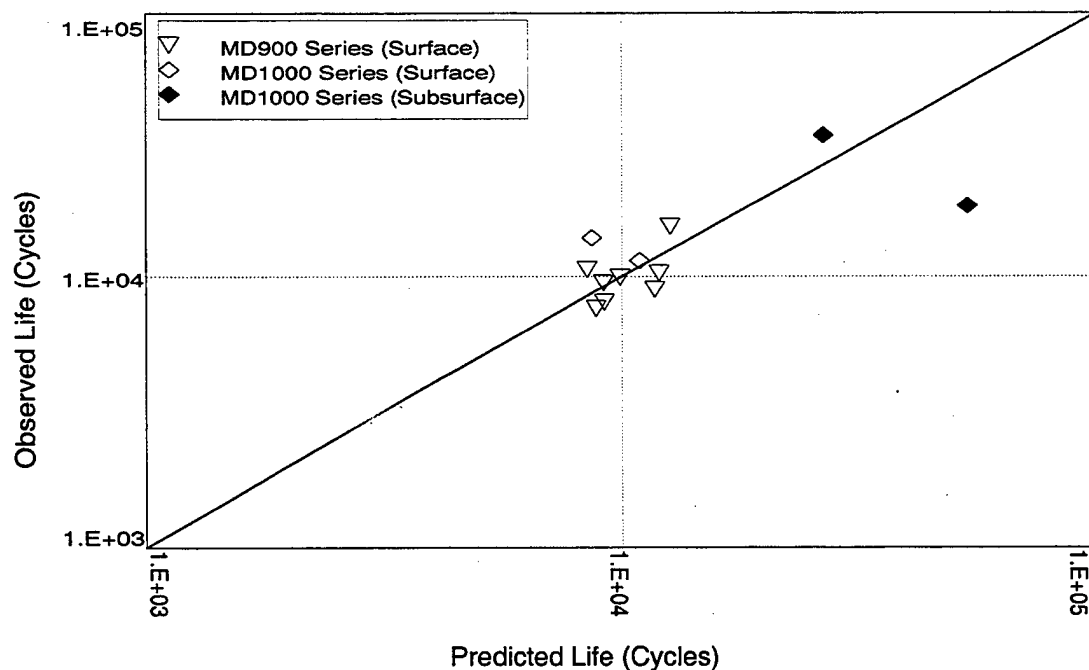


Figure 119. Individual Fracture Mechanics Calculations.

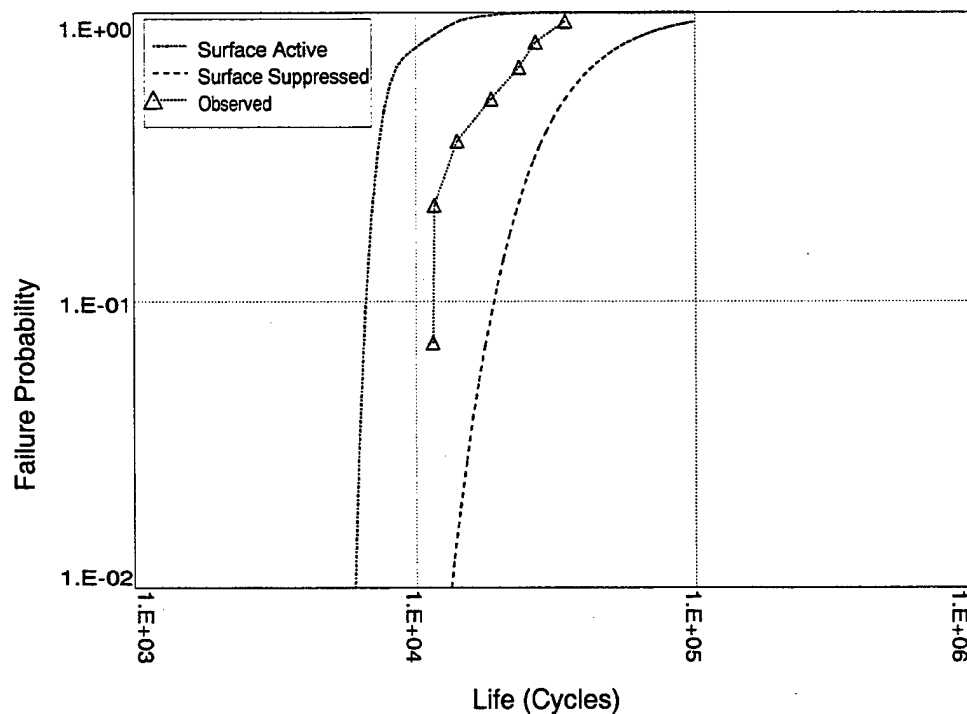


Figure 120. MD-10 Comparison of Predicted and Observed Failure Distributions.

formation. The residual stresses of the second peening should have held.

While these model disk results are encouraging, it is frustrating that the results must be taken at face value; far less post-mortem analysis is possible. Lessons which have been learned from push-pull specimen testing would be difficult to glean from the more complicated tests:

- The sample sizes are too small to hope to detect stratification effects.
- Temperature profiles are less well mapped and controlled.
- Actual stresses cannot be measured without additional expensive instrumentation.
- Post-test fractography is also more difficult given damage on high energy breakup (reduced but not eliminated by the aluminum/kevlar containment).

16.0 Summary and Discussion

A significant body of testing has been presented which supports PFM methodology, including small model disks representative of engine hardware. The work described amply demonstrates the utility of using seeded material for such testing. By careful tailoring of seeding distributions, a spectrum of failure distributions may be generated, from very narrow to very broad, allowing wide ranging assessment of the effectiveness of the probabilistic algorithms.

Precision in PFM calculations requires detailed understanding of mechanisms and variability in underlying material properties. In *Figures 81, 116-118 and 120*, a total of 229 specimen tests are presented in comparisons with predicted failure distributions. A small number of tests (7) were deleted from the analysis and do not show in these plots. Reasons given for the deletions follow:

- One specimen failed from a pair of nearby (and apparently interacting) inclusions.
- One specimen failed from a large badly oriented seeded inclusion lying very near the surface.
- One specimen failed from a very large buried inclusion at a lower than expected life; it and the specimen failing from the badly oriented, near surface inclusion are tied to a common forging. All specimens from this forging were underachievers. Forging variability is suggested.
- Four peened specimens failed from surface intersecting inclusions not suppressed by peening.

Current PFM technology *cannot yet* adequately address these effects, but they must be dealt with for design applications. Specifically: It can be assumed that initiation interactions are

ignorably rare in unseeded production material. It can be assumed that surface intersecting inclusions act as sharp cracks.

The point of the validation program was to validate those features of the PFM analysis which *can* be accounted for. The limited censoring of the data was felt appropriate.

There is another list of effects which were incorporated into the validation analyses but which are challenges for design applications:

Lot-to-Lot Variability in Inclusion Distribution

Seeding distributions were ascertained prior to manufacture of all seeded material.

It is known that there are differences in inclusion distribution between lots of production materials. It is not currently practical, however, to quantify and apply these differences in the PFM process, but it was shown in Section 9.2 that using an average distribution is actually conservative provided that the population captured in the average does not drift. (While mathematically demonstrable, this is counter-intuitive. It helps to understand that use of an average distribution assumes conservatively that every part contains some fraction of dirtier material.)

Inclusion Orientation

Orientation could be ignored for the As-HIP specimen set of Section 13. For the specimen sets of Sections 14 and 15 which were machined from pancake forgings, metallographic evidence supported one orientation assumption for the hourglass and cylindrical specimen sets, and another orientation assumption for the model disk specimen sets. The assumptions were independently supported by comparison of

observed distributions of initiation sizes to predicted distributions.

Orientation of inclusions in production forgings is considerably more complex. Models exist, but they are not yet incorporated into the PFM process. It may be conservatively assumed that the stress field always sees the maximum inclusion crosssections.

Yield Strength Variability

Min and Max test stresses were measured for the push-pull tests of Sections 14 and 15. The cylindrical specimen sets showed significant stratification implying yield stress variability. The effect of this variability was captured in μ -distributions of inclusion behavior which were integrated into the PFM analyses.

Incorporating yield stress variability into design applications of PFM is some way off. While it could be done, the needed response surfaces of elastic-plastic stress analyses require a significant computational commitment.

Lot-to-Lot Variability in Inclusion Behavior

Differences could be quantified between the data sets of Sections 14 and 15. Hourglass specimen inclusions behaved slightly differently than did cylindrical specimen inclusions. The differences were captured in the μ -distributions and integrated into the analyses.

While PM René 88 DT design applications incorporate the variability assessed from a large number of pancake forgings, evaluation of production material is still limited.

Where there are questions and concerns which can not be set aside with specific conservative assumptions, provision must be made to manage the potential risk. This is the *Outer Ring* action of the PFM Target discussed in Section 15.3.1 and more fully in Section 9 *Protection against the Unknown*. Engines may be removed from service at some fraction of a PFM calculated life or an inspection plan implemented.

This validation program does support the premise that adding precision to the inputs of a PFM analysis will improve the precision of the output. Conservatisms which have been added can often be subtracted, but at a cost.

For example, shotpeening has been shown to effectively suppress surface initiations at lower stresses, but its benefit gradually disappears as stress level increases. PFM calculations which assume full surface activity should lower bound hardware fatigue capability, but the conservatism may be extreme; better modeling of the effects of peening on surface inclusion behavior is called for and is being pursued.

In closing, it is pointed out that effects which impact probabilistics often also impact deterministics (e.g. yield strength variability), but while the latter is constrained by principle to *Middle Ring* conservatism, probabilistics offer the potential for hitting the *Bull's Eye* with safety.

Phase III References

1. Huron, E.S. and Roth, P.G., "The Influence of Inclusions on Low Cycle Fatigue Life in a P/M Nickel-Base Disk Superalloy," in Superalloys 1996, Ed. by R. D. Kissinger et. al., TMS-AIME, Warrendale, PA, 1996, p. 359.
2. Gibbons, JD, Nonparametric Statistical Inference, McGraw-Hill, Inc., 1971, p. 226.
3. Gibbons, JD, Nonparametric Statistical Inference, McGraw-Hill, Inc., 1971, p. 75.
4. Roth, P.G., and Paxson, A.J., *Electron Beam Melt Flotation as a Tool for Investigation of Ceramic Defect Distribution in Superalloys -- Development and Application to VIM-VAR Inconel 718*, Exists as Section 3.4.2.5 of AF-1 ENSIP Final Report, R89AEB236, June 1989.
5. Huron, E.S., "Serrated Yielding in a Nickel-Base Superalloy," in Superalloys 1992, Ed. by S. D. Antolovich et. al., TMS-AIME, Warrendale, PA, 1992, p. 675.
6. Roth, P.G., Murray, J.C., Morra, J.E., and Hyzak, J.M., "Heavy Liquid Separation: A Reliable Method to Characterize Inclusions in Metal Powder," Characterization, Testing and Quality Control, Advances in Powder Metallurgy & Particulate Materials - 1994, 2, Metal Powder Industries Federation, Princeton, NJ (1994).
7. Domas, P.A., and Roth, P.G., Fatigue '96, Proceedings of the Sixth International Fatigue Conference, Ed. by G. Lutjering and H. Nowack, Pergamon Press, p. 1251 (1996).
8. Prevay, P.S., Stress reversal conjecture by Prevay based on earlier work documented in "The Measurement of Subsurface Residual Stress and Cold Work Distributions in Nickel Base Alloys," *Residual Stress in Design, Process and Material Selection*, Ed. by W.B. Young, ASM, Metals Park, OH, 1987, p. 11.

Phase IV – Application

17.0 An Introduction to Design Optimization

Loosely speaking, artists produce drawings. They may be two dimensional as in a canvas, or three dimensional as in a sculpture, or may be more abstract and flow through time and mind as a piece of music or a poem. In broad terms, a designer's job also is to produce drawings but with the intention of making something (a building, an instrument, a machine); the drawings only serve as the specifications.

As a design progresses through concept and then engineering, drawings are iteratively re-worked, ideally with each edition improved in some way over its predecessor. Initially the dual notion of 'better or worse' used to judge each trial in the evolution may be loosely based on rules, or may be intuitive, or even aesthetic (this is equally true of an evening gown or a hypersonic transport). Almost invariably, however, 'better or worse' eventually becomes somehow quantitative. Leaving evening gowns alone, and focusing on mechanical designs, goals are set for performance, for reliability, for cost; and limits are set on controllable design parameters such as part dimensions, operating temperatures and applied loads.

In the simplest case, all goals are met by any point in the rectangular window defined by the parameter limits (for example, *Figure 121*); all designs in the window are said to be feasible.

It seems more often to be the case that most points in the fixed window fail one or more of the design goals, and assuming that it takes some effort to check if a potential design works, finding a feasible solution can be a time consuming endeavor (*Figure 122*).

And finding a feasible design is often not the end of the process; the designer is usually expected to find the best such design, where best means (of course) highest performance,

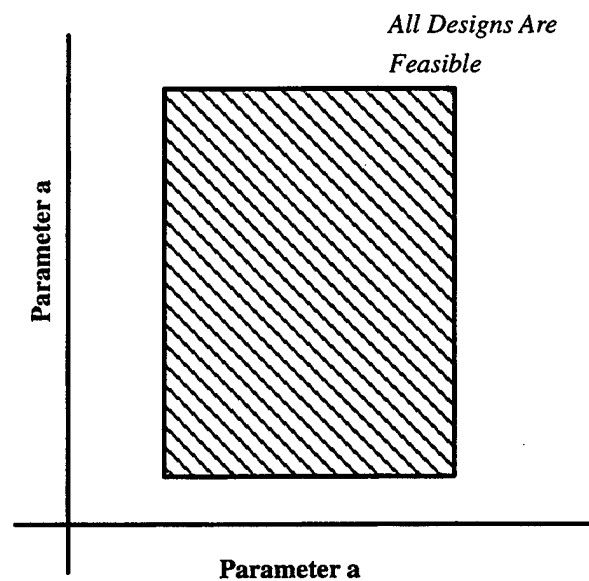


Figure 121. Rectangular Window.

most reliable and lowest cost. When, as is usually the case, these goals are mutually inconsistent (e.g. high performance conflicts with low cost), another discipline may be brought to bear to eliminate the conflict by redefining the problem (e.g. minimizing life

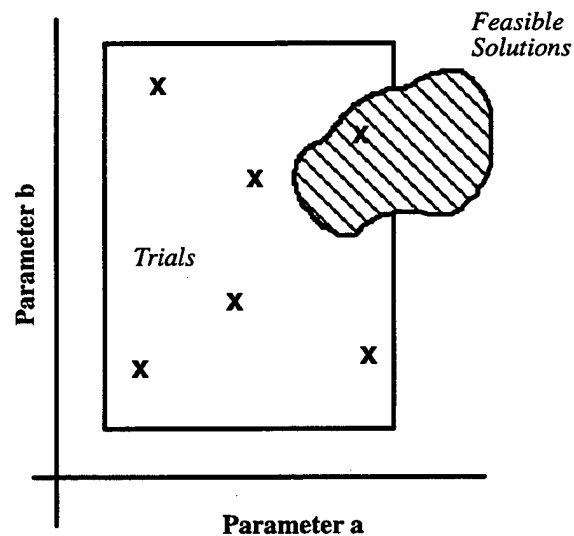


Figure 122. Trials - Feasible Solutions.

cycle cost defines tradeoffs between performance, reliability and cost).

If finding a feasible solution is time consuming; finding an optimal solution must clearly be more so (**Figure 123**). With any luck, response variables are reasonably well behaved functions of design parameters, allowing powerful tools to be applied.

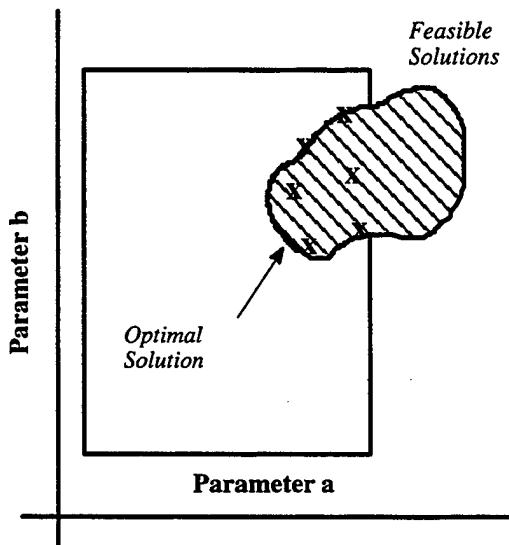


Figure 123. Optimal Solution.

Most engineers initially encounter optimization in their first calculus course. They are introduced to the derivative and then shown that it can be used to find maximas and minimas of nice functions. Later in the calculus sequence their concept of derivative is expanded into multiple dimensions, and they learn the use of the gradient for identifying extreme values of higher dimensional nice functions.

Note: Until otherwise noted, function will be taken to mean nice function will be taken to mean infinitely differentiable function.

The relative simplicity of gradient based optimization fades away at the introduction of constraints. A parameter limit is the simplest type of a constraint. It's not so bad in one dimension. It is learned in the early calculus

training that a function $f(x)$ of one variable restricted to an interval $[a, b]$ always:

- Has a maximum value and a minimum value over $[a, b]$.
- If a maximum or minimum occurs at an interior point of $[a, b]$, its derivative at that point is 0.
- It follows that if the derivative is non-0 over the interior, then the maximum and minimum values must occur at the endpoints, a and b .

Thus one identifies what is hopefully a very finite set of potential extreme values (the endpoints along with the so called *critical points* at which the derivative is 0) and then simply compares $f(x)$ over this set.

The theory is similar in multiple dimensions, but it doesn't help as much. A function $g(x, y)$ of two variables restricted to a rectangle $[a_1, b_1] \times [a_2, b_2]$ always:

- Has a maximum value and a minimum value over $[a_1, b_1] \times [a_2, b_2]$.
- If a maximum or minimum occurs at an interior point of the rectangle, its gradient at that point is $(0, 0)$.
- It follows that if the gradient is non-0 over the interior, then the maximum and minimum values must occur on the boundary of the rectangle.

As the set of potential extreme values contains the rectangular boundary, one can not rely on a finite number of comparisons. Another step must be taken. Restricting $g(x, y)$ to the sides of the rectangle yields four functions of one variable restricted to intervals: $g(a_1, y)$ and $g(a_2, y)$ restricted to $b_1 \leq y \leq b_2$, and $g(x, b_1)$ and $g(x, b_2)$ restricted to $a_1 \leq x \leq a_2$. The one dimensional theory may be applied to each of these to determine local maximas and minimas

which can be simply compared against critical point values in the interior (if any).

Optimizations of the sort sketched in the early paragraphs of this section tend to be subject to more complicated functional constraints, often stated in one of the following forms (in two dimensions): $c(x, y) \leq v$, $c(x, y) = v$, $c(x, y) \geq v$, or $u \leq c(x, y) \leq w$. The constraints define a feasible set which is likely more comtorted than a simple rectangle.

In many cases there is again theory to assure that $g(x, y)$:

- Has a maximum value and a minimum value over the feasible set.
- If a maximum or minimum occurs at an interior point of the feasible set, its gradient at that point is (0, 0).
- It follows that if the gradient is non-0 over the interior, then the maximum and minimum values must occur on the boundary.

But now the set of potential extreme values contains the boundary of the feasible set. If the boundary can be represented as a finite patchwork of simple functions of the form $\beta(s) = (\beta_x(s), \beta_y(s))$ each defined on the interval $[0, 1]$, then $g(\beta_x(s), \beta_y(s))$ can be optimized on each patch and the local maximas and minimas compared against any critical point values in the interior.

In practice, we are seldom so lucky, and iterative techniques must be utilized which move stepwise in promising directions (*References 1-3*). The optimization of the

XTC-76/3 High Pressure Turbine Disk presented in Section 20 utilizes the commercially available ADS (Automated Design System, *Reference 4*) package of optimization routines incorporated into PDAS (refer to Section 11.12).

Example (ADS test case):

$$\begin{aligned} \text{Minimize: } & 2^{3/2} x + y \\ & 0.01 \leq x \leq 1 \quad 0.01 \leq y \leq 1 \\ \text{Constraints: } & (2x + 2^{1/2} y) / (2x(x + 2^{1/2} y)) \leq 1 \\ & 1 / (2(x + 2^{1/2} y)) \leq 1 \end{aligned}$$

The objective function with the minimum identified is displayed in *Figure 124*. The constraint functions are displayed in *Figures 125* and *126*.

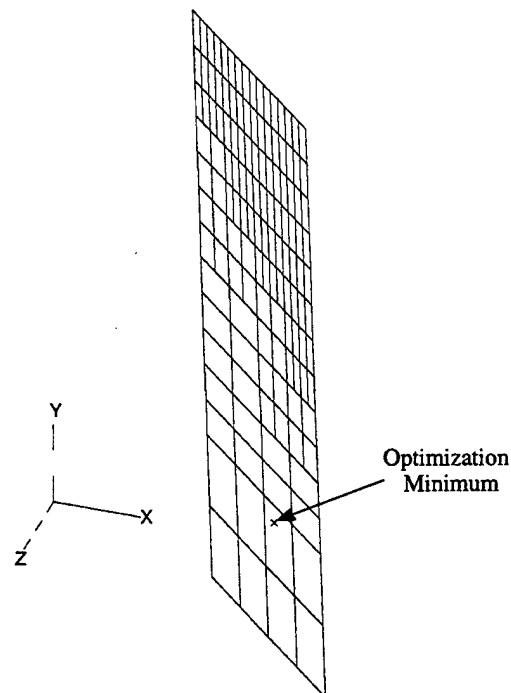


Figure 124. Objective Function $2^{3/2} x + y$.

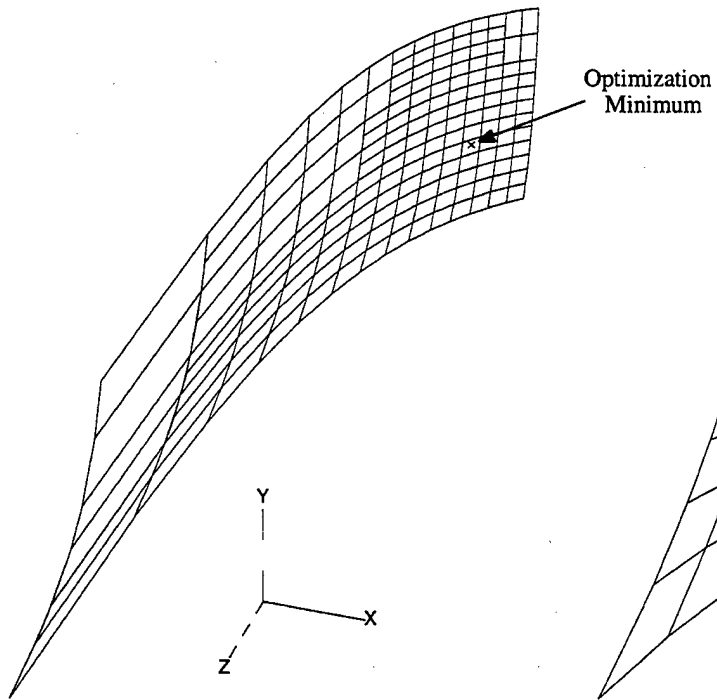


Figure 125. Constraint Function $(2x + 2^{1/2}y)/(2x(x + 2^{1/2}y))$

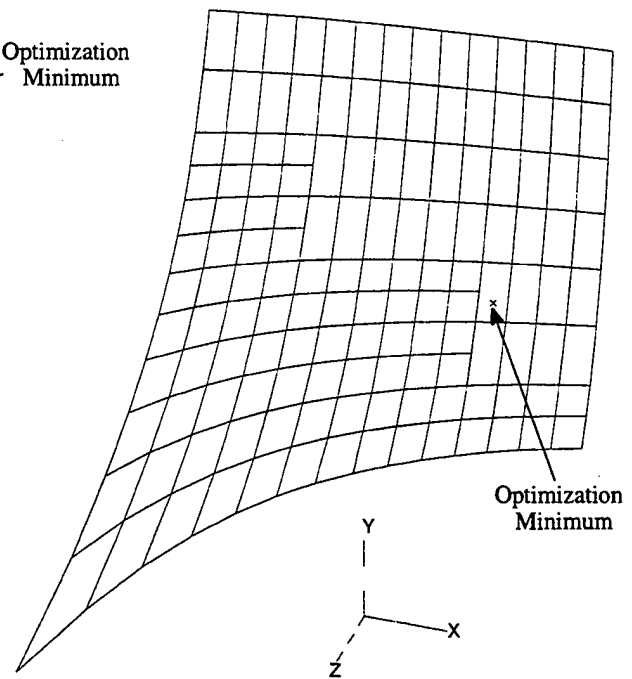


Figure 126. Constraint Function $1/2(x + 2^{1/2}y)$

18.0 Probabilistic Fracture Mechanics

18.1 Outline of the PFM Risk Calculation

The following is a brief summary of the theory layed out in Sections 8 and 12.

Algorithm 1

Let $G(N, a)$ denote the geometric failure probability . . . the probability of failure by life N given a single flaw of size a . Let $s(a)$ denote the probability density function of the flaw size distribution. $G(N, a)$ and $s(a)$ are integrated to yield $R(N)$. . . the probability of failure given a single randomly sized flaw.

$$R(N) = \int_0^{\infty} G(N, a) s(a) da$$

To calculate $F(N)$. . . the failure probability given competing flaws . . . the Poisson model for flaw occurrence will be assumed:

The probability that there are n flaws in a component volume is $e^{-V\lambda} (V\lambda)^n/n!$ where λ the average flaw frequency (number per cubic inch) and V is the volume.

$$\begin{aligned} F(N) &= \text{Prob}(1 \text{ defect present} -- \text{it fails by } N) \\ &+ \text{Prob}(2 \text{ defects present} -- \text{one or both fail by } N) \\ &+ \text{Prob}(3 \text{ defects present} -- \text{one or more fails by } N) \\ &+ \dots \\ &= e^{-\lambda V} (\lambda V)^1/1! (1 - (1 - R(N))^1) \\ &+ e^{-\lambda V} (\lambda V)^2/2! (1 - (1 - R(N))^2) \\ &+ e^{-\lambda V} (\lambda V)^3/3! (1 - (1 - R(N))^3) + \dots \\ &= e^{-\lambda V} (e^{\lambda V} - 1 - e^{\lambda V} (1 - R(N)) + 1) \\ &= 1 - e^{-\lambda V R(N)} \\ F(N) &= 1 - e^{-\lambda V R(N)} \end{aligned}$$

Algorithm 2

Algorithm 1 assumes that the life of any given flaw at any component location can be predicted exactly. In reality, there is scatter about the predicted life due to many factors (variability in flaw shape, variability in matrix properties, variability in actual loading, etc.).

1. Assume that the scatter can be modelled by a distribution of life multipliers: Let μ denote the ratio of predicted to observed life for a single inclusion, and let $m(\mu)$ denote the probability density function of the μ distribution.
2. Assume also that the distribution of μ predominantly represents testing variability (i.e. specimen-to-specimen rather than inclusion-to-inclusion). The distribution of life is derived from the basic PFM risk algorithm as a kind of convolution:

$$\int [1 - e^{-\lambda V \cdot R(N\mu)}] m(\mu) d\mu$$

19.0 Probabilistic Design Analysis System

PDAS (Probabilistic Design Analysis System) is a program developed at GEAE to facilitate complex design calculations. As was described in detail in Section 11, PDAS is really more a programming language than a program ... it does not define an analysis, but provides words and concepts which help the user define the analysis.

Computer programs have much structure in common: There may be blocks of input/output code, a sorting routine, random number generators and so on. Some of the overlap can be eliminated by linking programs with libraries of standard subroutines, but this requires careful attention to assure that calling sequences be exactly right. Arrays must be dimensioned; files opened and closed. Often the lines dedicated to actual computations are outnumbered many times by the wrapping.

Using PDAS ...

```
table 1 input x.dat
```

causes the file x.dat to be opened and keyword-defined data to be entered into a table identified as 1.

```
table 1 set y = EXP(LOG(X) +  
SIN(X**2))
```

creates a y-column in table 1 from the x-column of data in table 1 transformed by the expression following the equal sign.

```
distribution make d (table) 1 x
```

creates the empirical distribution d from the x-column data of table 1.

```
x = (random) d
```

generates a random parameter from the d-distribution.

Other commands enable manipulation of a MISSYDD database. Models, missions and computations can be defined and operated on as directed by simple template programs.

There are core GEAE-developed modules for selected functions such as spreadsheet management, distributional handling, finite element model interfacing and life calculations. There are also links to external functions such as Unigraphics, Patran and ANSYS, ensuring that the best tools can be applied to any given problem.

The following list of primary keywords summarizes current PDAS functionalities (for further details refer back to Section 11):

TABL	Table Manipulation	
TEXT	Text Entries	
EXPR	Expression Definition	
ALGE	Algebraic Operations	
DIST	Distribution Handling	
REGR	Regression Functions	
LOOP	Loops	
OPTI	Optimization	
PLOT	Plotting	
MODL	Model Library	} Probabilistic Fracture Mechanics Management
MSSN	Mission Library	
COMP	Computation Library	
LIFE	Life Calculations	
RISK	Risk Calculations	

20.0 Optimization of the IHPTET HPT Disk

The application vehicle for PRDS optimization was the HPT disk of the XTC-76/3 IHPTET engine. Through the course of the design process it was planned to machine the disk from a dual alloy forging comprised of fine mesh powder alloy products similar to the René 88 DT used in Phase III validation. Given preliminary data indicating that the dual alloy components were comparable to René 88 DT in crack growth characteristics, and superior in strength, René 88 DT properties were assumed applicable (though conservative) for the design calculations. This pullback position was later justified when technical concerns with the dual alloy forging forced a change in material selection to straight René 88 DT.

The disk was modeled parametrically, with seven dimensions selected for volume optimization of the bore and web regions. These are (refer to **Figure 127**):

BTHK	Bore Thickness
WANG	Web Angle
WTHK	Web Thickness
BOFF	Bore Offset
WOFF	Web Offset
FWAN	Forward Angle
ROFF	Rabbet Offset

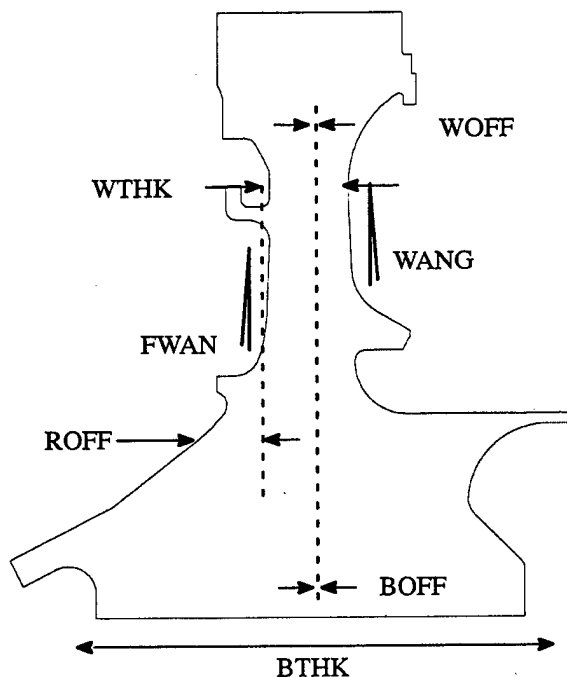


Figure 127. Volume Optimization.

Three computed quantities were constrained:

H_{AV} (AS11) - Average hoop stress over part crosssection (to be bounded above)

R_{Max} (MXRD) - Maximum of radial stress averages over part thickness at fixed radii (also to be bounded above)

$L_{0.001}$ (QLIF) Probabilistic fracture mechanics life at failure probability 1/1000 (to be bounded below)

The seven dimensional parameters were chosen for disk sizing. Clearly many more parameters are needed to define the disk shape: Fillet radii, Bore dimensions, Rim dimensions. While some of these are constrained by other design considerations, it would theoretically have been possible to open more of them up for optimization.

Adding parameters increases the computational load of an optimization. This becomes prohibitive if the time required for a single design evaluation is measured in hours. Consequently, it must be accepted that most design optimizations are technically only design improvements: Optimal (or at least locally optimal) designs are found assuming that most of the design is fixed. This is not a criticism. Optimization techniques should always move a design in the right direction.

In the case of our HPT disk, adjustable parameters were selected based on their probable impact on part volume. Others, particularly some of the fillet radii, impact the control variables (life and averaged stresses) but were felt to have less impact on volume.

The need to restrict the dimension of the design space was particularly strong given the following problems with partial derivative calculations required by the gradient based optimization routines. Consider the sequence of steps:

1. Part geometry defined for parameter vector $(\alpha_0, \beta_0, \gamma_0, \dots)$.
2. Geometry meshed and thermal/stress analysis executed.
3. Volume V_0 calculated based on (2).
4. Probabilistic fracture mechanics calculation set up and executed based on (2).
5. Life L_0 corresponding to a 0.001 failure probability calculated based on (4).
6. Part geometry defined for perturbed parameter vector $(\alpha_1, \beta_0, \gamma_0, \dots)$.
7. Steps (1) through (5) repeated for new geometry yielding volume V_1 and life L_1 .
8. Partial derivative estimated: $\partial(V, L)/\partial\alpha = (V_1 - V_0, L_1 - L_0)/(\alpha_1 - \alpha_0)$.
9. Steps repeated as necessary to estimate $\partial(V, L)/\partial\beta, \partial(V, L)/\partial\gamma, \partial\alpha, \dots$

As was discussed in Section 11.12.1, evaluations of the partial derivatives are compromised by discretization of the finite element mesh and Monte Carlo sampling variations.

The following alternative was adopted:

- A small region about the initial guess is defined. V and L are calculated at design points within and on the boundary of the region.
- Local response surfaces $V(\alpha, \beta, \gamma, \dots)$ and $L(\alpha, \beta, \gamma, \dots)$ are fit to the calculations.
- V is minimized in the region subject to the constraint that L remain above a specified value.
- The solution defines a new local region, and the process continues until a convergence criterion is satisfied.

This approach relies on larger perturbations in model geometry which are designed to result in larger (and less easily masked) differences in V and L ; it also tends to average out the noise inherent in the meshing and lifing operations.

20.1 First Step of Optimization

The HPT design engineer began sizing his disk using an ADS-based stacked shell optimization program producing the rough outline shown in **Figure 128**. Flanges and a rim were added as shown in **Figure 129**. Initial values of bore, web and rabbet offsets (BOFF, WOFF and ROFF) were set by judgement (**Figure 130**). PDAS was then used to optimize the parametrically defined finite element model for weight first by varying bore and web thicknesses (BTHK and WTHK), and then web thickness and angles (WTHK, WANG and FWAN ... WANG and FWAN held equal). Hoop and radial stress averages (AS11 and MXRD) were constrained. The optimized outline is shown in **Figure 131** superimposed on the starting point. Significant weight was added to meet the constraints.

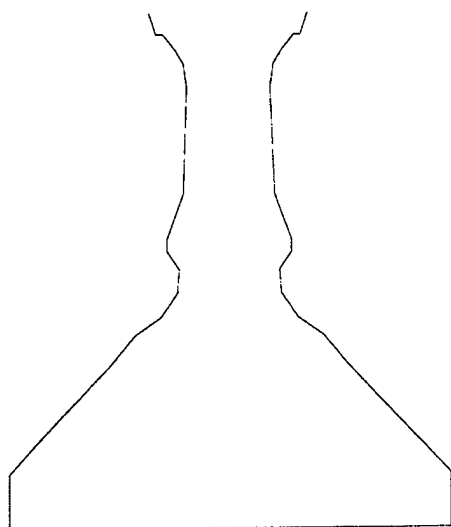


Figure 128. ADS-based Stacked Shell Optimization Program. Rough Outline

20.2 Second Step of Optimization

The second optimization step fixed BTHK (it pushed up against the constraint of forging thickness) but opened all six remaining variables to change. A thirty-two run matrix was

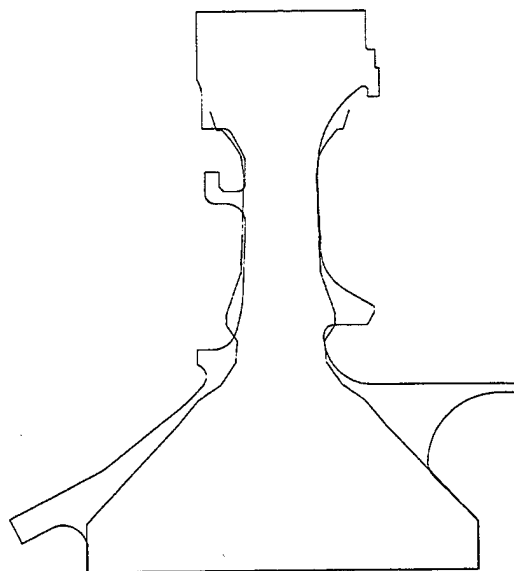


Figure 129. ADS-based Stacked Shell Optimization Program. Flanges and a Rim added.

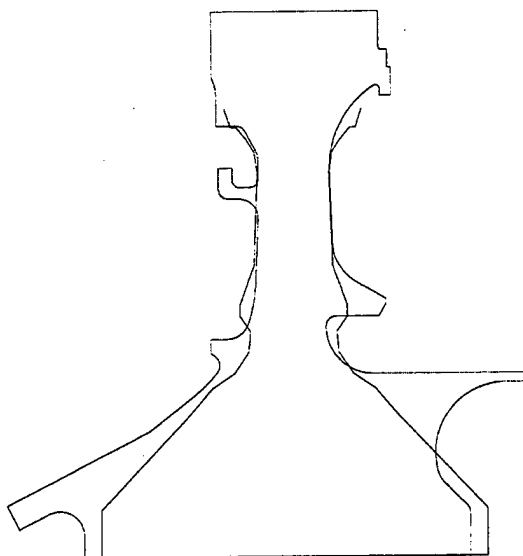


Figure 130. BOFF, WOFF AND ROFF Judgement.

constructed for the parameters WANG, WTHK, BOFF, WOFF, FWAN and ROFF to assess all first order effects and first order interactions of these dimensions on the four design response variables V , H_{Av} , R_{Max} and $L_{0.001}$ (see **Table 30**; refer to **Appendix D** for an introduction to factorial designs).

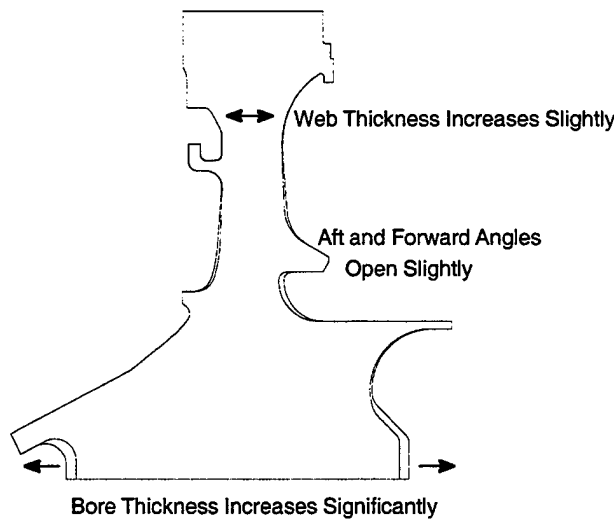


Figure 131. Optimized Outline.

PDAS was programmed to run this screening study. Each row (I_a, I_b, \dots, I_f) of **Table 30** defines a perturbation of part geometry:

$$(a_0, b_0, \dots, f_0) = (a_0, b_0, \dots, f_0) + (\delta_a I_a, \delta_b I_b, \dots, \delta_f I_f)$$

where $\delta_a, \delta_b, \dots, \delta_f$ are deviations fixed for the study. PDAS looped over the table performing the following sequence of steps for each row:

1. Edited part parameter file to reflect the perturbation.
2. Launched geometric modeling (via Unigraphics accessing the parameter file), followed by finite element meshing (via Patran), followed by thermal and stress analysis (via Ansys), followed by postprocessing (via GEAE's SIESTA programs) yielding a part database.
3. Computed V using a PDAS part database function.
4. Computed H_{Av} using another PDAS part database function.
5. Computed R_{Max} by first using a PDAS part database function to generate a table of thickness averaged radial stresses over a list of radii encompassing the model, and then taking the maximum of the table.

6. Set up and executed a probabilistic fracture mechanics calculation to determine $L_{0.001}$.
7. Added the results to a holding file.

Following the thirty-two runs, regression functions of PDAS were called to fit the following local functional form for each of the four response variables:

$$\begin{aligned} Z = & \varphi_0 + \varphi_A A + \varphi_B B + \varphi_C C + \varphi_D D + \varphi_E E + \\ & \varphi_F F + \varphi_{AB} AB + \varphi_{AC} AC + \varphi_{AD} AD + \varphi_{AE} AE + \\ & \varphi_{AF} AF + \varphi_{BC} BC + \varphi_{BD} BD + \varphi_{BE} BE + \\ & \varphi_{BF} BF + \varphi_{CD} CD + \varphi_{CE} CE + \varphi_{CF} CF + \\ & \varphi_{DE} DE + \varphi_{DF} DF + \varphi_{EF} EF \end{aligned}$$

where A, B, C, D, E and F are normalized deviations from the initial design (E.g. $A = (a - a_0)/\delta_a$). The results are presented in **Table 31**. Several observations are made.

- Volume is significantly impacted only by dimension B .
- Average hoop stress is not strongly impacted by any of the six dimensions. It will be kept as a constraint, but it will not significantly control the optimization.
- Maximum average radial stress is most strongly controlled by B and to a lesser extent by E . The signs of their effects on this response variable are both negative. The effects of B and E on part volume are both positive. Decreasing either dimension decreases volume but increases stress.
- Life at 1/1000 failure probability is strongly controlled by B and even more so by D . While B has a positive effect on both volume and life (decreasing B decreases volume but also life), the signs of the effects of D are opposite (decreasing D decreases volume and increases life).
- The life response is very weakly affected by variables A and C .
- Most of the interaction terms are negligible when compared to the main effects; the largest four are BD, DE, DF and EF connected with the life response.

Table 30. Fractional Factorial Design.

A (WANG)	B (WTHK)	C (BOFF)	D (WOFF)	E (FWAN)	F (ROFF)
-1	-1	-1	-1	-1	-1
1	-1	-1	-1	-1	1
-1	1	-1	-1	-1	1
1	1	-1	-1	-1	-1
-1	-1	1	-1	-1	1
1	-1	1	-1	-1	-1
-1	1	1	-1	-1	-1
1	1	1	-1	-1	1
-1	-1	-1	1	-1	1
1	-1	-1	1	-1	-1
-1	1	-1	1	-1	-1
1	1	-1	1	-1	1
-1	-1	1	1	-1	-1
1	-1	1	1	-1	1
-1	1	1	1	-1	1
1	1	1	1	-1	-1
-1	-1	-1	-1	1	1
1	-1	-1	-1	1	-1
-1	1	-1	-1	1	-1
1	1	-1	-1	1	1
-1	-1	1	-1	1	-1
1	-1	1	-1	1	1
-1	1	1	-1	1	1
1	1	1	-1	1	-1
-1	-1	-1	1	1	-1
1	-1	-1	1	1	1
-1	1	-1	1	1	1
1	1	-1	1	1	-1
-1	-1	1	1	1	1
1	-1	1	1	1	-1
-1	1	1	1	1	-1
1	1	1	1	1	1

Based on these results, the following local approximating form was selected for V , H_{AV} and R_{Max} :

$$Z = \phi_0 + \phi_A A + \phi_B B + \phi_C C + \phi_D D + \phi_E E + \phi_F F \\ + \phi_{BD} BD + \phi_{DE} DE + \phi_{DF} DF + \phi_{EF} EF$$

All six dimensional parameters were retained given that the computations required for their

determination could be executed with acceptable speed (steps 1-5 of the analysis loop).

By contrast, parameters A and C (WANG and BOFF) were pulled from the approximating form for $L_{0.001}$ given that the probabilistic fracture mechanics calculations require several hours apiece (step 6 of the analysis loop):

Table 31. Normalized Deviations Results.

Normalized Response Term	Part Volume	Average Hoop Stress	Maximum Average Radial Stress	Life at 1/1000 Failure Probability
A (WANG)	0.001	0.000	-0.002	-0.004
B (WTHK)	0.013	-0.001	-0.056	0.081
C (BOFF)	0.001	-0.001	0.000	-0.001
D (WOFF)	0.001	-0.001	0.002	-0.102
E (FWAN)	0.003	-0.001	-0.010	0.019
F (ROFF)	0.002	-0.001	0.000	0.018
AB	0.000	0.000	-0.001	-0.001
AC	0.000	0.000	0.000	0.008
AD	0.000	0.000	0.000	-0.006
AE	0.000	0.000	0.002	0.008
AF	0.000	0.000	0.000	0.007
BC	0.000	0.000	0.000	-0.006
BD	0.000	0.000	0.000	-0.019
BE	0.000	0.000	0.000	-0.004
BF	0.000	0.000	0.000	-0.004
CD	0.000	0.000	0.000	-0.001
CE	0.000	0.000	0.000	0.002
CF	0.000	0.000	0.000	0.003
DE	0.000	0.000	0.000	0.023
DF	0.000	0.000	0.000	0.024
EF	0.000	0.000	0.000	-0.027

$$Z = \varphi_0 + \varphi_B B + \varphi_D D + \varphi_E E + \varphi_F F + \varphi_{BD} BD + \varphi_{DE} DE + \varphi_{DF} DF + \varphi_{EF} EF$$

The interactions BD, DE, DF and EF were retained based on their impact on $L_{0.001}$.

New optimization runs were made with constraints on H_{Av} , R_{Max} and $L_{0.001}$. Recapping the procedure:

1. A small region about a design point (a_0, b_0, \dots, f_0) is defined by the seventeen perturbations ($\delta_a I_a, \delta_b I_b, \dots, \delta_f I_f$) tabulated in **Table 32**. V , H_{Av} , R_{Max} and $L_{0.001}$ are calculated at the perturbed points as called for (coded Y or N in **Table 32**).
2. Local response surfaces $V(a, b, c, d, e, f)$, $H_{Av}(a, b, c, d, e, f)$, $R_{Max}(a, b, c, d, e, f)$ and $L_{0.001}(b, d, e, f)$ are fit to the calculations.

3. V is minimized in the region subject to constraints bounding H_{Av} and R_{Max} above, and bounding $L_{0.001}$ below.
4. The solution defines a new local region and the process continues until a convergence criterion is satisfied.

The shape produced by the initial two-parameter optimization was used to start the program. Convergence was achieved after two iterations with little change from the starting geometry.

20.3 Recognizing Other Variabilities

It must be acknowledged that the stress constraints in the above optimization conform to GEAE's deterministic design practices. Given that the dual alloy disk concept was new and untested, and that funding was explicitly

Table 32. Design Point Defined by Seventeen Perturbations.

A	B	C	D	E	F	Volume	Average Hoop Stress	Max Average Radial Stress	1/1000 Life
0	0	0	0	0	0	Y	Y	Y	Y
0	0	0	1	1	1	Y	Y	Y	Y
0	0	0	1	1	-1	Y	Y	Y	Y
0	0	0	1	-1	1	Y	Y	Y	Y
0	0	0	1	-1	-1	Y	Y	Y	Y
0	0	0	-1	1	1	Y	Y	Y	Y
0	0	0	-1	1	-1	Y	Y	Y	Y
0	0	0	-1	-1	1	Y	Y	Y	Y
0	0	0	-1	-1	-1	Y	Y	Y	Y
1	0	0	0	0	0	Y	Y	Y	N
-1	0	0	0	0	0	Y	Y	Y	N
0	1	0	1	0	0	Y	Y	Y	Y
0	1	0	-1	0	0	Y	Y	Y	Y
0	-1	0	1	0	0	Y	Y	Y	Y
0	-1	0	-1	0	0	Y	Y	Y	Y
0	0	1	0	0	0	Y	Y	Y	N
0	0	-1	0	0	0	Y	Y	Y	N

excluded from the contract for generating distributional input data, the risk involved with backing away from the most basic of GEAE's disk design practices could not be justified.

Incorporating a probabilistic version of the constraint would have been straight forward.

Figure 132 plots:

$$\text{Prob}(H_{Av}(a, b, c, d, e, f) \leq H_{Limit} \text{ or } R_{Max}(a, b, c, d, e, f) \leq R_{Limit})$$

where truncated normal distributions were assumed for a, b, c, d, e and f, and lognormal distributions were assumed for H_{Limit} and R_{Limit} . (Scatter Parameter in the plot equals $\exp(\mu + \sigma) - \exp(\mu)$ where μ is a lognormal mean and σ a lognormal standard deviation. H_{Limit} and R_{Limit} were assigned different

means but were assumed to have a common standard deviation.)

(A simple PDAS template estimated the probabilities in **Figure 132** by executing 100,000 run Monte Carlo simulations for each selected value of the scatter parameter.)

Also, in Section 9.1 it was shown how to integrate dimensional variability into PFM calculations:

Compute $F(N: x_1, x_2, x_3)$, the conditional probability of failure given part dimensions x_1, x_2 and x_3 , and then integrate against $\rho(x_1, x_2, x_3)$, the joint density of the dimensions:

$$\int \times F(N: x_1, x_2, x_3) \rho(x_1, x_2, x_3) dx_1 dx_2 dx_3$$

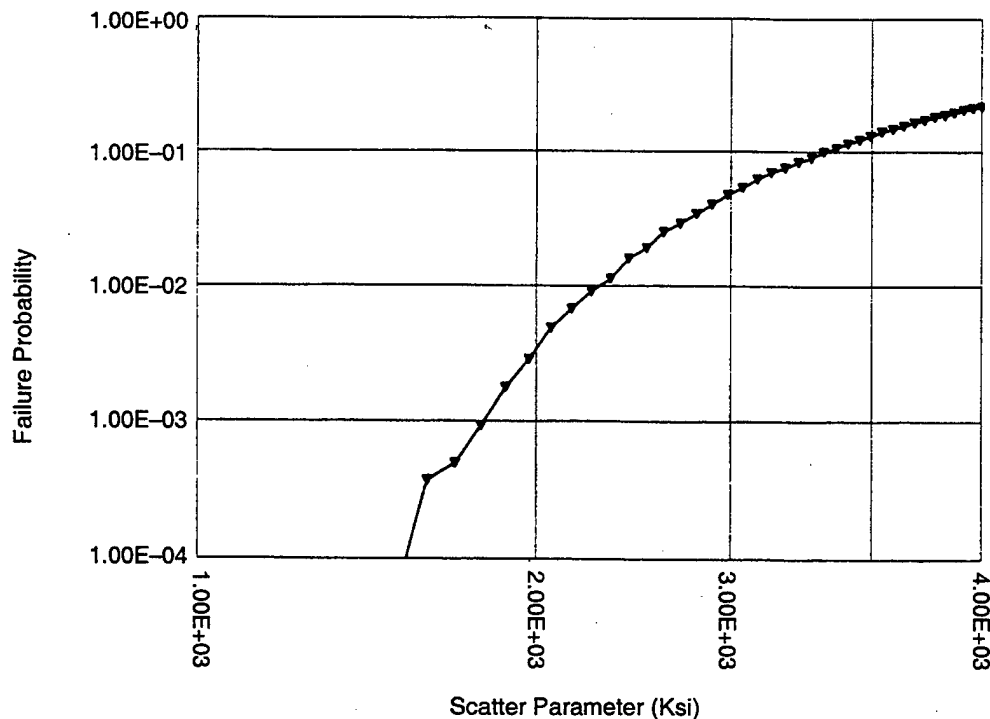


Figure 132. Dual Alloy Disk Concept Variability; PDAS Probabilities.

In the XTC-76 application, the screening study in Section 20.2 found only minimal sensitivity of $L_{0.001}$ to minor perturbations of the seven dimensional parameters. Also, the value of $L_{0.001}$ stayed well above the constraint minimum. Had $L_{0.001}$ been more sensitive to dimensional perturbations, or had its value been closer to the constraint limit, a simple response surface approximating $F(N: a, b, c, d, e, f)$ would have been developed and integrated as above.

20.4 Optimization Results

Figures 133-143 show the evolution of the design parameters BTHK, WANG, WTHK, BOFF, WOFF, FWAN and ROFF, and the response parameters V, AS11, MXRD and QLIF (Volume, H_{Av} , R_{Max} and $L_{0.001}$). In these plots, iterations 1 and 2 correspond to the overlaid outlines in **Figure 131**; 3 and 4 correspond to the iterations of the subsequent six parameter optimization.

Figures 133, 134, 135 and 138 show pronounced changes in bore and web thicknesses

and web angles from iteration 1 to iteration 2. These pushed H_{Av} and R_{Max} down to meet the stress constraints, and pushed $L_{0.001}$ up to meet the life constraint.

The disk outline changed very little from iteration 2 to iteration 3 ... V decreased slightly (by about 0.4 in^3); H_{Av} held essentially constant (as expected from the DOE study); R_{Max} increased slightly (bumping into its constraint); and $L_{0.001}$ moved down slightly but stayed well above the life constraint. It would appear that the constraint on MXRD was principally responsible for inhibiting further movement from iteration 3 to iteration 4. **Figures 144-148** detail the minor outline changes between iterations 2 and 4.

The optimization was successful; the disk geometry was pushed in the right direction. There are, however, caveats:

- At the point in the design process at which this exercise was performed, there were still significant unknowns: Material properties were assumed. Boundary conditions for the

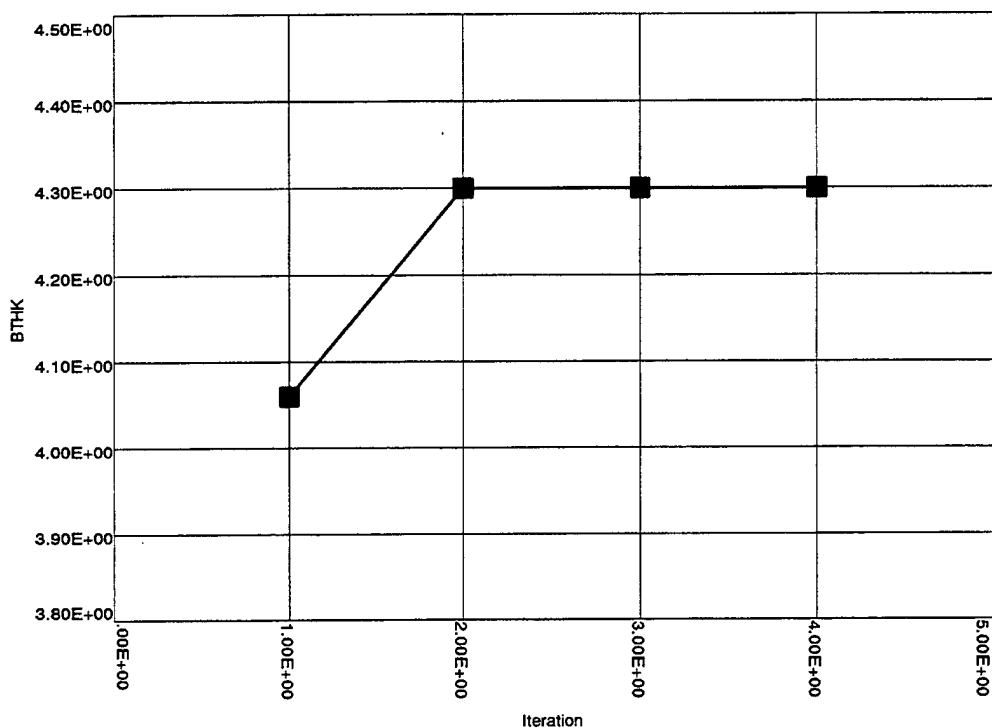


Figure 133. Evolution of Design and Response Parameters.

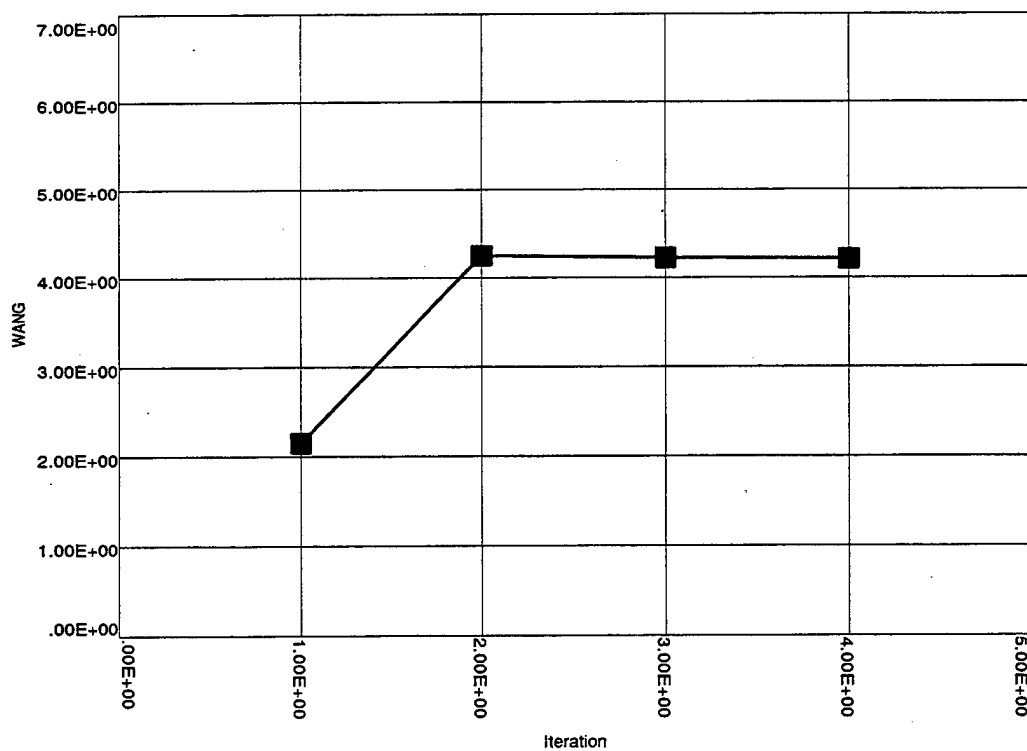


Figure 134. Evolution of Design and Response Parameters.

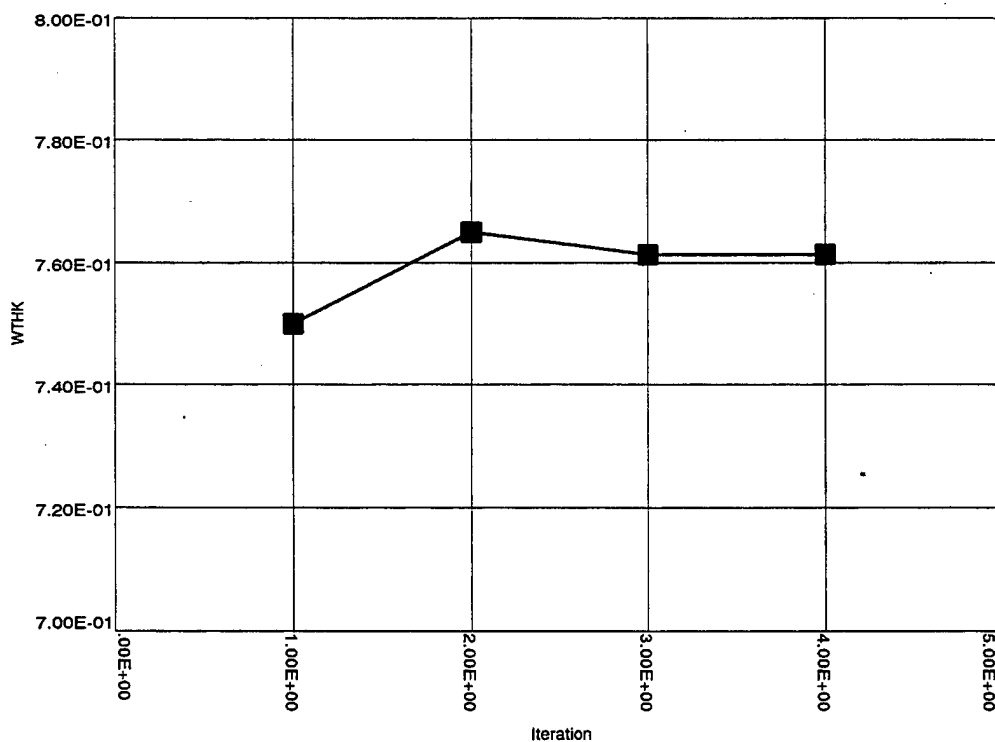


Figure 135. Evolution of Design and Response Parameters.

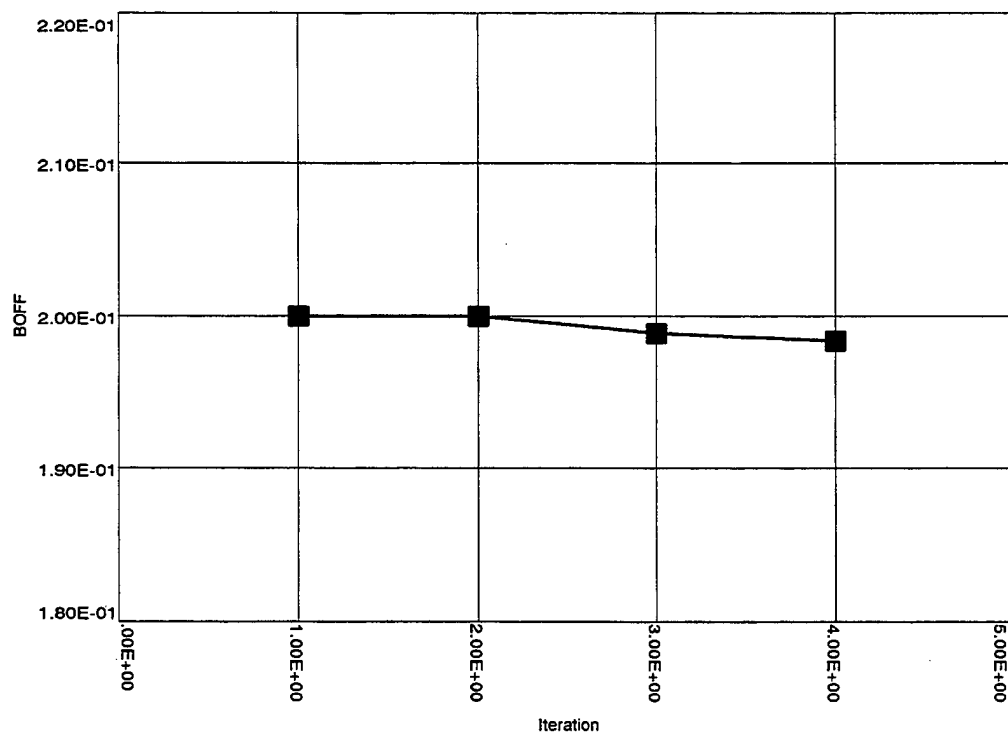


Figure 136. Evolution of Design and Response Parameters.

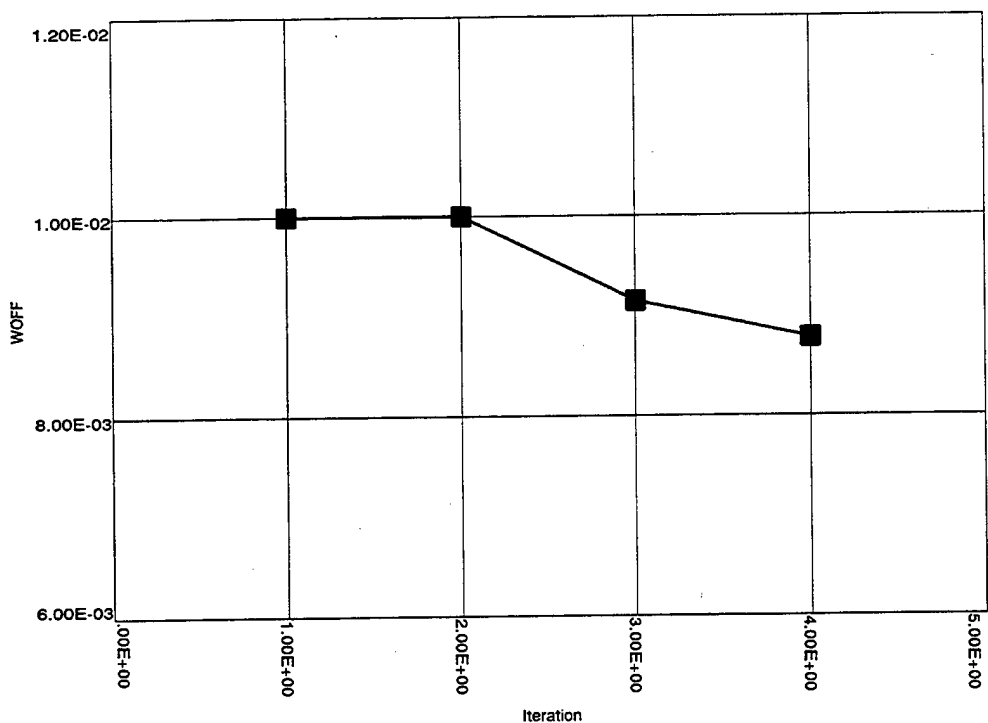


Figure 137. Evolution of Design and Response Parameters.

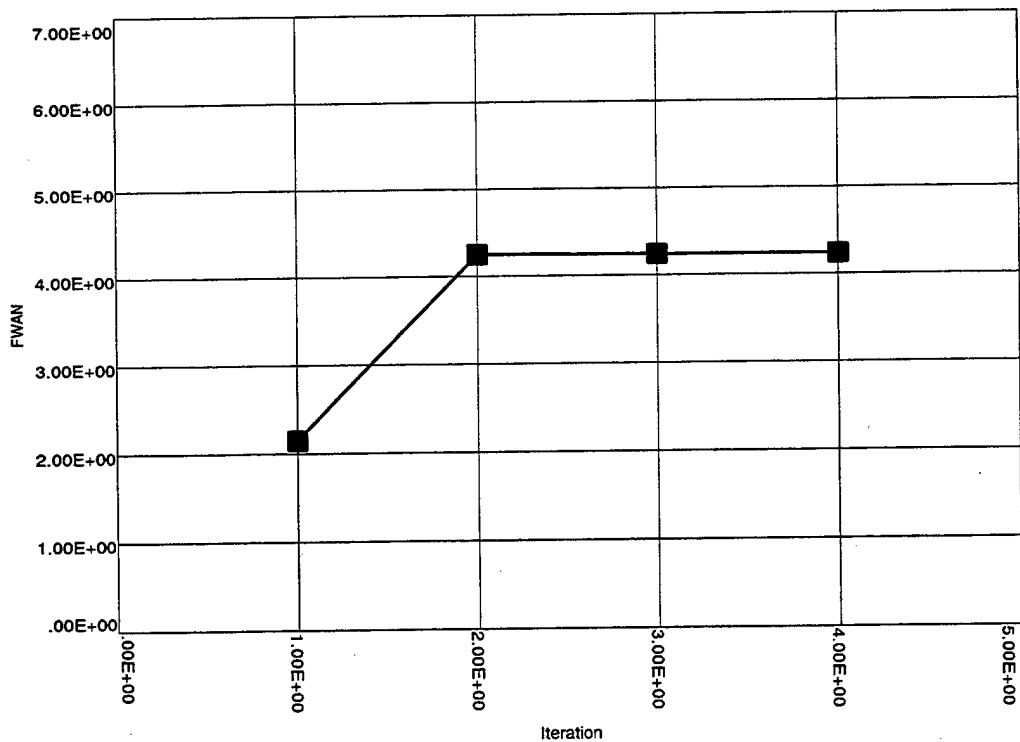


Figure 138. Evolution of Design and Response Parameters.

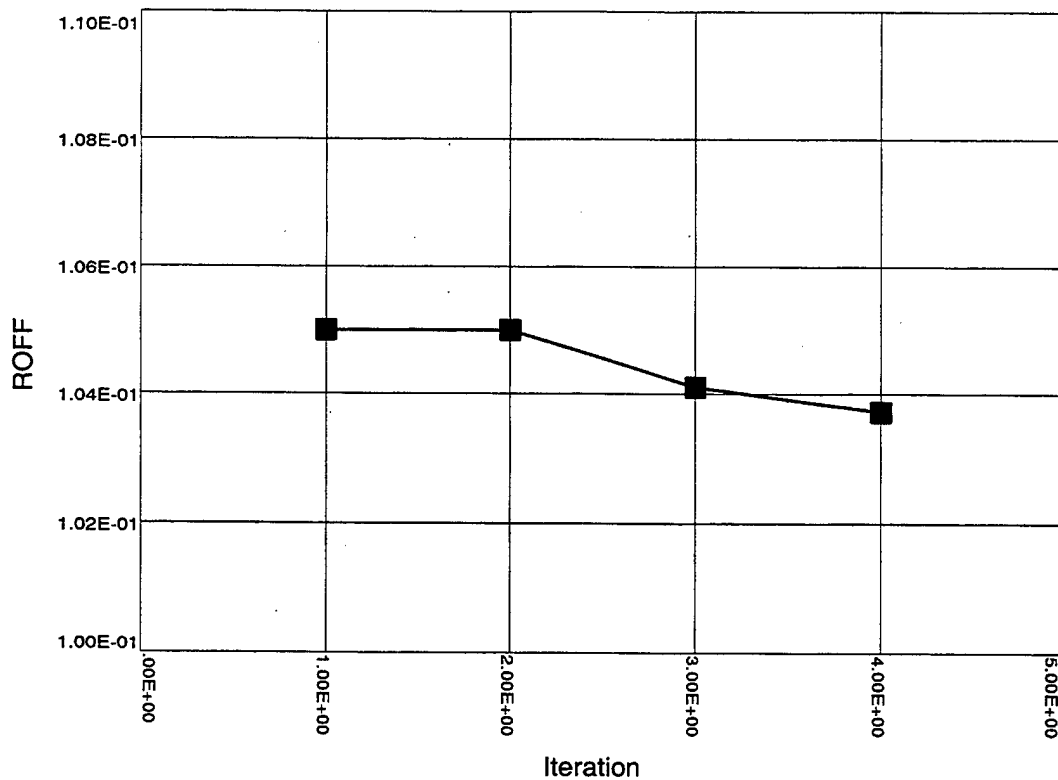


Figure 139. Evolution of Design and Response Parameters.

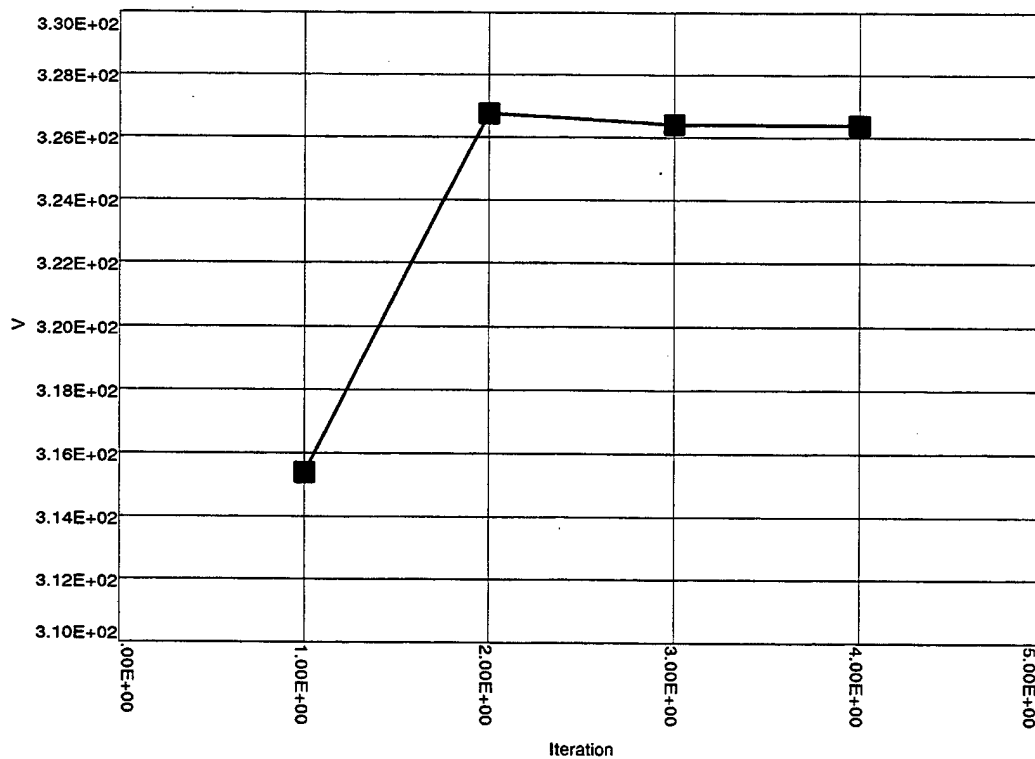


Figure 140. Evolution of Design and Response Parameters.

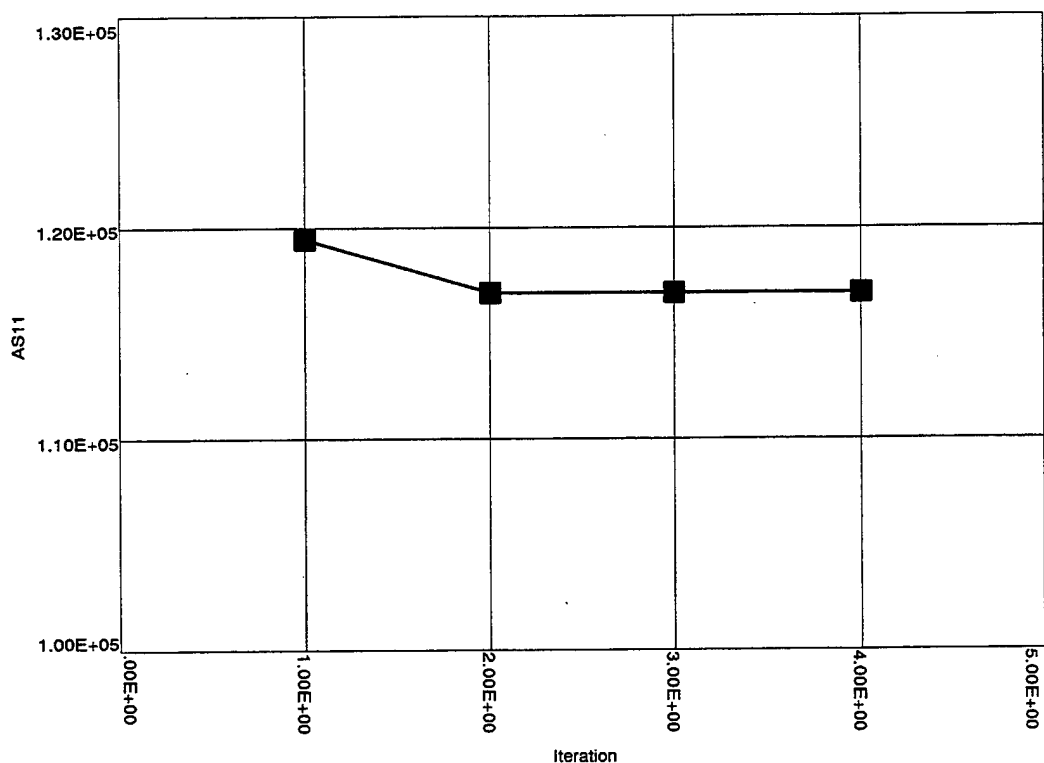


Figure 141. Evolution of Design and Response Parameters.

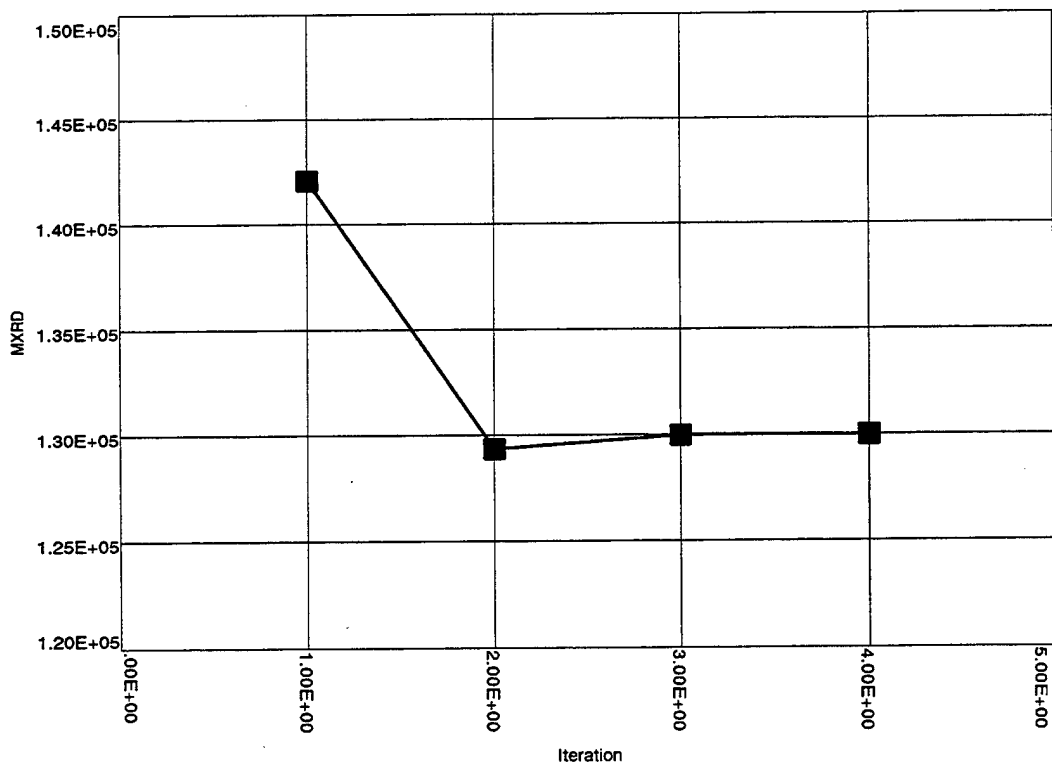


Figure 142. Evolution of Design and Response Parameters.

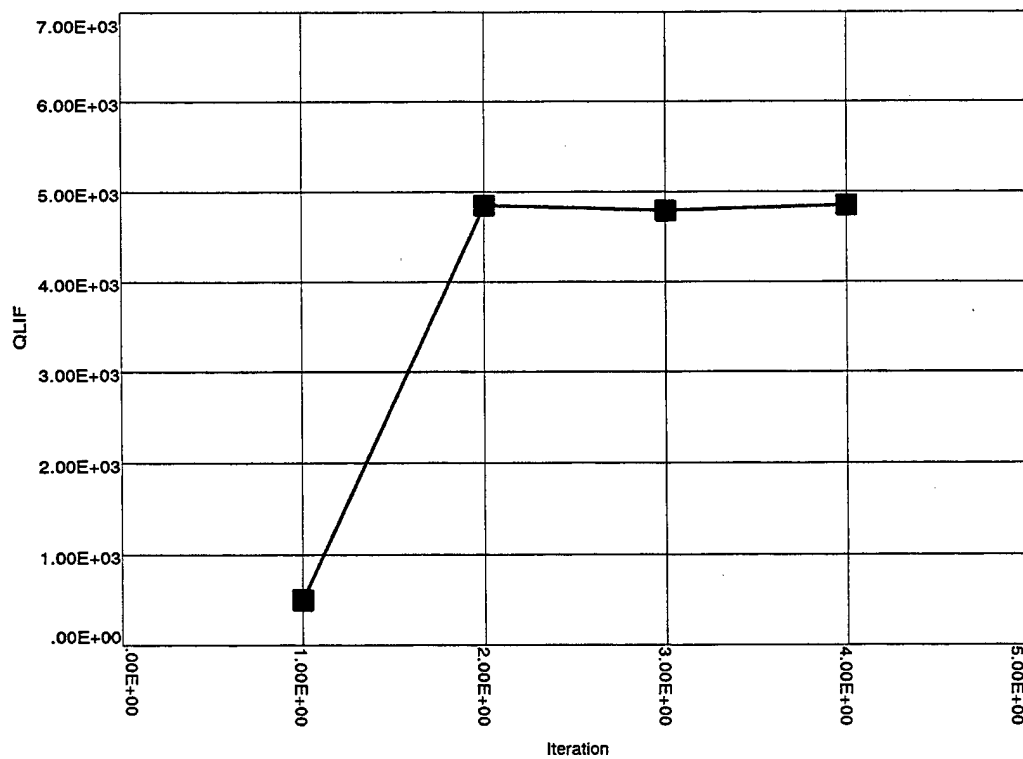


Figure 143. Evolution of Design and Response Parameters.

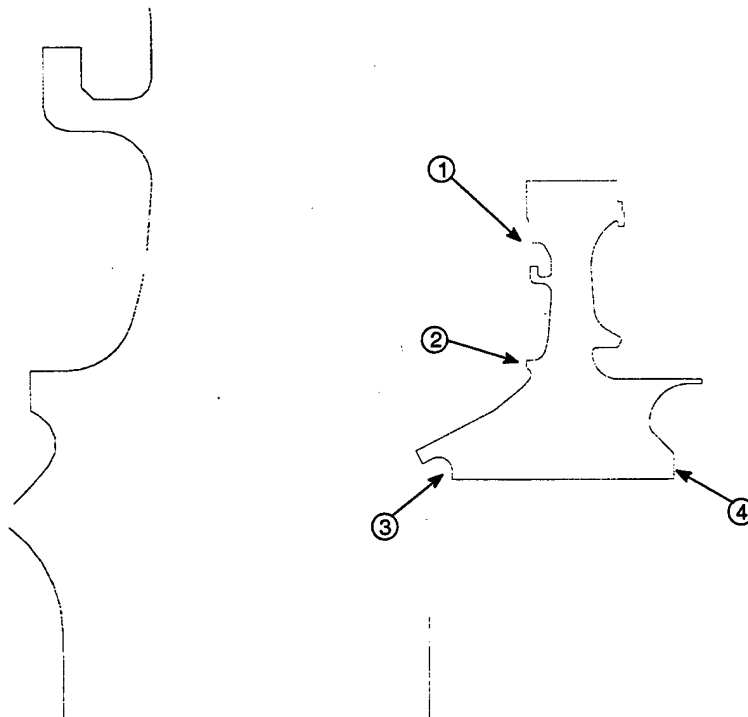


Figure 144. Minor Outline Changes Between Iteration 2 and 4.

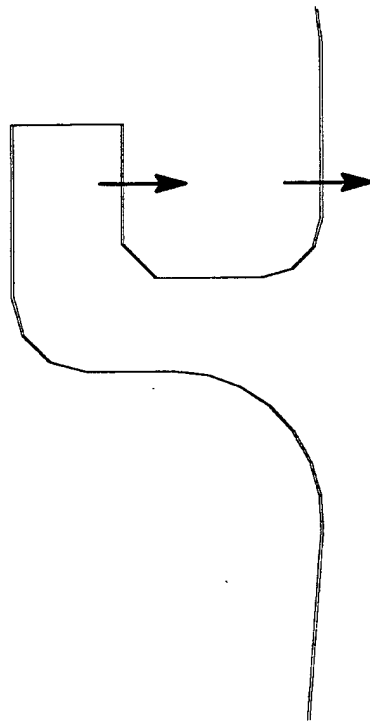


Figure 145. Location 1: Web Narrows Slightly.

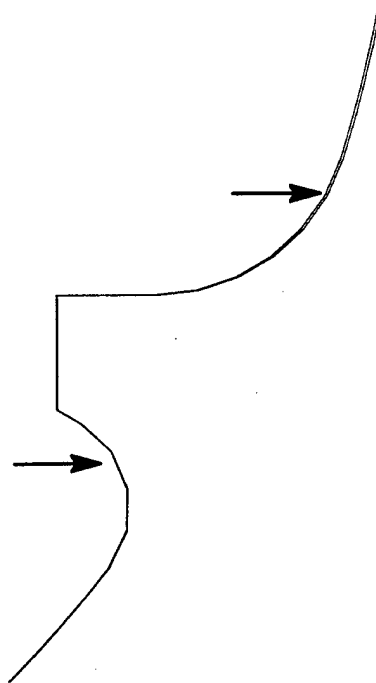


Figure 146. Location 2: Web Narrows Slightly.

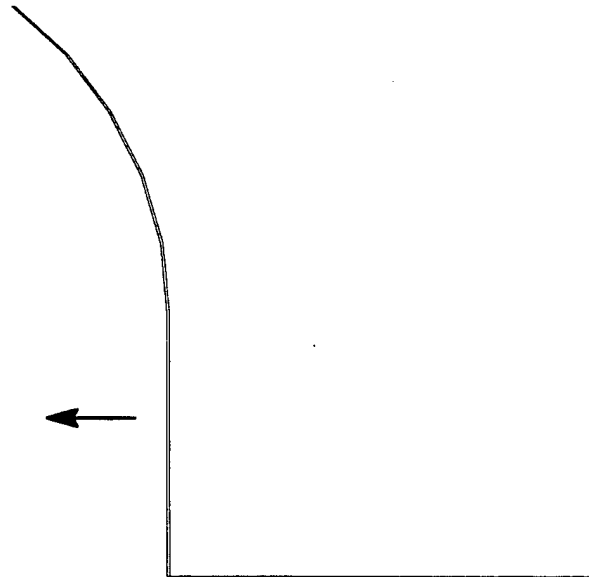


Figure 147. Location 3: Bore Shifts Slightly.

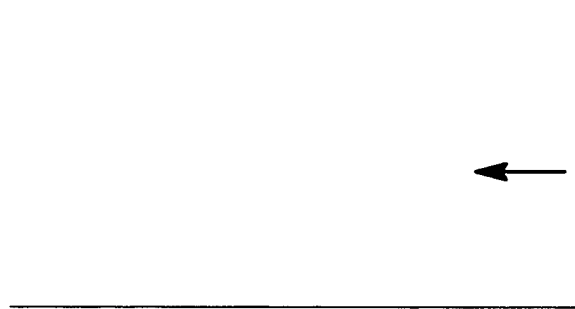


Figure 148. Location 4: Bore Shifts Slightly.

heat transfer were preliminary. The mission requirement was specified as a simple min-max-min cycle.

- The rim was not modeled in detail, and therefore its risk of failure was not incorporated into the analysis. While this is appropriate for an IHPTET demonstration engine, application to a production engine would have to be (and could be) more comprehensive in scope.

The optimization produced a viable design, but only in the context of the assumptions required by the engineer. There is always the risk that one or more assumptions will someday be found to be inappropriate, and the design will have to be modified.

21.0 Closing Thoughts

The prerequisite for this optimization was the construction of a parametric model for the disk geometry having a modest number of meaningful dimensions. One could alternatively define a disk shape by a large number of surface nodes (or drops), and vary these independently for optimization. While this would add flexibility, it would also exponentially increase computational burden. The chosen seven parameter parametric model was adequate to provide tremendous variety in crosssectional shape. We note that parametric modeling is not as cleanly developed in 3-D as in 2-D, and therefore that optimizations of 3-D features (which commonly control life) are not yet as readily undertaken.

Given models to push around, optimization is limited by the quality of the physical theory underlying constraint and objective function calculations and by the ability to carry the computational burden of response surface constructions. Patience seems the best answer to the latter limitation; hardware has been improving faster than basic algorithms over the past decade. Elastic stress analyses having on the order of 100,000 degrees of freedom are executed with ease on today's desktop machines. Introducing plasticity increases cycle time but is feasible. Adding creep effects may now push into unfriendly territory, but wait a few years and new hardware will have redefined the frontier.

Limitations in the underlying theory are harder to overcome.

While fracture mechanics technology is relatively well developed, many aspects still need much work:

- 3-D stress intensity formulations are limited.
- Crack closure remains an unsettled topic.

- It is not clear how to characterize or incorporate variability in crack growth data. (Is it necessary to deal with cycle-to-cycle variations in growth rate? Are cycle-to-cycle variations correlated? Are crack-to-crack variations more significant?)

Burst prediction is currently based on calculations of H_{Av} and R_{Max} . While finite element analysis would seem a better alternative, there are fundamental questions needing answers:

- Are location-to-location variations in yielding behavior important, or does load redistribution average out the differences?
- Does the answer for radial burst differ from that for hoop burst?
- If important, how does one statistically characterize locational variations?

A number of limitations to current PFM technology were discussed in Section 16 following the Phase III validation work:

- One seeded specimen was reported to have failed from a pair of nearby inclusions which apparently interacted. We can not currently model this effect, but can demonstrate that initiation interaction
- Four peened seeded specimens failed from surface intersecting inclusions. These failures demonstrate that peening is not fully effective in suppressing surface initiations. While we can demonstrate that surface intersecting inclusions do not all initiate sharp cracks early under cyclic loading, we can not yet model the incubation phenomenon well enough to incorporate into our design practice, and must submit to the sharp crack assumption.
- Our analyses use average inclusion distributions; lot-to-lot variability is ignored. This was shown in Section 9.2 to be

conservative provided that the populations captured in the averages do not drift.

- Our analyses conservatively assume that the stress field always sees maximum inclusion crosssections.
- Yield strength variability which was discussed above in connection with burst calculations also impacts life calculations. It is not explicitly recognized.
- Variability in inclusion behavior can be incorporated into our analyses, but the relevant distributions have been inferred largely from aggressively seeded pancake forgings; evaluation of production material is limited (though that which is available does seem to fit).

Optimization moves the target - The bull's eye computations move with the design. The middle and outer rings move with the bull's eye. As technologies improve and middle ring sensitivities are integrated into the bull's eye, an optimal design may be found not to be optimal after all. At this point, newly recognized conservatism could be reduced by redesign, or offset by broadening an operational envelope, or part life could be extended.

Summarizing - Probabilistics is a discipline which can improve the aim of engineering analysis. Optimization is a discipline which can improve the location of an engineering target. Both attempt to make the best use of available information, and if the information changes both can be used to quantify the impact of the changes and to identify options for responding.

Phase IV – References

1. G.N. Vanderplaats, Numerical Optimization Techniques for Engineering Design: With Applications, McGraw-Hill, 1984.
2. G.L. Nemhauser, AHG Rinnooy Kan and M.J. Todd, editors, Handbooks in Operations Research and Management Science, Volume 1, Optimization, North-Holland, 1989.
3. R.T. Haftka, Z. Gurdal and M.P. Kamat, Solid Mechanics and Its Applications, Volume 1, Elements of Structural Optimization, 3rd Edition, Dordrecht (Boston): Kluwer Academic Publishers, 1990.
4. ADS (Automated Design Synthesis), Developed by GN Vanderplaats under sponsorship of NASA and supported by Engineering Design Optimization, Inc., Santa Barbara, CA, 1987.
5. GEP Box and NR Draper, Empirical Model Building and Response Surfaces, John Wiley & Sons,
6. A Dey, Orthogonal Fractional Factorial Designs, Halsted Press, John Wiley & Sons, 1985.

Phase VI – Method Extension

22.0 Conservatism

During the course of this contract, a strategy for a phased implementation of probabilistics has taken shape. Throughout, it has been emphasized that the tools are not universally applicable. Ground rules were set down in Phase I, (Section 6.2). It was observed that probabilistics assume predictability even in randomness: Populations may be sampled repeatedly and repeatably. Statistical distributions can be derived from basic principles or inferred by preliminary sampling, and then applied to predict the results of subsequent sampling.

GE Aircraft Engine's first conscious entry into this discipline was with Probabilistic Fracture Mechanics (PFM) as detailed in Phase II, (Section 8). The need for this technology was obvious: Fatigue testing of powder metal alloy specimens showed that life was largely controlled by ceramic inclusions which were intrinsic to the product given the refractory ceramics used in the meltstock production, in the remelt for atomization and in the atomization. Large inclusions yielded lower lives than small inclusions, and surface inclusions were more damaging than buried ones of the same size. Statistical size effects had to be acknowledged: Large volumes were more likely to hold limiting inclusions than small volumes. The probability of surface intersections increased with surface area.

MISSYDD (MISsion SYnthesis given Defect Distribution), GEAE's principal PFM analysis tool, integrates the probability of failure *if* a flaw is present (determined by the spatial stress/temperature distribution of the component) with the probability that the flaw *is* present (the flaw distribution). Logically, given the distribution of flaws, given that flaws fracture and initiate sharp growing cracks, and given that the cycles to failure can be predicted, MISSYDD *should* be able to predict a failure dis-

tribution. This purely conceptual assurance is backed by a growing validation database (much of which was documented in Phase III, Section 12-16) which convincingly demonstrates that PFM does work given the right inputs.

In Phase II, (Section 9) the probabilistics implementation strategy was clarified and the concept of the target was developed (*Figure 149*):

1. *The Bull's Eye* — Apply what is known as well as is known how. E.g. PFM is actively being used to quantify product capability for powder alloy components.
2. *The Middle Ring* — Evaluate sensitivities to potential deviations and bound the results. E.g. Assess dependance of fatigue calculations on part dimensions; fall back to conservative assumptions.
3. *The Outer Ring* — Back off from the calculations until accumulated experience justifies doing otherwise. E.g. Apply safety factors to initial computed life limits. Grow the factors as confidence is improved by analysis, testing and field experience.

The Phase III validation results supported the bull's eye location of PFM: 229 specimen fatigue tests yielded excellent comparisons between predicted and observed failure distributions. However, 7 push-pull tests also pointed to effects which are not adequately addressed by available PFM technology and are handled in practice with middle and outer ring actions:

- One specimen failed from a pair of nearby (and apparently interacting) inclusions.
 - Standard practice ignores interactions based on statistical arguments showing that they should be extremely rare in unseeded production material. (*Middle Ring*)

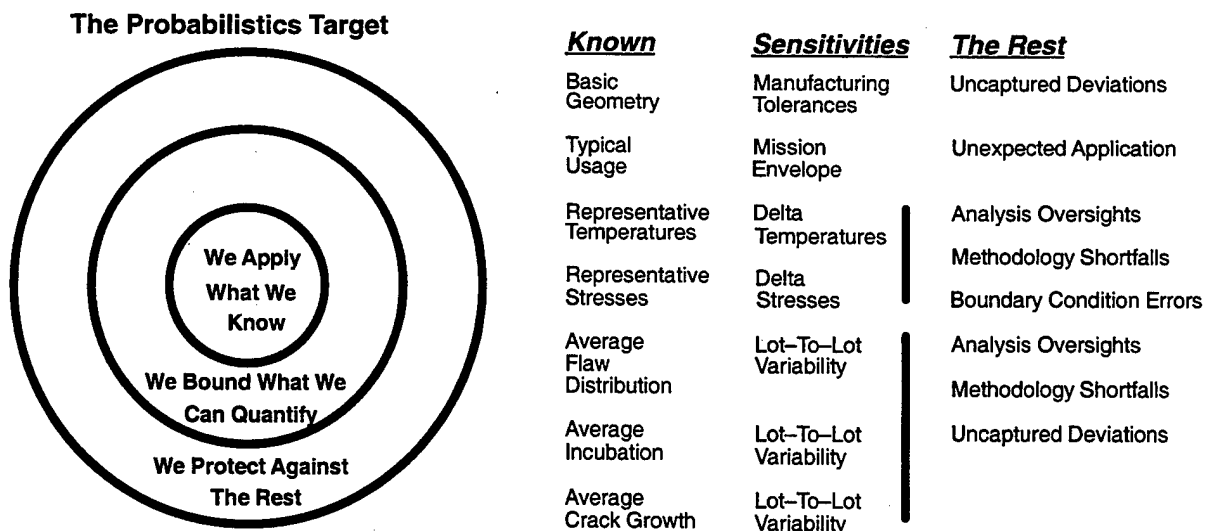


Figure 149. Strategy for Implementation of Probabilistics.

- One specimen failed from a large badly oriented seeded inclusion lying very near the surface.
 - Standard practice assumes that the stress field always sees maximum inclusion crosssections. (*Middle Ring*)
 - The validation PFM predictions assumed that all inclusions in the pancake forgings were oriented tangentially. Data shows this to be a good assumption, but not perfect.
 - Four peened specimens failed from surface intersecting inclusions.
 - The suppression by peening of thousands of other surface inclusions is currently ignored... Standard practice assumes that surface intersecting inclusions initiate sharp cracks upon first loading. (*Middle Ring*)
 - The validation PFM predictions assumed peening effectively seals surfaces from initiation. While four tests conflict with this assumption, the majority of experience supports it.
- Work is underway to better quantify surface inclusion behavior (see the next section).
- One specimen failed from a very large buried inclusion at a lower than expected life. It and the specimen failing from the badly oriented, near surface inclusion are tied to a common forging; all specimens from this forging were underachievers. Forging variability is suggested.
 - Standard practice applies safety factors until such issues can be dealt with. (*Outer Ring*)
 - The validation PFM predictions did incorporate the variability inferred from a fair number of pancake forgings, but the smoothed distribution which was fit to the data did not capture the apparent outlier. Standard practice could eventually incorporate a somewhat broader distribution that more conservatively encompassed production experience (*Another Middle Ring Solution*).

Two other effects were accounted for in the validation PFM predictions:

- Yield stress variability was recognized and incorporated.
 - Pushing this into standard practice is some way off. (*See the comments on burst calculations in Section 21 of Phase IV.*)
- Precise inclusion distributions were ascertained prior to manufacture of all seeded material.
 - It is recognized that inclusion distributions differ between lots of production materials. It is not currently practical, however, to quantify these differences and integrate them into the PFM process, but it was shown in Section 9.2 of Phase II that using an average distribution is actually

conservative provided that the population captured in the average does not drift (*Another Middle Ring Solution*).

- While mathematically demonstrable, this conservatism is counterintuitive. It helps to understand that use of an average distribution assumes that every part contains some fraction of dirtier material. (*This point will be important in subsequent discussions on manufacturing damage.*)

Summarizing to this point, the validation program substantiated elements of PFM technology which *could* be accounted for, supported assumptions and conservatisms made in production applications, and indicated directions for future developments.

23.0 Damage Tolerance

The damage tolerance requirements in the ENSIP MIL SPEC 1783 (*Reference 1*) direct that all fracture critical components be able to survive for a prescribed interval a sharp crack of a size which could be missed by inspection placed at any part location.

Sharp cracks result from tensile overloads or fatigue, and it is seldom possible to generate such cracks in manufacture. The few exceptions known to the author include quench cracks arising from overly aggressive heat treatment, and high cycle fatigue cracking resulting from improper inertia welding. To deliberately create cracks for NDE methods calibration and crack growth rate testing, notches are EDMed into fatigue specimens; the specimens are cycled to start cracks growing, and then the notches are machined off.

It seems clear, therefore, that ENSIP manufacturing inspections are not in place to catch cracks but other kinds of damage: Nicks or gouges resulting from tool breaks and the like. Field inspections may catch new damage introduced during repair and rework, or cracking from manufacturing flaws which were missed by the initial inspection.

If field inspections find fatigue cracks in undamaged material, they are likely traceable to a shortfall in the design analysis (possibly a missed or underestimated stress concentration). If so, the fracture mechanics calculations used to base the inspection intervals are also affected.

If ENSIP were to explicitly focus on protecting against randomly inflicted manufacturing damage, probabilistics would offer more realistic modeling by recognizing the following:

1. *Flaws are rare* – Assuming that all parts are damaged is not supportable by experience.
2. *Flaws are not attracted to stress concentrations* – Cracks may develop at stress

concentrations, but randomly inflicted damage rarely will fall at limiting locations.

3. *Flaws are not sharp cracks* – There is considerable evidence that small surface flaws often are slow to initiate macroscopic cracks. Also, nicks and scratches may be more inspectable than like-sized cracks. (By contrast it is noted that large hard alpha inclusions in titanium alloys *do* appear to initiate cracks upon initial loading and can be difficult to find despite their size.) We expand on each point.

23.1 Flaws are Rare

Clearly not every bolthole has a 15x30 flaw or parts would never make it out of manufacturing. Parts may be rejected by an initial inspection pass, but almost always make it through a repeat inspection after minor rework (often requiring no more than the removal of a fraction of a mil of material). Refer to the POD (Probability of Detection) curve shown in *Figure 150*. A 15x30 (353 mil²) crack is inspectable with 90% POD. The POD of a crack half this size (7.5x15 or 88 mil²) is nearly 0. Despite the assumed nondetectability of 7.5x15 flaws, they are not likely to occur with any significant frequency if detectable flaws 15x30 and larger are found to be rare: Given the assumed randomness of shop damage, it stretches credulity to postulate the existence of a narrow size distribution of nicks and gouges lurking below the NDE threshold, large enough to be threatening but small enough to elude detection.

None-the-less, assume a Weibull flaw distribution which is much narrower than the narrowest seeding distribution used in the Phase III validation testing (-270/+325 mesh Norton ANSI 240 alumina, see *Figure 151*). Locate the median of the distribution, a_{med} , beneath but close to the 15x30 inspection limit as follows:

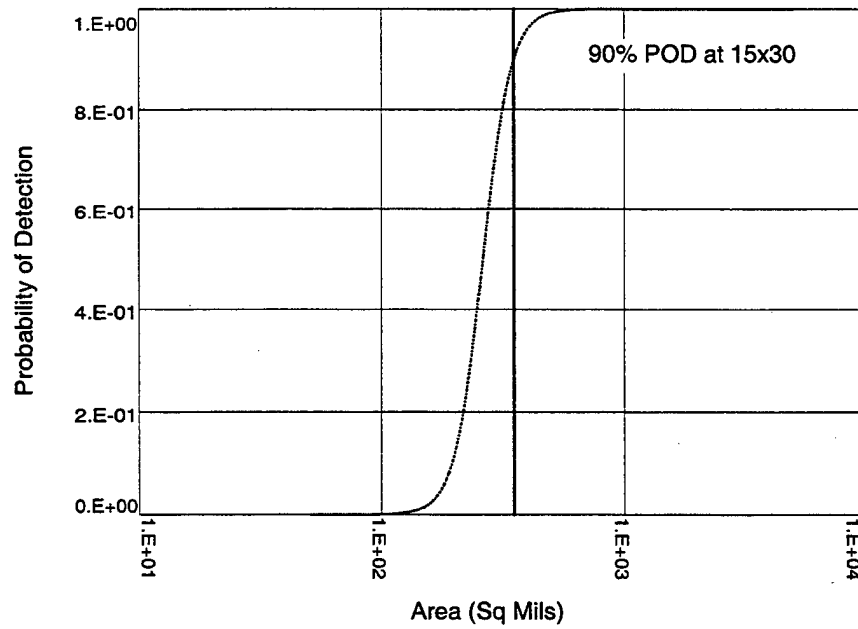


Figure 150. POD Function.

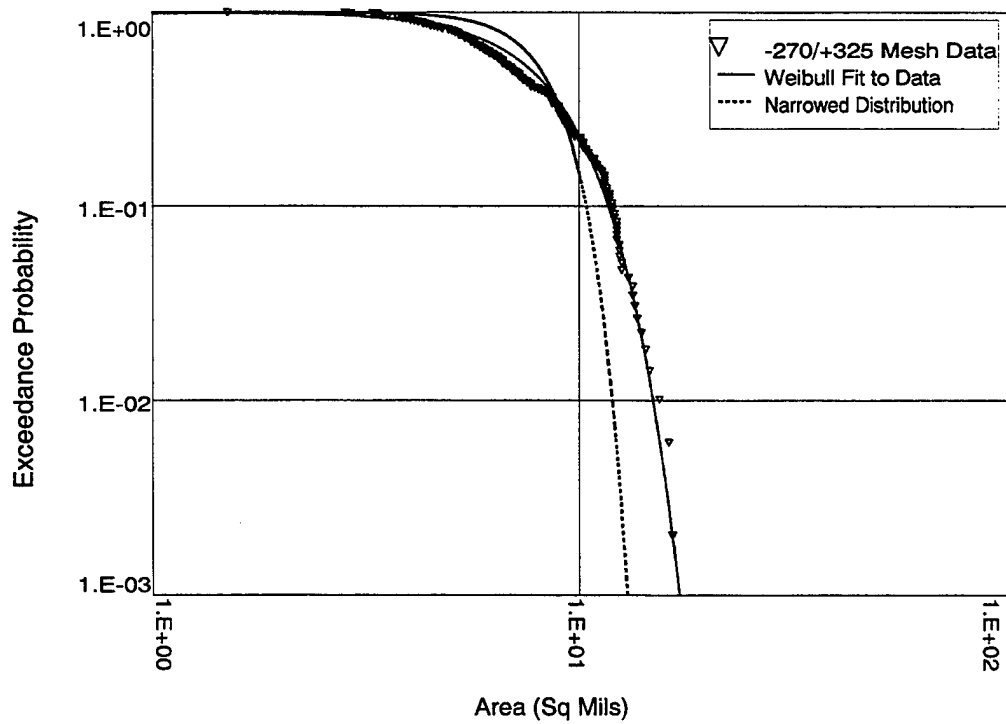


Figure 151. Size Distributions.

Call the distribution $S_\alpha(a)$. It has the form:

$$S_\alpha(a) = \exp[-(a/\alpha)^5]$$

$$\text{where } \alpha = a_{\text{med}}/[-\ln(0.5)]^{1/5} \Leftrightarrow$$

$$\alpha_{\text{med}} = \alpha \cdot [-\ln(0.5)]^{1/5}$$

The probability that a single flaw from this distribution will be detected is the integral:

$$\int_0^\infty \text{POD}(a) s_\alpha(a) da$$

where $\text{POD}(a)$ is the function shown in **Figure 152** and $s_\alpha(a)$ is the probability density function corresponding to $S_\alpha(a)$.

This integrated probability of detection is shown as a function of median flaw size in **Figure 152**. Given that flaws have been found only rarely in the tens of thousands of parts manufactured during the production history of GEAE's

F110 engine, we argue that the integrated probability of detection should not exceed the modestly remote value of 0.01.

Solving:

$$\int_0^\infty \text{POD}(a) s_\alpha(a) da = 0.01$$

for α leads to a median flaw size of about 130 mil²

Given a 130 mil² median, the Weibull probability of a 15x30 flaw is about 10⁻⁴⁵. Designing to a 15x30 seems very conservative given this scenario.

23.2 Flaws Are Not Attracted to Stress Concentrations

The following discussion will move around an example constructed using the F110 HPT bolt-hole geometry shown in **Figure 153**. So that this work could be published, the finite element

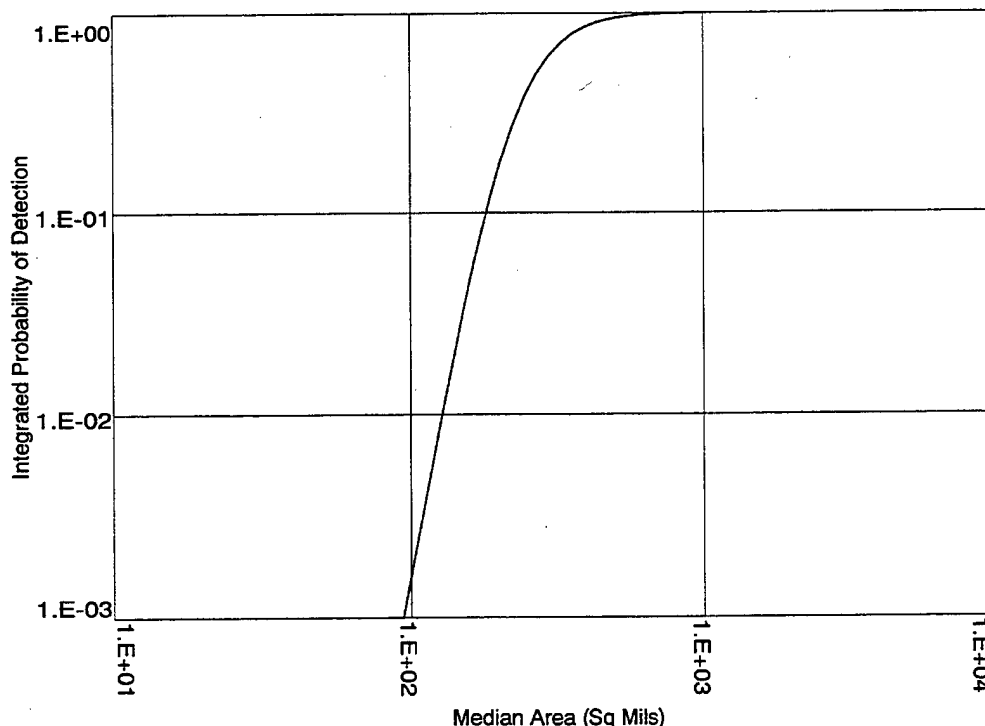


Figure 152. Integrated POD.

Limiting Location

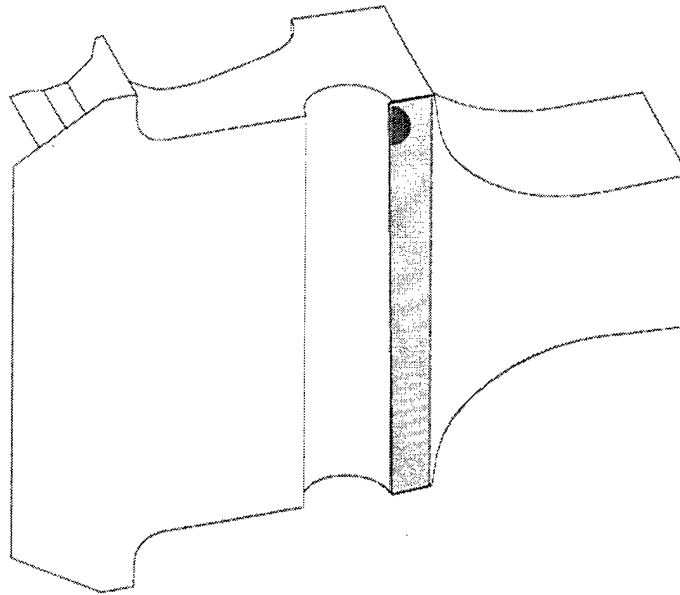


Figure 153. F110 Bolthole Model.

stress analysis was scaled to yield 2900 cycles from a 15x30 crack at the critical location shown. The scaling preserved the stress distribution which is such that fracture mechanics life increases quickly as the crack is positioned away from the concentration.

It will be shown that the probability of failure from a 15x30 crack is low if it is assumed that the crack is randomly placed rather than set squarely on the concentration. It will then be shown that the risk is even lower if the crack is randomly selected from the damage distribution constructed in the last section.

The PFM theory underpinning MISSYDD may be extended to encompass random surface damage. In particular, assuming a Poisson distribution of surface damage modeled as flaws characterized by a size parameter a , the following expression can be used to compute part or feature failure probability:

where ρ is the average number of flaws per square inch, A is the relevant part or feature surface area, $G_{sur}(N, a)$ is the surface geometric failure distribution at life N for flaw size a ,

$$F_{sur}(N) =$$

$$1 - \exp \left[-\rho A \cdot \int_0^{\infty} G_{sur}(N, a) s_{sur}(a) da \right]$$

and s_{sur} is the probability density function of the flaw distribution.

A PDAS template program was written to estimate G_{sur} by Monte Carlo simulation; **Figure 154** shows the random surface placements; **Figure 155** compares G_{sur} at 5,000 cycles with the POD as functions of flaw size. The geometric probability of failure given a single randomly placed flaw is found to be 0.0012 for a 15x30 (353 mil²) flaw. Detection probability decreases rapidly with flaw size, but then so does geometric failure probability. Between 15x30 and 7.5x15 we are much more likely to find the flaw than to fail from it, and if (as was argued above) flaws are present with any frequency, then there should be a range of sizes, some of which should be readily found.

The probability of failure given a single randomly selected flaw from the distribution S_{α} (assumed to be one of the Weibull family con-

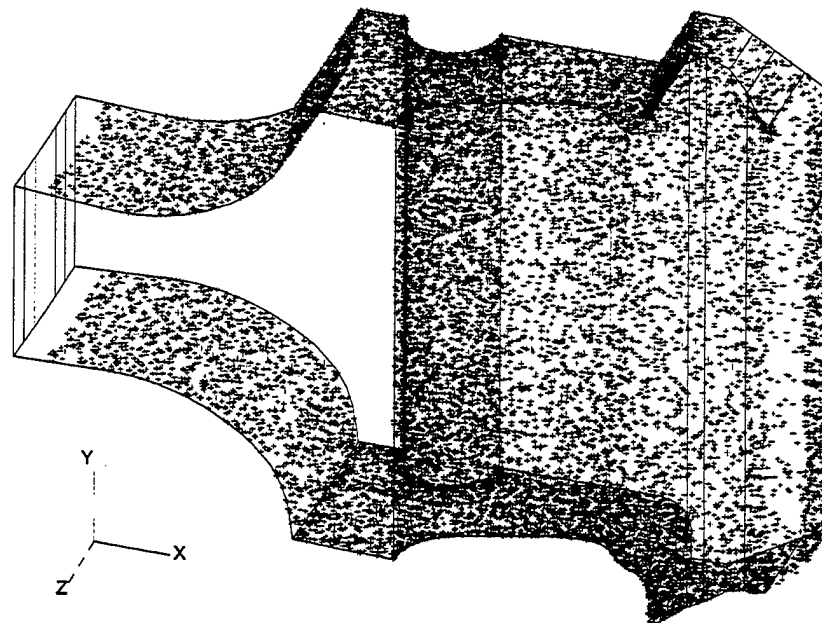


Figure 154. Monte Carlo Simulation.

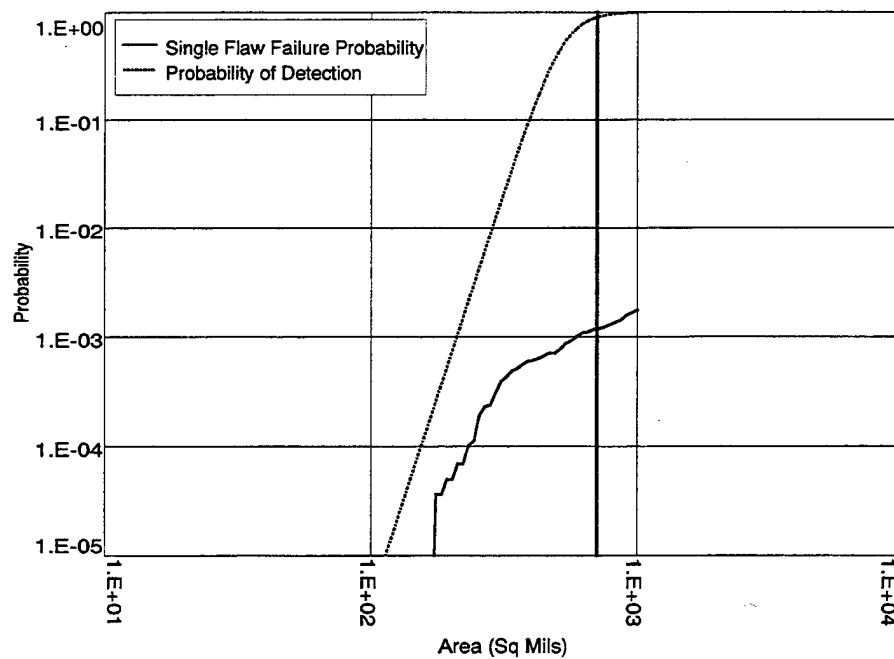


Figure 155. Geometric Failure Probability at 5,000 Cycles Compared to POD Function.

sidered in the last section) is given by the integral:

$$\int_0^{\infty} G_{\text{sur}}(N, a) s_a(a) da$$

Figure 156 shows this integral at 5,000 cycles as a function of the median flaw size. Accepting that the median is less than or equal to 130 mil² based on the rarity of detected flaws, the probability of failure for the feature is no greater than about 2.3×10^{-6} . This risk is acceptably remote by most people's standards, justifying a proposed life of 5,000 cycles (compared to the 2,900 cycles obtained deterministically).

23.3 Flaws Are Not Sharp Cracks

As was discussed briefly in Section 15.1 of Phase III and at greater length in *Reference 2*, small buried inclusions typical of powder al-

loys enjoy an incubation period prior to initiation of classical growing cracks. There is reason to believe that this may also be true of many surface intersecting inclusions and other surface flaws. (Again, the behavior of large hard alpha inclusions in titanium alloys argues for careful quantification of this phenomenon. Different material classes and different flaw types must be evaluated individually.)

Current ENSIP guidelines do not recognize the incubation phenomenon. Repeating the model disk calculations of Section 15.3.3 without benefit of the subsurface incubation model yields new failure distributions shown in **Figures 157 and 158**. Surface and subsurface inclusions now compete fairly evenly for both the MD9 and MD10 geometries entries. Some subsurface initiated failures would have been expected in both series of tests. None were observed in the MD9 tests; two in the MD10 tests.

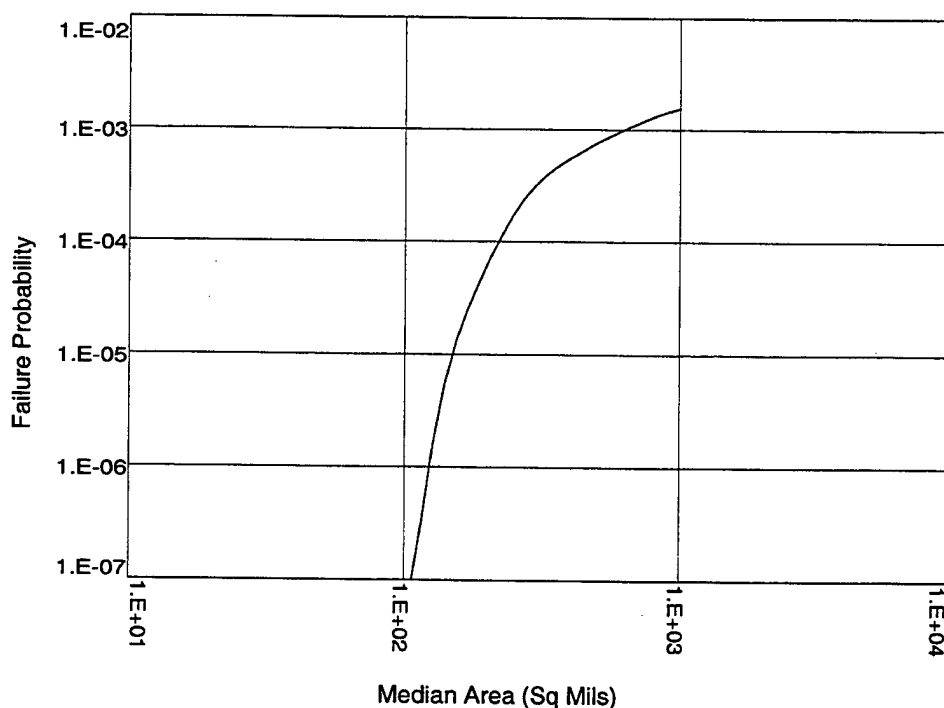


Figure 156. Integrated Failure Probability at 5,000 Cycles.

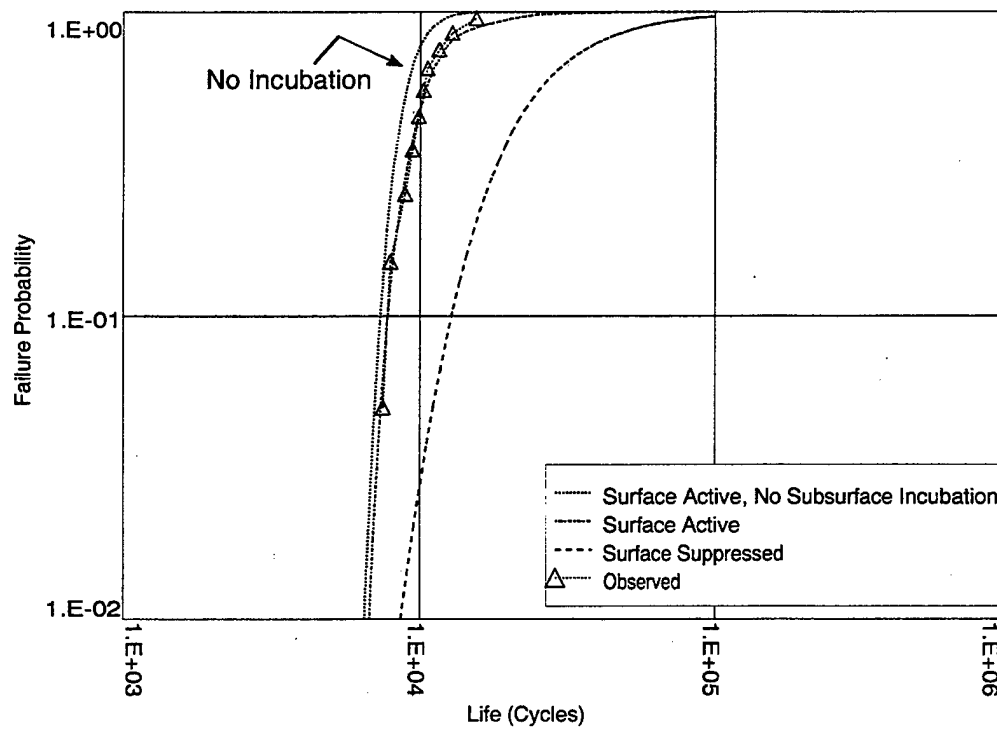


Figure 157. Revised MD9 Predictions.

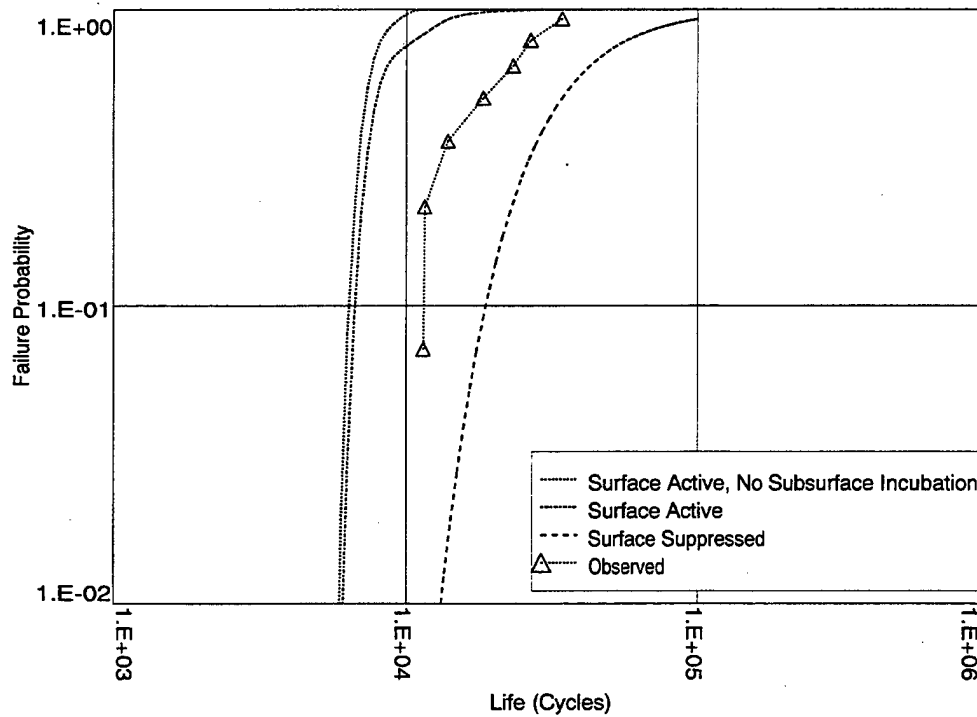


Figure 158. Revised MD10 Predictions.

The observed distribution in the MD10 tests is well above the prediction assuming the surface is fully active (that shotpeening has no impact). Were it assumed that shotpeening did enhance surface life, the subsurface would control. **Figure 159** shows the two subsurface failures

treated as a separate population. While doing so may not properly recognize the effect of surface competition, the points clearly are better described by the surface suppressed distribution with subsurface incubation recognized.

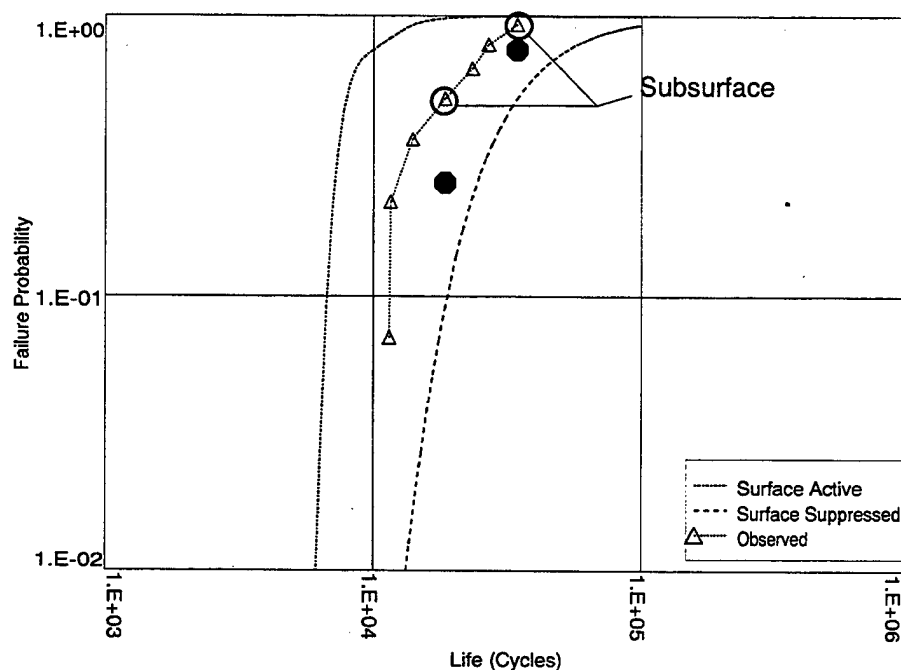


Figure 159. MD10 Internal Initiations.

We make four points supporting an incubation phenomenon:

- While fracture mechanics accurately predicts crack growth life for many inclusions and provides lower bound predictions for most, it is in many cases very conservative (**Figures 160–167**). This is most evidently true for buried inclusions, but it is also true for surface inclusions as is most clearly apparent in the large As-HIP –150 mesh database at 1000°F (**Figures 166 and 167**).
- Given that incubation is observed for inclusions of all sizes, the phenomenon probably cannot be attributed to crack growth threshold. It is also observed that incubation life is stress range dependent for the strain controlled tests (**Figures 161, 163, 165 and 167**). This is not the case for the fracture mechanics predictions which are approximately max-stress controlled for negative stress R-ratios.
- Referring to the As-HIP database: At 0.78% strain range, 71.8% of the characterized failures are surface initiated. At 0.66% strain range, this fraction falls to 30.8%. The inclusion content (in particular, the distribution of surface intersecting inclusions) is not expected to depend on testing conditions. It can be concluded, therefore, that surface inclusions are suppressed at lower stresses. PFM analyses indicate that the suppression is not due to crack growth threshold.

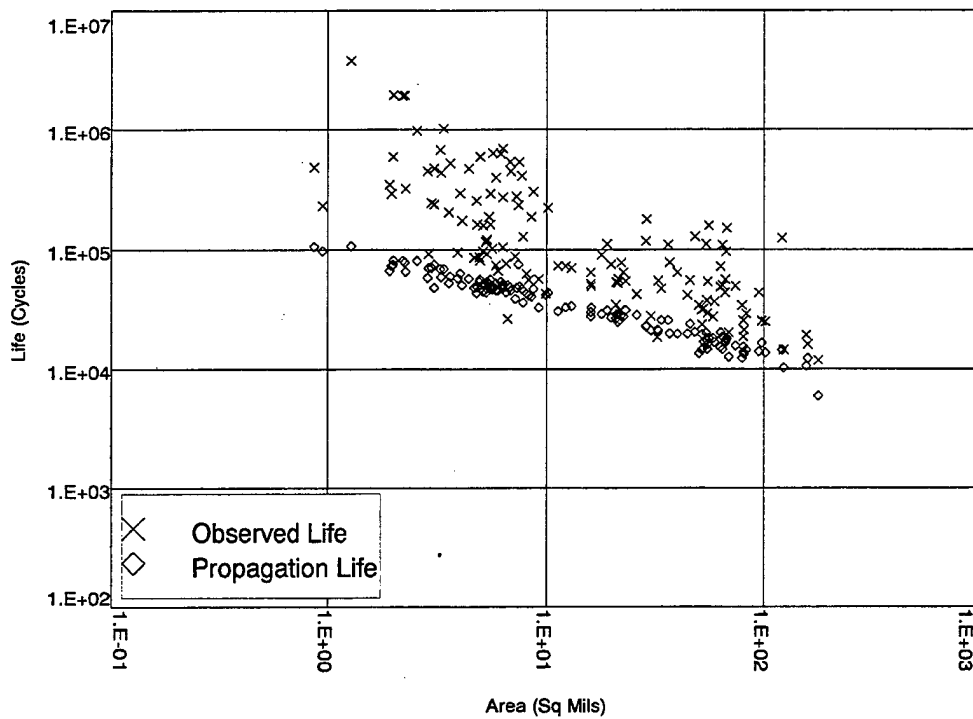


Figure 160. René 88 DT, Subsurface.

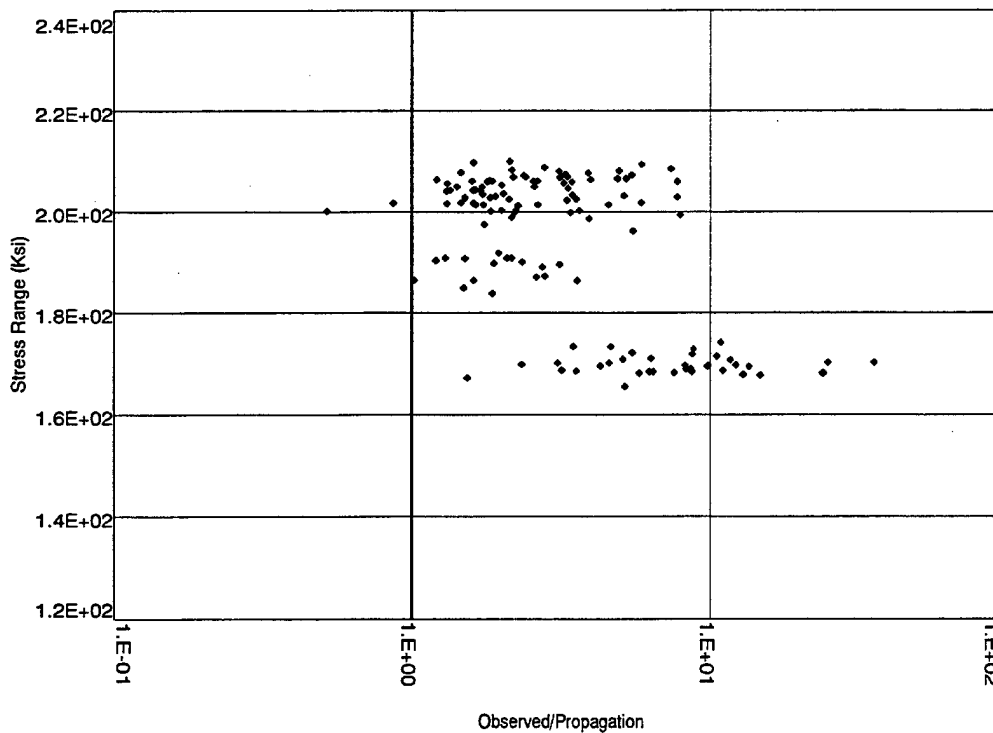


Figure 161. René 88 DT, Subsurface.

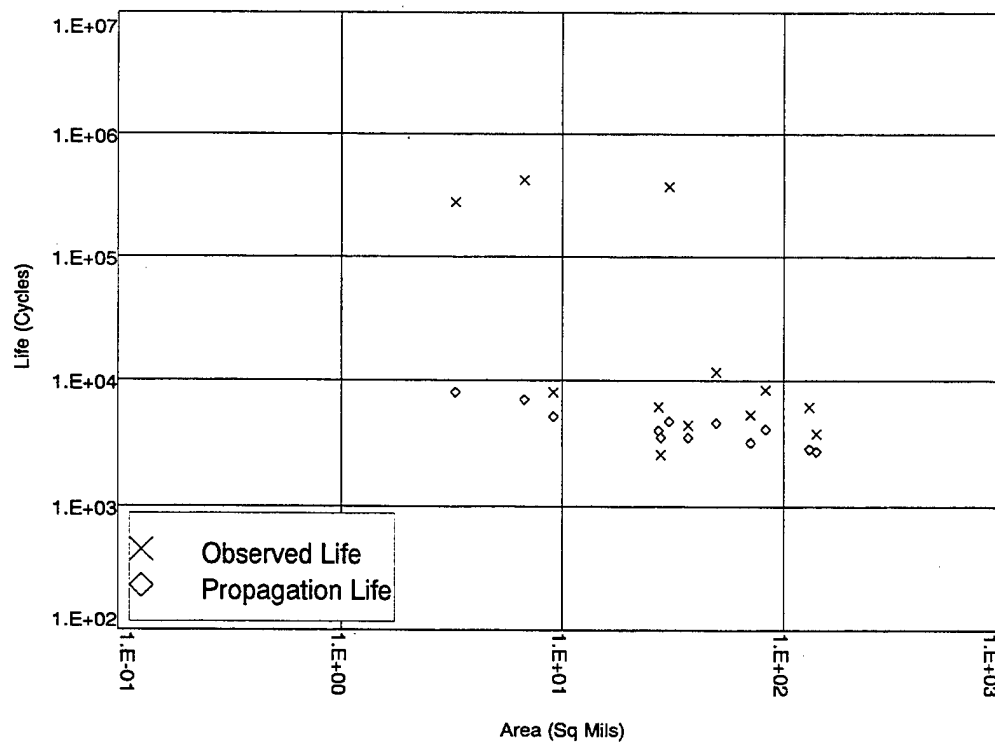


Figure 162. René 88 DT, Surface.

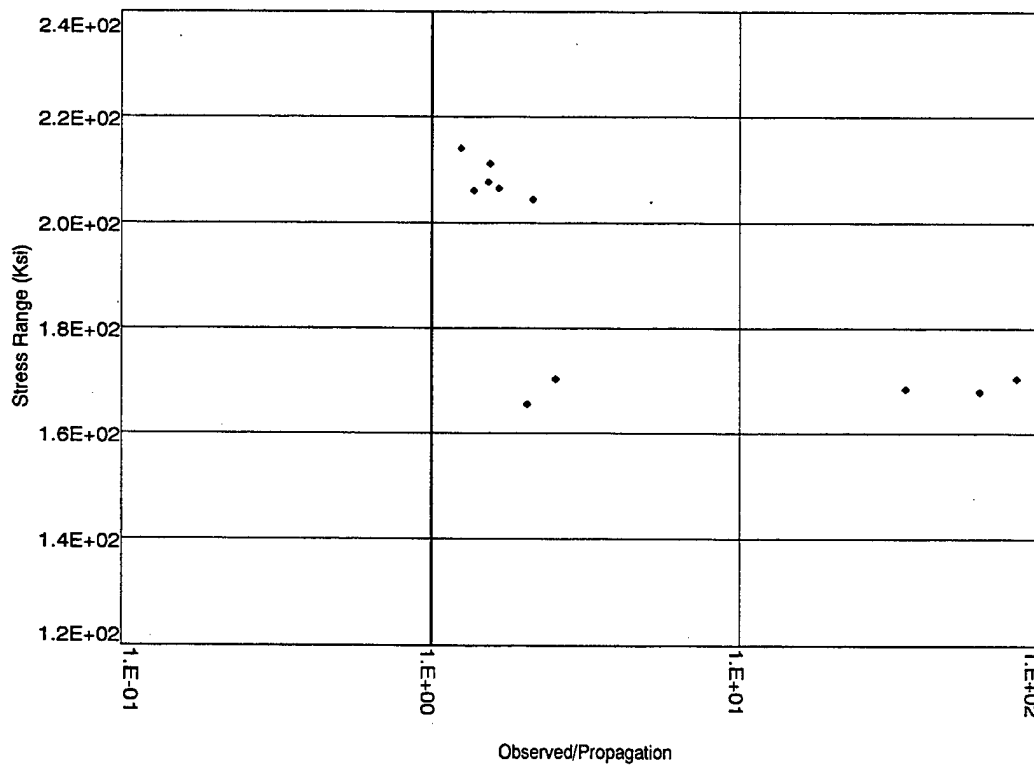


Figure 163. René 88 DT, Surface

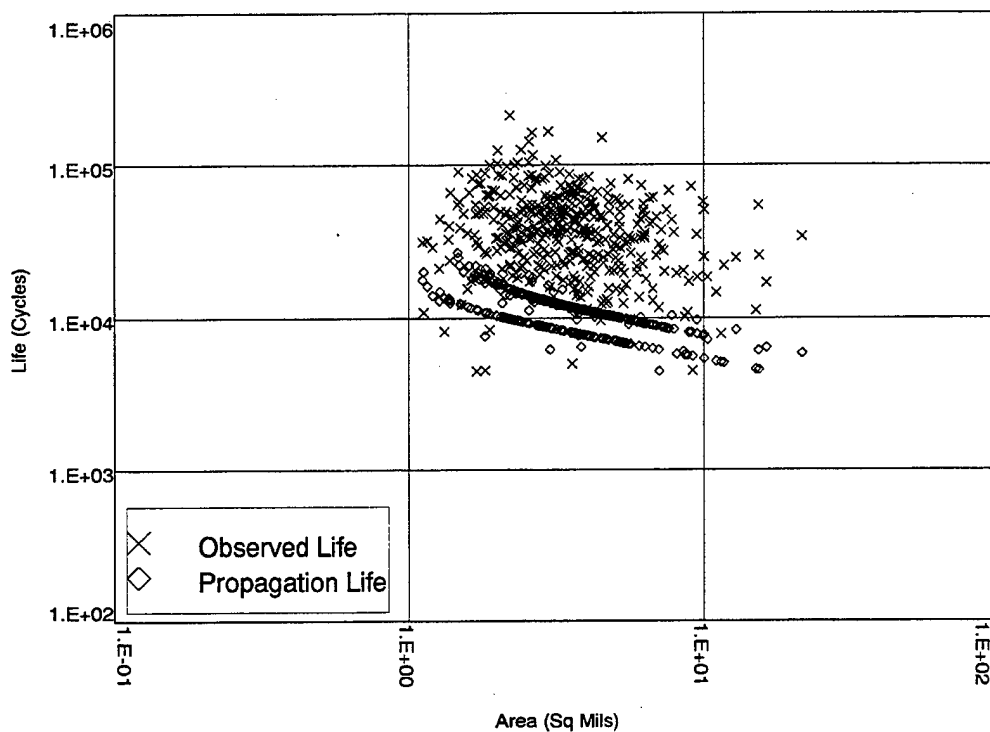


Figure 164. As-HIP René 95, Subsurface.

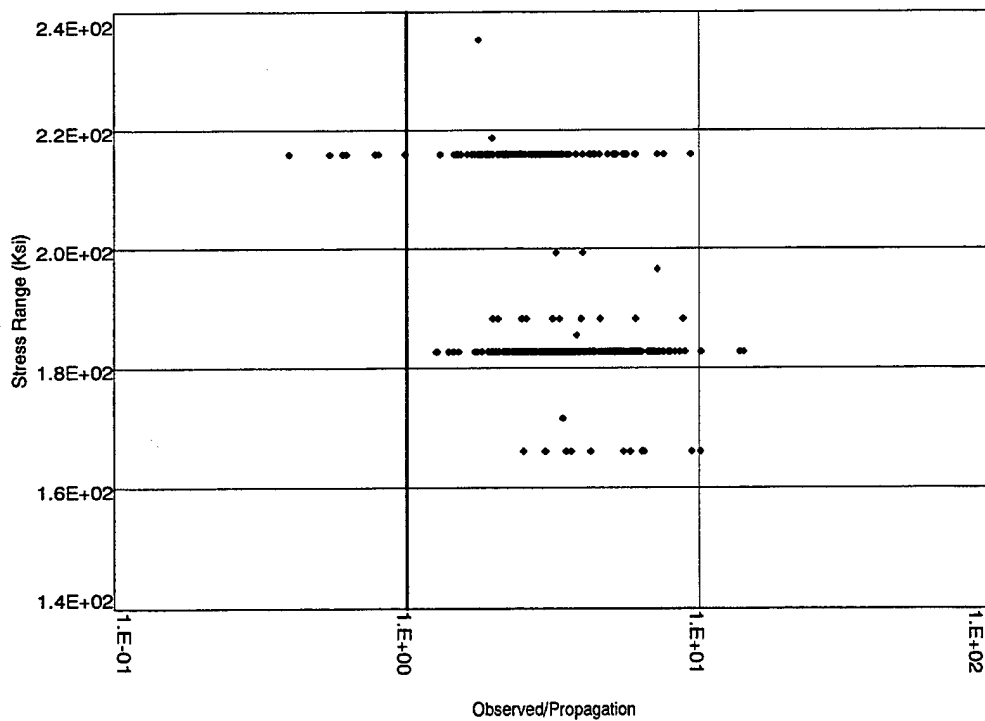


Figure 165. As-HIP René 95, Subsurface.

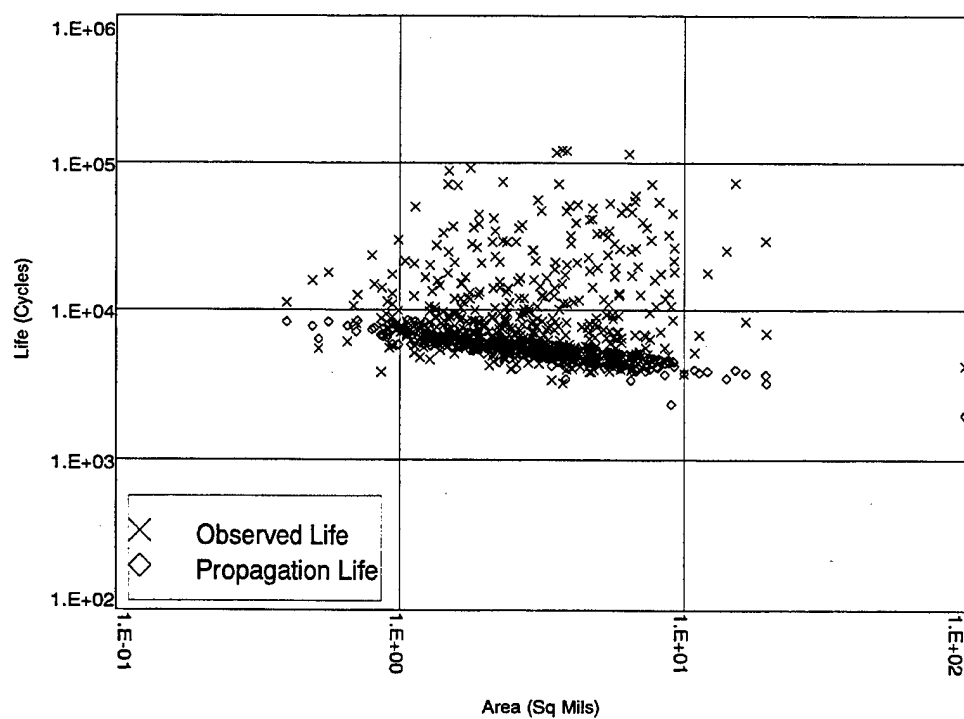


Figure 166. As-HIP René 95, Surface.

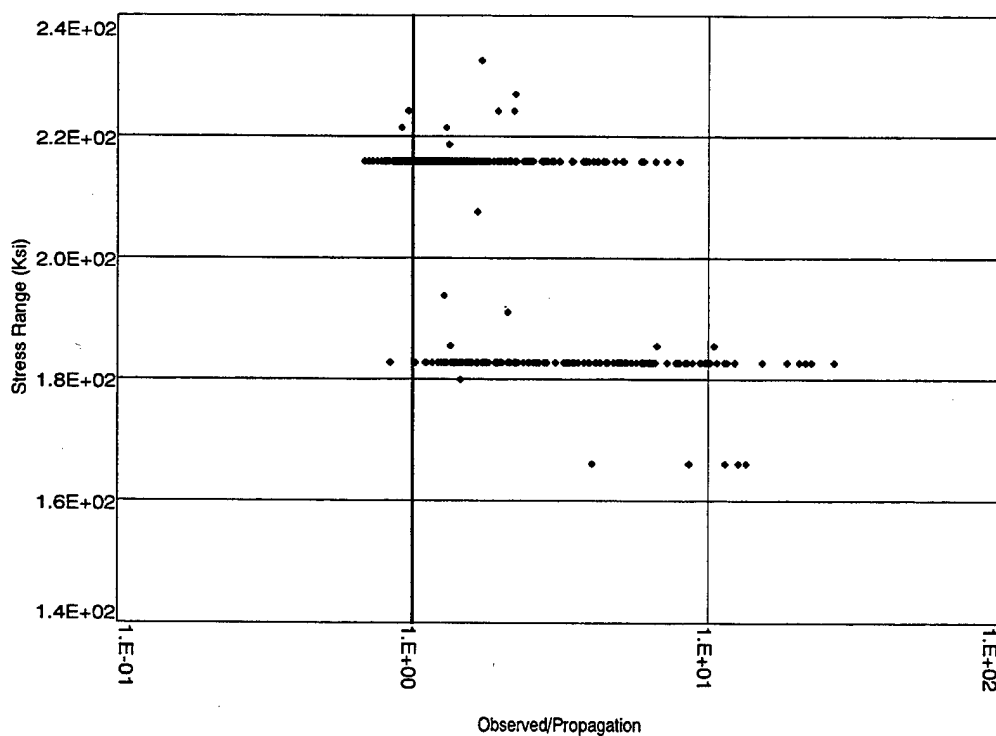


Figure 167. As-HIP René, Surface.

- There is direct evidence that incubation is a real phenomenon in that most inclusions in a failed fatigue specimen have no discernable cracks emanating from them. This is so for both buried and surface intersecting inclusions.

In closing this section we also note that data was presented in Section 3.8.3 suggesting that eddy current inspections may find nicks and scratches more readily than comparably sized sharp cracks.

24.0 Recommendations

The conservatism of the ENSIP MIL SPEC 1783 was appropriate at the time it was developed back in the early 1980's. Hardware was failing – From Section 4.6 of the specification:

There have been numerous Class A incidents on Air Force aircraft and engines due to structural failures caused by material defects, manufacturing defects or fatigue induced cracks. Causes have been: (1) use of high strength, low fracture toughness materials, (2) improper detail designs resulting in high stress levels and structural discontinuities, and (3) lack of adequate quality control requirements (both in production and depot maintenance). Many of the incidents could have been avoided by proper material selection, control of stress levels, use of fracture resistant design concepts, manufacturing and process controls and by use of reliable inspection methods during production and in-service maintenance.

Referring to the target analogy, 1970's technology was not able to hit the bull's eye: Finite element methods were limited, compromising understanding of complex part features. Manufacturing and maintenance processes introduced nicks and scratches; process controls did not always weed them out.

By tying designs to inspection capabilities, ENSIP encouraged both tighter process controls and better analysis. Requiring tolerance to cracks from 10 to 30 mils in length at all fracture critical locations aimed at the middle ring of the target. Risk was reduced, but by how much was not known.

Advances in probabilistic fracture mechanics technology now allow us to aim closer to the target center. The Phase III validation testing documented in Sections 12–16 demonstrates that risk can be accurately assessed under controlled conditions. While manufacturing flaws

are not likely to be statistically distributed in the same rigorous sense as are the ceramic inclusions addressed in the validation, their occurrence can be reasonably bounded, and their placement is likely to be random.

Rather than assuming that a 15x30 flaw is present at the limiting location, the analysis in the preceding section would:

1. Protect against a narrow distribution of flaws. (The distribution nudges against the POD curve (*Figure 168*), but lies well to the left of the 15x30 requirement.)
2. Recognize that flaws are not likely to hit a limiting location exactly. (Given random placement and accurate life predictions at all locations, geometric failure distributions can be estimated with great precision.)

The geometric failure probability was integrated against the flaw distribution yielding a failure probability of 2.3×10^{-6} at 5,000 cycles compared to the deterministic limit of 2,900 cycles.

Details of this approach can certainly be questioned, but we feel that any concerns can be addressed. The following critique is likely not comprehensive, but a conscientious effort has been made to dispassionately review our principal assumptions:

Concern – The narrowness of the flaw distribution ($\beta = 5$) may not truly reflect the randomness likely to be inherent in a production process gone awry.

Response – The analysis was repeated with $\beta = 1$ (a very broad distribution). The failure probability increased slightly from 2.3×10^{-6} to 4.9×10^{-6} .

Concern – Manufacturing damage does not seem to meet the criteria in Section 22 for application of probabilistics. The location and orientation of a nick can likely be treated

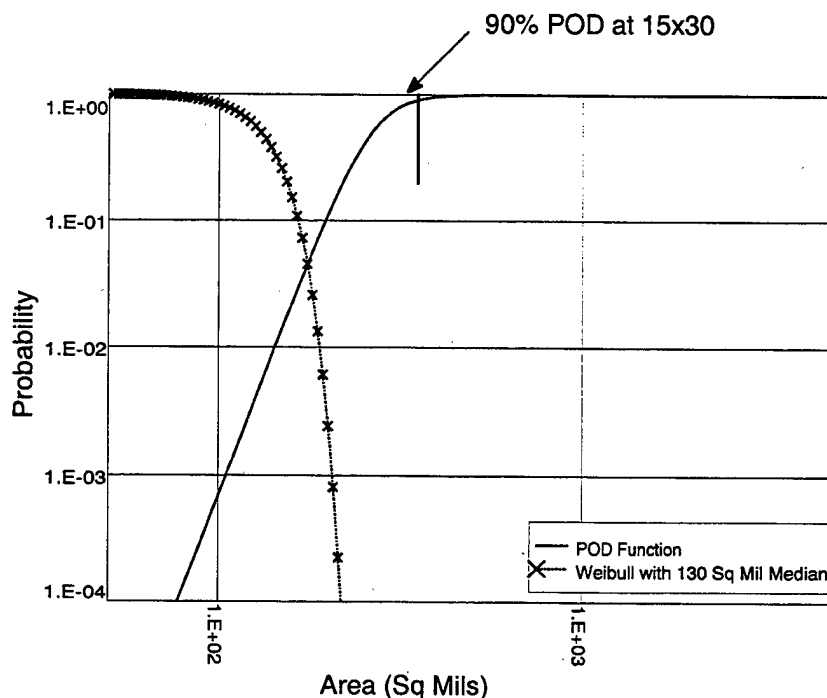


Figure 168. Flaw Distribution Compared to POD Function.

probabilistically; there should be some level of randomness which can be reasonably (though maybe not simply) modeled. The geometry of a nick is, however, probably random in the most colloquial sense of the word; there is no obvious basis for a distribution . . . Any two samples will likely check out as significantly different if statistical tests are tried.

Response – We are suggesting that designs be evaluated against distributions constructed to capture experience. It makes little difference that experience does not support a strict probabilistic interpretation. Neither does experience support the assumption of minimum inspectable cracks at all critical locations. We are merely trading one design criterion for another which better captures the rarity of manufacturing flaws.

Concern – Randomness in placement may not be statistically uniform (e.g. nicks might be more likely to occur at bolthole corners).

Response – This can be factored into the calculations if it is quantified.

Concern – The example considered a single randomly chosen, randomly placed flaw; the failure probability will be higher if there are multiple flaws.

Response – This is true. The integrated risk expression

$$\int_0^{\infty} G_{\text{sur}}(N, a) s_a(a) da$$

does address a single flaw, as does the integrated POD expression

$$\int_0^{\infty} \text{POD}(a) s_{\alpha}(a) da$$

for the probability that a single flaw will be detected. The Poisson risk expression:

$$1 - \exp[-\rho A \cdot \int_0^{\infty} G_{\text{sur}}(N, a) s_{\alpha}(a) da]$$

is based on the possibility of multiple flaws; its value increases as ρA increases. There is an analogous expression for the probability of detection given multiple flaws:

$$1 - \exp[-\rho A \cdot \int_0^{\infty} \text{POD}(a) s_{\alpha}(a) da]$$

For a given value of α this probability also increases as ρA increases. The fact remains, however, that nicks and scratches are rarely found; if ρA is larger, α will have to be smaller, and the net effect on the estimated failure probability will be minimal.

The area term, A , covers a single part in the Poisson risk expression. It should be noted that in the Poisson POD expression, the area term could encompass all inspected parts. . . All inspected parts can contribute to the definition of ρ and $S_{\alpha}(a)$.

Concern – Confidence in the estimated geometric failure distribution depends on the accuracy of the life predictions.

Response – Yes, but the existing ENSIP approach depends equally on this accuracy. Moreover, we have demonstrated one approach to directly integrating statistical variability in the life calculations into the risk expression (Section 9.3):

- Assume that the scatter can be modelled by a distribution of life multipliers: Let μ

denote the ratio of predicted to observed life for a single flaw, and let $m(\mu)$ denote the probability density function of the μ distribution.

- Assume that the distribution of μ predominantly represents testing variability (i.e. Specimen-to-Specimen rather than Flaw-to-Flaw).

With these assumptions, the distribution of life is derived from the Poisson risk expression as a kind of convolution:

$$\int [1 - e^{-\lambda V \cdot R(N \cdot \mu)}] m(\mu) d\mu$$

The existing ENSIP spec acknowledges life scatter by dividing fracture mechanics calculations by 2.

To this point, discussion has focused on a possible probabilistic revision to ENSIP damage tolerance requirements. This attention is appropriate given the perception that the suggestion is a radical departure from a comfortably conservative position. Lost in these considerations, however, is the fact that more could potentially be gained by addressing the sharp crack behavioral assumptions. In particular, the data detailed in Section 23.3 strongly argues for recognition of an incubation mechanism.

24.1 Specific Recommendations

It is recommended:

1. That the ENSIP Spec be amended to permit a probabilistic approach along the lines which we have outlined. Note that additional probabilistic elements could be added as appropriate. Examples:
 - The POD function can be integrated into the risk calculation as shown in Phase I, Section 5.8.
 - Part dimensional variability can be incorporated as shown in Section 9.1.

2. That the acceptable risk ceiling be set at 1/10,000 at full life. This is an order of magnitude lower than the value 1/1,000 proposed in Section 6.3. Given that FAA data suggested that commercial aviation was operating at a level of 7.2/1,000, we cautioned against adding zeroes just to feel good, but feeling good is a strong instinctual drive. More people are comfortable with the lower number.

(It is recognized that the 1/10,000 criterion is already called-out in the ENSIP Spec for embedded defect analysis.)

3. That depot maintenance shops evaluate all rejected parts in detail characterizing any damage or cracking found. This will cost money, but the payoffs in life extensions could be huge if the data supported the accepted belief that flaws are rare and better quantified the distributional bounds required for the proposed probabilistic methodology.

(Some progress in this direction is already being made for the F110 as a CIP activity. An FAA sponsored contract is also looking for such data in the commercial fleet.)

4. That positive incubation and surface enhancement mechanisms be recognized, and also negative time dependent effects on crack growth which are currently ignored in ENSIP calculations. Much has been done (and is continuing to be done) to model inclusion behavior in René 88 DT. Work is needed to address other alloys and other flaw types representative of pertinent manufacturing processes.
5. That greater emphasis be placed on Lead-the-Fleet programs. Endurance testing attempts to catch engineering oversights, but operational usage may produce conditions not adequately represented in testing.

Finally, we suggest that these changes initially be explored in the context of Task V of MIL SPEC 1783 (Life Management). As experience accrues and technology improves, we would expect that Task II (Design) would assimilate elements of these changes as seems appropriate. Furthermore, we suggest that the USAF create a government/industry working group to debate the ideas proposed, and (when consensus is reached) to hammer out the language of a spec revision and details of an implementation strategy.

Phase VI – References

1. ENSIP MIL-STD-1783 (USAF, November 30, 1984).
2. Huron, E.S., and Roth, P.G., "The Influence of Inclusions on Low Cycle Fatigue Life in a P/M Nickel-Base Disk Superalloy," in Superalloys 1996, Ed. by Kissinger, R.D. et.al., TMS-AIME, Warrendale, PA, 1996, p. 359.

Appendix A – Statement of Work

Appendix A – Statement of Work

The following is the current Statement of Work for USAF Contract F33615-90-C-2070.

1.0 Introduction

The Integrated High Performance Turbine Engine Technology (IHPTET) Initiative has set the goal of doubling the performance of gas turbine engines by the year 2000. Achievement of this goal will place new demands on existing materials and will require the use of advanced material systems such as intermetallics and composites. Conventional, deterministic design methods are inherently conservative, and cannot be readily applied to composite material systems. Probabilistic design methodology offers a method of analyzing the interaction of the statistical distribution of design parameters. This reduces the conservatism of the design to a known, acceptable level, and gives the ability to deal with the complex interactions in composite material systems. This program will develop, validate and apply a probabilistic design system.

2.0 Scope

This program will consist of 6 phases. In Phase I, design and operating data will be collected and analyzed to form the basis of later work. In Phase II, the probabilistic design system will be developed, and in Phase III, the system will be validated through testing. Phase IV will apply the design system to a component which will be tested in Phase V. Finally, in Phase VI, the future application of the probabilistic design method will be explored, with particular reference to composite material systems.

3.0 Background

Conventional design systems are based on a deterministic approach, where a single value is assumed for each design factor. Safety is ensured by applying an arbitrary safety factor, or

worst-case assumption. When several safety factors are combined in a design, the end result may be a very safe, but very conservative design. Achievement of IHPTET goals will require the use of new material systems and design concepts where it will be very difficult to determine satisfactory single values for design and safety factors. An alternative design system which has been developing in recent years is the probabilistic approach. In this approach, instead of single values, the statistical distributions of design factors are considered. The interaction of the distributions is analyzed, to predict an overall distribution of the life, or strength, of the total design. From the analysis, operating limitations or component life can be identified for a chosen probability of success. The main resultant benefits are weight reduction, through reduced design conservatism, and improved safety, through better definition of the probability of failure. The method can also be used to analyze an existing design to examine its sensitivity to the variability of influential factors.

4.0 Technical Requirements

The Contractor shall furnish all manpower, facilities and equipment to conduct the program. The Contractor shall exercise administrative and financial management functions during the course of this effort, including: scheduling of activities and milestones; describing status; outlining Contractor activity and progress towards accomplishment of objectives; planning, forecasting and making recommendations on funding and funding changes; program planning; describing in detail the overall results of the effort; and documenting any new technological breakthroughs (CDRL Sequence Nos. 1, 2, 3, 5, 7, 8, 9). The program shall be conducted in 6 phases:

4.1 Phase I – Data Acquisition

In this phase, the Contractor shall collect, review and analyze data on rotor design, operation and failure, to provide a basis for the later phases of the program. Operating and failure data relating to compressor and turbine rotor disks shall be collected from published reports, laboratory experience, engine and component test results, and from field operations. The Contractor shall review and analyze the data to identify the factors which influence the strength and life of rotor disks and the variability of the influential factors. The failure modes of the disks shall also be determined.

4.1.1 Data Acquisition

The Contractor shall collect relevant data from laboratory, spin pit, test engine and field experience for evaluation and analysis. The Contractor shall compile the data from the Contractor's data bases, from available engine overhaul records, published reports, and other sources.

4.1.2 Correlation of Failure Experience

The Contractor shall identify the loadings, temperatures, and gradients that influence the structural longevity of turbine and compressor rotors. The Contractor shall further identify and quantify the probabilistic uncertainties associated with these variables. Potential failure modes shall also be identified.

4.1.3 Evaluation of Loads and Temperatures

The Contractor shall identify the loadings, temperatures, and gradients that influence the structural longevity of turbine and compressor rotors. The Contractor shall further identify and quantify the probabilistic uncertainties associated with these variables. Potential failure modes shall also be identified.

4.1.4 Probabilistic Rotor Design System Parameters

The Contractor shall identify the life-limiting parameters that place a structure at risk from the potential failure modes identified in Paragraph 4.1.3. The probabilistic influence of other risk concerns, such as manufacturing tolerances, imperfect non-destructive evaluation, and mission variability shall also be considered. The Contractor shall formulate an algorithmic architecture that will permit assessment of the overall probability of failure from competing failure modes, considering at least the primary, secondary, and tertiary threats.

4.1.5 Development of Acceptable Risk Criteria

The Contractor shall review available failure data. Data shall be sorted by failure mode at the component level whenever possible to identify specific trends in failure risk levels. Analytical trade studies shall be conducted using probabilistic methods to quantify actual failure risk levels for various peacetime and wartime scenarios. Study results shall be correlated to actual field experience whenever possible. The Contractor shall survey Government and industry sources to help define acceptable risk criteria based on current experience and on the results generated by the studies above. The results of Phase I shall be reviewed in an oral presentation to the Air Force (CDRL Sequence No. 4).

4.1.6 The Contractor shall obtain written approval from the Contracting Officer before proceeding with Phase II.

4.2 Phase II – Method Development

In this phase the Contractor shall review its existing probabilistic design methods and develop them as required for application to compressor and turbine rotor disks. Models shall be selected or developed for all significant failure modes, including cyclic fatigue, fracture, burst, creep, vibration and growth. The models shall address the statistical variations of influential

design factors, including mission profiles, material properties, inspection reliability and manufacturing capability. The Contractor shall also select and study an alternative model program, such as NESSUS (Numerical Evaluation of Stochastic Structures Under Stress), which shall be used later for comparison.

4.2.1 Failure Models Development

The Contractor shall assess existing probabilistic life cyclic fatigue and fracture models and modify them based on the results of Phase 1. The Contractor shall modify or develop probabilistic models for burst, creep, vibration, and growth failure modes.

4.2.2 Statistical Analysis Models

The Contractor shall construct the statistical models required as input to the analysis developed in task 4.2.1. These models shall include statistical variations of life drivers, regression models, and other analytical models. Statistical variation of life drivers shall include variations in the operating environment as well as the uncertainty in engineering analyses and models.

4.2.3 Methodology Description

The Contractor shall prepare a description of the analysis techniques contained in the code and the assumptions used or implicit in the methodology. At the completion of Phase II, the Contractor shall make an oral presentation to the Air Force (CDRL Sequence No. 4).

4.2.4 The Contractor shall obtain written approval from the Contracting Officer before proceeding with Phase III.

4.3 Phase III – Validation

In this phase the Contractor shall demonstrate the validity of the Probabilistic Rotor Design System (PRDS) design tool. This shall be done by designing specimens, and testing them to failure in a series of controlled experiments. All

test hardware shall be designed, fabricated and tested in accordance with AFR 800-16 and the standards of MIL-STD-882B. The specimens shall be designed to simulate the failure behavior of a turbine rotor disk, and the testing shall aim to produce representative failures in the specimens. The specimen design shall be analyzed using the probabilistic design method and the probability distribution of its failure shall be determined. The test plan shall be designed to produce a statistically significant validation of the predicted results, using a design of experiments methodology.

4.3.1 Test Definition

The Contractor shall determine the test articles and necessary tests to be used for validating the PRDS. The test articles and test methods shall be designed so as to provide a clear validation of the probabilistic life methodology. The Contractor shall perform both a deterministic and probabilistic life analysis of the test articles. The Contractor shall then determine the tests required to verify the predictions and their applicability to future testing (CDRL Sequence No. 6). The Contractor shall review and approve the fabrication of the specialized tooling required to cyclic spin selected test articles in a government facility.

4.3.2 Test Evaluation

The Contractor shall fabricate the approved test articles and monitor the PRDS validation testing in accordance with the approved test plan. The contractor shall monitor cyclic spin testing of selected components until each has failed or until economic life has been attained. Fractographic examination of selected test articles will be conducted to characterize the location (surface, near-surface, subsurface, etc.) and nature (ceramic, oxide, nitride, void, crystallographic, etc.) of the origin of the fracture. All raw test data shall be compiled (CDRL Sequence No. 10) and the Contractor shall make

an oral presentation to the Air Force (CDRL Sequence No. 4).

4.3.3 PRDS Design Tool Refinement

Based on the results of the validation tests the Contractor shall make improvements to the PRDS design tool as required.

4.3.4 The Contractor shall obtain written approval from the Contracting Officer before proceeding with Phase IV.

4.4 Phase IV – Application

In this phase the Contractor shall apply the Probabilistic Rotor Design System (PRDS) to one turbine rotor disk from an advanced technology engine. The selected component shall be used for a case study addressing the use of the PRDS design tool as a means of reducing weight. Representative engine cycle parameters (stress and temperature histories) and available materials data will be identified and analyzed with the refined methodology resulting from Phase II, to establish a baseline weight and survival probability of the selected components for a specifically defined life.

4.4.1 Probabilistic Redesign

The Contractor shall redesign and analyze the component for the same life as the baseline design using the PRDS code, in sufficient detail to determine the survival probability and weight for comparison to the baseline design. The objective of this task is to identify an alternative design that provides a significant weight reduction as compared to the baseline design, with an acceptable survival probability identified in Phase I. At the completion of Phase IV, the results shall be reviewed with the Air Force (CDRL Sequence No. 4).

4.4.2 The Contractor shall obtain written approval from the Contracting Officer before proceeding with Phase V.

4.5 Phase V – Application Test

In this phase the Contractor shall monitor testing of the rotor disk which was redesigned in Phase IV. The disk shall be provided from a separately funded contract as GFE. Under a separately funded contract, the Contractor shall install the disk in a test engine to be run for a predetermined number of cycles. After the engine test, the Contractor shall monitor the disk installation in a government facility spin rig and monitor testing of the disk to failure. Failure analysis shall be conducted and all test results shall be evaluated to demonstrate the integrity of the design.

4.5.1 Rotor Components Detail Design

The Contractor shall establish and document the design details of the selected rotor disk using the Probabilistic Rotor Design System (PRDS). The acceptable risk criteria defined during Phase I shall be integrated with probabilistic methods to establish the design allowables. These allowables shall then be used in conjunction with standard design analysis procedures such as finite element analysis to establish the final component. This detail design shall include the statistical probability of failure for all primary failure modes. The Contractor shall also evaluate the weight and performance payoff obtained by redesigning the component using probabilistic design concepts.

4.5.2 Rig Test and Validation for Gas Generator Testing

The Contractor shall monitor and analyze the test of the GFE rotor disk to provide final verification of the PRDS and applicability for advanced demonstrator engine testing. The Contractor shall: (1) prepare a test plan defining post-engine component testing, (2) review and approve design and fabrication of necessary test rig adaptive hardware, (3) perform a complete stress survey. The Contractor shall identify and document all instrumentation require-

ments. The Contractor shall identify the design conditions and cycles to be simulated. The Contractor shall define evaluation methods for analysis and test correlation. The Contracting Officer, within 7 days after submittal of the test plan (CDRL Sequence No. 6), will inform the Contractor by letter if work may proceed on the Phase V test items. Following approval by the Air Force Contracting Officer, the Contractor shall provide the PRDS component for testing in a separately funded advanced demonstrator engine test. The Contractor shall conduct engine testing in such a manner as to obtain data for verification of the design predictions and the applicability of advanced PRDS components in advanced turbopropulsion weapon systems.

4.5.3 Hot Cyclic Spin of Component

The Contractor shall monitor a hot cyclic spin test of the GFE rotor disk until it fails. This test shall be completed after all potential advanced gas generator testing has occurred. The Contractor shall conduct a post-test failure analysis of the rotor component. The results shall be compared against predictions from the Probabilistic Rotor Design System to determine the accuracy of the system. The Contractor shall review the results of Phase V in an oral presentation to the Air Force (CDRL Sequence No. 4).

4.5.4 The Contractor shall obtain written approval from the Contracting Officer before proceeding with Phase VI.

4.6 Phase VI – Method Extension

In this phase the Contractor shall examine the extension of the probabilistic design method to other component types and materials. Advanced materials, and engine components other than rotor disks, shall be classified according to their properties, manufacturing methods and failure modes, and the applicability of the probabilistic design system shall be determined.

Recommendations shall be made for further work, including modification or extension of the design system.

4.6.1 PRDS for Metal Matrix Composite (MMC) Rotors

The Contractor shall gather information on the properties, behavior and failure modes for MMC materials. This information shall be evaluated to determine the possibilities and requirements for developing statistical models for a design system. The Contractor shall determine the benefits of a Probabilistic Rotor Design System for meeting MIL-STD-1783 Engine Structural Integrity Program (ENSIP) and IHPTET Requirements for MMC materials.

4.6.2 Modifications to Military Standard 1783

The Contractor shall develop a modified Military Standard 1783 that incorporates PRDS. The modification shall be in a form that can be submitted to the Government Committee on Military Standards for consideration.

4.6.3 PRDS Modifications

The probabilistic life-prediction methodology, resulting from Phase II, shall be modified or supplemented as applicable to address the failure mechanisms determined by Paragraph 4.6.1, and the information obtained in Phases III, IV and V. A plan addressing the comprehensive application of the PRDS methodology shall be prepared. The plan shall be developed to include both isotropic and anisotropic materials. The results of Phase VI shall be reviewed in an oral presentation to the Air Force (CDRL Sequence No. 4).

5.0 Data and Other Deliverables

5.1 Data are listed on the CDRL (DD Form 1423).

5.2 The Contractor shall plan for six status reviews in the form of oral presentations to the Air Force at Wright-Patterson Air Force Base (CDRL Sequence No. 4).

Appendix B – Sampler Scatter

Appendix B – Sampling Scatter

The scatter inherent in small scale sampling is significant and absolutely unavoidable. Repeat samples of size 20 could be expected to yield distributions as shown in *Figures B.1* through *B.4*. (A count somewhere on the order of 20

inclusions is not untypical for a single half-pound HLS sample.)

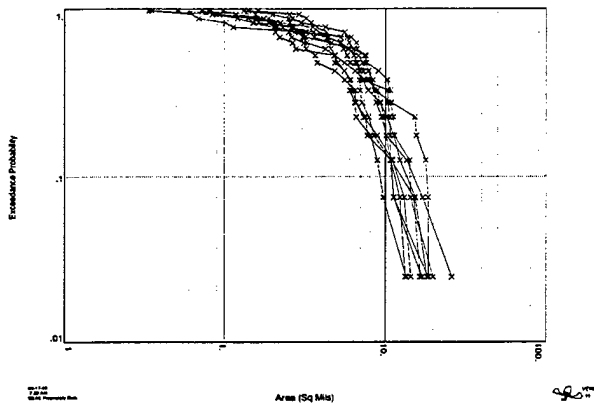


Figure B.1. Reproducibility – 10 Random Samples of Size 20.

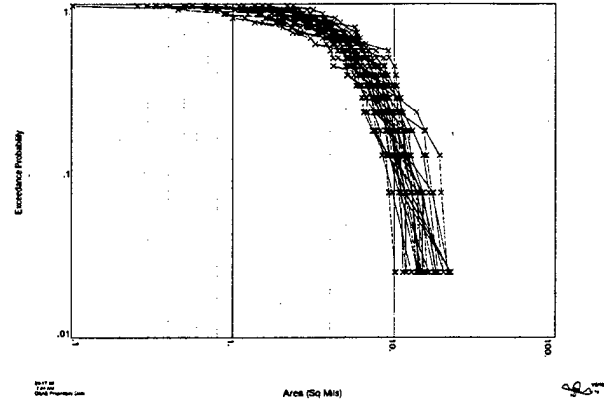


Figure B.3. Reproducibility – 30 Random Samples of Size 20.

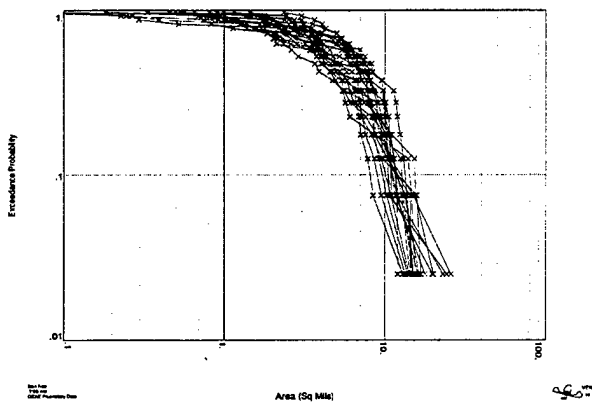


Figure B.2. Reproducibility – 20 Random Samples of Size 20.

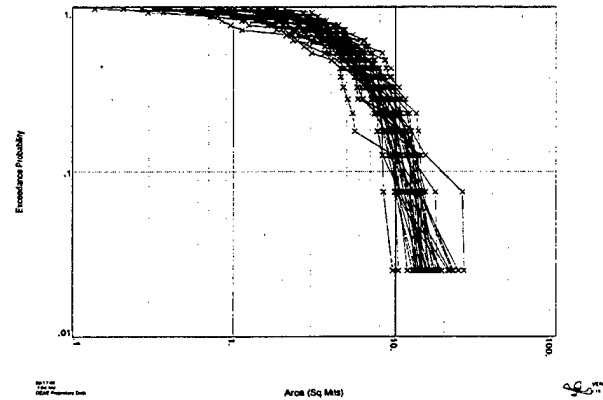


Figure B.4. Reproducibility – 40 Random Samples of Size 20.

Appendix C – PDAS Analysis Templates

Appendix C – PDAS Analysis Templates

The following templates were used to produce the analyses presented in Section 7.1.

Direct Integration

```
table 1 initialize
table 1 column Z from -6 to 6 # 1000
table 1 set Z = Z + 0
table 1 set PROB = (1/sqrt(2*pi))*exp(-((Z-0)**2)/2)
```

Define X-distribution

```
distribution input X (table) 1 Z (format) density
```

```
table 1 initialize
table 1 column Z from -6 to 6 # 1000
table 1 set Z = Z + 0
table 1 set PROB = (1/sqrt(2*pi))*exp(-((Z-3)**2)/2)
```

Define Y-distribution

```
distribution input Y (table) 1 Z (format) density
```

```
table 2 initialize
V = 0.7
table 2 write new# V
V = 1.3
table 2 write new# V
V = 2.0
table 2 write new# V
```

Construct table of V-values

```
loop start
loop over (table) 2
```

Loop over the V-table

```
expr B : (X+V)**2 + (X-V)**2 - 2
expr C : (X**2-v**2)**2 - (X+V)**2 - (X-V)**2
expr DSCR : B**2 - 4*C
```

Define expressions used to
compute Y-limits of
integration

```
table 1 initialize (width) 30
table 1 column X from -3.3 to 3.3 # 1000
```

Construct table of X-values

Direct Integration (continued)

table 1 set B = (expr) B table 1 set C = (expr) C table 1 set DSCR = (expr) DSCR table 1 flag DSCR .ge. 0 table 1 set YSQ = (-B + sqrt(DSCR))/2 table 1 flag YSQ .ge. 0 table 1 set YLIM = sqrt(YSQ)	Determine Y-limits of integration for each X
loop start loop over (table) 1	Loop over the X-table
expr : unsf(YLIM - Y) * unsf(YLIM + Y) algebra replace YLIM	Define Y-integrand as 1 between \pm YLIM and 0 elsewhere
Y_INT = (integral) LAST wrt Y table 1 writ Y_INT	Evaluate the Y-integral and write to the X-table
loop stop	End of the X-table loop
expr : (dig) (table) 1 Y_INT (lin) X (lin)	Define X-integrand as the X-digitized function of the Y-integral
X_INT = (integral) LAST wrt X table 2 write X_INT	Integrate this function; Write to the V-table. (X_INT estimates failure probability)
loop stop	End of the V-table loop
submit rm example.1.out done	Remove the file example.1.out (if it exists)
table 2 output V X_INT example.1.out	Output V and X_INT to example.1.out

Monte Carlo Integration

table 1 initialize table 1 column Z from -6 to 6 # 1000 table 1 set Z = Z + 0 table 1 set PROB = (1/sqrt(2*pi))*exp(-((Z-0)**2)/2) S = 0 table 1 set S = S + PROB table 1 read row# 1000 SUM = S table 1 set PROB = S/SUM dist input X (table) 1 Z (format) cumulative table 1 initialize table 1 column Z from -6 to 6 # 1000 table 1 set Z = Z + 3 table 1 set PROB = (1/sqrt(2*pi))*exp(-((Z-3)**2)/2) S = 0 table 1 set S = S + PROB table 1 read row# 1000 SUM = S table 1 set PROB = S/SUM dist input Y (table) 1 Z (format) cumulative table 2 initialize V = 0.7 table 2 write new# V V = 1.3 table 2 write new# V V = 2.0 table 2 write new# V loop start loop over (table) 2 table 1 init (width) 15 table 1 rand X Y # 1000000 table 1 set DEN1 = (X - V)**2 + Y**2	Define X-distribution; First the probability density function Then, integrate to yield the cumulative distribution function Input the distribution Define Y-distribution First the probability density function Then, integrate to yield the cumulative distribution function Input the distribution Construct table of V-values Loop over the V-table Construct table of 1,000,000 randomly chosen (X, Y) points Compute pressure at each point
---	--

```
table 1 set DEN2 = (X + V)**2 + Y**2
table 1 set P = 1e10
table 1 flag DEN1 .gt. 0 DEN2 .gt. 0
table 1 set P = 1/DEN1 + 1/DEN2
```

```
table 1 flag P .ge. 1
table 1 set COUNT = 1
SUM = (table) 1 (sum) COUNT
FRACTION = SUM/1000000
table 2 write FRACTION
```

```
loop stop
```

```
submit
rm example.2.out
done
```

```
table 2 output V FRACTION
example.2.out
```

Flag points with pressure greater than or equal to 1; Count the rows and divide by 1,000,000; Write to the V-table. (FRACTION estimates failure probability)

End of the V-table loop

Remove the file example.2.out (if it exists)

Output V and FRACTION to example.2.out

First Order Reliability Approximation

```
table 1 initialize
table 1 column Z from -6 to 6 # 1000
table 1 set Z = Z + 3
table 1 set PROB = (1/sqrt(2*pi))*exp(-((Z-3)**2)/2)
```

```
distribution input Z (table) 1 Z (format) density
```

```
table 2 initialize
V = 0.7
table 2 write new# V
V = 1.3
table 2 write new# V
V = 2.0
table 2 write new# V
```

```
loop start
loop over (table) 2
```

```
expr B : (X+V)**2 + (X-V)**2 - 2
expr C : (X**2-V**2)**2-(X+V)**2-(X-V)**2
expr DSCR : B**2 - 4*C
```

Define Z-distribution

Input probability density function

Construct table of V-values

Loop over the V-table

Define expressions used to compute Y-bounds

table 1 initialize (width) 30 table 1 column X from -3.3 to 3.3 # 1000	Construct table of X-values
table 1 set B = (expr) B table 1 set C = (expr) C table 1 set DSCR = (expr) DSCR table 1 flag DSCR .ge. 0 table 1 set YSQ = (-B + sqrt(DSCR))/2 table 1 flag YSQ .ge. 0 table 1 set YBND = sqrt(YSQ)	For each X, determine Y-bound
YBND = (table) 1 (max) YBND	Determine maximum Y-bound
expr : unsf(-Z + YBND) algebra replace YBND	Define Z-integrand as 1 below YBND and 0 above
Z_INT = (integral) LAST wrt z table 2 write X_INT	Integrate this function; Write to the V-table. (Z_INT estimates failure probability)
loop stop	End of the V-table loop
submit rm example.3.out done	Remove the file example.3.out (if it exists)
table 2 output V X_INT example.3.out	Output V and Z_INT to example.3.out

**Appendix D – Introduction to Response
Surface Methodology and Factorial Designs**

Appendix D - Introduction to Response Surface Methodology and Factorial Designs

Consider 2 dimensions - Fitting a function of the form $f(x, y) = a_x x + a_y y + c$ can be done with a minimum of 3 points. E.g.:

$$(0, 0), (\delta, 0) \text{ and } (0, \delta),$$

but the risk of noise is great. Using the following 4 point factorial design improves the fit:

$$(\delta/2, \delta/2), (\delta/2, -\delta/2), (-\delta/2, \delta/2) \\ \text{and } (-\delta/2, -\delta/2).$$

The parameter vector of the least square fit of $f(x, y)$ to the data $(x_1, y_1, o_1), \dots, (x_n, y_n, o_n)$ is computed as follows (p 63, **Reference 10**) 5 of Phase IV:

$$\begin{bmatrix} a_x \\ a_y \\ c \end{bmatrix} = (J^T J)^{-1} J^T \begin{bmatrix} o_1 \\ \dots \\ o_n \end{bmatrix}$$

where the Jacobian:

$$J = \begin{bmatrix} \partial f / \partial a_x(x_1, y_1) & \partial f / \partial a_y(x_1, y_1) & \partial f / \partial c(x_1, y_1) \\ \dots & \dots & \dots \\ \partial f / \partial a_x(x_n, y_n) & \partial f / \partial a_y(x_n, y_n) & \partial f / \partial c(x_n, y_n) \end{bmatrix}$$

$$= \begin{bmatrix} x_1 & y_1 & 1 \\ \dots & \dots & \dots \\ x_n & y_n & 1 \end{bmatrix}$$

Fitting $f(x, y)$ to the three points $(0, 0)$, $(1, 0)$ and $(0, 1)$ yields:

$$\begin{bmatrix} a_x \\ a_y \\ c \end{bmatrix} = \begin{bmatrix} -1 & 1 & 0 \\ -1 & 0 & 1 \\ 1 & 0 & 0 \end{bmatrix} \begin{bmatrix} o_1 \\ o_2 \\ o_3 \end{bmatrix}$$

$$a_x = o_2 - o_1$$

$$a_y = o_3 - o_1$$

$$c = o_3 - o_1$$

Assume that the observations o_1, o_2 and o_3 have identical and independent random noise components having a standard deviation σ . Then the estimator $a_x = o_2 - o_1$ will have slightly greater noise (a standard deviation of $2^{1/2}\sigma$) as it is a linear combination of two random variables; similarly for $a_y = o_3 - o_1$. The scatter in the c estimator is σ .

Now, fit $f(x, y)$ to the four points $(1, 1)$, $(1, -1)$, $(-1, 1)$ and $(-1, -1)$...

$$\begin{bmatrix} a_x \\ a_y \\ c \end{bmatrix} = 0.25 \begin{bmatrix} 1 & 1 & -1 & -1 \\ 1 & -1 & 1 & -1 \\ 1 & 1 & 1 & 1 \end{bmatrix} \begin{bmatrix} o_1 \\ o_2 \\ o_3 \\ o_4 \end{bmatrix}$$

$$a_x = 0.25 (o_1 + o_2 - o_3 - o_4)$$

$$a_y = 0.25 (o_1 - o_2 + o_3 - o_4)$$

$$c = 0.25 (o_1 + o_2 + o_3 + o_4)$$

Thus each parameter estimate is a linear combination of four random variables. The standard deviations of the estimators are all $\sigma/2$... There is significant noise reduction.

Noise reduction increases as dimension increases.

Fitting a function of the form $f(x) = a_1 x_1 + a_2 x_2 + \dots + a_n x_n + c$, let J_n be the Jacobian for the following full factorial design in n dimensions:

$$p_1 = (1, \dots, 1, 1, 1)$$

$$p_2 = (1, \dots, 1, 1, -1)$$

$$p_3 = (1, \dots, 1, -1, 1)$$

$$p_4 = (1, \dots, 1, -1, -1)$$

$$p_5 = (1, \dots, -1, 1, 1)$$

$$p_6 = (1, \dots, -1, 1, -1)$$

$$p_7 = (1, \dots, -1, -1, 1)$$

$$p_8 = (1, \dots, -1, -1, -1)$$

Consider $J_1 \dots$

$$J_1 = \begin{bmatrix} 1 & 1 \\ -1 & 1 \end{bmatrix}$$

The columns are orthogonal. Now, assume that the columns of J_n are mutually orthogonal.

Adding one dimension doubles the size of the factorial design in a simple fashion...

$$(1, p_1), (1, p_2), (1, p_3), \dots \\ (-1, p_1), (-1, p_2), (-1, p_3), \dots$$

J_{n+1} is blocked ...

$$J_{n+1} = \begin{bmatrix} u & J_n \\ -u & J_n \end{bmatrix} \text{ where } u = \begin{bmatrix} 1 \\ \dots \\ 1 \end{bmatrix}$$

The dot product of first column of J_{n+1} with any other column has the form $u \cdot u_i - u \cdot u_i$ where u_i is the relevant column of J_n ; the dot product vanishes, and therefore the first column of J_{n+1} is orthogonal to every other column. The dot product of any two columns to the right of the first has the form $u_i \cdot u_j - u_i \cdot u_j$ where u_i and u_j are the relevant columns of J_n . The dot products all vanish; it follows that the right hand columns of J_{n+1} are mutually orthogonal, and hence that all columns are mutually orthogonal.

By mathematical induction, for any dimension n , the columns of J_n are mutually orthogonal.

Since $(J_n^T J_n)^{-1} = (1/2^n) I$, the least squares fit estimator is:

$$\begin{bmatrix} a \\ c \end{bmatrix} = (1/2^n) J_n^T o$$

Each of the parameter estimators a_1, a_2, \dots, a_n and c is thus a linear combination of the 2^n observations in the factorial design. The coefficients are either $1/2^n$ or $-1/2^n$. It follows that the standard deviation of each estimator is $2^{-n/2} \sigma$.

The same factorial design can be used to fit the much more general functional form obtained by adding in any number of interaction terms:

First order interaction terms:

$$a_{12}x_1x_2, a_{13}x_1x_3, a_{14}x_1x_4, \dots \\ a_{23}x_2x_3, a_{24}x_2x_4, \dots$$

Second order interaction terms:

$$a_{123}x_1x_2x_3, a_{124}x_1x_2x_4, a_{125}x_1x_2x_5, \dots \\ a_{234}x_2x_3x_4, a_{235}x_2x_3x_5, \dots$$

One $(n-1)$ 'st order interaction term:

$$a_{123\dots n}x_1x_2x_3 \dots x_n$$

The Jacobian column of an interaction term is the component product of the corresponding linear term columns. For example: The column of the second order interaction term $a_{ijk}x_i x_j x_k$ is computed by taking the i, j and k linear term columns and multiplying component by component:

$$\begin{bmatrix} j_{1i} \cdot j_{1j} \cdot j_{1k} \\ j_{2i} \cdot j_{2j} \cdot j_{2k} \\ j_{3i} \cdot j_{3j} \cdot j_{3k} \\ \dots \end{bmatrix} \text{ where } j_{pq} \text{ is the } p,q \text{ entry of } J_{\text{linear}}$$

We will show that all columns generated in this fashion sum to 0.

Consider $J_1 \dots$

$$J_1 = \begin{bmatrix} 1 & 1 \\ -1 & 1 \end{bmatrix}$$

The only column product is:

$$\begin{bmatrix} 1 \times 1 \\ -1 \times 1 \end{bmatrix} = \begin{bmatrix} 1 \\ -1 \end{bmatrix}$$

The sum of the entries is 0.

Now, assume that any product of distinct columns of J_n sum to 0.

J_{n+1} is blocked ...

$$J_{n+1} = \begin{bmatrix} u & J_n \\ -u & J_n \end{bmatrix} \text{ where } u = \begin{bmatrix} 1 \\ \vdots \\ 1 \end{bmatrix}$$

Any column product of J_{n+1} which includes the first column has the form:

$$\begin{bmatrix} 1 & x & p \\ -1 & x & p \end{bmatrix}$$

where p is a column product of J_n .

Any column product of J_{n+1} which does not include the first column has the form:

$$\begin{bmatrix} p \\ p \end{bmatrix}$$

where p is a column product of J_n .

In either case, the sum of the entries is 0.

The desired result follows by mathematical induction.

Since $(J_n^T J_n)^{-1} = (1/2^n) I$, the least squares fit estimator again has the form:

$$\begin{bmatrix} a \\ c \end{bmatrix} = (1/2^n) J_n^T o$$

and the standard deviation of each estimator is $2^{-n/2} \sigma$.

By comparison, let J_n be the Jacobian for the following minimal design in n dimensions:

$$\begin{aligned} p_1 &= (0, 0, 0, \dots, 0) \\ p_2 &= (1, 0, 0, \dots, 0) \\ p_3 &= (0, 1, 0, \dots, 0) \\ p_4 &= (0, 0, 1, \dots, 0) \\ p_{n+1} &= (0, 0, 0, \dots, 1) \end{aligned}$$

$$J_n^T J_n = \begin{bmatrix} 1 & 0 & 0 & \dots & 1 \\ 0 & 1 & 0 & \dots & 1 \\ 0 & 0 & 1 & \dots & 1 \\ \dots & & & & \\ 1 & 1 & 1 & \dots & n \end{bmatrix}$$

$$(J_n^T J_n)^{-1} = \begin{bmatrix} 2 & 1 & 1 & \dots & -1 \\ 1 & 2 & 1 & \dots & -1 \\ 1 & 1 & 2 & \dots & -1 \\ \dots & & & & \\ -1 & -1 & -1 & \dots & 1 \end{bmatrix}$$

$$\begin{bmatrix} a \\ c \end{bmatrix} = (J_n^T J_n)^{-1} J_n^T o$$

$$= \begin{bmatrix} -1 & 1 & 0 & \dots & 1 \\ -0 & 0 & 1 & \dots & 1 \\ -1 & 0 & 0 & \dots & 1 \\ \dots & & & & \\ 1 & 0 & 0 & \dots & 0 \end{bmatrix} \begin{bmatrix} o_1 \\ o_2 \\ \dots \\ o_n \\ o_{n+1} \end{bmatrix}$$

Therefore, $a_i = o_{i+1} - o_i$, and $c = o_1$; the standard deviations of the a_i estimators are all $2^{1/2} \sigma$; the standard deviation of the c estimator is σ .

Any experimental design which has the property that the columns of the Jacobian are orthogonal is called an orthogonal design. Subsets of a full factorial design which are orthogonal are called fractional factorial (*References 5 and 6* of Phase IV). They provide some of the benefit of variance reduction, but will not allow incorporation of all possible interaction terms. This may not be a problem if one is only interested in the lower order interactions. For example, in the HPT disk optimization discussed in Section 20, a 6 parameter model was assumed with a constant term, 6 linear terms and all 15 first order interactions. The full factorial design for six parameters requires 64 points. A 32 point

fractional factorial design was used to accomplish the fits.

The lack of quadratic terms (A^2 , B^2 , etc.) in the response surface approximations is probably more a potential concern for the application of Section 20 than is the absence of higher order interactions (ABC, ABD, ABE, etc.). Consider, for example, the dependence of H_{Av} (Average Hoop Stress) on BOFF (Bore Offset) as shown in *Figure D.1*.

The points plotted in the *Figure D.1* represent all calculations required for the last two iterations of the optimization. There are two sets of three points connected by line segments; each set of three isolates dependence on just the parameter BOFF. While there is a hint of quadratic behavior, the first order effects are small, and the second order effects even smaller; adding a quadratic term in BOFF would not have significantly affected the optimization.

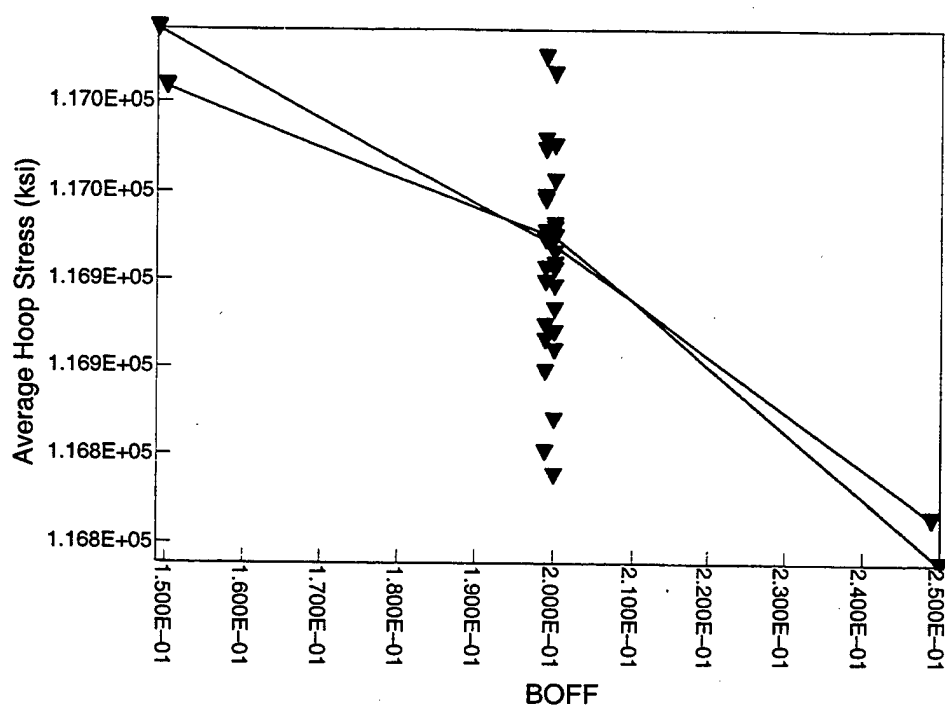


Figure D.1. Average Hoop Stress on Bore Offset.